Decoherence and relaxation of a pair of interacting spins coupled to independent environments

Von der Fakultät Mathematik und Physik der Universität Stuttgart
zur Erlangung der Würde eines Doktors der
Naturwissenschaften (Dr. rer. nat.) genehmigte Abhandlung

vorgelegt von

Peter Nägele

aus Schwäbisch Gmünd

Hauptberichter: Prof. Dr. Ulrich Weiß
Mitberichter: Prof. Dr. Günter Mahler

Tag der mündlichen Prüfung: 29.Oktober 2009

II. Institut für Theoretische Physik der Universität Stuttgart
2009

Contents

Notations and Symbols

NIBA	noninteracting-blip approximation
RDM	reduced density matrix
SBE	spin-boson environment
SQUIDS	superconducting quantum interference devices
TSS	two-state system
$\mathcal{A}$	path integral amplitude
$\mathcal{B}$	spin-spin coupling path integral amplitude
$\vec{B}$, $B_{x,y,z}$	magnetic field
B_n	bias factor
b, $b^\dagger$	boson annihilation and creation operators
C_g	gate capacitance
C_J	Josephson capacitance
c_α	coupling strength to bath mode α
D	denominator
E_C	charging energy
E_J	Josephson energy
$E_1,\ E_2,\ E_3,\ E_4$	eigenenergies
e	elementary charge
$\|e\rangle$	excited state
$\|e_1\rangle,\ \|e_2\rangle,\ \|e_3\rangle,\ \|e_4\rangle$	energy eigenstates
$\mathcal{F}$	Feynman-Vernon influence functional
F_i	bath coupling
$\|g\rangle$	ground state
H	Hamilton operator
Im	imaginary part
$J(\omega)$, $J_\mathrm{lf}(\omega)$	spectral density of bath, low frequency part hereof

$J_{m,n}$	conditional propagators
K, $K_{1,2}$	Kondo parameter
$\mathcal{K}$, $k_{1,2}^{(\pm)}$, and $k_{1,2}^{(\mathrm{s/a})}$	kernels, symmetric and antisymmetric
$k_{1,2}^{\pm}$	forward and backward rate
k_{B}	Boltzmann constant
L	self-inductance
lim	limit
N	numerator
n	number operator of Cooper pair charges
n_{g}	gate induced charges
$P(t)$	population
P	purity
Q	quality factor, charge
$Q = Q' + \mathrm{i}\,Q''$	bath correlation function, real and imaginary part
Q_i	position operator
$\|R\rangle$, $\|L\rangle$	eigenstates of σ_z
$\|RR\rangle$, $\|RL\rangle$, $\|LR\rangle$, and $\|LL\rangle$	eigenstates of σ_z and τ_z
Re	real part
Res	residue, amplitude
$S(\omega)$	power spectrum of bath
sgn	signum function
T	temperature
$T_{1,2}$, and T_2^*	relaxation time T_1, dephasing time T_2, and ensemble averaged dephasing time T_2^*
tr	trace
U	diagonalization matrix
V_{g}	gate voltage
$v_{x,y,z}$	spin-spin coupling
$W_{n,m}$	transition rate $m \to n$
X	bath coupling operator
β	inverse temperature

$\Gamma^{\pm}$	Golden Rule rates
γ	gyromagnetic ratio
γ, γ_{r}	relaxation and dephasing rates
$\gamma_{n,m}$	damping rate
$\Delta_{1,2}$	tunneling matrix
Δ_{r}	renormalized tunneling matrix
Δ_{T}	renormalized and temperature dependent tunneling matrix
δ	eigenfrequency, δ function
$\epsilon_{1,2}$	bias
ϵ_{c}	critical bias
$\zeta = 1, 2$	spin 1, spin 2; bath 1, bath 2
η	symmetric spin path
Θ	superconducting phase, Heaviside function
$\Theta_{1,2}$	mixing angles
$\vartheta_{1,2}$, $\theta_{1,2}$	scaled temperature, generalized temperature
ϑ^*	crossover temperature
κ	relaxation and dephasing rates
Λ	blip-blip correlations
λ	Laplace variable
ξ	antisymmetric spin path
ρ	density matrix
ρ_{eq}	equilibrium density matrix
$\rho_{i,j}^{(0)}$	initial state of density matrix
$\Sigma^{(\mathrm{s/a})}$	self energy
$\sigma_{\mathrm{i,f}}$	initial and final spin state
$\sigma_{x,y,z}$, $\tau_{x,y,z}$	Pauli matrices
σ, τ	spin 1, spin 2
τ_{c}	correlation time
τ_j	blip lengths
Φ, Φ_x	magnetic flux
Φ_0	flux quantum
Ω, Ω_+, Ω_-	eigenfrequencies

ω_α	frequency of bath oscillator α
ω_c	high-frequency cutoff

Zusammenfassung

Quantale dissipative Systeme werden schon seit den 1980er Jahren intensiv untersucht. Dennoch ist das Interesse für solche Systeme nach wie vor ungebremst. Dies liegt unter anderem an der fortwährenden Miniaturisierung elektronischer Bauelemente. Die Entwicklung der Halbleiterindustrie, insbesondere das Mooresche Gesetz, ist hierbei ein bekanntes Beispiel. Moores Gesetz besagt, dass sich die Zahl der Transistoren auf einem Mikrochip ungefähr alle zwei Jahre verdoppelt. Das Wachstum wird durch zwei Faktoren begrenzt: zum einen können Bauteile strukturbedingt nicht kleiner werden als ein paar wenige Atome, zum anderen jedoch wird die Funktionalität der Bauteile durch das Auftreten von Quanteneffekten begrenzt, bzw. verändert. Diese Quanteneffekte treten schon bei Strukturgrößen auf, die kleiner als 200nm sind, wobei aktuelle kommerziell verfügbare Mikrochips mit 45nm großen Strukturen fabriziert werden. Dies verdeutlicht das große Interesse und die Notwendigkeit neue Konzepte und Methoden zu entwickeln.

Zudem entwickelte sich insbesondere in den letzten Jahren eine Nanowissenschaft. Diese umfasst die verschiedene Bereiche wie die Nanobiologie, Nanochemie, Nanoelektronik und den Nanomagnetismus. Die Gemeinsamkeit dieser Bereiche liegt in der Erforschung mesoskopischer Strukturen. Diese Strukturen umfassen einen Größenbereich zwischen mehreren Atomen und 200nm und sind daher durch das Vorhandensein von Quanteneigenschaften charakterisiert. Es sind insbesondere zwei Eigenschaften die gegenüber der klassischen Physik wichtig werden: Erstens, für ein Zwei–Zustands–System, z.B. ein Spin mit den zwei Einstellmöglichkeiten Spin–Up und Spin–Down, erlaubt die Quantenphysik auch eine Superposition beider Zustände, also eine Mischung aus Spin–Up und Spin–Down. Gerade diese Eigenschaft führt zu neuen Anwendungen wie bspw. den Quantencomputer. Die zweite bedeutende Änderung betrifft die Wechselwirkung mit der Umgebung, die zu Dissipation und Dekohärenz führt. Während man klassische Systeme getrennt von der restlichen Welt einigermaßen gut beschreiben kann, gilt dies für mesoskopische Systeme nicht mehr. Alleine schon das Messen eines Quantenzustands durch ein Messgerät entspricht einer Interaktion mit der Umgebung. Aber auch schon die gewöhnliche Umgebung eines System stellt einen wichtigen Faktor dar: wirkt die Umgebung zu stark auf das System, geht dieses schnell in einen klassischen Zustand über und Vorteile der Quantenwelt gehen verloren.

Aus rein theoretischer Sicht ist die Dekohärenz ein Grund für Kontroversen. Insbesondere der Messprozess eines Quantenzustands wird oft mit einem Kollaps der Wellenfunktion gleichgesetzt. Der Kollaps aber ist ein Postulat, welches mit anderen grundsätzlichen Postulaten der Quantenmechanik im Widerspruch steht, dem Superpositionsprinzip und der unitären Zeitentwicklung von Zuständen. Betrachtet man allerdings den Messapparat als Umgebung, welche kontinuierlich auf das Quantensystem einwirkt, so erhält man einen stetigen unitären Übergang zu einem Eigenzustand des Systems, wie er nach einer Messung vorzufinden ist, ohne dabei einen Kollaps der Wellenfunktion postulieren zu müssen.

So dient die Untersuchung von quantalen dissipativen Systemen auch der Klärung von Grundsatzfragen der Physik.

Das dissipative quantenmechanische Zwei–Zustands–System, z.B. ein Spin mit dissipativer Umgebung, findet sich in vielen Problemstellungen der Physik. Diese umfassen verschiedene Bereiche wie Störstellentransport in Kristallen, Tunnelprozesse in Metallen oder Gläsern und Elektronentransferprozesse wie in der Photosynthese. Die theoretische Formulierung dieser Systeme wurde daher schon eingehend studiert [1, 2]. Basierend auf den daraus erworbenen Erkenntnissen werden wir in dieser Arbeit zwei verschiedene Methoden benutzen, um zwei gekoppelte Spins mit dissipativer Umgebung zu untersuchen.

Die erste Methode basiert auf dem Pfadintegralformalismus und einer perturbativen Entwicklung des Tunnelmatrixelements zwischen den zwei möglichen Zuständen. Der Pfadintegralformalismus für dissipative Quantensysteme wurde bereits 1963 von Feynman und Vernon entwickelt. Hier wird jeder mögliche Pfad (Propagator) von einem festen Anfangszustand zu einem festen Endzustand durch einen Phasenfaktor gewichtet. Pfade, die von dem klassischen Pfad abweichen, tendieren zur Interferenz. Ist die Wirkung im Vergleich zu $\hbar$ groß, so tragen am Ende nur Pfade mit einer Wirkung in einem (schmalen) Kanal der Größenordnung $\hbar$ um den klassischen Pfad effektiv bei. Ist die Wirkung jedoch von derselben Größenordnung wie $\hbar$, so liefern auch entferntere Pfade einen Beitrag. Die Beschreibung von Spins vereinfacht die Benutzung des Pfadintegralformalismus, da die Anzahl der möglichen Anfangs- und Endzustände begrenzt ist (2^{2N} für N gekoppelte Spins).

Bloch und Redfield entwickelten die hier verwendete zweite Methode, welche perturbativ den Einfluss der Umgebung berücksichtigt. Aufgrund dieser Vorgehensweise liefert sie nur für kleine Temperaturen und schwacher Kopplung an die Umgebung ein richtiges Ergebnis. Dieser Bereich wird von Ein–Boson Austausch–Prozessen zwischen System und bosonischem Wärmebad dominiert. Die Bloch–Redfield–Methode beschreibt die Zeitentwicklung der reduzierten Dichtematrix mittels einer generalisierten Mastergleichung. Die reduzierte Dichtematrix beschreibt dabei die effektive Dichtematrix des Systems unter der Wirkung des Bades. Der Einfluss der dissipativen Umgebung auf die Übergangsmatrixelemente wird im so genannten Redfield–Tensor zusammengefasst. Dieser wächst schnell mit der Anzahl Spins an, genauer gesagt mit 2^{4N} für N gekoppelte Spins. Dies erschwert die Benutzung dieser Methode für $N \geq 3$ deutlich. Allerdings zeigt es sich, dass im Allgemeinen der Redfield–Tensor nur spärlich besetzt ist. Aus diesem Grund können relevante numerische Ergebnisse für einigermaßen großes N erzielt werden.

Wir leiten in dieser Arbeit die Dynamik zweier gekoppelter Spins von kleinen Temperaturen und schwacher Kopplung an ein bosonisches Wärmebad bis zu hohen Temperaturen und/oder starker Kopplung an ein bosonisches Wärmebad her. Nach einer Einführung in das Thema, wird in Kapitel 2 zunächst für hohe Temperaturen und für einen Spin ein Lösungsweg mittels der Pfadsummenmethode entwickelt, der alle möglichen Pfade einschließt und annimmt, dass die Umgebung das System nur beeinflusst, wenn dieses sich in einem klassisch nicht möglichen Kohärenzzustand befindet. Die hohe Temperatur hat zur Folge, dass wir uns zunächst im sogenannten Markov–Regime befinden, in welchem Gedächtniseffekte des Bades vernachlässigbar sind. Dies erlaubt uns die gekoppelten Bewegungsgleichungen des Systems iterativ zu lösen und wir erhalten dadurch

einen detaillierten Einblick in die interne Dynamik des Spins. Im Markov–Regime wird die Wechselwirkung zwischen System und Bad durch Multi–Boson Austausch–Prozesse beliebiger Ordnung beschrieben. Geht man über zu kleineren Temperaturen, so führt die Markov–Annahme zu einer fehlerhaften Dynamik und Gedächtniseffekte des Bades sind nicht mehr vernachlässigbar. Stattdessen berücksichtigten wir nun Badkorrelationen in erster Ordnung. Diese Korrelationen beschreiben Ein–Boson Austausch–Prozesse zwischen System und Wärmebad. Hier zeigt sich eine Übereinstimmung mit der perturbativen Bloch–Redfield–Methode, die nur für Ein–Boson Austausch–Prozesse, d.h. für kleine Temperaturen und schwacher Kopplung ans Wärmebad, gültig ist.

Bevor wir auf die Bloch–Redfield–Methode eingehen, führen wir in Kapitel 3 für zwei gekoppelte Spins zunächst eine iterative Behandlung der Systemdynamik mit Hilfe der Pfadsummenmethode durch. Zunächst führen wir eine Ising–Kopplung zwischen den Spins ein, um dann im Markov–Regime die Dynamik des Spins zu berechnen (Abschnitt 3.1–3.3). Anschließend untersuchen wir verschiedene Parameterbereiche, wie die Ein–Boson–Korrektur und die Grenzfälle großer Spin–Spin Kopplung und/oder hoher Temperatur (Abschnitt 3.4–3.5).

Wir behandeln in Abschnitt 3.6 verschiedene Linearkombinationen longitudinaler und transversaler Kopplungsarten der Spins, wie z.B. die XY–, YZ– und Heisenbergkopplung. Ferner führen wir einen möglichen Bias ein, welcher die Entartung der lokalisierten Zustände, wie z.B. Spin–Up und Spin–Down, bei verschwindendem Tunnelmatrixelement aufhebt. Es zeigt sich, dass eine analytische Lösung, welche alle Kopplungsarten und Bias beinhaltet, nicht möglich ist.

Insbesondere die YZ–Kopplung zeigt einen neuartigen Effekt, bei dem man eine Verringerung der Dekohärenz erhält, sobald bestimmte Eigenfrequenzen des Systems entarten. Wir erhalten zwei Grundzustände mit derselben Energie, welche sich aber gegenseitig ausschließen. Dies führt zu einer *Frustration der Dekohärenz*, d.h. zu verlängerten Dephasierungs– und Relaxationszeiten (Abschnitt 3.7). Eine Untersuchung der sogenannten Purity, welche ein Maß für die Reinheit eines quantenmechanischen Zustands darstellt, bestätigt diesen Effekt (Abschnitt 3.8).

Von allgemein hohem Interesse ist ein System, in welchem ein Spin σ mit einem Spin τ wechselwirkt, wobei letzterer an ein bosonisches Bad gekoppelt ist. Der τ–Spin wirkt auf den σ–Spin als ein resonantes nicht–lineares Wärmebad. Im physikalischen Sinne repräsentiert er eine bistabile Störstelle, welche auf den σ–Spin einwirkt. Die Parametermittelung von vielen Störstellen führt letztendlich zu $1/f$–Rauschen. Dieses stellt für kleine Temperaturen die dominierende Quelle für Dekohärenz in Festkörpern dar und ist daher von besonderer Bedeutung. Dies wird in Abschnitt 3.9 beschrieben. Interessant ist hierbei der Fall hoher Temperatur. Dabei befindet sich σ in einem Kondo–artigen Zustand, jedoch mit dominierenden kohärenten Beiträgen.

Ein Vergleich mit früheren Resultaten, welche von Dubé und Stamp berechnet wurden und im Wesentlichen nur für große Temperaturen gültig sind, findet sich im Abschnitt 3.10. Wie erwartet, zeigen sich für mittlere Temperaturen deutliche Abweichungen von den neu abgeleiteten Ergebnissen. Dies verdeutlicht, dass die hier gemachten Erweiterungen und gefundenen Resultate von praktischer Relevanz sind und eine qualitative und quantitative Verbesserung darstellen.

Im Kapitel 4 wird die perturbative Bloch–Redfield–Methode behandelt. Nach einer allgemeinen Einführung in Abschnitt 4.1, wenden wir im Folgenden Abschnitt 4.2 die Methode auf einen einzelnen Spin an. Danach behandeln wir auf diese Art zwei auf Ising–Art gekoppelte Spins in Abschnitt 4.3. Insbesondere sind hier Terme zu erwähnen, die zusätzlich zur üblichen Säkularnäherung notwendig sind, um eine korrekte Beschreibung der Systemdynamik zu erhalten. Diese Terme ergeben sich aus zufälligen Entartungen des Energiespektrums. Es zeigt sich, dass in einem mittleren Temperaturbereich die Bloch–Redfield Ergebnisse mit den Ein–Boson Resultaten der Pfadsummenmethode exakt übereinstimmen. Die Prozedur wird in Abschnitt 4.4 für zwei auf YZ–Art gekoppelte Spins wiederholt. Auch hier stimmen die Resultate mit den entsprechenden der Pfadsummenmethode überein. Abschließend untersuchen wir in Abschnitt 4.5 die Frustration der Dekohärenz mit der Bloch–Redfield–Methode. Minimale Dämpfungsraten finden sich auch hier, sobald bestimmte Eigenwerte entarten, wieder.

Die vorliegende Arbeit schließt erstmals analytisch die Lücke zwischen perturbativen Ergebnissen der Bloch–Redfield–Methode für kleine Temperaturen und Pfadsummen–Ergebnissen für große Temperaturen im Markov–Regime. Die exakte Übereinstimmung der Ergebnisse, die mit Bloch–Redfield und Pfadsummenmethoden berechnet wurden, ist deswegen interessant, da die zwei Methoden auf unterschiedlichen Vorgehensweisen basieren und deshalb keineswegs zwingend identische Resultate liefern müssen. So beginnt die Bloch–Redfield–Methode mit einer perturbativen Entwicklung der System–Bad–Kopplung, während die Pfadsummenmethode auf einer Entwicklung des Tunnelmatrixelements beruht. Andererseits unterscheiden sich die beiden Methoden nur unwesentlich in den benutzten Vereinfachungen. So benutzen beide die Markov–Annahme, es wird angenommen, dass die Dichtematrix von System und Bad separierbar ist und beide vernachlässigen Effekte die auf einer kleinen Zeitskala ablaufen. Die Übereinstimmung der beiden Methoden ermöglicht es, zwei gekoppelte Spins mit schwacher Badankopplung für alle Temperaturen adäquat zu beschreiben.

Abstract

In this thesis, a scheme for calculating the dynamics of two coupled dissipative spins is developed, where each of the spins is coupled to its own boson bath. We derive analytic path sum results both in the Markov-regime and in the one-boson exchange regime. The analysis is also performed with the Bloch-Redfield method. It is shown that the two different approaches lead to identical results for the dynamics. This is not obvious a priori because both methods are based on different procedures.

The path sum method gives detailed insight into the internal dynamics of two coupled spins because we consider every path sequence that contributes to the time evolution.

While most studies of coupled spins are restricted to one type of coupling, e.g., Ising type, we will generalize here to linear combinations of possible couplings. Especially interesting is the occurrence of a frustration of decoherence, if the spins are interacting via a linear combination of longitudinal and transverse coupling and, when in addition, some of the eigenfrequencies become degenerate. Our analysis shows that degenerate but mutual exclusive ground states lead to increased coherence times. Maximization of coherence is one of the crucial goals of quantum state engineering.

Another topic of interest is the impact of non-linear quantum environments, formed by surrounding dissipative spins. A distribution of bistable background charges is known to be responsible for $1/f$ noise in solid state devices, like the superconducting quantum interference devices. Since $1/f$ noise is seemingly the dominating source of decoherence at very low temperature, there is a profound theoretical interest in modeling it. Therefore, we analyze two interacting spins, where one of them is coupled to a boson bath and thereby represents a resonant non-linear quantum environment. We study the crossover from a non-linear to a linear bath and study the corresponding time scale for the relevant bath correlations. Interestingly, for large and increasing temperature we find a decreasing decoherence for the central spin.

1 Introduction

Although quantum dissipative systems have been studied intensely since the 1980's [1, 2] there are still many open topics that allow for a deeper theoretical and experimental understanding. There is even an increasing interest in the theoretical description of such systems as the possibility to produce small devices which show quantum effects has reached everyday life, like giant magnetoresistance [3], or is on its way to do so, like quantum computation. This nanoscience can be found in different areas as nanobiology, nanochemistry, nanoelectronics, and nanomagnetism [4]. A topic of special interest is the quantum computer [5, 6, 7, 8, 9]. Its value would not be restricted to pure number factoring but it could also be used as a quantum simulator, for example to simulate chemical dynamics [10, 11].

Apart from everyday life, there is also a pure theoretical motivation to study quantum dissipative systems. We can study on the one hand quantum mechanics on a macroscopic scale and on the other hand test quantum mechanics itself, e.g., with quantum state engineering [12]. In addition, we can study details of the measurement process. Furthermore, we can examine the transition from quantum to classical physics and may ask at which point in the parameter space the transition occurs, or if a continuous transition from quantum to classical was more realistic. It is certainly very challenging, if not impossible, to completely isolate a quantum system of its environment. Particularly the measurement apparatus itself acts like an environment for the quantum system. A continuous measurement of the system by its environment is therefore an intrinsic feature of any quantum system. This leads to a continuously decohering quantum system [13, 14] and a non-abrupt emergence of classical states. A further point is the concept of wave-function collapse, which is in contradiction with the superposition principle and the unitarity of quantum dynamics. But as was shown recently, the wave-function collapse is made obsolete by decoherence [15].

The description of quantum dynamics is complicated by the inevitable coupling to environmental modes [16]. We will discriminate two sources of decoherence [17, 18]: first, the localized modes, such as nuclear and paramagnetic spins and defects. They dominate at low temperature. Second, the delocalized modes, such as electrons, phonons, etc. The localized modes might be a collection of bistable impurities leading to $1/f$-noise. These could be for example background-charge-fluctuators or two-level-fluctuators, residing in the neighborhood of a solid state device [19, 20, 21, 22]. In the literature, a bath of bistable impurities is also referred to as a spin-bath. It is shown in Ref. [22] that an ensemble of two-level fluctuators with degenerate level splitting is equivalent to a single two-level fluctuator with renormalized, stronger coupling strength. Thus, the study of a single localized mode already reveals the basic physics of a whole ensemble.

A setup in which both sources of decoherence are involved consists of two coupled spins

where only one of them is coupled to a boson bath. This can be considered as a dissipative bistable impurity acting on the other spin as environment. In the literature, this setup is known as a spin-boson environment (SBE) [23, 24, 25]. An interesting feature of the SBE is the possibility to study the transition from Gaussian to non-Gaussian behavior [24, 26, 27, 28]. Non-Gaussian behavior is characterized by the possibility of the system to resolve dynamics of the environment. The Markov approximation is no longer valid and therefore the standard master equation approach fails for such systems. We have to apply more sophisticated methods like the influence functional method [1, 2].

Of special importance are parameter regimes with minimal influence of the environment. There are so-called *sweet-spots* where coupling to off-diagonal states is zero in first order. Since the environment acts primarily on the system while being off-diagonal we have minimized dissipation. Another way to minimize dissipation is to use the so-called frustration of decoherence phenomenon [29, 30]. Here, non-commutative properties of the Hamiltonian are utilized. These might be different environments coupled to two non-commuting variables of the system or two non-commuting variables of the system itself, leading to equally preferred but mutually exclusive ground states. Yet another way is to tune the energy level splitting of the system to a value near to the variance of the stochastic fluctuations of the environment and thereby introduce a stochastic resonance between the involved states [31].

There are several proposals for the realization of qubits: entangled ions [32], nanomagnets [4], fullerenes [33], nitrogen-vacancy (NV) centers [34, 35], nuclei in nuclear magnetic resonance (NMR) [36], photons [37], atomic impurities and quantum dots [38, 35]. NV centers show quantum coherent dynamics even at room temperature. An advanced realization for quantum dissipative systems are Josephson junctions [12, 39, 40, 41, 42, 43, 44, 45]. Compared to other possible realizations of qubits, they share an advantage with the quantum dots; they can be embedded into existing micro-electronic circuits. And once implemented, it should be possible to scale them up to large numbers of qubits. This is important because, for example, to directly factorize a n-bit number we need more than $2n$ qubits. Current RSA (R. L. Rivest, A. Shamir, and L. Adleman) encryption keys are typically $1024 - 2048$ bits long [46, 47].

A single Josephson junction consists of two superconductors, which are separated by a small insulating tunnel junction. Cooper-pair charges that tunnel through the junction constitute the Josephson current. The number of Cooper-pairs is controlled via a gate voltage, as shown in Fig. 1.1. Two Josephson junctions are easily connected either capacitively or inductively, allowing for example an Ising-type coupling [41]. It is remarkable that these superconducting qubits can be implemented in such a way that strong coupling and no coupling can be controlled locally by electronic means.

Reversely, we can use Josephson junctions as a spectrum analyzer or probe for the noise of the environment [48, 49, 50]. A significant contribution of $1/f$-noise for low temperature is observed, leading on the one hand to the demand of enhancing theoretical descriptions of dissipative systems to include a spin-bath at low temperature. On the other hand, experimental enhancements that suppress low-frequency noise have been developed such as the transmon and quantronium, which are smart variations of Josephson junction

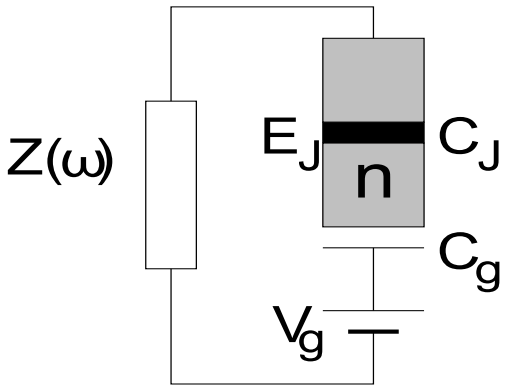

Figure 1.1: Single Josephson junction formed by a superconducting charge box with n excess Cooper pair charges. The environment is characterized by the impedance $Z(\omega)$. The tunnel junction has capacitance C_J and Josephson coupling energy E_J. Its typical thickness is about 2-3 nm and Cooper pairs can tunnel the barrier coherently. A gate capacitor C_g is connected to tune the system via the voltage V_g. The single-electron charging energy $e^2/2(C_g + C_J)$ has to be much larger than the thermal energy. For a temperature of 1K, we need $(C_g + C_J)$ to be much less than 1fF. Figure is taken from [12].

qubits [51, 52].

1.1 Theoretical perspective

A basic and fertile theoretical model for the description of spin systems is the two-state system (TSS), which may be thought of as a quartic potential with two energy minima at comparable energies. At low temperature only the ground states of the two minima will be relevant and we obtain an effective TSS. A possible bias lifts the degeneracy of the ground states in the absence of tunneling. The two ground states are coupled quantum mechanically via a tunneling matrix element. In a realistic scenario we also have a dissipative environment acting on the TSS, which is due to the inevitable coupling to environmental modes. The TSS plus a bosonic environment is represented by the thoroughly studied *spin-boson model*. Although it is the simplest quantum dissipative system that shows quantum interference effects, it is a very useful model for different situations. These include defect motion in crystals, tunneling of light particles in metals, glasses or amorphous metals, and electron transfer processes as in photosynthesis [2]. There are still some new developments and extensions in recent years, like the weakly interacting blip approximation in [53, 54] and the already mentioned studies of the SBE [23, 24, 25].

There are several theoretical tools to describe the spin-boson model. Two of them are the influence-functional technique based on path sums [1, 2] and the perturbative Bloch-Redfield method [55]. A comparison of the Bloch-Redfield and path sum approach can be found for example in [56, 57]. Their common goal is to describe the dynamics of the reduced density matrix (RDM). The RDM contains all information concerning the

time evolution of the system under the influence of the bath. It is called reduced density matrix because the trace with respect to the bath is performed. All physical information about measurements of the system is captured by the RDM.

The path integral method for quantum dissipative systems was introduced by Feynman and Vernon [58] in 1963. Every possible propagator from a fixed initial state to a fixed end state is weighted by an amplitude. An integration over all paths leads to a cancellation of neighboring paths which have large phases. In a semi-classical approximation, where the action is much larger than $\hbar$, only paths near the classical path significantly contribute to the overall propagator. If the action is of the order of $\hbar$ also paths contribute that are not near the classical path. For the two simplest physical model systems, the free particle and the harmonic oscillator, only the classical path is relevant and the propagator is readily calculated. Unfortunately, the method becomes rapidly difficult for other models, e.g., if we include a dissipative environment via the Feynman-Vernon influence functional method [58]. The description of one or more spins eases the use of path integrals because there are only *few* possible states (4 for a single spin, 16 for two coupled spins, 2^{2N} for N coupled spins). It is possible to derive a formally exact description of the system dynamics under the influence of the bath. However, its solution is often restricted to special parameter regimes, or numerical techniques.

The Bloch-Redfield approach is a perturbative theory; it can be used for small bath influences only. It describes the time evolution of the reduced density matrix (RDM) via a generalized master equation. The dissipative environment is specified via the Redfield-tensor. Since it links all matrix elements of the RDM, it grows quickly with the number of spins, i.e., like 2^{4N} for N coupled spins. Fortunately, many of the tensor elements are zero, and therefore reliable results are commonly obtained with suitable computer software.

A theoretical analysis of two coupled spins with an Ising-type coupling and based on path sum methods was first given in [59]. But, crude approximations were made in which all inter- and intrablip correlations, where both spins are involved, are disregarded (see Section 3.10). The parameter regime may be divided in three main areas:

1. a perturbative regime, in which the coupling between the spins can be treated perturbatively
2. a so-called locked phase regime, in which the spin-spin coupling is dominant so that the two spins are locked together and can be treated as a single spin with effective frequency coupled to a heat bath
3. a strong coupling regime, in which we have strong spin-spin coupling and either high temperature or small coupling to the bath. In this case, all interblip correlations for each spin and between the spins can safely be neglected. Furthermore, path sequences in which both spins are off-diagonal at the same time interval can be disregarded.

So, unless we deal with the perturbative regime, the results derived in [59] are limited to either large spin-spin coupling and high temperature or small coupling to the bath.

We shall derive in this work an exact solution for two coupled spins in the Markov-regime, where each spin is coupled to its own boson bath. For low temperature and small bath coupling we will solve the relevant Bloch-Redfield equations. They are well suited for this regime because they are based on a perturbative approach [60, 61]. Increasing temperature decreases the validity of the Bloch-Redfield method. Then, the Feynman-Vernon influence-functional method becomes more adequate [1, 2]. The influence-functional method leads to exact results in the Markov limit, regardless of the mutual coupling strength [59]. The Markov-regime is already valid for temperatures of the order of or larger than the system energies. For lower temperature, inter- and intrablip correlations become important and the Markov-results will not render anymore a correct description of the system dynamics. For weak coupling to the bath, one-boson exchange processes between system and bath are dominating. We shall derive exact expressions for the system's dynamics this regime.

The results will be derived for the case of two independent boson baths for the two spins. Large deviations for the cases of interacting baths or one single bath are not expected. This is true as long as the two spins are spatially separated in such a way that retardation effects can be neglected. In other words, we assume that there are no direct bath-mediated correlations between the two spins. As an estimation, this requires the two spins to be separated more than 50 μm for an ohmic electron bath. However, smaller separation leads only to a renormalization of the spin-spin coupling strength [59]. Therefore, the results should be valid for a single boson bath and for independent boson baths, too.

The next step would be to apply the methods developed in this thesis for the description of N spins. Experiments are already feasible, e.g., 8 entangled ions in [32], 12 magnetic nuclei with NMR in [36], 6 photons in [37]. But, since the Hilbert space of the system is growing with 2^N, a straightforward application of the new developed methods seems unpromising [62]. Nevertheless, numerical and/or approximative variants should be applicable for larger numbers of coupled spins.

1.2 Experimental perspective: qubits

The physical realization of a qubit has attracted a lot of different proposals in many areas of physics [63]. This is possible because a qubit is based on a two-state system (TSS) and a TSS can be found in almost every branch of quantum physics.
One example is an electron in a quantum dot, where the spin of the electron couples to an external magnetic field. The Hamiltonian is then given by (we put $\hbar = 1$)

$$H = -\frac{\gamma}{2}\,\vec{\sigma}\,\vec{B}, \tag{1.2.1}$$

with the gyromagnetic ratio γ, the Pauli matrices[1] $\vec{\sigma} = (\sigma_x, \sigma_y, \sigma_z)$ describing the spin of the electron, and the external magnetic field $\vec{B}$. Choosing the magnetic field to be parallel to the z-axis, $\vec{B} = B_z\,\hat{z}$, we obtain a TSS with Hamiltonian

$$H = -\frac{\gamma}{2}\,\sigma_z\,B_z \tag{1.2.2}$$

and eigenvalue equations

$$H\,|R\rangle = -\frac{\epsilon}{2}\,|R\rangle\;, \qquad H\,|L\rangle = \frac{\epsilon}{2}\,|L\rangle. \tag{1.2.3}$$

Here, we have defined the bias frequency $\epsilon = \gamma\,B_z$. The state vectors $|R\rangle$ and $|L\rangle$ are chosen such that they are eigenstates of σ_z, i.e., $\sigma_z\,|R\rangle = +\,|R\rangle$ and $\sigma_z\,|L\rangle = -\,|L\rangle$. Further, we can apply a magnetic field along the x-axis to induce tunneling between the two eigenstates of σ_z with frequency $\Delta = \gamma\,B_x$. Then we obtain the generic Hamiltonian of a TSS

$$H = -\frac{\Delta}{2}\,\sigma_x - \frac{\epsilon}{2}\,\sigma_z. \tag{1.2.4}$$

Other devices are SQUIDS, which are based on Josephson junctions [12, 45]. These are promising candidates for quantum state engineering, e.g., quantum oscillations in two coupled Josephson junction qubits were observed in [41]. There exist two basic types of Josephson qubits depending on the parameter regime. The first is based on a charge degree of freedom and is therefore called *charge qubit*, where charge refers to the number of Cooper pairs on an island. The second is based on a flux (phase) degree of freedom and is called *flux qubit*. Here, a superconducting ring is interrupted by a number of Josephson junctions. Additionally, the ring is traversed by a magnetic flux. Josephson junctions that exploit special working parameters as the transmon or the quantronium are, for example, described in [51, 52].

The size of Josephson junctions ranges between $0.1 \times 0.1\mu\text{m}^2$ for charge qubits and $1 \times 1\mu\text{m}^2$ for phase qubits. Charge qubits are patterned using shadow evaporation and electron-beam lithography, while phase qubits are patterned photolithographically. Usually, $\text{Al}-\text{Al}_\text{x}\text{O}_\text{y}-\text{Al}$ compounds are used for the fabrication. The relevant qubit frequencies are between 5 and 10 GHz ($\sim 0.25 - 0.5$ K), which necessitates the use of dilution refrigerators ($10 - 30$ mK) to minimize thermal population of the upper state. Cooling is indispensable to minimize decoherence, too. And, cooling leads to unexpected techniques like Sisyphus cooling and amplification of a LC-resonator [64, 65].

For a *charge qubit*, the tunable Josephson energy and the charging energy, i.e.,

$$\Delta = E_J(\Phi_x) \qquad \text{and} \qquad E_C = \frac{e^2}{2(C_g + C_J)}\;, \tag{1.2.5}$$

[1] We use the representation $\sigma_x = \begin{pmatrix} 0 & 1 \\ 1 & 0 \end{pmatrix}$, $\sigma_y = \begin{pmatrix} 0 & -\mathrm{i} \\ \mathrm{i} & 0 \end{pmatrix}$ and $\sigma_z = \begin{pmatrix} 1 & 0 \\ 0 & -1 \end{pmatrix}$.

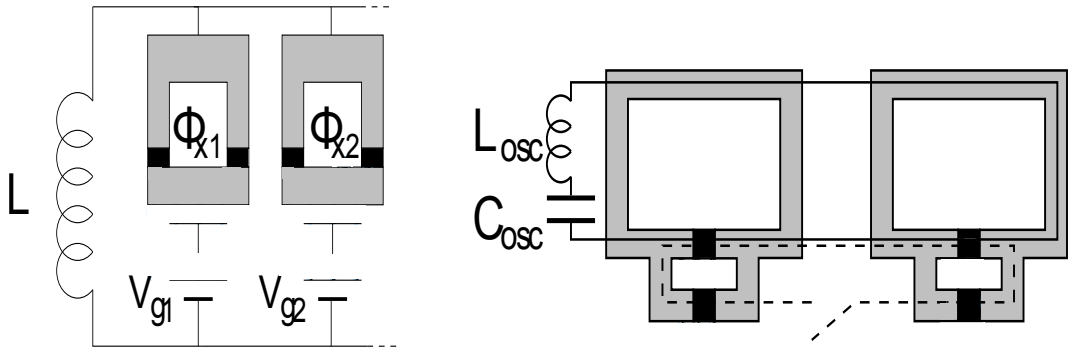

Figure 1.2: Left: coupled charge qubits with coupling $\propto \sigma_y \tau_y$. Right: coupled flux qubits, either inductively (dashed line) or with a LC-circuit (solid line). Here, the coupling is $\propto \sigma_x \tau_x$ and $\propto \sigma_z \tau_z$. The superconducting areas are light gray and the tunnel junctions are black. Figures are taken from [12].

are the two relevant energy scales describing the system. C_J and C_g are the tunnel junction capacitance and gate capacitance, respectively, and e is the elementary charge (see Figs. 1.1 and 1.2). The loop is threaded by a magnetic flux Φ_x. The Hamiltonian reads

$$H = 4E_C(n - n_g)^2 - E_J \cos\Theta \,, \tag{1.2.6}$$

where n is the number operator of Cooper pair charges on the island and Θ is the phase of the superconducting order parameter of the island. Number and phase operator are canonically conjugate $n = -\mathrm{i}\partial/\partial\Theta$. The effect of the gate voltage is captured by $n_g = C_g V_g/(2\,e)$.

If we choose $\Delta_s \gg E_C \gg E_J \gg k_B T$, where Δ_s is a superconducting gap, only Cooper pairs will tunnel through the junction and the number n of Cooper pairs is a well-defined basis. Further, choosing n_g close to a half-integer, only charge states with $n = 0, 1$ remain relevant. Higher charge states have much larger energy and can be ignored. The level splitting, which is now controlled by the gate voltage, reads

$$\epsilon = 4\,E_C\,(1 - 2\,n_g) \,. \tag{1.2.7}$$

For the tunable Josephson energy we obtain

$$\Delta = 2\,E_J\,\cos(\pi\,\Phi_x/\Phi_0) \,, \tag{1.2.8}$$

with the flux quantum $\Phi_0 = h/(2\,e)$. Hence, the system reduces to a TSS and is described by the Hamiltonian of Eq. (1.2.4). A coupling between charge qubits is realized either inductively or capacitively with $H_{\rm int} \propto \sigma_y\tau_y$ or $H_{\rm int} \propto \sigma_z\tau_z$ [12]. An example is shown in Fig. 1.2.

The *flux qubit* is based on the regime $E_J \gg E_C$, where the flux gives a well-defined basis. Flux qubits are also called persistent current qubits. Its Hamiltonian is given by

$$H = -E_{\rm J} \cos\left(2\pi\frac{\Phi}{\Phi_0}\right) + \frac{(\Phi - \Phi_x)^2}{2\,L} + \frac{Q^2}{2\,C_{\rm J}} \,, \tag{1.2.9}$$

where Φ is a flux traversing the loop in multiples of the flux quantum Φ_0 and Φ_x is an applied bias. L is the self-inductance of the loop. The charge Q is canonically conjugate to the flux Φ, i.e., $Q = -\mathrm{i}\partial/\partial\Phi$. For large enough self-inductance ($\beta_\mathrm{L} \equiv E_\mathrm{J}/(\Phi_0^2/4\pi^2 L) \gg 1$) and Φ_x close to $\Phi_0/2$ the Hamiltonian describes a double-well potential near $\Phi = \Phi_0/2$. If additionally temperature is low enough, only the two lowest lying states will be relevant and the resulting TSS is again described by the Hamiltonian of Eq. (1.2.4). An example is shown in Fig. 1.2.

Especially important quantities are the relaxation time T_1 and the dephasing time T_2. A running quantum computer/simulator needs to perform many operations, while the qubit is coherent. Thus we need large $T_{1,2}$. These are two of the main quantities that will be considered and calculated in this thesis. The relaxation time is the time required to relax from the excited state to the ground state by dissipating energy into the environment. The dephasing time is the timescale, where phase correlations between the eigenstates become randomized. Both are due to the coupling to the environment and the goal is to maximize them. This can be done for example by a clever design as in the transmon or quantronium and/or by cooling to lower temperature.

The relaxation time T_1 can be measured by irradiating the qubit with microwaves of frequency Δ for a period much longer than T_1. After turning off the pulse, the probability of being in the excited state is measured, which decays exponentially with $\exp(-t/T_1)$.

To observe Rabi oscillations, which are characteristic for a TSS, the qubit is again irradiated with microwaves of frequency Δ for a time τ and the magnetic field component is aligned along the y-axis. As long as the pulse is applied, the state vector rotates in the y-z plane. A subsequent measurement of the qubit state shows Rabi oscillations as a function of τ. Rabi oscillations confirm that we deal with a TSS and are used to calibrate the microwave field.

And finally, Ramsey fringes and the spin-echo technique are used to determine the dephasing time. Here, we have to differ the intrinsic dephasing time of a single qubit T_2 and the observed dephasing time $T_2^* < T_2$, which is an ensemble average. We deal with an ensemble because we have to rerun the measurement many times in order to obtain precise data. But fluctuations on the timescale of a single measurement, i.e., low-frequency noise, lead to deviations between different measurements. Ramsey fringes are measured by applying two $\pi/2$ microwave pulses at frequency f_m, where the second is delayed by τ_d. The first pulse rotates the Bloch vector into the x-y plane, where it precesses around a static magnetic field. Due to dephasing, the magnitude decreases. Then, the second $\pi/2$ pulse is applied. A subsequent measurement of the qubit gives either a projection to $|0\rangle$ or $|1\rangle$. By plotting the switching probability versus the delay time τ_d, we obtain the free evolution of the qubit. If f_m matches Δ, we observe coherent oscillations that decay with $\exp(-t/T_2^*)$. To circumvent dephasing due to low-frequency noise, the spin-echo technique can be used. We only have to apply a π-pulse in the middle of the two $\pi/2$ pulses. A fluctuation that induced a phase delay will now advance the phase and vice versa. Fluctuations on a timescale well below the measurement time become irrelevant. Thus, we can measure T_2.

These are only the basic measurement protocols and many other sophisticated methods have been developed since the invention of nuclear magnetic resonance.

1.3 Outline of the thesis

In Chapter 2 we discuss the path sum method for the TSS, where the environment is in the Markov-regime. Interblip interactions cancel out exactly in this regime, so that the well-studied noninteracting-blip approximation (NIBA) becomes exact. As a result, the influence functional takes a convolutive form so that the dynamics can be solved by Laplace transformation. After a discussion of the resulting dynamics, we expand our results to the quantum-noise regime, where we include interblip correlations to first order in the coupling strength. This regime is dominated by one-boson exchange contributions between system and bath. Higher order exchange contributions may be neglected.

The newly developed methods of Chapter 2 are applied to two coupled spins in Chapter 3. First, we concentrate on Ising coupling of the spins and derive path sum results within the Markov-regime in the Sections 3.1 – 3.3. For this purpose, a detailed analysis of all spin paths is performed. Afterwards, we examine and discuss different regimes, including the one-boson exchange regime, and the large spin-spin coupling and/or high temperature regime in Sections 3.4 and 3.5. An analytic solution including all spin-spin coupling types and a bias of the spins energy states, is not possible. But, we show in Section 3.6 which coupling and bias types are accessible in analytic form. Of course, approximative solutions are always possible.

Following that, we study several features of two coupled spins in Sections 3.6 – 3.10. We explore the case of linear combinations of longitudinal and transverse spin-spin coupling and especially simultaneous YZ spin-spin coupling in Section 3.6. If some of the systems eigenfrequencies become degenerate, it turns out that there are two equally preferred ground states, which are mutually exclusive. Thereupon, a noticeable decrease of decoherence occurs. This effect was dubbed *frustration of decoherence* for a similar case in [29] and is studied in Section 3.7. We examine in the subsequent Section 3.8 the purity, which measures how pure or mixed a quantum state is. The purity also shows a dip in its effective damping rate, if the corresponding eigenfrequencies become degenerate.

Especially interesting is a setup, where only one of the spins is coupled to a boson bath, leading to a non-linear environment for the other spin. Some previous work and newly found results are presented in Section 3.9. Surprisingly, if temperature is large enough, we find the spin without bath in a Kondo-like regime, but with dominating coherent contributions.

A comparison of the new results with previous results obtained by Dubé and Stamp in [59] is given in Section 3.10. As expected, we obtain an agreement in the high temperature regime, where Dubé and Stamp derived their results. But, the old results clearly deviate from the more precise new results for lower temperature. Thus, we have succeeded to generalize the analytic treatment of two coupled spins to lower temperatures.

The perturbative Bloch-Redfield method is introduced in Chapter 4. We begin with a general introduction in Section 4.1 and discuss afterwards the solution of a TSS in Section 4.2. Following that, we solve the relaxation equations for Ising coupling in Section 4.3 and YZ spin-spin coupling in Section 4.4. Due to degeneracies in the energy spectrum,

there are terms beyond the usual secular approximation, which cannot be neglected. Although the Bloch-Redfield and the path sum method are based on different assumptions and simplifications, we obtain a smooth crossover of both approaches for intermediate temperature. This closes the gap between low and high temperature. Finally, the frustration of decoherence is studied with Bloch-Redfield method in Section 4.5. Again, we find minimal damping rates, if the eigenfrequencies become degenerate.

The results of this thesis are derived with the Bloch-Redfield method, valid for low temperature, and with the path sum method, here used for high temperature. However, they smoothly match on each other at intermediate temperature. This is not obvious a priori. The Bloch-Redfield method is based on a perturbative expansion of the system-bath coupling, while the path sum method utilizes an expansion of the tunnel matrix element. On the other side, both methods differ only marginally in the applied simplifications. Both use the Markov-assumption, it is assumed that the density matrix of system and bath is separable, and both neglect any dynamics on a short time scale. It is now possible to adequately describe two interacting spins for all temperatures with the restriction that they are weakly coupled to a boson bath.

2 Path sum description of the dissipative two-state system

As was shortly discussed in the introduction, the dissipative two-state system (TSS) is a basic model for the theoretical study of the decoherence phenomenon [1, 2]. This is due to the simplicity and the comprehensible mathematics and physics involved in its solution. Here, we give an introduction to the solution of a TSS with the path sum method and briefly introduce the methods and procedures that will be applied later to the case of two coupled spins.

The TSS might be a double well potential at low temperature, such that only the ground state of each well is relevant. The two ground states are coupled via a tunneling matrix Δ, describing transitions between the wells. Additionally, we have a bias ϵ, making the two localized states non-degenerate in the absence of tunneling. We then obtain the genuine spin-boson Hamiltonian for a TSS with bath coupling

$$H = -\frac{\Delta}{2}\,\sigma_x - \frac{\epsilon}{2}\,\sigma_z - \frac{X}{2}\,\sigma_z + \sum_\alpha \omega_\alpha b_\alpha^\dagger b_\alpha \ , \tag{2.0.1}$$

where σ_x, σ_y and σ_z are the standard Pauli matrices. Here, we employ the representation, in which σ_z is diagonal. Then the eigenstates of σ_z with eigenvalue $+1$ (-1) are the localized states in the right (left) well. To model the boson environment we included in (2.0.1) the fluctuating forces

$$X(t) = \sum_\alpha c_\alpha \left[b_\alpha(t) + b_\alpha^\dagger(t)\right] \ , \tag{2.0.2}$$

which are coupled to σ_z and therefore result in a fluctuating bias. Here, $b^\dagger$ and b are creation and annihilation operators of the environmental bosons and c_α is the coupling strength of bath mode α to the TSS. The last term in the Hamiltonian (2.0.1) describes the energy of the environment. The fluctuating bias is zero on average, i.e., $\langle X(t)\rangle_\beta = 0$. Thereby, it does not provide a systematic force acting on the system. For a harmonic bath, all effects of the environmental coupling are captured by the force-force autocorrelation function $\langle X(t)X(0)\rangle_\beta$. It is convenient to use the power spectrum $S(\omega)$, which is the Fourier transform of the force-force autocorrelation function

$$S(\omega) = \mathrm{Re}\int_{-\infty}^{\infty} \mathrm{d}t\, \mathrm{e}^{\mathrm{i}\omega t}\langle X(t)X(0)\rangle_\beta = J_{\mathrm{lf}}(\omega)\coth(\beta\,\omega/2) \ . \tag{2.0.3}$$

We introduced on the rhs the spectral density $J_{\mathrm{lf}}(\omega)$ of the bath coupling. From now on, we restrict ourselves to an ohmic spectral density

$$J_{\mathrm{lf}}(\omega) = \sum_\alpha c_\alpha^2 \delta(\omega - \omega_\alpha) = 2K\omega\ \mathrm{e}^{-|\omega|/\omega_{\mathrm{c}}} \ , \tag{2.0.4}$$

where ω_c is a high-frequency cutoff and K is the usual dimensionless Kondo parameter, which characterizes the effective bath coupling.

2.1 Undamped two-state system

Before we start to analyze the dissipative TSS with the path sum method, we first state a few basic properties of the undamped system. The Hamiltonian for a single two-state system without coupling to an environment,

$$H = -\frac{\Delta}{2}\,\sigma_x - \frac{\epsilon}{2}\,\sigma_z\,, \tag{2.1.1}$$

can be rewritten in matrix notation as

$$H = \begin{pmatrix} -\epsilon/2 & -\Delta/2 \\ -\Delta/2 & \epsilon/2 \end{pmatrix}\,, \tag{2.1.2}$$

where the basis states $|R\rangle$ and $|L\rangle$ are eigenstates of σ_z with the eigenvalues ± 1. The Hamiltonian is diagonalized by the matrix

$$U = \begin{pmatrix} \cos(\Theta/2) & -\sin(\Theta/2) \\ \sin(\Theta/2) & \cos(\Theta/2) \end{pmatrix}\,, \tag{2.1.3}$$

with the mixing angles $\tan(\Theta) = -\Delta/\epsilon$. In the energy eigenbasis the Hamiltonian reads

$$\widetilde{H} = U\,H\,U^{-1} = -\frac{\Omega}{2}\,\sigma_z\,, \tag{2.1.4}$$

with the eigenfrequency $\Omega = \sqrt{\Delta^2 + \epsilon^2}$. The ground state $|g\rangle$ and excited state $|e\rangle$ in the energy basis are superpositions of the σ_z eigenstates,

$$|g\rangle = \cos(\Theta/2)\,|R\rangle - \sin(\Theta/2)\,|L\rangle\,, \qquad |e\rangle = \sin(\Theta/2)\,|R\rangle + \cos(\Theta/2)\,|L\rangle\,. \tag{2.1.5}$$

If we prepare our system in $|R\rangle$ at $t = 0$, the time evolution of $\langle\sigma_z(t)\rangle = |\langle R(t)|R\rangle|^2$ in the energy basis is readily calculated with

$$|R\rangle = \cos(\Theta/2)\,|g\rangle + \sin(\Theta/2)\,|e\rangle\,, \quad |L\rangle = -\sin(\Theta/2)\,|g\rangle + \cos(\Theta/2)\,|e\rangle\,, \tag{2.1.6}$$

and

$$|e(t)\rangle = \mathrm{e}^{-\mathrm{i}\,\frac{\Omega}{2}t}\,|e\rangle\,, \qquad |g(t)\rangle = \mathrm{e}^{\mathrm{i}\,\frac{\Omega}{2}t}\,|g\rangle\,. \tag{2.1.7}$$

We then get

$$\langle\sigma_z(t)\rangle = |\langle R(t)|R\rangle|^2 = \frac{\epsilon^2}{\Omega^2} + \frac{\Delta^2}{\Omega^2}\cos\Omega t\,. \tag{2.1.8}$$

Another important quantity is the thermal equilibrium state reached at long times. This is generally determined by the canonical state of the reduced density matrix, $\rho_{\mathrm{eq}} = \mathrm{e}^{-\beta H}$, and reads

$$\langle A\rangle_{\mathrm{eq}} \equiv \langle A(t\to\infty)\rangle = \frac{\mathrm{tr}(A\,\rho_{\mathrm{eq}})}{\mathrm{tr}(\rho_{\mathrm{eq}})} = \frac{\mathrm{tr}(A\,\mathrm{e}^{-\beta\,H})}{\mathrm{tr}(\mathrm{e}^{-\beta\,H})}\,, \tag{2.1.9}$$

where A stands for σ_z, σ_x, or σ_y, respectively. For example, the thermal equilibrium state of $\langle\sigma_z\rangle_{\rm eq}$ is found as

$$\langle\sigma_z\rangle_{\rm eq} = \frac{\epsilon}{\Omega}\tanh\left(\frac{\beta\,\Omega}{2}\right)\ . \tag{2.1.10}$$

It is convenient to solve the coupled equations of motion for a TSS in the Heisenberg picture, in which the time dependence of an operator formally is

$$A(t) = \mathrm{e}^{\mathrm{i}\,H\,t}\,A\,\mathrm{e}^{-\mathrm{i}\,H\,t}\ . \tag{2.1.11}$$

Hence, the time evolution of an operator is[1] given by

$$\frac{\mathrm{d}}{\mathrm{d}t}A(t) = \mathrm{i}[H,A(t)] = \mathrm{i}\,\mathrm{e}^{\mathrm{i}\,H\,t}\,[H,A]\,\mathrm{e}^{-\mathrm{i}\,H\,t}\ . \tag{2.1.12}$$

Here, $[\cdot,\cdot]$ is the usual commutator. In Laplace space[2], we then get three coupled equations

$$\begin{aligned}
\lambda\,\langle\sigma_z(\lambda)\rangle &= 1 - \Delta\,\langle\sigma_y(\lambda)\rangle\ ,\\
\lambda\,\langle\sigma_y(\lambda)\rangle &= \Delta\,\langle\sigma_z(\lambda)\rangle - \epsilon\langle\sigma_x(\lambda)\rangle\ ,\\
\lambda\,\langle\sigma_x(\lambda)\rangle &= \epsilon\langle\sigma_y(\lambda)\rangle\ .
\end{aligned} \tag{2.1.13}$$

Solving them for $\langle\sigma_z(\lambda)\rangle$ yields

$$\langle\sigma_z(\lambda)\rangle = \frac{1}{\lambda + \Delta\frac{1}{1+\frac{1}{\lambda}\epsilon\frac{1}{\lambda}\epsilon}\frac{1}{\lambda}\Delta} = \frac{1}{\lambda + \mathcal{K}^{(\mathrm{s})}_{\sigma_z}(\lambda)}\ , \tag{2.1.14}$$

where on the rhs the kernel $\mathcal{K}^{(\mathrm{s})}_{\sigma_z}(\lambda)$ was introduced. This kernel describes all (symmetric) irreducible transition sequences together with all possible bias phase factors included in the geometrical series $(1+\epsilon^2/\lambda^2)^{-1}$. Higher order transitions in Δ make a visit of at least one diagonal state at intermediate times and therefore are reducible contributions. Summing them up leads to a geometrical series for the kernel resulting in $\langle\sigma_z(\lambda)\rangle$. The time evolution of (2.1.14) is given by the inverse Laplace transform and coincides with (2.1.8).

2.2 Dissipative two-state system

Feynman and Vernon developed a method to include dissipative effects based on the path integral approach [58]. They introduced the so-called Feynman-Vernon influence

[1] Remember that the time evolution of the density matrix $\rho(t) = \sum_i p_i\,\mathrm{e}^{-\mathrm{i}\,Ht}\,|\alpha_i\rangle\langle\alpha_i|\,\mathrm{e}^{\mathrm{i}\,Ht}$ is governed by the von-Neumann equation, i.e., $\frac{\partial}{\partial t}\rho(t) = -\mathrm{i}[H,\rho(t)]$ (observe the minus sign).

[2] We define the Laplace transform as $f(\lambda) = \int_0^\infty \mathrm{d}t\exp(-\lambda t)f(t)$ and the corresponding inverse transform as $f(t) = (2\pi\,\mathrm{i})^{-1}\int_{-\mathrm{i}\,\infty+c}^{\mathrm{i}\,\infty+c}\mathrm{d}\lambda\exp(\lambda t)f(\lambda)$. The integration contour is the standard Bromwich contour and the constant $c\in\mathbb{R}$ is chosen such that all singularities are to the left of the integration path.

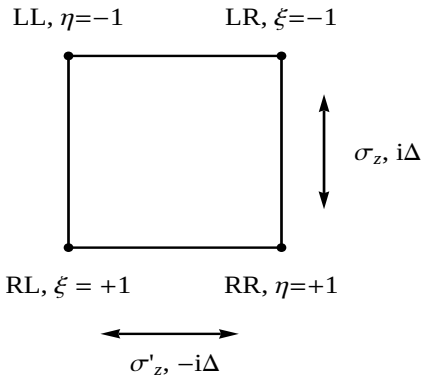

Figure 2.1: The four states of the density matrix and the possible paths for σ_z, σ'_z with the corresponding signs $-\,\mathrm{i}\,\Delta$ for $RL \leftrightarrow RR$ and $LL \leftrightarrow LR$, $+\,\mathrm{i}\,\Delta$ for $RR \leftrightarrow LR$ and $RL \leftrightarrow LL$.

functional to deal with the environmental effects on the system. We will follow the discussions and the reviews of [1, 2] for a two-state system. The reduced density matrix (RDM) for a TSS can be written as a double path sum in the form

$$\rho_{\sigma_\mathrm{f}\sigma'_\mathrm{f}}(t) = \int \mathcal{D}\sigma\mathcal{D}\sigma'\, \mathcal{A}[\sigma]\, \mathcal{A}^*[\sigma']\, \mathcal{F}[\sigma,\sigma'] \;, \tag{2.2.1}$$

where $\mathcal{A}[\sigma]$ is the bare amplitude of the system to follow the path $\sigma(t')$ without the environment and $\mathcal{F}[\sigma,\sigma']$ is the Feynman-Vernon influence functional that describes the environmental effects on the system. At time $t = 0$ we prepare the double paths $\sigma(t')$ and $\sigma'(t')$ in the $|R\rangle$ eigenstate. The final states σ_f and σ'_f at time t are one of the two diagonal states $|R\rangle$ or $|L\rangle$. It is useful to introduce the symmetric and antisymmetric paths

$$\xi(t') = \frac{1}{2}\left[\sigma(t') - \sigma'(t')\right] \qquad \text{and} \qquad \eta(t') = \frac{1}{2}\left[\sigma(t') + \sigma'(t')\right] \;. \tag{2.2.2}$$

Here, $\xi(t')$ is 0 (± 1), if we are on a diagonal (off-diagonal) state of the density matrix and likewise $\eta(t')$ is ± 1 (0), if we are on a diagonal (off-diagonal) state (cf. Fig. 2.1). The time spend in a diagonal state is called sojourn and the time spend in an off-diagonal state is named blip. With these paths the influence functional takes the form

$$\mathcal{F}[\xi,\eta] = \exp\left\{\int_0^t \mathrm{d}t' \int_0^{t'} \mathrm{d}t'' \left[\dot{\xi}(t')Q'(t'-t'')\dot{\xi}(t'') \;+\; \mathrm{i}\,\dot{\xi}(t')Q''(t'-t'')\dot{\eta}(t'')\right]\right\} \;. \tag{2.2.3}$$

$Q(t)$ is the second integral of the force autocorrelation function

$$\begin{aligned} Q(t) =\; & Q'(t) + \mathrm{i}\,Q''(t) \\ =\; & \int_0^\infty \mathrm{d}\omega\, \frac{J_\mathrm{lf}(\omega)}{\omega^2}\left[\coth(\beta\omega/2)(1-\cos(\omega t)) + \mathrm{i}\sin(\omega t)\right] \\ =\; & 2K\left[\ln\left(\frac{\beta\omega_\mathrm{c}}{\pi}\right) + \ln\sinh\left(\frac{\pi|t|}{\beta}\right)\right] + \mathrm{i}\,\pi K\,\mathrm{sgn}(t) \;, \end{aligned} \tag{2.2.4}$$

where the last line holds in the ohmic scaling limit, in which the cutoff frequency ω_c is the largest energy scale of the system and $J_{\rm lf}(\omega) = 2K\omega \exp(-|\omega|/\omega_c)$. As usual, the Kondo parameter K denotes the coupling strength. $Q(t)$ is known as the bath correlation function. It is a two-point correlation function and we will write it abbreviated as $Q_{j,k} \equiv Q(t_j - t_k)$. A path that starts and ends in a sojourn can be divided into $2n$ transitions parametrized as

$$\eta^{(n)}(t') = \sum_{j=0}^{n} \eta_j \left[\Theta(t' - t_{2\,j}) - \Theta(t' - t_{2\,j+1})\right] , \tag{2.2.5}$$

$$\xi^{(n)}(t') = \sum_{j=1}^{n} \xi_j \left[\Theta(t' - t_{2\,j-1}) - \Theta(t' - t_{2\,j})\right] . \tag{2.2.6}$$

Now, the influence functional can be written as

$$\begin{aligned} \mathcal{F}^{(n)} = \exp\left[-\sum_{j=1}^{n} Q'_{2\,j,2\,j-1}\right] \exp\left[-\sum_{j=2}^{n}\sum_{k=1}^{j-1} \xi_j\,\xi_k\,\Lambda_{j,k}\right] \\ \times \exp\left[\mathrm{i}\,\pi K \sum_{k=0}^{n-1} \xi_{k+1}\,\eta_k\right] . \end{aligned} \tag{2.2.7}$$

Here, $\Lambda_{j,k}$ describes the blip-blip-correlations

$$\Lambda_{j,k} = Q'_{2\,j,2\,k-1} + Q'_{2\,j-1,2\,k} - Q'_{2\,j,2\,k} - Q'_{2\,j-1,2\,k-1} . \tag{2.2.8}$$

The influence phase factors in the second line of (2.2.7) are a simplifying feature of the ohmic scaling limit. They describe correlations of sojourns with subsequent blips.

Remarkably, the first line of Eq. (2.2.7) suppresses off-diagonal states exponentially in time. Therefore, the system is driven diagonal by the persistent measurement of the environment. It behaves more classical the stronger the coupling to the environment (see [13, 14]).

Still to do is the summing over all possible paths,

$$\sum_{\text{all paths}} \cdots \longrightarrow \sum_{n_1=0}^{\infty} \sum_{\{\eta_j=\pm1\}} \sum_{\{\xi_j=\pm1\}} \int_{t_\mathrm{i}}^{t_\mathrm{f}} \mathrm{d}t_{2n_1} \int_{t_\mathrm{i}}^{t_{2n_1}} \mathrm{d}t_{2n_1-1} \cdots \int_{t_\mathrm{i}}^{t_2} \mathrm{d}t_1 \cdots , \tag{2.2.9}$$

where t_i denotes the initial time (here $t_i = 0$). The sum is composed of three steps:

1. the sum over all possible intermediate sojourn and blip states the paths with a given number of transitions can visit

2. the integration over the time-ordered jumps of these paths

3. the sum over the possible number of transitions the system may undergo.

Further, we rewrite the double path sum as transition sequences of the four possible states of Fig. 2.1. The amplitude to flip the current state is $\pm \mathrm{i}\Delta/2$. The weight to stay in a sojourn state is unity, whereas the weight to stay in the blip state j is $\exp(\mathrm{i}\epsilon\,\xi_{\mathrm{j}}\,\tau_{\mathrm{j}})$. Here, we have used the blip lengths $\tau_j = t_{2j} - t_{2j-1}$. These blip factors accumulate for n blip states in the overall bias factor

$$B_n = \exp\left(\mathrm{i}\epsilon \sum_{\mathrm{j}=1}^{\mathrm{n}} \xi_{\mathrm{j}}\,\tau_{\mathrm{j}}\right) . \tag{2.2.10}$$

This overall bias factor has to be included in the double path sum (2.2.1), unless the bias equals zero.

The above expressions describe the exact formal solution for the dynamics of the RDM of the TSS in the ohmic scaling limit. But, the nonconvolutive form of the bath correlations in the influence functional (2.2.7) prevents to perform the path sum in analytic form.

2.3 Markov limit

We will not give a detailed description of the justifications and implications of the NIBA [1, 2] but a brief overview of the main results. The main assumption of the NIBA is that the system dwells most of its time on a diagonal state, leading to two simplifications. First, interblip interactions $\Lambda_{j,k}$ are negligible, and second, correlations between sojourns and blips are only included for a sojourn with its subsequent blip.

The bath correlations from Eq. (2.2.4) simplify considerably in the Markov limit to

$$Q(t) = \vartheta\,|t| + \mathrm{i}\,\pi\,K\,\mathrm{sgn}(t) + 2K \ln\left(\frac{\omega_{\mathrm{c}}}{2\pi T}\right) , \tag{2.3.1}$$

where we introduced the scaled temperature $\vartheta = 2\pi K T$. This is a natural choice for the temperature as it drops out of the bath spectral density $S(\omega)$ in the high temperature limit, $S(\omega \ll 1/\beta) = 2\vartheta/\pi$. The logarithmic term in (2.3.1) is an adiabatic Franck-Condon factor including all environmental modes in the frequency range $2\pi T \leq \omega \leq \omega_{\mathrm{c}}$. It is advantageous to absorb these high-frequency modes into a renormalized temperature-dependent tunneling matrix element,

$$\Delta_T^2 = \left(\frac{2\pi T}{\Delta_{\mathrm{r}}}\right)^{2K} \Delta_{\mathrm{r}}^2 , \tag{2.3.2}$$

where $\Delta_{\mathrm{r}}^{1-K} = \Delta/\omega_{\mathrm{c}}^K$ is the standard renormalized tunneling matrix for $K < 1$ [2]. In the following, we will always refer to Δ_T when writing Δ. The validity for the high temperature limit is given for

$$K \lesssim 0.3 \qquad \text{and} \qquad \Omega \lesssim T \ll \omega_{\mathrm{c}} . \tag{2.3.3}$$

The second inequality is due to the doubly exponential dependence on temperature in the influence functional. It follows that the high temperature limit is already valid for temperatures comparable or larger than the largest frequency of the system. This illustrates how effectively the bath destroys correlations.

For the form (2.3.1) of the bath correlations, the interblip correlations vanish, i.e., $\Lambda_{j,k} = 0$ in (2.2.7). Thus the influence functional (2.2.7) simplifies to

$$\mathcal{F}_{\mathrm{NIBA}}^{(n)} = \prod_{j=1}^{n} \exp\left[-Q'(\tau_j) + \mathrm{i}\,\xi_j\,\eta_{j-1}\,Q''(\tau_j)\right] . \tag{2.3.4}$$

With this expression for the influence functional, each term of the infinite series for the elements of the RDM becomes a convolution. This feature makes the path sum feasible.

The bath is only visible to the system, while it stays off-diagonal. The form (2.3.1) in (2.3.4) leads to a shift of the Laplace variable in the respective time-period, $\lambda \to \lambda + \vartheta$. The integral representation for the $\langle\sigma_z\rangle$ kernel in the Markov limit takes the form

$$\begin{aligned} \mathcal{K}_{\sigma_z}(\lambda) &= -\frac{1}{\lambda^2}\,\Delta^2 \frac{1}{2} \int_0^\infty \mathrm{d}\tau_1\, \mathrm{e}^{-\lambda\,\tau_1}\, \mathrm{e}^{-\vartheta\,\tau_1} \left[\mathrm{e}^{\mathrm{i}\,\pi\,K + \mathrm{i}\,\epsilon\,\tau_1} + \mathrm{e}^{-\mathrm{i}\,\pi\,K - \mathrm{i}\,\epsilon\,\tau_1}\right] \\ &= -\frac{1}{\lambda^2}\,\Delta^2 \int_0^\infty \mathrm{d}\tau_1\, \cos(\pi\,K + \epsilon\,\tau_1)\, \mathrm{e}^{-(\lambda+\vartheta)\,\tau_1} . \end{aligned} \tag{2.3.5}$$

Using $\cos(a+b) = \cos(a)\cos(b) - \sin(a)\sin(b)$ the previous equation can be rewritten as (putting $\sin(\pi K) \approx \pi K$)

$$\mathcal{K}_{\sigma_z}(\lambda) = -\frac{1}{\lambda^2}\,\left[\mathcal{K}_{\sigma_z}^{(\mathrm{s})}(\lambda) - \pi\,K\,\mathcal{K}_{\sigma_z}^{(\mathrm{a})}(\lambda)\right] , \tag{2.3.6}$$

with the symmetric kernel

$$\mathcal{K}_{\sigma_z}^{(\mathrm{s})}(\lambda) = \frac{\Delta^2\,(\lambda+\vartheta)}{(\lambda+\vartheta)^2 + \epsilon^2} , \tag{2.3.7}$$

which was already defined in Eq. (2.1.14) in the absence of the bath coupling and the antisymmetric kernel

$$\mathcal{K}_{\sigma_z}^{(\mathrm{a})}(\lambda) = \frac{\Delta^2\,\epsilon}{(\lambda+\vartheta)^2 + \epsilon^2} . \tag{2.3.8}$$

$\mathcal{K}_{\sigma_z}^{(\mathrm{a})}(\lambda)$ gives only one contribution. Therefore, $\langle\sigma_z(\lambda)\rangle$ modifies to

$$\langle\sigma_z(\lambda)\rangle = \frac{1 + \frac{\pi K}{\lambda}\,\mathcal{K}_{\sigma_z}^{(\mathrm{a})}(\lambda)}{\lambda + \mathcal{K}_{\sigma_z}^{(\mathrm{s})}(\lambda)} = \frac{1}{\lambda}\,\frac{\pi K \Delta^2 \epsilon + \lambda\,[(\lambda+\vartheta)^2 + \epsilon^2]}{\lambda\,[(\lambda+\vartheta)^2 + \epsilon^2] + \Delta^2(\lambda+\vartheta)} . \tag{2.3.9}$$

It is interesting to note an alternative approach to obtain $\langle\sigma_z(\lambda)\rangle$. Since the expectation values $\langle\sigma_j\rangle$, with $j = x, y, z$, are related to the reduced density matrix by[3]

$$\rho(\lambda) = \frac{1}{2}\begin{pmatrix} 1/\lambda + \langle\sigma_z(\lambda)\rangle & \langle\sigma_x(\lambda)\rangle - \mathrm{i}\langle\sigma_y(\lambda)\rangle \\ \langle\sigma_x(\lambda)\rangle + \mathrm{i}\langle\sigma_y(\lambda)\rangle & 1/\lambda - \langle\sigma_z(\lambda)\rangle \end{pmatrix} = \begin{pmatrix} RR & RL \\ LR & LL \end{pmatrix} , \tag{2.3.10}$$

[3]Remember that the RDM can generally be written as a linear combination of the Pauli matrices and the unit matrix, $\rho(\lambda) = \frac{1}{2}\left[\frac{1}{\lambda}\mathbb{1} + \sum_{j=x,y,z}\langle\sigma_j(\lambda)\rangle\sigma_j\right]$.

it is possible to rewrite the coupled equations of motion given in Eq. (2.1.13) by the states of the RDM. Then, we obtain instead of (2.1.13) a new set of coupled equations of motion

$$\begin{aligned} 1 &= \lambda\, RR + \frac{\mathrm{i}}{2}\,(RL - LR)\;, \\ 0 &= \lambda\, LL + \frac{\mathrm{i}}{2}\,(LR - RL)\;, \\ 0 &= (\lambda + \vartheta)\, LR + \frac{\mathrm{i}}{2}\left[\Delta\left(I^{(+)}LL - I^{(-)}RR\right) + 2\,\epsilon\, LR\right]\;, \\ 0 &= (\lambda + \vartheta)\, RL - \frac{\mathrm{i}}{2}\left[\Delta\left(I^{(-)}LL - I^{(+)}RR\right) + 2\,\epsilon\, RL\right]\;. \end{aligned} \tag{2.3.11}$$

We have included influence phase factors arising from transitions, where we start in a diagonal state and end in an off-diagonal state. These are

$$I^{(+)} = \mathrm{e}^{\mathrm{i}\,\pi K} \quad \text{and} \quad I^{(-)} = \mathrm{e}^{-\mathrm{i}\,\pi K}\;. \tag{2.3.12}$$

Solving for $\langle\sigma_z(\lambda)\rangle = RR - LL$ gives the same result as Eq. (2.3.9). The coupled equations of (2.3.11) give a detailed picture of the intrinsic dynamics of the TSS in the Markov-regime. Every single contribution to $\langle\sigma_z(\lambda)\rangle$ can be understood by the transitions between the four states of the density matrix (see also Fig. 2.1).

For non-zero bias, the dynamics of $\langle\sigma_z(\lambda)\rangle$ is determined by four poles located at λ_j, with $j = 1, \ldots, 4$. For vanishing bias two poles $\lambda_{1,2}$ remain.

For the symmetric case $\epsilon = 0$ there is a crossover temperature at $\vartheta^* = 2\,\Delta$. Below this crossover temperature the system shows damped oscillations, above ϑ^* only incoherent damping. Then, the two poles $\lambda_{1,2}$ of $\langle\sigma_z(\lambda)\rangle$ are located at

$$\lambda_1 = \frac{1}{2}\left(-\vartheta - \sqrt{\vartheta^2 - 4\Delta^2}\right)\;, \qquad \lambda_2 = \frac{1}{2}\left(-\vartheta + \sqrt{\vartheta^2 - 4\Delta^2}\right)\;. \tag{2.3.13}$$

The rate $\gamma_1 = -\mathrm{Re}[\lambda_1]$ is growing with increasing temperature and approaches the limiting form

$$\gamma_1 = \vartheta\;, \tag{2.3.14}$$

whereas the rate $\gamma_2 = -\mathrm{Re}[\lambda_2]$ is decreasing with growing temperature and shows the Kondo-like temperature dependence $\gamma_2 \propto T^{2K-1}$. Remember that we are actually using the renormalized temperature-dependent tunneling matrix element from Eq. (2.3.2). Only the residue describing the Kondo-behavior survives for high temperature [2].

The asymmetric case $\epsilon \neq 0$ shows a richer behavior (Figs. 2.2–2.3). Here, the denominator of $\langle\sigma_z(\lambda)\rangle$ is a polynomial of degree four in λ, with four zeros λ_j. One of the zeros, say λ_4, leads to a non-zero equilibrium value (see below). The other three give rise to coherent and incoherent contributions, depending on the parameters. Below the critical bias

$$\epsilon_{\mathrm{cr}} = \frac{\Delta}{2\sqrt{2}} \tag{2.3.15}$$

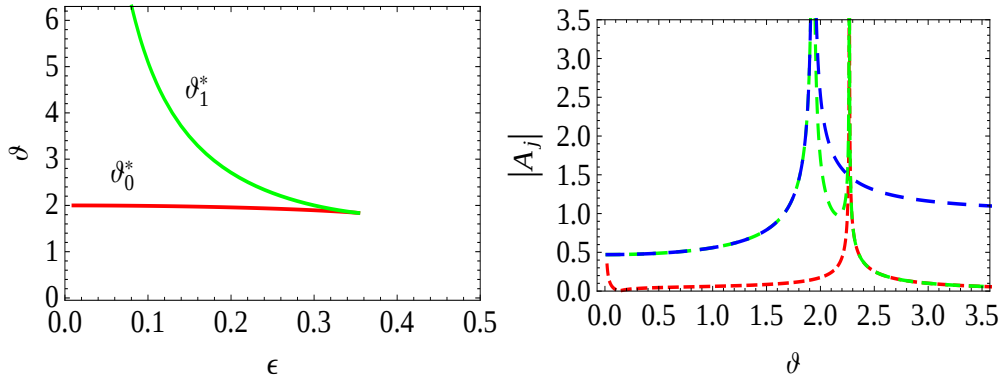

Figure 2.2: Left: crossover temperatures ϑ_0^* and ϑ_1^*, which are separating the coherent and incoherent regime ($\Delta = 1$). Right: absolute values of the amplitudes of $\langle\sigma_z(\lambda)\rangle$ with $\Delta = 1$, $\epsilon = 0.25$, and $K = 0.01$. The colors red, green, and blue denote the amplitudes $|A_j|$, with $j = 1, 2, 3$. See text for details.

there are two crossover temperatures ϑ_0^*, and ϑ_1^*. For temperatures below $\vartheta < \vartheta_0^*$ the main contribution is a damped oscillation plus a negligible incoherent contribution. Coming closer to ϑ_0^* the incoherent contribution gains more weight and for temperatures between $\vartheta_0^* < \vartheta < \vartheta_1^*$ all contributions are relevant and incoherent. Above $\vartheta > \vartheta_1^*$ the smallest relaxation pole, the Kondo-pole, dominates the system and the dynamics is therefore incoherent.
Above $\epsilon_{\rm cr}$ we have a real root and a complex conjugate pair of poles for all temperatures. They all contribute, whereat high temperature the Kondo-pole dominates.
A plot in the time and Fourier regime is shown in Fig. 2.4. We clearly see the transition from the coherent regime for low temperature to pure incoherent damping for high temperature.

In order to obtain $\langle\sigma_z(t)\rangle$ in the time regime, it is useful to rewrite the denominator of $\langle\sigma_z(\lambda)\rangle$ in (2.3.9) to $\lambda(\lambda-\lambda_1)(\lambda-\lambda_2)(\lambda-\lambda_3)$. The pole at $\lambda = 0$ leads to a non-zero equilibrium residue

$$\langle\sigma_z\rangle_{\rm eq} = \pi K\epsilon/\vartheta\ . \tag{2.3.16}$$

Below the critical bias $\epsilon_{\rm cr}$ and for temperatures $\vartheta < \vartheta_0^*$ and $\vartheta > \vartheta_1^*$, the other zeros give rise to a relaxation term and to damped oscillations. Then the zeros read

$$\lambda_1 = -\gamma_{\rm r} \quad \text{and} \quad \lambda_{2,3} = -\gamma \pm {\rm i}\,\Omega\ . \tag{2.3.17}$$

The new variables have to comply with the Vieta relations

$$\begin{aligned} \gamma_{\rm r} + 2\gamma &= 2\vartheta\ , \qquad \gamma_{\rm r}\left(\gamma^2+\Omega^2\right) = \Delta^2\vartheta\ , \\ \gamma^2 + 2\gamma\gamma_{\rm r} + \Omega^2 &= \Delta^2 + \epsilon^2 + \vartheta^2\ . \end{aligned} \tag{2.3.18}$$

By transformation of the Vieta relations we obtain

$$\gamma = \vartheta - \gamma_{\rm r}/2 \qquad \text{and} \qquad \Omega^2 = \epsilon^2 + \Delta^2 + \gamma_{\rm r}^2/4 - \gamma\gamma_{\rm r}\ . \tag{2.3.19}$$

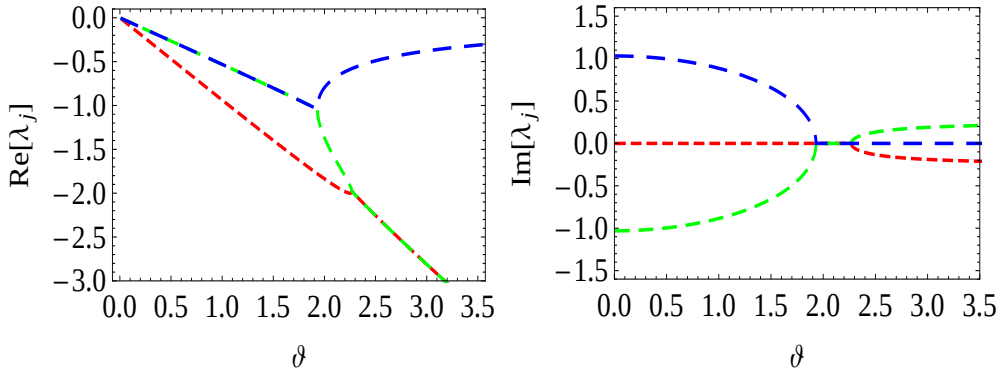

Figure 2.3: $\langle\sigma_z\rangle$: real (left) and imaginary (right) part of the three poles λ_j of $\langle\sigma_z(\lambda)\rangle$. At low ϑ, $\langle\sigma_z(t)\rangle$ is a superposition of two damped oscillations. There is only incoherent relaxation for intermediate temperature. It remains one relevant relaxation contribution for high ϑ. The parameters are $\epsilon = 0.25$, $\Delta = 1$. The colors red, green, and blue label $\mathrm{Re}\,[\lambda_j]$ and $\mathrm{Im}\,[\lambda_j]$, with $j = 1, 2, 3$.

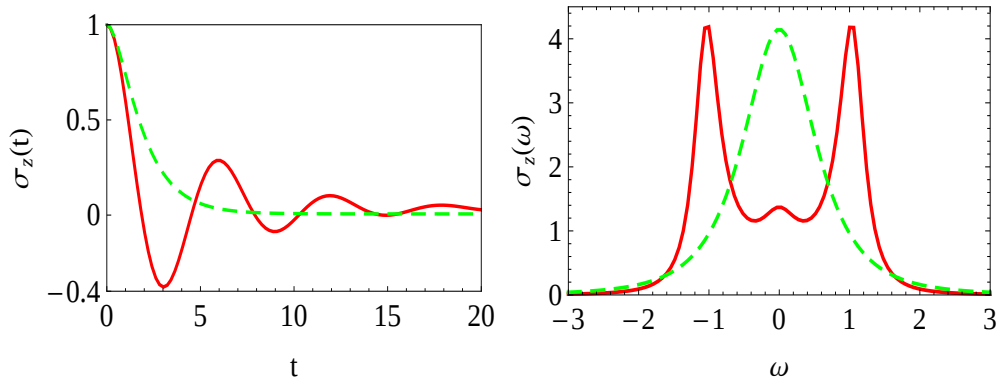

Figure 2.4: $\langle\sigma_z\rangle$: plots of $\langle\sigma_z\rangle$ in the time regime (left) and Fourier regime (right), with $\epsilon = 0.4$, $\Delta = 1$, and $K = 0.01$. For $T = 6$ (red) a coherent oscillation plus a small incoherent contribution occurs. Increasing temperature removes the coherent part and only one incoherent contribution remains, which is shown for $T = 32$ (green, dashed).

In the high temperature limit, i.e., well above ϑ_1^*, the rates γ, $\gamma_{\rm r}$ and the oscillation frequency Ω are given by

$$\gamma = \vartheta - \frac{\Delta^2}{2\vartheta}\,, \qquad \gamma_{\rm r} = \frac{\Delta^2}{\vartheta} \qquad \text{and} \qquad \Omega = \epsilon\,. \tag{2.3.20}$$

Thus, for increasing temperature the eigenfrequency approaches ϵ and the coherent contribution is strongly damped. On the other side, the relaxation part is weakly damped for high temperature. For temperatures well below ϑ_0^*, i.e., in the low temperature limit of the Markov-regime, the rates γ, $\gamma_{\rm r}$ and the oscillation frequency Ω read

$$\gamma = \frac{\Delta^2 + 2\,\epsilon^2}{2\,(\Delta^2+\epsilon^2)}\,\vartheta\,, \qquad \gamma_{\rm r} = \frac{\Delta^2}{\Delta^2+\epsilon^2}\,\vartheta \qquad \text{and} \qquad \Omega^2 = \Delta^2 + \epsilon^2\,. \tag{2.3.21}$$

Both rates γ and $\gamma_{\rm r}$ grow linearly with ϑ to leading order, whereas the oscillation frequency is constant. Finally, the time dependence of $\langle\sigma_z(t)\rangle$ is obtained by a Bromwich contour integration

$$\langle\sigma_z(t)\rangle = a_1\,{\rm e}^{-\gamma_{\rm r}t} + \Big[\Big(1 - a_1 - \langle\sigma_z\rangle_{\rm eq}\Big)\cos\Omega t + a_2\sin\Omega t\Big]\,{\rm e}^{-\gamma t} + \langle\sigma_z\rangle_{\rm eq}\,, \tag{2.3.22}$$

where

$$a_1 = \Big[\Omega^2 + \gamma^2 - \Delta^2 - \big(\Omega^2+\gamma^2\big)\,\langle\sigma_z\rangle_{\rm eq}\Big] \,/\, \big[\Omega^2 + (\gamma-\gamma_{\rm r})^2\big]\,, \tag{2.3.23}$$

$$a_2 = \Big[(\gamma_{\rm r}-\gamma)a_1 + \gamma\,\Big(1 - \langle\sigma_z\rangle_{\rm eq}\Big)\Big] \,/\, \Omega\,. \tag{2.3.24}$$

The first term in (2.3.22) describes pure relaxation, while the second term is responsible for dephasing. The probability to be in the state R at time t, when we start in state R at time $t=0$, is defined as $P(t) \equiv P_{R,R}(t) = \frac{1}{2}(1 + \langle\sigma_z(t)\rangle)$. We can split $P(t)$ into a relaxation and dephasing part, $P(t) = \mathit{relaxation} + \mathit{dephasing}$. The relaxation part is only present for asymmetric systems where $\epsilon \neq 0$.

2.4 One-boson self-energy

For temperatures lower than Ω, i.e., in the quantum-noise regime, the neglect of interblip interactions leads to wrong results. We will follow the discussion in [2] and examine the one-boson exchange contribution, where interblip correlations are included to first order in the coupling strength. Instead of the Markov form (2.3.1), we now employ the full quantum mechanical form (2.2.4), i.e., ${\rm Re}\,[\langle X(t)X(0)\rangle_T] = Q'(t)$, with the frequency-integral representation

$$Q'(t) \;=\; \int_0^\infty {\rm d}\omega\;\frac{S(\omega)}{\omega^2}\,[\,1-\cos(\omega t)\,]\,, \quad \text{and} \quad S(\omega) \;=\; 2K\,\omega\coth\Big(\frac{\omega}{2T}\Big)\,. \tag{2.4.1}$$

It is convenient to introduce self-energies, which are defined as the kernels of Eq. (2.3.9) minus the kernels of the undamped system

$$\Sigma^{(\rm s)}(\lambda) \equiv \mathcal{K}^{(\rm s)}_{\sigma_z}(\lambda) - \lambda\,\Delta^2/(\Delta^2+\epsilon^2)\,, \qquad \Sigma^{(\rm a)}(\lambda) \equiv \mathcal{K}^{(\rm a)}_{\sigma_z}(\lambda)\,. \tag{2.4.2}$$

We are interested in the shift of the relaxation and dephasing rate due to the interblip correlations. Thus, we have to calculate the symmetric self-energy and examine the shift of the poles in the denominator of Eq. (2.3.9). Technically, we have to sum all irreducible multiblip diagrams up to order Δ^4 in which two blips are correlated via a one-boson exchange. These correlated interblip contributions vanish in the Markov-regime. Within the time interval spanned by the correlated blips any number of uncorrelated transitions has to be included. A direct calculation of the self-energy can be found in [2].

It is illustrative to describe an alternative way, in which all possible transition sequences and correlations are summed up to obtain the self-energy. First, we need the conditional propagators $J_{m,n}$ from all four initial states m to the four final states n (cf. Fig. 2.1). Since all information on the time evolution of the TSS is contained in the RDM, we can express the conditional propagators by the RDM. The indices $m, n \in \{RR, RL, LR, LL\}$ correspond to the states of the RDM in Eq. (2.3.10). For example, if the initial and final state is RR, we obtain the conditional propagator

$$J_{RR,RR}(\lambda) = \frac{1}{2}\left[1/\lambda + \langle\sigma_z(\lambda)\rangle\right] \ . \tag{2.4.3}$$

Likewise, if we end in state RL we obtain

$$J_{RR,RL}(\lambda) = \frac{1}{2}\left[\langle\sigma_x(\lambda)\rangle - \mathrm{i}\langle\sigma_y(\lambda)\rangle\right] \ . \tag{2.4.4}$$

We obtain similar conditional propagators if we start in one of the coherent states. For example, starting in the state RL, with $\langle\sigma_x(t=0)\rangle = 1$ and $\langle\sigma_y(t=0)\rangle = \mathrm{i}$, and going to the final state RR yields

$$J_{RL,RR}(\lambda) = \frac{1}{2}\langle\sigma_z(\lambda)\rangle \ . \tag{2.4.5}$$

Second, we need the contributions when the system flips its state, say $F_{m,n}(\lambda)$. These are obtained by expanding the conditional propagators to first order in Δ.

Consider now the irreducible multiblip contribution where the outer charges are correlated. There are four possible paths

$$\begin{aligned} &F_{RR,RL}(\lambda)\, J_{RL,RL}(\lambda+\mathrm{i}\,\omega)\, F_{RL,RR}(\lambda) \ , \qquad &&-F_{RR,RL}(\lambda)\, J_{RL,LR}(\lambda+\mathrm{i}\,\omega)\, F_{LR,RR}(\lambda) \ , \\ &F_{RR,LR}(\lambda)\, J_{LR,LR}(\lambda+\mathrm{i}\,\omega)\, F_{LR,RR}(\lambda) \ , \qquad &&-F_{RR,LR}(\lambda)\, J_{LR,RL}(\lambda+\mathrm{i}\,\omega)\, F_{RL,RR}(\lambda) \ . \end{aligned} \tag{2.4.6}$$

Observe the shift of $\lambda \to \lambda + \mathrm{i}\,\omega$ due to the correlation between the outer charges. The attractive (repulsive) dipole-dipole interaction of the blips leads to the alternating sign +(-) in (2.4.6). Summing up the four path contributions results in

$$-\frac{\Delta^2\left(\Delta^2 + (\lambda+\mathrm{i}\,\omega)^2\right)}{\lambda^2(\lambda+\mathrm{i}\,\omega)\left(\Delta^2+\epsilon^2+(\lambda+\mathrm{i}\,\omega)^2\right)} \ . \tag{2.4.7}$$

We have to repeat this step for the interaction of the first with the third charge and the second with the fourth, which are equal because of symmetry,

$$\frac{\Delta^4\,\epsilon^2}{\lambda^2\left(\lambda^2+\epsilon^2\right)(\lambda+\mathrm{i}\,\omega)\left(\Delta^2+\epsilon^2+(\lambda+\mathrm{i}\,\omega)^2\right)} \tag{2.4.8}$$

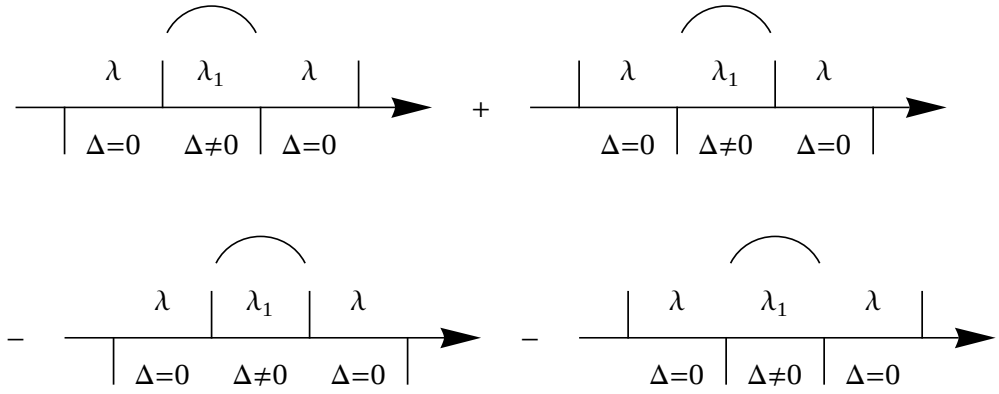

Figure 2.5: Example for systematic weak damping approximation. The up and down lines denote the different paths in the charge picture. Every line stands for a transition of the spin. An up (down) line would be a positive (negative) charge, i.e in Fig. 2.1, we would be in the state RL (LR). The shifted variable $\lambda_1 = \lambda + \mathrm{i}\,\omega$ characterizes the correlated part. There are no transitions allowed between the two charges while $\Delta = 0$. The arrow indicates the time direction.

and for the interior charges (see Fig. 2.5)

$$-\frac{\Delta^4\,\epsilon^2\,(\epsilon^2+(\lambda+\mathrm{i}\,\omega)^2)}{\lambda^2\,(\lambda^2+\epsilon^2)^2\,(\lambda+\mathrm{i}\,\omega)\,(\Delta^2+\epsilon^2+(\lambda+\mathrm{i}\,\omega)^2)}\;. \tag{2.4.9}$$

The self-energy is obtained by doing the integration over ω and thus by summing the residues of ω, leading to

$$\begin{aligned}\Sigma(\lambda) = -\frac{1}{2}\pi\Bigg[&\frac{\Delta^4\lambda^2\,S(\mathrm{i}\,\lambda)}{\Omega^2\,(\lambda^2+\Omega^2-\Delta^2)^2}\\ &+\frac{\Delta^2\,(\Omega^2-\Delta^2)\,(\lambda-\mathrm{i}\,\Omega)^2\,S(\mathrm{i}\,\lambda-\Omega)}{2\Omega^2\,(\lambda^2+\Omega^2-\Delta^2)^2}+\frac{\Delta^2\,(\Omega^2-\Delta^2)\,(\lambda+\mathrm{i}\,\Omega)^2\,S(\mathrm{i}\,\lambda+\Omega)}{2\Omega^2\,(\lambda^2+\Omega^2-\Delta^2)^2}\Bigg]\;.\end{aligned} \tag{2.4.10}$$

It is convenient to introduce generalized temperatures, describing one-boson transfers from the system to the bath or vice versa. To be more precise, $S(\pm\Omega)$ describe one-boson transfers from or to the bath, while $S(0)$ describes flipless dephasing processes [2, 56]. The generalized temperatures are obtained by matching the result for the self-energy (2.4.10) with the known result ϑ in the high temperature limit. We have to set $\lambda = \pm\,\mathrm{i}\,\Omega$ and $\lambda = 0$, respectively, in Eq. (2.4.10) because these are the poles of the undamped denominator in Eq. (2.3.9). Then, we obtain for the generalized temperatures

$$\theta^{(\Omega)} = \frac{\pi}{2}\frac{\Delta^2\,S(\Omega)+2\,\epsilon^2\,S(0)}{\Delta^2+2\,\epsilon^2} \qquad \text{and} \qquad \theta^{(0)} = \frac{\pi}{2}\,S(\Omega)\;. \tag{2.4.11}$$

Now, we insert the generalized temperatures (2.4.11) in the low temperature rates of $\langle\sigma_z\rangle$ given in Eq. (2.3.21). This yields

$$\gamma_\mathrm{r} = \frac{\Delta^2}{\Omega^2}\,\theta^{(0)} \qquad \text{and} \qquad \gamma = \frac{\Delta^2+2\,\epsilon^2}{2\,\Omega^2}\,\theta^{(\Omega)}\;. \tag{2.4.12}$$

The rates in Eq. (2.4.12) simplify to the relaxation and dephasing rate of the TSS in the one-boson regime [2]

$$\gamma_{\mathrm{r}} = \frac{\Delta^2}{\Omega^2}\,\frac{\pi}{2}\,S(\Omega) \qquad \text{and} \qquad \gamma = \frac{\gamma_{\mathrm{r}}}{2} + \frac{\epsilon^2}{\Omega^2}\,\frac{\pi}{2}\,S(0)\ . \tag{2.4.13}$$

Therefore, the generalization from the white-noise regime to the quantum-noise regime is done by replacing ϑ with $\frac{\pi}{2}\,S(0)$ and $\frac{\pi}{2}\,S(\Omega)$, depending on whether we have a flipless dephasing process $\propto \epsilon$, or a one-boson exchange process $\propto \Delta$.

3 Path sum method for two dissipative coupled spins and results

The interest in an accurate description of two coupled spins is still increasing as the fabrication of coupled spin systems becomes more and more feasible, e.g., with coupled Josephson devices [41]. The prospect of a quantum computer or simulator is a rather strong motivation to couple more and more spins because applications and algorithms are already known. But the need for a virtually complete decoupling from environmental modes to yield sufficiently long coherence times shifts the realization of a functional quantum computer with a few dozen qubits at least into the medium-term future. However, a detailed knowledge of the involved dissipative processes is inevitable. Also the process of decoherence, the mechanism that makes the difference of classical and quantum physics, can be studied thoroughly with two coupled spins.

Here, we derive the dynamics of two coupled spins from low temperature and weak damping to high temperature and/or strong damping. Thus, the results can be applied to a large area of the parameter space. Before we proceed with different types of spin-spin coupling in Section 3.6, we give a detailed analysis of sole v_z coupling. The methods, developed and applied for this particular coupling, can be used straightforward for general spin-spin coupling. Parts of this chapter have been published in [30, 66].

3.1 Two undamped coupled spins

The model Hamiltonian for two coupled spins without environmental effects is (we choose $\Delta_1 > \Delta_2$)

$$H = -\frac{\Delta_1}{2}(\sigma_x \otimes \mathbb{1}_2) - \frac{\Delta_2}{2}(\mathbb{1}_2 \otimes \tau_x) - \frac{v_z}{2}(\sigma_z \otimes \tau_z)\,. \tag{3.1.1}$$

We have used the tensor product $\otimes$, which connects the Hilbert spaces of the two spins. Our model consists of two two-state systems, σ and τ, with a coupling term $\propto v_z$. The tunnel matrices $\Delta_{1,2}$ describe transitions of the two states of spin σ and τ, respectively. We postpone possible bias terms until Section 3.6. If we use the basis states $|RR\rangle$, $|RL\rangle$, $|LR\rangle$, and $|LL\rangle$, which are eigenstates of σ_z and τ_z, we can rewrite the Hamiltonian in matrix notation to

$$H = \frac{1}{2}\begin{pmatrix} -v_z & -\Delta_2 & -\Delta_1 & 0 \\ -\Delta_2 & v_z & 0 & -\Delta_1 \\ -\Delta_1 & 0 & v_z & -\Delta_2 \\ 0 & -\Delta_1 & -\Delta_2 & -v_z \end{pmatrix}\,. \tag{3.1.2}$$

The Hamiltonian can be diagonalized with the matrix

$$U = \frac{1}{2}\begin{pmatrix} \sqrt{1+\sin(\Theta_1)} & \frac{\cos(\Theta_1)}{\sqrt{1+\sin(\Theta_1)}} & \frac{\cos(\Theta_1)}{\sqrt{1+\sin(\Theta_1)}} & \sqrt{1+\sin(\Theta_1)} \\ -\sqrt{1+\sin(\Theta_2)} & \frac{\cos(\Theta_2)}{\sqrt{1+\sin(\Theta_2)}} & -\frac{\cos(\Theta_2)}{\sqrt{1+\sin(\Theta_2)}} & \sqrt{1+\sin(\Theta_2)} \\ -\sqrt{1-\sin(\Theta_2)} & -\frac{\cos(\Theta_2)}{\sqrt{1-\sin(\Theta_2)}} & \frac{\cos(\Theta_2)}{\sqrt{1-\sin(\Theta_2)}} & \sqrt{1-\sin(\Theta_2)} \\ \sqrt{1-\sin(\Theta_1)} & -\frac{\cos(\Theta_1)}{\sqrt{1-\sin(\Theta_1)}} & -\frac{\cos(\Theta_1)}{\sqrt{1-\sin(\Theta_1)}} & \sqrt{1-\sin(\Theta_1)} \end{pmatrix} \tag{3.1.3}$$

and the mixing angles

$$\Theta_1 = \arctan\left[v_z/(\Delta_1+\Delta_2)\right] \qquad \text{and} \qquad \Theta_2 = \arctan\left[v_z/(\Delta_1-\Delta_2)\right]. \tag{3.1.4}$$

The four energy eigenstates $|e_1\rangle \ldots |e_4\rangle$, with $|e_1\rangle$ the lowest and $|e_4\rangle$ the highest lying state, are composed of the eigenstates of σ_z and τ_z,

$$\begin{aligned} |e_1\rangle &= \sqrt{1+\sin(\Theta_1)}\,|RR\rangle - \sqrt{1+\sin(\Theta_2)}\,|RL\rangle \\ &\qquad - \sqrt{1-\sin(\Theta_2)}\,|LR\rangle + \sqrt{1-\sin(\Theta_1)}\,|LL\rangle\,, \\ &\vdots \\ |e_4\rangle &= \sqrt{1+\sin(\Theta_1)}\,|RR\rangle + \sqrt{1+\sin(\Theta_2)}\,|RL\rangle \\ &\qquad + \sqrt{1-\sin(\Theta_2)}\,|LR\rangle + \sqrt{1-\sin(\Theta_1)}\,|LL\rangle\,. \end{aligned} \tag{3.1.5}$$

The diagonalized Hamiltonian reads

$$\widetilde{H} = U\,H\,U^{-1} = -\frac{\Omega}{2}\,(\sigma_z \otimes \mathbb{1}) - \frac{\delta}{2}\,(\mathbb{1} \otimes \tau_z)\,, \tag{3.1.6}$$

with

$$\begin{aligned} \Omega = \frac{1}{2}(\Omega_+ + \Omega_-), \qquad \delta = \frac{1}{2}(\Omega_+ - \Omega_-)\,, \\ \Omega_\pm = \sqrt{(\Delta_1 \pm \Delta_2)^2 + v_z^2}\,. \end{aligned} \tag{3.1.7}$$

These are the eigenfrequencies of the undamped system.

The expectation value of an operator A is generally given by $\langle A\rangle = \mathrm{tr}(\rho\,A)$, where ρ is the density matrix of the system. While the system relaxes for $t \to \infty$ to equilibrium, the density matrix approaches a Boltzmann distribution, $\rho_{\mathrm{eq}} = \mathrm{e}^{-\beta H}$. Thus, the thermodynamical equilibrium value of an operator A, which was already written in Eq. (2.1.9), reads

$$\langle A\rangle_{\mathrm{eq}} \equiv \langle A(t\to\infty)\rangle = \frac{\mathrm{tr}(A\,\rho_{\mathrm{eq}})}{\mathrm{tr}(\rho_{\mathrm{eq}})} = \frac{\mathrm{tr}(A\,\mathrm{e}^{-\beta\,H})}{\mathrm{tr}(\mathrm{e}^{-\beta\,H})}\,. \tag{3.1.8}$$

For our model, A stands for σ_z, τ_z, $\sigma_z\tau_z$, and so on. For example, in the basis of the σ_z- and τ_z-eigenstates the numerator is given by

$$\mathrm{tr}\left[A\,U^{-1}\begin{pmatrix} \mathrm{e}^{-\beta\,E_1} & 0 & 0 & 0 \\ 0 & \mathrm{e}^{-\beta\,E_2} & 0 & 0 \\ 0 & 0 & \mathrm{e}^{-\beta\,E_3} & 0 \\ 0 & 0 & 0 & \mathrm{e}^{-\beta\,E_4} \end{pmatrix} U\right], \tag{3.1.9}$$

where E_1, E_2, E_3, and E_4 are the eigenvalues of the Hamiltonian. This leads to

$$\langle \sigma_z \rangle_{\mathrm{eq}} = \langle \tau_z \rangle_{\mathrm{eq}} = 0 \tag{3.1.10}$$

and

$$\langle \sigma_z \tau_z \rangle_{\mathrm{eq}} = \frac{v_z}{\Omega_+ \, \Omega_-} \frac{\Omega_+ \, \sinh\left(\frac{\beta \, \Omega_-}{2}\right) + \Omega_- \, \sinh\left(\frac{\beta \, \Omega_+}{2}\right)}{\cosh\left(\frac{\beta \, \Omega_+}{2}\right) + \cosh\left(\frac{\beta \, \Omega_-}{2}\right)} \tag{3.1.11}$$

or written as a function of Ω and δ

$$\langle \sigma_z \tau_z \rangle_{\mathrm{eq}} = \frac{v_z}{\Omega^2 - \delta^2} \left[\Omega \, \tanh\left(\frac{\beta \, \Omega}{2}\right) - \delta \, \tanh\left(\frac{\beta \, \delta}{2}\right) \right] . \tag{3.1.12}$$

For vanishing coupling of the spins we regain the correct result for a single spin without bias

$$\lim_{v_z \to 0} \langle \sigma_z \tau_z \rangle_{\mathrm{eq}} = 0 \, . \tag{3.1.13}$$

The density matrix of a two-spin system $\rho_{n,m}(t)$ has 16 entries, where we decide that $n = 1, \ldots, 4$ ($m = 1, \ldots, 4$) denotes the σ-spin (τ-spin). Alternatively, we can label the entries with $m, n \in \{RR, RL, LR, LL\}$ for σ and τ, respectively. The probability to be in the state $\sigma_z \, \sigma'_z, \tau_z \, \tau'_z$ at time t when we start in the state RR, RR at time t_0 is given by $\rho_{\sigma_z \, \sigma'_z, \tau_z \, \tau'_z}(t)$. Then the probability to be in the state RR, RR at time t reads

$$\begin{aligned} \rho_{RR,RR}(t) &= \frac{1}{2} \left[1 + \langle \sigma_z(t) \rangle \right] \frac{1}{2} \left[1 + \langle \tau_z(t) \rangle \right] \\ &= \frac{1}{4} \left[1 + \langle \sigma_z(t) \rangle + \langle \tau_z(t) \rangle + \langle \sigma_z \tau_z(t) \rangle \right] . \end{aligned} \tag{3.1.14}$$

The other diagonal entries of the density matrix are

$$\begin{aligned} \rho_{RR,LL}(t) &= \frac{1}{4} \left[1 + \langle \sigma_z(t) \rangle - \langle \tau_z(t) \rangle - \langle \sigma_z \tau_z(t) \rangle \right] , \\ \rho_{LL,RR}(t) &= \frac{1}{4} \left[1 - \langle \sigma_z(t) \rangle + \langle \tau_z(t) \rangle - \langle \sigma_z \tau_z(t) \rangle \right] , \\ \rho_{LL,LL}(t) &= \frac{1}{4} \left[1 - \langle \sigma_z(t) \rangle - \langle \tau_z(t) \rangle + \langle \sigma_z \tau_z(t) \rangle \right] . \end{aligned} \tag{3.1.15}$$

Consider that $\langle \sigma_z \rangle$ is actually $\langle \sigma_z \rangle \otimes \mathbb{1}_2$ and $\langle \tau_z \rangle$ is $\mathbb{1}_2 \otimes \langle \tau_z \rangle$, i.e., we have to regard the product Hilbert space of the two spins. We can also revert the upper expressions and express $\langle \sigma_z \rangle$, $\langle \tau_z \rangle$, and $\langle \sigma_z \tau_z \rangle$ by the density matrix

$$\begin{aligned} \mathbb{1}_2 \otimes \mathbb{1}_2 &= \rho_{RR,RR}(t) + \rho_{RR,LL}(t) + \rho_{LL,RR}(t) + \rho_{LL,LL}(t) \, , \\ \langle \sigma_z(t) \rangle \otimes \mathbb{1}_2 &= \rho_{RR,RR}(t) + \rho_{RR,LL}(t) - \rho_{LL,RR}(t) - \rho_{LL,LL}(t) \, , \\ \mathbb{1}_2 \otimes \langle \tau_z(t) \rangle &= \rho_{RR,RR}(t) - \rho_{RR,LL}(t) + \rho_{LL,RR}(t) - \rho_{LL,LL}(t) \, , \\ \langle \sigma_z \tau_z(t) \rangle &= \rho_{RR,RR}(t) - \rho_{RR,LL}(t) - \rho_{LL,RR}(t) + \rho_{LL,LL}(t) \, . \end{aligned} \tag{3.1.16}$$

This can be done for the off-diagonal elements of the density matrix, too. For example, $\langle\sigma_x\tau_y(t)\rangle$ is

$$\langle\sigma_x\tau_y(t)\rangle = \mathrm{i}\left[\rho_{LR,LR}(t) - \rho_{LR,RL}(t) + \rho_{RL,LR}(t) - \rho_{RL,RL}(t)\right]. \tag{3.1.17}$$

The restriction for initial states to start in RR is not as strong as might seem. For example, if we start in a mixture of the RR and LL states, we can deduce everything from the case discussed above. This is described in Appendix A.1.

It is convenient to use the Heisenberg picture to derive the time evolution of the expectation values. The time dependence of an operator A in the Heisenberg picture and the corresponding time evolution read

$$A(t) = \mathrm{e}^{\mathrm{i}Ht}\,A\,\mathrm{e}^{-\mathrm{i}Ht} \quad \text{and} \quad \frac{\mathrm{d}}{\mathrm{d}\,t}A(t) = \mathrm{i}[H, A(t)] = \mathrm{i}\,\mathrm{e}^{\mathrm{i}Ht}\,[H, A]\,\mathrm{e}^{-\mathrm{i}Ht}\,, \tag{3.1.18}$$

where $[H, A]$ is the usual commutator. For example, we may calculate $\frac{\mathrm{d}}{\mathrm{d}\,t}\langle\sigma_z\tau_z(t)\rangle$,

$$\frac{\mathrm{d}}{\mathrm{d}\,t}\langle\sigma_z\tau_z(t)\rangle = -\Delta_1\,\langle\sigma_y\tau_z(t)\rangle - \Delta_2\,\langle\sigma_z\tau_y(t)\rangle. \tag{3.1.19}$$

For $\frac{\mathrm{d}}{\mathrm{d}\,t}\langle\sigma_y\tau_z(t)\rangle$ we obtain

$$\frac{\mathrm{d}}{\mathrm{d}\,t}\langle\sigma_y\tau_z(t)\rangle = \Delta_1\,\langle\sigma_z\tau_z(t)\rangle - \Delta_2\,\langle\sigma_y\tau_y(t)\rangle - v_z\,\langle\sigma_x(t)\rangle\,. \tag{3.1.20}$$

Similarly, we obtain for $\frac{\mathrm{d}}{\mathrm{d}\,t}\langle\sigma_y\tau_y(t)\rangle$ the expression

$$\frac{\mathrm{d}}{\mathrm{d}\,t}\langle\sigma_y\tau_y(t)\rangle = \Delta_1\,\langle\sigma_z\tau_y(t)\rangle + \Delta_2\,\langle\sigma_y\tau_z(t)\rangle\,. \tag{3.1.21}$$

It is useful to note that commutators of the form $[\sigma_y\tau_y, \sigma_z\tau_z]$ are zero in the product Hilbert space. At the end, we obtain a set of coupled equations. The full set of coupled equations is written in Appendix A.2. Explicitly, we retain in the case studied here six coupled equations for $\langle\sigma_z\,\tau_z\rangle$ and four coupled equations for $\langle\sigma_z\rangle$ and $\langle\tau_z\rangle$. They can be readily solved in Laplace space.

As an example, we study the coupled equations that we need to solve $\langle\sigma_z\rangle$. The initial conditions are chosen such that

$$\begin{aligned}\langle\sigma_z(t=0)\rangle &= 1\,,\\ \langle\tau_z(t=0)\rangle &= \langle\sigma_z\,\tau_z(t=0)\rangle = 0\,.\end{aligned} \tag{3.1.22}$$

We end up with four coupled equations for $\langle\sigma_z\rangle$:

$$\begin{aligned}\lambda\,\langle\sigma_z(\lambda)\rangle &= 1 - \Delta_1\,\langle\sigma_y(\lambda)\rangle\,,\\ \lambda\,\langle\sigma_y(\lambda)\rangle &= \Delta_1\,\langle\sigma_z(\lambda)\rangle - v_z\,\langle\sigma_x\sigma_z(\lambda)\rangle\,,\\ \lambda\,\langle\sigma_x\sigma_z(\lambda)\rangle &= -\Delta_2\,\langle\sigma_x\sigma_y(\lambda)\rangle - v_z\,\langle\sigma_y(\lambda)\rangle\,,\\ \lambda\,\langle\sigma_x\sigma_y(\lambda)\rangle &= \Delta_2\,\langle\sigma_x\sigma_z(\lambda)\rangle\,.\end{aligned} \tag{3.1.23}$$

Solving them yields the undamped dynamics of, e.g., $\langle\sigma_z(\lambda)\rangle$,

$$\langle\sigma_z(\lambda)\rangle = \frac{\lambda(\lambda^2+\Delta_2^2+v_z^2)}{\lambda^2 v_z^2+(\lambda^2+\Delta_1^2)(\lambda^2+\Delta_2^2)}\,. \tag{3.1.24}$$

Analogously, for $\langle\tau_z(\lambda)\rangle$ and $\langle\sigma_z\tau_z(\lambda)\rangle$ we calculate

$$\begin{aligned}\langle\tau_z(\lambda)\rangle &= \frac{\lambda(\lambda^2+\Delta_1^2+v_z^2)}{\lambda^2 v_z^2+(\lambda^2+\Delta_1^2)(\lambda^2+\Delta_2^2)}\,,\\ \langle\sigma_z\tau_z(\lambda)\rangle &= \frac{(\lambda^2+v_z^2)(\lambda^2+\Delta_1^2+\Delta_2^2+v_z^2)}{\lambda\,(\lambda^2+(\Delta_1+\Delta_2)^2+v_z^2)(\lambda^2+(\Delta_1-\Delta_2)^2+v_z^2)}\,.\end{aligned} \tag{3.1.25}$$

Following this procedure all the other parts can be calculated, too. To simplify the denominators it is useful to recall the definitions from Eq. (3.1.7)

$$\begin{aligned}\Omega_\pm &= \sqrt{(\Delta_1\pm\Delta_2)^2+v_z^2}\,,\\ \Omega = \frac{1}{2}(\Omega_+ + \Omega_-), &\qquad \delta = \frac{1}{2}(\Omega_+ - \Omega_-)\,.\end{aligned} \tag{3.1.26}$$

They satisfy the Vieta relations

$$\begin{aligned}\Omega_+^2+\Omega_-^2 &= 2\,(\Delta_1^2+\Delta_2^2+v_z^2)\,, &\qquad \Omega_+^2\,\Omega_-^2 &= (\Delta_1^2+\Delta_2^2+v_z^2)^2-4\,\Delta_1^2\,\Delta_2^2\,,\\ \Omega^2+\delta^2 &= \Delta_1^2+\Delta_2^2+v_z^2\,, &\qquad \Omega^2\,\delta^2 &= \Delta_1^2\,\Delta_2^2\,.\end{aligned} \tag{3.1.27}$$

Now, using these relations we can rewrite $\langle\sigma_z(\lambda)\rangle$, $\langle\tau_z(\lambda)\rangle$ and $\langle\sigma_z\tau_z(\lambda)\rangle$ to

$$\begin{aligned}\langle\sigma_z(\lambda)\rangle &= \frac{\lambda(\lambda^2+\Delta_2^2+v_z^2)}{(\lambda^2+\Omega^2)(\lambda^2+\delta^2)}\,, \qquad \langle\tau_z(\lambda)\rangle = \frac{\lambda(\lambda^2+\Delta_1^2+v_z^2)}{(\lambda^2+\Omega^2)(\lambda^2+\delta^2)}\,,\\ \langle\sigma_z\tau_z(\lambda)\rangle &= \frac{(\lambda^2+v_z^2)(\lambda^2+\Delta_1^2+\Delta_2^2+v_z^2)}{\lambda\,(\lambda^2+\Omega_+^2)(\lambda^2+\Omega_-^2)}\,.\end{aligned} \tag{3.1.28}$$

We see that the frequencies $\Omega_\pm$, Ω and δ correspond to the zero-temperature eigenfrequencies of the system.

After having solved the equations in Laplace space, we may calculate the probability $\rho_{RR,RR}(t)$ from Eq. (3.1.14) in the time regime. Alternatively, we could use a propagator approach as described in Appendix A.3. We obtain

$$\begin{aligned}\rho_{RR,RR}(t) = \frac{1}{4}\Bigg[&\frac{1}{2}\,(1+\cos\Omega_-\,t)+\frac{1}{2}\,(1+\cos\Omega_+\,t)+\cos\Omega\,t+\cos\delta\,t\\ &+\frac{v_z^2}{\Omega_-^2}\,\frac{1}{2}\,(1-\cos\Omega_-\,t)+\frac{v_z^2}{\Omega_+^2}\,\frac{1}{2}\,(1-\cos\Omega_+\,t)+\frac{v_z^2}{\Omega_-\,\Omega_+}\,(\cos\delta\,t-\cos\Omega\,t)\Bigg]\,.\end{aligned} \tag{3.1.29}$$

Or, ordered by contributions from $\langle\sigma_z(t)\rangle+\langle\tau_z(t)\rangle$ and $\langle\sigma_z\tau_z(t)\rangle$

$$\begin{aligned}\langle\sigma_z(t)\rangle+\langle\tau_z(t)\rangle &= \cos\Omega\,t+\cos\delta\,t+\frac{v_z^2}{\Omega_-\,\Omega_+}\,(\cos\delta\,t-\cos\Omega\,t)\,,\\ \langle\sigma_z\tau_z(t)\rangle &= \frac{1}{2}\,(\cos\Omega_-\,t+\cos\Omega_+\,t)+\frac{v_z^2}{\Omega_-^2}\,\frac{1}{2}\,(1-\cos\Omega_-\,t)+\frac{v_z^2}{\Omega_+^2}\,\frac{1}{2}\,(1-\cos\Omega_+\,t)\,.\end{aligned} \tag{3.1.30}$$

3.2 Two dissipative coupled spins

Now, we are ready to introduce a specific model for the environment. We choose a generalization of the spin-boson Hamiltonian to a second spin. Starting with Eq. (3.1.1) and modeling the environment as uncorrelated baths of harmonic oscillators, we obtain the Hamiltonian for two dissipative coupled spins (cf. Eq. (2.0.1))

$$H = -\frac{\Delta_1}{2}\sigma_x \,-\, \frac{\Delta_2}{2}\tau_x \,-\, \frac{v_z}{2}\sigma_z\tau_z \,-\, \frac{X_1}{2}\sigma_z \,-\, \frac{X_2}{2}\tau_z \,+\, \sum_{\zeta=1,2}\sum_{\alpha}\omega_{\zeta,\alpha}b^\dagger_{\zeta,\alpha}b_{\zeta,\alpha}\,. \quad (3.2.1)$$

The collective bath modes $X_\zeta(t) = \sum_\alpha c_{\zeta,\alpha}[\, b_{\zeta,\alpha}(t) \,+\, b^\dagger_{\zeta,\alpha}(t)\,]$ with $\zeta = 1, 2$ induce fluctuating bias forces acting on the spin system. The double sum at the end of the generalized spin-boson Hamiltonian describes the energy of the disjointed baths of harmonic oscillators. As usual, the fluctuating forces cancel on average, i.e., $\langle X_\zeta(t)\rangle_{\beta_\zeta} = 0$. All the environmental effects are characterized by the power spectrum of the force-force autocorrelation function

$$\begin{aligned} S_{\zeta,\zeta'}(\omega) &= \frac{1}{2}\int_{-\infty}^{\infty}\mathrm{d}t\,\mathrm{e}^{\mathrm{i}\omega t}\,\left\langle X_\zeta(t)X_{\zeta'}(0) \,+\, X_{\zeta'}(0)X_\zeta(t)\right\rangle_{\beta_{\zeta,\zeta'}} \\ &= \delta_{\zeta,\zeta'}S_\zeta(\omega) = \delta_{\zeta,\zeta'}\,J_{\mathrm{lf},\zeta}(\omega)\coth\left(\frac{\beta_\zeta\omega}{2}\right), \end{aligned} \quad (3.2.2)$$

with the spectral density of the coupling

$$J_{\mathrm{lf},\zeta}(\omega) = \sum_\alpha c^2_{\zeta,\alpha}\delta(\omega-\omega_{\zeta,\alpha}) = 2K_\zeta\,\omega\,\mathrm{e}^{-|\omega|/\omega_c}\,, \qquad \zeta = 1,\,2\,. \quad (3.2.3)$$

We have chosen an ohmic bath with an intrinsic high-frequency cutoff ω_c. The influence of one common bath for both spins is discussed in [59, 67, 68]. As long as the spatial distance of the qubits is large enough, the sole effect of a single bath is to renormalize the spin-spin coupling v_z. Also the effect of bath mediated entanglement seems to be irrelevant for most realizable setups [69].

To solve the RDM of the two-spin system with the Feynman-Vernon method we have to analyze the quadruple path integral

$$\rho_{\sigma_\mathrm{f}\sigma'_\mathrm{f},\tau_\mathrm{f}\tau'_\mathrm{f}}(t) = \int \mathcal{D}\sigma\,\mathcal{D}\sigma'\,\mathcal{D}\tau\,\mathcal{D}\tau'\;\mathcal{A}[\sigma]\,\mathcal{A}^*[\sigma']\,\mathcal{A}[\tau]\,\mathcal{A}^*[\tau']\,\mathcal{B}[\sigma,\sigma';\tau,\tau']\,\mathcal{F}[\sigma,\sigma';\tau,\tau']\,. \quad (3.2.4)$$

Every path $\sigma(t'), \sigma'(t'), \tau(t'), \tau'(t')$ is prepared to start in the eigenstate $|R\rangle$ at time $t = 0$. At time t they end up in the final states σ_f, σ'_f, τ_f, $\tau'_\mathrm{f} \in \{|R\rangle, |L\rangle\}$. The functional $\mathcal{A}[\sigma]$ is the bare amplitude for the path $\sigma(t')$ without environment and $\mathcal{B}[\sigma,\sigma';\tau,\tau']$ describes the coupling of the spins among each other. The environmental effects are included in the influence functional $\mathcal{F}[\sigma,\sigma';\tau,\tau']$.

Since each spin is coupled to its own bath, we can factorize the influence functional

$$\mathcal{F}[\sigma,\sigma';\tau,\tau'] \;=\; \mathcal{F}_1[\xi_1,\eta_1]\;\mathcal{F}_2[\xi_2,\eta_2]\,. \quad (3.2.5)$$

Therefore, the functional of each bath is the same as in the spin-boson model for a single bath (cf. Sec. (2.2))

$$\ln \mathcal{F}_\zeta[\xi_\zeta,\eta_\zeta] = \int_0^t \mathrm{d}t' \int_0^{t'} \mathrm{d}t'' \left[\dot{\xi}_\zeta(t') Q'_\zeta(t'-t'') \dot{\xi}_\zeta(t'') \,+\, \mathrm{i}\, \dot{\xi}_\zeta(t') Q''_\zeta(t'-t'') \dot{\eta}_\zeta(t'')\right] \,. \quad (3.2.6)$$

ξ_ζ and η_ζ are the usual symmetric and antisymmetric spin paths,

$$\begin{aligned} \xi_1(t') &= \frac{1}{2}[\sigma(t') - \sigma'(t')] \,, \qquad & \eta_1(t') &= \frac{1}{2}[\sigma(t') + \sigma'(t')] \,, \\ \xi_2(t') &= \frac{1}{2}[\tau(t') - \tau'(t')] \,, \qquad & \eta_2(t') &= \frac{1}{2}[\tau(t') + \tau'(t')] \,. \end{aligned} \quad (3.2.7)$$

The bath correlations $Q_\zeta(t) = Q'_\zeta(t) + \mathrm{i}\, Q''_\zeta(t)$ are the second integral of the force autocorrelation functions $\langle X_\zeta(t) X_\zeta(0)\rangle_\beta$. This correlator reads in the ohmic scaling limit

$$Q_\zeta(t) \;=\; 2K_\zeta \left[\ln\left(\frac{\beta_\zeta \omega_\mathrm{c}}{\pi}\right) + \ln\sinh\left(\frac{\pi|t|}{\beta_\zeta}\right)\right] + \mathrm{i}\pi K_\zeta \,\mathrm{sgn}(t) \,. \quad (3.2.8)$$

K_ζ is the coupling strength for the spin ζ. If we label the sojourn and blip states with charges $\eta_{1,j}$, $\xi_{1,j}$ and $\eta_{2,j}$, $\xi_{2,j}$ for spin 1 and spin 2, respectively, each with the possible values ± 1, we can write the factorized influence functionals in the form

$$\begin{aligned} \mathcal{F}_\zeta^{(n_\zeta)} \;=\; & \exp\Big[-\sum_{j=1}^{n_\zeta} Q'_{\zeta;2j,2j-1}\Big] \exp\Big[-\sum_{j=2}^{n_\zeta}\sum_{k=1}^{j-1} \xi_{\zeta,j}\xi_{\zeta,k}\Lambda_{\zeta;j,k}\Big] \\ & \times \exp\Big[\mathrm{i}\,\pi K_\zeta \sum_{k=0}^{n_\zeta - 1} \xi_{\zeta,k+1}\eta_{\zeta,k}\Big] \,. \end{aligned} \quad (3.2.9)$$

Here, we used the abbreviations $Q_{\zeta;j,k} = Q_\zeta(t_j - t_k)$ and

$$\Lambda_{\zeta;j,k} \;=\; Q'_{\zeta;2j,2k-1} + Q'_{\zeta;2j-1,2k} - Q'_{\zeta;2j,2k} - Q'_{\zeta;2j-1,2k-1} \,. \quad (3.2.10)$$

The first line in (3.2.9) renders the intra- and interblip correlations, where $\Lambda_{\zeta;j,k}$ describes bath correlations between the blip pair $\{j,k\}$ of spin ζ. The influence phase term in the second line is an intrinsic feature of the ohmic scaling limit and describes correlations of sojourns with subsequent blips.

To solve the path integral (3.2.4), it is necessary to examine all possible transition

sequences. They can be parametrized for each spin separately with

$$\begin{aligned}
\eta_1^{(n_1)}(t') &= \sum_{j=0}^{n_1} \eta_{1,j} \left[\Theta(t'-t_{2j}) - \Theta(t'-t_{2j+1})\right] \ , \\
\xi_1^{(n_1)}(t') &= \sum_{j=1}^{n_1} \xi_{1,j} \left[\Theta(t'-t_{2j-1}) - \Theta(t'-t_{2j})\right] \ , \\
\eta_2^{(n_2)}(t') &= \sum_{j=0}^{n_2} \eta_{2,j} \left[\Theta(t'-s_{2j}) - \Theta(t'-s_{2j+1})\right] \ , \\
\xi_2^{(n_2)}(t') &= \sum_{j=1}^{n_2} \xi_{2,j} \left[\Theta(t'-s_{2j-1}) - \Theta(t'-s_{2j})\right] \ .
\end{aligned} \tag{3.2.11}$$

These sequences describe $2n_1$ and $2n_2$ transitions. Since we start and end in a sojourn state, they always have to enclose an even number of transitions. The flips occur at times t_j for spin 1 and at times s_j for spin 2. Each flip of spin ζ has an amplitude $\pm \mathrm{i}\,\Delta_\zeta/2$.

The sum over all transition sequences, i.e., the sum over all possible paths of the quadruple path integral (3.2.4), has to be conducted in the following way:

1. the sum over all possible intermediate sojourn and blip states of the two spins the paths with a given number of transitions can visit
2. the integration for each spin over the time-ordered jumps of these paths
3. the sum over the possible number of transitions the two spins can take, i.e.,

$$\begin{aligned}
\sum_{\text{all paths}} \cdots \ \rightarrow \ & \sum_{n_1=0}^{\infty} \sum_{\{\eta_{1,j}=\pm 1\}} \sum_{\{\xi_{1,j}=\pm 1\}} \int_{t_\mathrm{i}}^{t_\mathrm{f}} \mathrm{d}t_{2n_1} \int_{t_\mathrm{i}}^{t_{2n_1}} \mathrm{d}t_{2n_1-1} \cdots \int_{t_\mathrm{i}}^{t_2} \mathrm{d}t_1 \\
\times \ & \sum_{n_2=0}^{\infty} \sum_{\{\eta_{2,j}=\pm 1\}} \sum_{\{\xi_{2,j}=\pm 1\}} \int_{t_\mathrm{i}}^{t_\mathrm{f}} \mathrm{d}s_{2n_2} \int_{t_\mathrm{i}}^{s_{2n_2}} \mathrm{d}s_{2n_2-1} \cdots \int_{t_\mathrm{i}}^{s_2} \mathrm{d}s_1 \ \cdots .
\end{aligned} \tag{3.2.12}$$

As was outlined before, we want to calculate the system dynamics in an iterative way. Therefore, we need to rewrite the double path sum (3.2.12) as transition sequences for each spin with time-ordered flip times $\{t_j\}$, $\{s_i\}$. These are composed of the 16 possible states shown in Fig. 3.1. The coupling factor $\mathcal{B}$ in Eq. (3.2.4) only contributes, if one spin is diagonal while the other spin is off-diagonal for a period u_j. Otherwise, the coupling factor is unity. We obtain

$$\begin{aligned}
\mathcal{B}[\,j\,] \ &= \ \mathrm{e}^{+\mathrm{i}\,v_z u_j} \ , \qquad \text{for} \qquad j \ \in \ (1,2),\,(2,1),\,(4,3),\,(3,4) \ , \\
\mathcal{B}[\,j\,] \ &= \ \mathrm{e}^{-\mathrm{i}\,v_z u_j} \ , \qquad \text{for} \qquad j \ \in \ (1,4),\,(4,1),\,(2,3),\,(3,2) \ .
\end{aligned} \tag{3.2.13}$$

It is useful to note that the v_z coupling behaves like a mutual bias. This can be seen, if we compare the above form with the bias factor of a single-spin system $\mathrm{e}^{-\mathrm{i}\,\epsilon\,\xi\,\tau_j}$, where ϵ is a bias and τ_j a blip length. Thus, while being off-diagonal, the spin-spin coupling induces a bias for the other spin.

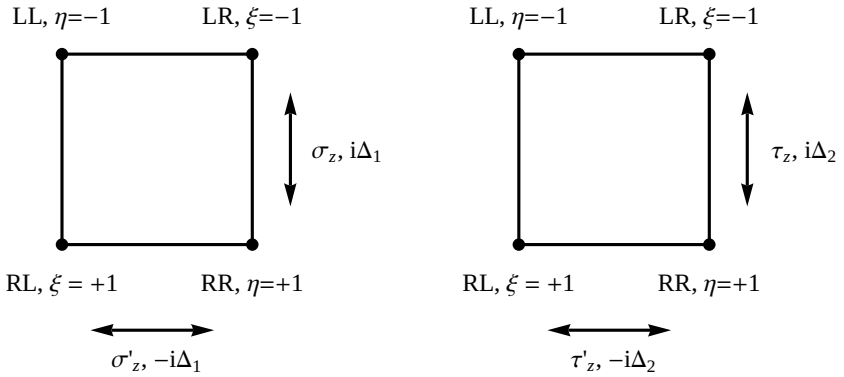

Figure 3.1: States of the density matrix and possible paths for σ_z, σ'_z, τ_z, τ'_z with the corresponding signs. $-\mathrm{i}\,\Delta_\zeta$ for $RL \leftrightarrow RR$ and $LL \leftrightarrow LR$, $+\mathrm{i}\,\Delta_\zeta$ for $RR \leftrightarrow LR$ and $RL \leftrightarrow LL$.

At this point, we have derived an exact formal solution for the RDM of the coupled spin system. An analytic solution of the path sum within all parameter regimes is not possible because of the nonconvolutive form of the bath correlations in the influence functional (3.2.9). Therefore, we will restrict ourselves in the next section to the white-noise regime.

3.3 Markov limit

Following the general specification of the model, we will now restrict ourselves to the high temperature regime of the two baths.

With the scaled temperature $\vartheta_\zeta = 2\pi\, K_\zeta\, T_\zeta$ that drops out naturally from the high temperature limit of Eq. (3.2.2), $S_\zeta(\omega \ll 1/\beta) = 2\vartheta_\zeta/\pi$, the bath correlations $Q_\zeta = Q'_\zeta + \mathrm{i}\, Q''_\zeta$ from Eq. (3.2.8) simplify to

$$Q_\zeta(t) = 2K_\zeta \,\ln\left(\frac{\omega_\mathrm{c}}{2\pi T_\zeta}\right) + \vartheta_\zeta\,|t| + \mathrm{i}\,\pi\, K_\zeta\,\mathrm{sgn}(t)\;. \tag{3.3.1}$$

The time independent term leads to an adiabatic renormalization of the tunneling matrix element due to modes in the frequency range $2\pi T_\zeta < \omega < \omega_\mathrm{c}$. The renormalized temperature-dependent tunneling matrix element together with the phase term reads

$$\bar{\Delta}_\zeta^2 = \Delta_{\zeta,T_\zeta}^2 \cos(\pi K_\zeta)\;, \qquad \text{with} \qquad \Delta_{\zeta,T_\zeta}^2 = (2\pi T_\zeta/\Delta_{\zeta,\mathrm{r}})^{2K_\zeta}\,\Delta_{\zeta,\mathrm{r}}^2\;, \tag{3.3.2}$$

where $\Delta_{\zeta,\mathrm{r}}^{1-K_\zeta} = \Delta_\zeta/\omega_\mathrm{c}^{K_\zeta}$ is the standard renormalized tunneling matrix element for $K < 1$. We tacitly assume for the following that the Δ's are already the renormalized ones. For a non-exponential cutoff for the high frequency modes of the spectral density we refer to [2]. The validity of the high temperature limit leading to Eq. (3.3.1) is given in the parameter range

$$K_\zeta \lesssim 0.3 \qquad \text{and} \qquad \Omega_\pm \lesssim T_\zeta \ll \omega_\mathrm{c}\;, \tag{3.3.3}$$

as will be shown in the following.

For the form (3.3.1) of the bath correlations, the interblip correlations vanish, i.e., $\Lambda_{\zeta;j,k} = 0$ in (3.2.9). Then, the influence phase factors from (3.2.9) simplify to the form

$$\mathcal{F}_{\zeta,\,\mathrm{NIBA}}^{(n_\zeta)} = \prod_{j=1}^{n_\zeta} \exp\left[-Q'_\zeta + \mathrm{i}\,\xi_{\zeta,j}\,\eta_{\zeta,j-1}\,Q''_\zeta\right] \tag{3.3.4}$$

and the NIBA becomes exact. With this simplified form of the influence functional, each term of the RDM becomes a convolution and the path sum is accomplishable.

Remember that the influence functionals for the two spins enter the path integral in a product form (cf. Eq. (3.2.5)). Thus, we obtain correlations between the two spin paths, which appear while one spin is off-diagonal and the other spin makes any even number of transitions. We will give a detailed discussion of these correlations in the next section.

3.4 σ_z

Although we could solve the coupled equations of motion in Appendix A.2 to directly obtain $\langle\sigma_z\rangle$, we choose Eq. (3.1.23) as the starting point. Solving (3.1.23) in an iterative way gives detailed insight into how the system evolves in time. We can deduce which transitions actually contribute to $\langle\sigma_z\rangle$. Thus, solving (3.1.23) iteratively leads to

$$\langle\sigma_z(\lambda)\rangle = \frac{1}{\lambda}\frac{1}{1+\frac{\Delta_1^2}{\lambda^2+v_z^2}}\,\frac{1}{1+\frac{\Delta_1^2\,\Delta_2^2}{(\lambda^2+v_z^2)^2}\,\frac{v_z^2}{\lambda^2}\,\frac{1}{\left(1+\frac{\Delta_1^2}{\lambda^2+v_z^2}\right)\left(1+\frac{\Delta_2^2}{\lambda^2+v_z^2}\right)}}\,. \tag{3.4.1}$$

The first part is due to the spin σ itself. The second part belongs to the correlated transitions of order $\Delta_1^2\,\Delta_2^2$. Within these correlated contribution an arbitrary number of single spin transitions may contribute, which manifests itself in the geometrical series

$$\frac{1}{\left(1+\frac{\Delta_1^2}{\lambda^2+v_z^2}\right)\left(1+\frac{\Delta_2^2}{\lambda^2+v_z^2}\right)}\,. \tag{3.4.2}$$

This can be derived by adding up every possible ordering of $\Delta_1^2\,\Delta_2^2$ (cf. Fig. 3.1). Only those transitions where σ starts and ends in the same diagonal state are relevant (see below). The contributing transition sequences and the corresponding coupling factors are shown in Table 3.1 (cf. Eq. (3.3.4)) After a Laplace transformation, we get an expression for the correlated contributions of order $\Delta_1^2\,\Delta_2^2$,

$$\frac{\Delta_1^2}{4}\,\frac{\Delta_2^2}{4}\,\frac{1}{\lambda^2}\left[4\,\frac{1}{(\lambda-\mathrm{i}\,v_z)^2}+4\,\frac{1}{(\lambda+\mathrm{i}\,v_z)^2}-8\,\frac{1}{(\lambda-\mathrm{i}\,v_z)\,(\lambda+\mathrm{i}\,v_z)}\right], \tag{3.4.3}$$

which is exactly the second part of Eq. (3.4.1),

$$-\frac{v_z^2}{\lambda^2}\,\frac{\Delta_1^2\,\Delta_2^2}{(\lambda^2+v_z^2)^2}\,. \tag{3.4.4}$$

All other sequences do not contribute because there is always a pair which differs only in the sign of the last transition and thus cancels each other (see Table 3.2).

Transition sequences of $\mathcal{O}(\Delta_1^2\,\Delta_2^2)$							Coupling factors			
$\mathrm{i}\,\Delta_1$	$\to$	$\mathrm{i}\,\Delta_2$	$\to$	$\mathrm{i}\,\Delta_2$	$\to$	$\mathrm{i}\,\Delta_1$	$+\mathrm{e}^{\mathrm{i}\,v_z}$	1	$\mathrm{e}^{\mathrm{i}\,v_z}$	1
$\mathrm{i}\,\Delta_1$	$\to$	$\mathrm{i}\,\Delta_2$	$\to$	$-\mathrm{i}\,\Delta_2$	$\to$	$\mathrm{i}\,\Delta_1$	$-\mathrm{e}^{\mathrm{i}\,v_z}$	1	$\mathrm{e}^{-\mathrm{i}\,v_z}$	1
$\mathrm{i}\,\Delta_1$	$\to$	$-\mathrm{i}\,\Delta_2$	$\to$	$\mathrm{i}\,\Delta_2$	$\to$	$\mathrm{i}\,\Delta_1$	$-\mathrm{e}^{\mathrm{i}\,v_z}$	1	$\mathrm{e}^{-\mathrm{i}\,v_z}$	1
$\mathrm{i}\,\Delta_1$	$\to$	$-\mathrm{i}\,\Delta_2$	$\to$	$-\mathrm{i}\,\Delta_2$	$\to$	$\mathrm{i}\,\Delta_1$	$+\mathrm{e}^{\mathrm{i}\,v_z}$	1	$\mathrm{e}^{\mathrm{i}\,v_z}$	1
$-\mathrm{i}\,\Delta_1$	$\to$	$\mathrm{i}\,\Delta_2$	$\to$	$\mathrm{i}\,\Delta_2$	$\to$	$-\mathrm{i}\,\Delta_1$	$+\mathrm{e}^{-\mathrm{i}\,v_z}$	1	$\mathrm{e}^{-\mathrm{i}\,v_z}$	1
$-\mathrm{i}\,\Delta_1$	$\to$	$\mathrm{i}\,\Delta_2$	$\to$	$-\mathrm{i}\,\Delta_2$	$\to$	$-\mathrm{i}\,\Delta_1$	$-\mathrm{e}^{-\mathrm{i}\,v_z}$	1	$\mathrm{e}^{\mathrm{i}\,v_z}$	1
$-\mathrm{i}\,\Delta_1$	$\to$	$-\mathrm{i}\,\Delta_2$	$\to$	$\mathrm{i}\,\Delta_2$	$\to$	$-\mathrm{i}\,\Delta_1$	$-\mathrm{e}^{-\mathrm{i}\,v_z}$	1	$\mathrm{e}^{\mathrm{i}\,v_z}$	1
$-\mathrm{i}\,\Delta_1$	$\to$	$-\mathrm{i}\,\Delta_2$	$\to$	$-\mathrm{i}\,\Delta_2$	$\to$	$-\mathrm{i}\,\Delta_1$	$+\mathrm{e}^{-\mathrm{i}\,v_z}$	1	$\mathrm{e}^{-\mathrm{i}\,v_z}$	1

Table 3.1: Contributing transition sequences of $\mathcal{O}(\Delta_1^2\,\Delta_2^2)$ and the corresponding coupling factors. We also need the sequences with $\Delta_1 \leftrightarrow \Delta_2$. The time variable is suppressed here.

Irrelevant transition sequences of $\mathcal{O}(\Delta_1^2\,\Delta_2^2)$							Coupling factors			
$\mathrm{i}\,\Delta_1$	$\to$	$\mathrm{i}\,\Delta_2$	$\to$	$\mathrm{i}\,\Delta_1$	$\to$	$\mathrm{i}\,\Delta_2$	$+\mathrm{e}^{\mathrm{i}\,v_z}$	1	$\mathrm{e}^{\mathrm{i}\,v_z}$	1
$\mathrm{i}\,\Delta_1$	$\to$	$\mathrm{i}\,\Delta_2$	$\to$	$\mathrm{i}\,\Delta_1$	$\to$	$-\mathrm{i}\,\Delta_2$	$-\mathrm{e}^{\mathrm{i}\,v_z}$	1	$\mathrm{e}^{\mathrm{i}\,v_z}$	1
$\mathrm{i}\,\Delta_1$	$\to$	$-\mathrm{i}\,\Delta_2$	$\to$	$\mathrm{i}\,\Delta_1$	$\to$	$\mathrm{i}\,\Delta_2$	$-\mathrm{e}^{\mathrm{i}\,v_z}$	1	$\mathrm{e}^{-\mathrm{i}\,v_z}$	1
$\mathrm{i}\,\Delta_1$	$\to$	$-\mathrm{i}\,\Delta_2$	$\to$	$\mathrm{i}\,\Delta_1$	$\to$	$-\mathrm{i}\,\Delta_2$	$+\mathrm{e}^{\mathrm{i}\,v_z}$	1	$\mathrm{e}^{-\mathrm{i}\,v_z}$	1

Table 3.2: Non-contributing transition sequences of $\mathcal{O}(\Delta_1^2\,\Delta_2^2)$ and the corresponding coupling factors, which sum up to zero. This always happens for a pair of sequences, which differs only in the sign of the last transition. This is the case for all remaining sequences. The time variable is suppressed here.

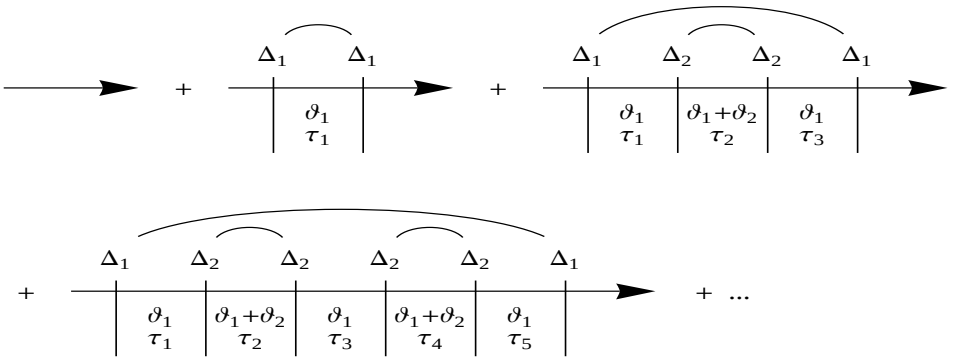

Figure 3.2: Series expansion of contributing transition sequences for $\langle\sigma_z\rangle$. The arrow indicates the time direction. If σ is off-diagonal, the spin τ can make any number of transitions. The system dwells in the blip state j for a time τ_j. See also text for explanation.

Transition sequences of $\mathcal{O}(\Delta_1^2)$					
$-$	RR, RR	$\rightarrow$	RL, RR	$\rightarrow$	RR, RR
$+$	RR, RR	$\rightarrow$	RL, RR	$\rightarrow$	LL, RR
$-$	RR, RR	$\rightarrow$	LR, RR	$\rightarrow$	RR, RR
$+$	RR, RR	$\rightarrow$	LR, RR	$\rightarrow$	LL, RR

Table 3.3: Contributing transition sequences of $\mathcal{O}(\Delta_1^2)$. Shown are the states of the density matrix and the corresponding sign of the contribution.

Transition sequences of $\mathcal{O}(\Delta_1^2\Delta_2^2)$								
$+$	RR, RR	$\rightarrow$	RL, RR	$\rightarrow$	RL, LR	$\rightarrow$	RL, RR	$\rightarrow$	RR, RR
$-$	RR, RR	$\rightarrow$	RL, RR	$\rightarrow$	RL, LR	$\rightarrow$	RL, RR	$\rightarrow$	LL, RR
$-$	RR, RR	$\rightarrow$	RL, RR	$\rightarrow$	RL, LR	$\rightarrow$	RL, LL	$\rightarrow$	RR, LL
$+$	RR, RR	$\rightarrow$	RL, RR	$\rightarrow$	RL, LR	$\rightarrow$	RL, LL	$\rightarrow$	LL, LL
$+$	RR, RR	$\rightarrow$	LR, RR	$\rightarrow$	LR, RL	$\rightarrow$	LR, RR	$\rightarrow$	RR, RR
$-$	RR, RR	$\rightarrow$	LR, RR	$\rightarrow$	LR, RL	$\rightarrow$	LR, RR	$\rightarrow$	LL, RR
$-$	RR, RR	$\rightarrow$	LR, RR	$\rightarrow$	LR, RL	$\rightarrow$	LR, LL	$\rightarrow$	RR, LL
$+$	RR, RR	$\rightarrow$	LR, RR	$\rightarrow$	LR, RL	$\rightarrow$	LR, LL	$\rightarrow$	LL, LL
$+$	RR, RR	$\rightarrow$	LR, RR	$\rightarrow$	LR, LR	$\rightarrow$	LR, RR	$\rightarrow$	RR, RR
$-$	RR, RR	$\rightarrow$	LR, RR	$\rightarrow$	LR, LR	$\rightarrow$	LR, RR	$\rightarrow$	LL, RR
$-$	RR, RR	$\rightarrow$	LR, RR	$\rightarrow$	LR, LR	$\rightarrow$	LR, LL	$\rightarrow$	RR, LL
$+$	RR, RR	$\rightarrow$	LR, RR	$\rightarrow$	LR, LR	$\rightarrow$	LR, LL	$\rightarrow$	LL, LL

Table 3.4: Contributing transition sequences of $\mathcal{O}(\Delta_1^2\Delta_2^2)$. Shown are the states of the density matrix and the corresponding sign of the contribution.

Now we can proceed and include the bath-induced damping (cf. Fig. 3.2). In the Markov limit we get a shift of λ to $\lambda + \vartheta_1$ if the first spin dwells in a blip state for a time τ_j. A shift of ϑ_2 occurs correspondingly, if the second spin dwells in a blip state for a time τ_j. And finally, if both spins are in a blip state, we obtain a shift of $\vartheta_1 + \vartheta_2$ (cf. Eq. (3.3.4)). We have four possibilities for the transitions of order Δ_1^2. These are $\mathrm{i}\,\Delta_1\,\mathrm{i}\,\Delta_1$, $-\mathrm{i}\,\Delta_1(-\mathrm{i}\,\Delta_1)$, $-\mathrm{i}\,\Delta_1\,\mathrm{i}\,\Delta_1$ and $\mathrm{i}\,\Delta_1(-\mathrm{i}\,\Delta_1)$. The lowest order contribution to $\langle\sigma_z\rangle$ is thus given by the sequences shown in Table 3.3. Considering Eq. (3.1.16), we get

$$-\frac{\Delta_1}{2}\left(\frac{2}{\lambda+\vartheta_1+\mathrm{i}\,v_z}+\frac{2}{\lambda+\vartheta_1-\mathrm{i}\,v_z}\right)\frac{\Delta_1}{2}\frac{1}{\lambda} \;=\; -\frac{\lambda+\vartheta_1}{\lambda}\,\frac{\Delta_1^2}{(\lambda+\vartheta_1)^2+v_z^2}\,. \tag{3.4.5}$$

This matches, besides a factor $1/\lambda$, with the symmetric kernel of the spin-boson model in Eq. (2.3.7). There are 16 sequences in order $\Delta_1^2\,\Delta_2^2$, which are shown in Table 3.4.

Together with Eq. (3.1.16) the contribution of order $\Delta_1^2\,\Delta_2^2$ reads

$$\begin{aligned}
&4\Bigg(\frac{\Delta_1}{2}\,\frac{1}{\lambda+\vartheta_1+\mathrm{i}\,v_z}\,\frac{\Delta_2}{2}\,\frac{1}{\lambda+\vartheta_1+\vartheta_2}\,\frac{\Delta_2}{2}\,\frac{1}{\lambda+\vartheta_1+\mathrm{i}\,v_z}\,\frac{\Delta_1}{2}\,\frac{1}{\lambda}\\
&\quad+\frac{\Delta_1}{2}\,\frac{1}{\lambda+\vartheta_1-\mathrm{i}\,v_z}\,\frac{\Delta_2}{2}\,\frac{1}{\lambda+\vartheta_1+\vartheta_2}\,\frac{\Delta_2}{2}\,\frac{1}{\lambda+\vartheta_1-\mathrm{i}\,v_z}\,\frac{\Delta_1}{2}\,\frac{1}{\lambda}\\
&\quad-\frac{\Delta_1}{2}\,\frac{1}{\lambda+\vartheta_1-\mathrm{i}\,v_z}\,\frac{\Delta_2}{2}\,\frac{1}{\lambda+\vartheta_1+\vartheta_2}\,\frac{\Delta_2}{2}\,\frac{1}{\lambda+\vartheta_1+\mathrm{i}\,v_z}\,\frac{\Delta_1}{2}\,\frac{1}{\lambda}\\
&\quad-\frac{\Delta_1}{2}\,\frac{1}{\lambda+\vartheta_1+\mathrm{i}\,v_z}\,\frac{\Delta_2}{2}\,\frac{1}{\lambda+\vartheta_1+\vartheta_2}\,\frac{\Delta_2}{2}\,\frac{1}{\lambda+\vartheta_1-\mathrm{i}\,v_z}\,\frac{\Delta_1}{2}\,\frac{1}{\lambda}\Bigg)\\
&=-\frac{\lambda+\vartheta_1}{\lambda}\,\frac{\Delta_1^2}{(\lambda+\vartheta_1)^2+v_z^2}\,\frac{v_z^2}{(\lambda+\vartheta_1)^2+v_z^2}\,\frac{\Delta_2^2}{(\lambda+\vartheta_1)(\lambda+\vartheta_1+\vartheta_2)}\,.
\end{aligned}\tag{3.4.6}$$

Consecutive calculation of higher orders reveals a geometrical series and we finally derive for $\langle\sigma_z(\lambda)\rangle$,

$$\langle\sigma_z(\lambda)\rangle=\frac{1}{\lambda}\,\frac{1}{1+\frac{\lambda+\vartheta_1}{\lambda}\,\frac{\Delta_1^2}{(\lambda+\vartheta_1)^2+v_z^2}\,A}\,,\tag{3.4.7}$$

with

$$A=\frac{(\lambda+\vartheta_1)\,\{(\lambda+\vartheta_1+\vartheta_2)\,[(\lambda+\vartheta_1)^2+v_z^2)]+(\lambda+\vartheta_1)\,\Delta_2^2\}+v_z^2\,\Delta_2^2}{(\lambda+\vartheta_1)\,[(\lambda+\vartheta_1+\vartheta_2)\,[(\lambda+\vartheta_1)^2+v_z^2)]+(\lambda+\vartheta_1)\,\Delta_2^2]}\,.\tag{3.4.8}$$

Until now, we did not include influence phase factors arising from blips interacting with preceding sojourns (see Eq. (3.3.4) and Fig. 3.2). These phase factors lead to additional contributions to $\langle\sigma_z(\lambda)\rangle$. A sophisticated way to include these phase factors is to rewrite the coupled equations of motion by identifying the expectation values with the corresponding entries in the RDM, as in the Eqs. (3.1.14) – (3.1.17). This is shown in Appendix A.2. However, we will first discuss one of the contributions in detail and then use the generalized coupled equations of motion to obtain the full result. This gives some additional insight into the internal dynamics.

The first contribution does not change,

$$\mathcal{K}_1(\lambda)=\frac{1}{\lambda}\,.\tag{3.4.9}$$

The second contribution, corresponding to the transition sequences from Table 3.3, now reads

$$\begin{aligned}
\mathcal{K}_2(\lambda)&=-\frac{1}{\lambda^2}\Delta_1^2\frac{1}{2}\int_0^\infty \mathrm{d}\tau_1\,\mathrm{e}^{-\lambda\,\tau_1}\,\mathrm{e}^{-\vartheta_1\,\tau_1}\,\left[\mathrm{e}^{\mathrm{i}\,\pi\,K_1+\mathrm{i}\,v_z\,\tau_1}+\mathrm{e}^{-\mathrm{i}\,\pi\,K_1-\mathrm{i}\,v_z\,\tau_1}\right]\\
&=-\frac{1}{\lambda^2}\Delta_1^2\int_0^\infty \mathrm{d}\tau_1\,\cos(\pi\,K_1+v_z\,\tau_1)\,\mathrm{e}^{-(\lambda+\vartheta_1)\,\tau_1}\,.
\end{aligned}\tag{3.4.10}$$

We obtain in order $\Delta_1^2\,\Delta_2^2$, i.e., for the transition sequences of Table 3.4

$$\begin{aligned}\mathcal{K}_3(\lambda) =& \frac{1}{\lambda^2}\,\Delta_1^2\,\Delta_2^2\,\frac{1}{2}\int_0^\infty \mathrm{d}\tau_1\,\mathrm{d}\tau_2\,\mathrm{d}\tau_3\,\mathrm{e}^{-\lambda(\tau_1+\tau_2+\tau_3)}\,\mathrm{e}^{-\vartheta_1(\tau_1+\tau_2+\tau_3)}\,\mathrm{e}^{-\vartheta_2\,\tau_2}\\ &\times\cos(\pi\,K_2)\,[\cos(\pi\,K_1+v_z\,\tau_1+v_z\,\tau_3)-\cos(\pi\,K_1+v_z\,\tau_1-v_z\,\tau_3)]\\ =& -\frac{1}{\lambda^2}\,\Delta_1^2\,\Delta_2^2\int_0^\infty \mathrm{d}\tau_1\,\mathrm{d}\tau_2\,\mathrm{d}\tau_3\,\mathrm{e}^{-\lambda(\tau_1+\tau_2+\tau_3)}\,\mathrm{e}^{-\vartheta_1(\tau_1+\tau_2+\tau_3)}\,\mathrm{e}^{-\vartheta_2\,\tau_2}\\ &\times\cos(\pi\,K_2)\,\sin(\pi\,K_1+v_z\,\tau_1)\,\sin(v_z\,\tau_3)\,.\end{aligned} \tag{3.4.11}$$

Higher orders, i.e., $\Delta_1^2\,\Delta_2^{2\,n+2}$ with $n=1,2,\ldots$, can be expressed as $\mathcal{K}_3(\lambda)$ times a factor which increases with the power of n,

$$\mathcal{K}_{n+3} = (-1)^n\mathcal{K}_3(\lambda)\,\left(\frac{(\lambda+\vartheta_1)\,\Delta_2^2\,\cos(\pi\,K_2)}{(\lambda+\vartheta_1+\vartheta_2)\,[(\lambda+\vartheta_1)^2+v_z^2]}\right)^n\,. \tag{3.4.12}$$

Introducing the kernels

$$\begin{aligned}k_1^{(+)}(\lambda) &\equiv -\frac{\Delta_1^2}{\lambda}\int_0^\infty \mathrm{d}\tau\,\mathrm{e}^{-(\lambda+\vartheta_1)\,\tau}\,\cos(\pi\,K_1+v_z\,\tau)\,,\\ k_1^{(-)}(\lambda) &\equiv -\frac{\Delta_1^2}{\lambda}\int_0^\infty \mathrm{d}\tau\,\mathrm{e}^{-(\lambda+\vartheta_1)\,\tau}\,\sin(v_z\,\tau+\pi\,K_1)\,,\end{aligned} \tag{3.4.13}$$

we can sum up all contributions

$$\begin{aligned}\mathcal{K}(\lambda) &= \frac{1}{\lambda}\left\{1+k_1^{(+)}+\lambda\,\mathcal{K}_3(\lambda)\,\left[1-\frac{(\lambda+\vartheta_1)\,\Delta_2^2\,\cos(\pi\,K_2)}{(\lambda+\vartheta_1+\vartheta_2)\,[(\lambda+\vartheta_1)^2+v_z^2]}\pm\ldots\right]\right\}\\ &= \frac{1}{\lambda}\left\{1+k_1^{(+)}+\lambda\,\mathcal{K}_3(\lambda)\,\frac{1}{1+\frac{(\lambda+\vartheta_1)\,\Delta_2^2\,\cos(\pi\,K_2)}{(\lambda+\vartheta_1+\vartheta_2)\,[(\lambda+\vartheta_1)^2+v_z^2]}}\right\}\\ &= \frac{1}{\lambda}\Bigg\{1+k_1^{(+)}+k_1^{(-)}\\ &\quad\times\frac{v_z\,\Delta_2^2\,\cos(\pi\,K_2)}{(\lambda+\vartheta_1+\vartheta_2)\,[(\lambda+\vartheta_1)^2+v_z^2]+\Delta_2^2\,\cos(\pi\,K_2)\,(\lambda+\vartheta_1)}\Bigg\}\,.\end{aligned} \tag{3.4.14}$$

Now it is convenient to split this expression into one part that is symmetric in v_z and another part that is antisymmetric in v_z,

$$\begin{aligned}C(\lambda) &= k_1^{(+)}+k_1^{(-)}\,\frac{v_z\,\Delta_2^2\,\cos(\pi\,K_2)}{(\lambda+\vartheta_1+\vartheta_2)\,[(\lambda+\vartheta_1)^2+v_z^2]+\Delta_2^2\,\cos(\pi\,K_2)\,(\lambda+\vartheta_1)}\,,\\ C(\lambda) &= C^{(s)}(\lambda)+C^{(a)}(\lambda)\,.\end{aligned} \tag{3.4.15}$$

Using standard trigonometric relations

$$\begin{aligned}\cos(a+b) &= \cos(a)\cos(b)-\sin(a)\sin(b)\,,\\ \sin(a+b) &= \sin(a)\cos(b)+\cos(a)\sin(b)\,,\end{aligned} \tag{3.4.16}$$

we get

$$\begin{aligned} C^{(s)}(\lambda) =& -\cos(\pi K_1)\, k_1^{(\mathrm{s})}(\lambda) - \cos(\pi K_1) \\ &\times k_1^{(\mathrm{a})}(\lambda)\, \frac{v_z\, \Delta_2^2\, \cos(\pi K_2)}{(\lambda+\vartheta_1+\vartheta_2)\, [(\lambda+\vartheta_1)^2+v_z^2] + \Delta_2^2\, \cos(\pi K_2)\, (\lambda+\vartheta_1)}\,, \\ C^{(a)}(\lambda) =& \sin(\pi K_1)\, k_1^{(\mathrm{a})}(\lambda) - \sin(\pi K_1) \\ &\times k_1^{(\mathrm{s})}(\lambda)\, \frac{v_z\, \Delta_2^2\, \cos(\pi K_2)}{(\lambda+\vartheta_1+\vartheta_2)\, [(\lambda+\vartheta_1)^2+v_z^2] + \Delta_2^2\, \cos(\pi K_2)\, (\lambda+\vartheta_1)}\,, \end{aligned} \tag{3.4.17}$$

with

$$\begin{aligned} k_1^{(\mathrm{s})}(\lambda) &= \frac{\Delta_1^2}{\lambda} \int_0^\infty \mathrm{d}\tau\, \mathrm{e}^{-(\lambda+\vartheta_1)\,\tau}\, \cos(v_z\,\tau) = \frac{\Delta_1^2}{\lambda}\, \frac{\lambda+\vartheta_1}{(\lambda+\vartheta_1)^2+v_z^2}\,, \\ k_1^{(\mathrm{a})}(\lambda) &= \frac{\Delta_1^2}{\lambda} \int_0^\infty \mathrm{d}\tau\, \mathrm{e}^{-(\lambda+\vartheta_1)\,\tau}\, \sin(v_z\,\tau) = \frac{\Delta_1^2}{\lambda}\, \frac{v_z}{(\lambda+\vartheta_1)^2+v_z^2}\,. \end{aligned} \tag{3.4.18}$$

The kernels $k_1^{(\mathrm{s})}(\lambda)$ and $k_1^{(\mathrm{a})}(\lambda)$ are, besides a factor $1/\lambda$, the symmetric and antisymmetric kernels for a single spin, which were already introduced in Eq. (2.3.7) and (2.3.8). Here, they describe the dynamics of one spin, while the other spin is fixed. We see again that the spin-spin coupling behaves like a mutual bias.

$C(\lambda)$ is still of order Δ_1^2. The summation over all higher orders results in

$$\frac{1}{\lambda}\left\{1+\frac{C^{(s)}(\lambda)+C^{(a)}(\lambda)}{1-C^{(s)}(\lambda)}\right\} = \frac{1}{\lambda}\,\frac{1+C^{(a)}(\lambda)}{1-C^{(s)}(\lambda)}\,. \tag{3.4.19}$$

This result only includes one additional antisymmetric contribution due to the influence phase factors. With the generalized form of the coupled equations of motion given in Appendix A.2, we obtain the complete form of $\langle\sigma_z(\lambda)\rangle$. We get with (A.2.8)

$$\begin{aligned} \langle\sigma_z(\lambda)\rangle &= N(\lambda)/D(\lambda)\,, \\ N(\lambda) &= \pi K_1 v_z \Delta_1^2 \Big\{ \Delta_1^2 \left((\lambda+\vartheta_2)\,(\lambda+\vartheta_1+\vartheta_2) - \Delta_2^2\right) + (\lambda+\vartheta_1+\vartheta_2)\left[v_z^2\,(\lambda+\vartheta_1+\vartheta_2)\right. \\ &\quad \left. + (\lambda+\vartheta_2)\left((\lambda+\vartheta_2)\,(\lambda+\vartheta_1+\vartheta_2) - \Delta_2^2\right)\right] \Big\} + \Big[v_z^2\,(\lambda+\vartheta_1+\vartheta_2) \\ &\quad + (\lambda+\vartheta_1)\left(\Delta_2^2 + (\lambda+\vartheta_1)\,(\lambda+\vartheta_1+\vartheta_2)\right)\Big] \Big[\Delta_1^2\left(\Delta_2^2 + \lambda\,(\lambda+\vartheta_2)\right) \\ &\quad + (\lambda+\vartheta_1+\vartheta_2)\left(\lambda v_z^2 + (\lambda+\vartheta_2)\left(\Delta_2^2 + \lambda\,(\lambda+\vartheta_2)\right)\right)\Big]\,, \\ D(\lambda) &= \Big[\Delta_1^2\left(\Delta_2^2 + \lambda\,(\lambda+\vartheta_2)\right) + (\lambda+\vartheta_1+\vartheta_2)\left(\Delta_2^2\,(\lambda+\vartheta_2) + \lambda\left(v_z^2 + (\lambda+\vartheta_2)^{\,2}\right)\right)\Big] \\ &\quad \times \Big\{\Delta_1^2\left(\Delta_2^2 + (\lambda+\vartheta_1)\,(\lambda+\vartheta_1+\vartheta_2)\right) + \lambda\big[v_z^2\,(\lambda+\vartheta_1+\vartheta_2) \\ &\quad + (\lambda+\vartheta_1)\left(\Delta_2^2 + (\lambda+\vartheta_1)\,(\lambda+\vartheta_1+\vartheta_2)\right)\big]\Big\}\,. \end{aligned} \tag{3.4.20}$$

The denominator $D(\lambda)$ is of order eight in λ and can be factorized into a product of two fourth order polynomials. The dynamics of $\langle\sigma_z(\lambda)\rangle$ is completely determined by the eight zeros of the denominator and the corresponding amplitudes. In leading order of the bath coupling and/or low temperature only four of the eight amplitudes have a non-vanishing weight (see next subsection).

The thermal equilibrium state of $\langle\sigma_z(t)\rangle$ for $t \to \infty$ is zero in accordance with the Boltzmann equilibrium value of Eq. (3.1.10). If we set $\Delta_2 = 0$, the spin-spin coupling v_z takes the role of a bias and we expect to obtain the result of Eq. (2.3.9). This is the case, as can be easily shown.

The result for $\langle\tau_z(\lambda)\rangle$ is the same as for $\langle\sigma_z(\lambda)\rangle$ but with $\vartheta_1 \leftrightarrow \vartheta_2$, $K_1 \leftrightarrow K_2$ and $\Delta_1 \leftrightarrow \Delta_2$. We have thus derived an analytical result for $\langle\sigma_z(\lambda)\rangle$ (and $\langle\tau_z(\lambda)\rangle$) in the Markov-regime, which is valid in the parameter range of (3.3.3).

3.4.1 Low temperature and one-boson self-energy

Here, we want to calculate the damping rates in a systematic low temperature approximation. In a second step we will derive the one-boson self-energy and expand the low temperature approximation to the quantum-noise regime. Below the parameter range given in (3.3.3), i.e., in the quantum-noise regime, the damping rates are not properly described by a linear temperature dependence. Thus, for temperatures below $\Omega_\pm$ corrections have to be applied. For example, the rates have to adopt a non-zero value for zero temperature because the baths can always absorb energy from the system. This also follows from a perturbative treatment of this regime (see Chapter 4). Afterwards we compare the results for $\langle\sigma_z\rangle$ in the limit $\Delta_2 \to 0$ with the spin-boson results that we derived earlier in Section 2.4.

The low-temperature rates within the Markov-regime can be obtained by performing a series expansion of the zeros of the denominator of $\langle\sigma_z(\lambda)\rangle$ from Eq. (3.4.20) up to first order in the temperatures ϑ_1 and ϑ_2. There is a superposition of four damped oscillations with frequencies

$$\begin{aligned} \lambda_{1,2} &= \pm\mathrm{i}\,\delta - \kappa_1\ , \quad \lambda_{3,4} = \pm\mathrm{i}\,\Omega - \kappa_2\ , \\ \lambda_{5,6} &= \pm\mathrm{i}\,\delta - \kappa_3\ , \quad \lambda_{7,8} = \pm\mathrm{i}\,\Omega - \kappa_4\ . \end{aligned} \tag{3.4.21}$$

The respective dephasing rates read

$$\begin{aligned} \kappa_1 &= \frac{\Omega^2 + \Delta_1^2 - 2\,\delta^2}{2\,(\Omega^2 - \delta^2)}\,\vartheta_1 + \frac{\Omega^2 - \Delta_2^2}{2\,(\Omega^2 - \delta^2)}\,\vartheta_2\,, \\ \kappa_2 &= \frac{2\,\Omega^2 - \Delta_1^2 - \delta^2}{2\,(\Omega^2 - \delta^2)}\,\vartheta_1 + \frac{\Delta_2^2 - \delta^2}{2\,(\Omega^2 - \delta^2)}\,\vartheta_2\,, \\ \kappa_3 &= \frac{\Omega^2 + \Delta_2^2 - 2\,\delta^2}{2\,(\Omega^2 - \delta^2)}\,\vartheta_2 + \frac{\Omega^2 - \Delta_1^2}{2\,(\Omega^2 - \delta^2)}\,\vartheta_1\,, \\ \kappa_4 &= \frac{2\,\Omega^2 - \Delta_2^2 - \delta^2}{2\,(\Omega^2 - \delta^2)}\,\vartheta_2 + \frac{\Delta_1^2 - \delta^2}{2\,(\Omega^2 - \delta^2)}\,\vartheta_1\,. \end{aligned} \tag{3.4.22}$$

Assuming that we have identical baths, we get for the amplitudes in order $\mathcal{O}(1/T)$ (remember that we still are in the Markov-regime and that $1/T$ is a small parameter)

$$\begin{aligned}
\mathrm{Res}\left[\sigma_z(\lambda_{1,2})\right] &= \frac{\Delta_2^2+v_z^2-\delta^2}{2(\Omega^2-\delta^2)} - \frac{v_z}{2T}\frac{\Delta_1^2\,(\Omega^2-\Delta_2^2)}{(\Omega^2-\delta^2)\,(\Delta_1^2-\Delta_2^2)}\,,\\
\mathrm{Res}\left[\sigma_z(\lambda_{3,4})\right] &= \frac{\Omega^2-\Delta_2^2-v_z^2}{2(\Omega^2-\delta^2)} - \frac{v_z}{2T}\frac{\Delta_1^2\,(\Delta_2^2-\delta^2)}{(\Omega^2-\delta^2)\,(\Delta_1^2-\Delta_2^2)}\,,\\
\mathrm{Res}\left[\sigma_z(\lambda_{5,6})\right] &= \frac{v_z}{2T}\frac{\Delta_1^2\,(\Omega^2-\Delta_2^2)}{(\Omega^2-\delta^2)\,(\Delta_1^2-\Delta_2^2)}\,,\\
\mathrm{Res}\left[\sigma_z(\lambda_{7,8})\right] &= \frac{v_z}{2T}\frac{\Delta_1^2\,(\Delta_2^2-\delta^2)}{(\Omega^2-\delta^2)\,(\Delta_1^2-\Delta_2^2)}\,.
\end{aligned} \tag{3.4.23}$$

Then, the dynamics of $\langle\sigma_z(t)\rangle$ reads

$$\begin{aligned}
\langle\sigma_z(t)\rangle = {}& 2\,\left\{\mathrm{Res}\left[\sigma_z(\lambda_{1,2})\right]\mathrm{e}^{-\kappa_1 t} + \mathrm{Res}\left[\sigma_z(\lambda_{5,6})\right]\mathrm{e}^{-\kappa_3 t}\right\}\cos(\delta\,t)\\
&+ 2\,\left\{\mathrm{Res}\left[\sigma_z(\lambda_{3,4})\right]\mathrm{e}^{-\kappa_2 t} + \mathrm{Res}\left[\sigma_z(\lambda_{7,8})\right]\mathrm{e}^{-\kappa_4 t}\right\}\cos(\Omega\,t)\,.
\end{aligned} \tag{3.4.24}$$

In leading order of the low-temperature and/or weak bath-coupling regime only four of the eight amplitudes in (3.4.23) have a non-vanishing weight.

As the next step, we want to generalize the temperature dependence for low temperature and weak damping, i.e., for the quantum-noise regime [2, 30]. The necessary steps are quite similar to the single-spin case in Section 2.4. In a systematic weak damping approximation the interblip correlations are included to first order in the correlation strength. For low temperatures the Markov assumption is no more valid and we have to consider the full bath correlation function

$$S_{1,2}(\omega) = J_{\mathrm{lf}}(\omega)\coth(\beta_{1,2}\,\omega/2), \tag{3.4.25}$$

with $J_{\mathrm{lf}}(\omega) = 2\,K_{1,2}\,\omega$ the low-frequency part of the spectral density. For high temperatures $S_{1,2}(\omega)$ reduces to the Markov expressions $2\vartheta_{1,2}/\pi$. Furthermore, we have to sum over all irreducible multiblip diagrams up to order $\Delta_{1,2}^4$ in which two blips interact via a one-boson exchange. Between these two blips any number of noninteracting and uncorrelated transitions can occur.

First of all, we have to consider every possible transition from the 16 initial states to the 16 final states, which gives us 256 possible propagators. As the second step, we have to account for interactions between the first and the fourth blip, the first with the third, the second with the fourth, and finally the second with the third blip. The second and third case are equal because of symmetry. The interaction of the second and the third blip is schematically shown in Fig. 3.3 for the coupling with bath 1. The result of the interaction between the first and the fourth blip is

$$-\frac{\Delta_1^2\,[\Delta_1^4 + 2\,\Delta_1^2(\lambda_\omega^2-\Delta_2^2) + (\lambda_\omega^2+\Delta_2^2)^2 + v_z^2(\lambda_\omega^2+\Delta_1^2+\Delta_2^2)]}{\lambda^2\,\lambda_\omega\,[\lambda_\omega^2+(\Delta_1-\Delta_2)^2+v_z^2]\,[\lambda_\omega^2+(\Delta_1+\Delta_2)^2+v_z^2]}\,. \tag{3.4.26}$$

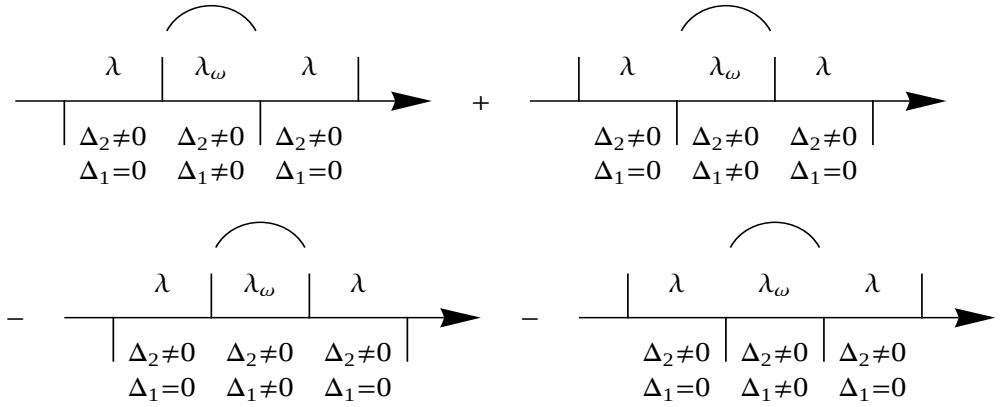

Figure 3.3: Example for systematic weak damping approximation. The up and down lines denote the different paths in the charge picture. Every line stands for a transition of the σ-spin. An up (down) line would be a positive (negative) charge, i.e., in Fig. 3.1 we would be in the state RL (LR). The correlated part is characterized by $\lambda_\omega = \lambda + \mathrm{i}\,\omega$. The notation $\Delta_{1,2} \neq 0$ ($\Delta_{1,2} = 0$) indicates that there is any (no) number of transitions allowed between the two charges. The arrow defines the time direction.

We obtain for the interaction of the first with the third and the second with the fourth blip

$$\frac{v_z^2\,\Delta_1^4\,[v_z^2\,\lambda + \Delta_1^2\,\lambda + \lambda\,\lambda_\omega^2 - \Delta_2^2(\lambda + 2\lambda_\omega)]}{\lambda^3(v_z^2 + \Delta_2^2 + \lambda^2)\lambda_\omega\,[v_z^2 + (\Delta_1 - \Delta_2)^2 + \lambda_\omega^2]\,[v_z^2 + (\Delta_1 + \Delta_2)^2 + \lambda_\omega^2]} \tag{3.4.27}$$

and the interaction of the second with the third blip leads to

$$N/D \tag{3.4.28}$$

with

$$\begin{aligned} N = &- v_z^2\,\Delta_1^4 \Big\{ v_z^4\,\lambda^2 + v_z^2\big(\Delta_1^2\,\lambda^2 + 2\,\lambda^2\,\lambda_\omega^2 + \Delta_2^2(\lambda^2 - 2\,\lambda\,\lambda_\omega - \lambda_\omega^2)\big) \\ &+ \lambda_\omega\Big[\Delta_1^2\big(\Delta_2^2(2\,\lambda - \lambda_\omega) + \lambda^2\,\lambda_\omega\big) - (\Delta_2^2 + \lambda_\omega^2)\big(-\lambda^2\,\lambda_\omega + \Delta_2^2(2\,\lambda + \lambda_\omega)\big)\Big]\Big\} \\ D = &\ \lambda^4(v_z^2 + \Delta_2^2 + \lambda^2)^2\lambda_\omega(v_z^2 + (\Delta_1 - \Delta_2)^2 + \lambda_\omega^2)(v_z^2 + (\Delta_1 + \Delta_2)^2 + \lambda_\omega^2)\,. \end{aligned} \tag{3.4.29}$$

The shift of $\lambda \to \lambda_\omega = \lambda + \mathrm{i}\,\omega$ is due to the correlation between the outer charges. We can calculate the self-energy via the residues of the poles in ω and summing up the expressions (3.4.26) – (3.4.29) (cf. Section 2.4). Matching the self-energy in the high temperature limit with the known result ϑ_1 for the corresponding eigenfrequencies Ω and δ of the system we can identify the generalized temperatures

$$\theta_1^{(\Omega)} = \frac{\pi}{2}\,\frac{2\,(\Omega^2 - \Delta_1^2)S_1(\delta) + (\Delta_1^2 - \delta^2)S_1(\Omega)}{2\Omega^2 - \Delta_1^2 - \delta^2} \tag{3.4.30}$$

and

$$\theta_1^{(\delta)} = \frac{\pi}{2} \frac{(\Omega^2 - \Delta_1^2) S_1(\delta) + 2(\Delta_1^2 - \delta^2) S_1(\Omega)}{\Omega^2 + \Delta_1^2 - 2\delta^2} \,. \tag{3.4.31}$$

The generalization for ϑ_2 is similar, e.g., in Fig. 3.3 we have to interchange Δ_1 with Δ_2. Eventually, only NIBA terms contribute and the generalization reads

$$\theta_2^{(\Omega)} = \frac{\pi}{2} S_2(\Omega) \qquad \text{and} \qquad \theta_2^{(\delta)} = \frac{\pi}{2} S_2(\delta) \,. \tag{3.4.32}$$

Finally, we have derived the generalization of the dephasing rates (3.4.22) to the white-noise regime. These are

$$\begin{aligned} \kappa_1 &= \frac{\Omega^2 + \Delta_1^2 - 2\,\delta^2}{2\,(\Omega^2 - \delta^2)}\, \theta_1^{(\delta)} + \frac{\Omega^2 - \Delta_2^2}{2\,(\Omega^2 - \delta^2)}\, \theta_2^{(\delta)} \,, \\ \kappa_2 &= \frac{2\,\Omega^2 - \Delta_1^2 - \delta^2}{2\,(\Omega^2 - \delta^2)}\, \theta_1^{(\Omega)} + \frac{\Delta_2^2 - \delta^2}{2\,(\Omega^2 - \delta^2)}\, \theta_2^{(\Omega)} \,. \end{aligned} \tag{3.4.33}$$

It it advantageous to identify in these rates the origin of the different terms. Therefore, we partition the rates into terms with $S_{1,2}(\omega)$,

$$\begin{aligned} \kappa_1 &= \frac{\pi}{4\,(\Omega^2 - \delta^2)} \left[(\Omega^2 - \Delta_1^2)\, S_1(\delta) + 2\,(\Delta_1^2 - \delta^2)\, S_1(\Omega) + (\Omega^2 - \Delta_2^2)\, S_2(\delta) \right] \,, \\ \kappa_2 &= \frac{\pi}{4\,(\Omega^2 - \delta^2)} \left[2\,(\Omega^2 - \Delta_1^2)\, S_1(\delta) + (\Delta_1^2 - \delta^2)\, S_1(\Omega) + (\Delta_2^2 - \delta^2)\, S_2(\Omega) \right] \,. \end{aligned} \tag{3.4.34}$$

For the rates $\kappa_{3,4}$, we only have to interchange the indices $1 \leftrightarrow 2$. Thus, the low-temperature generalizations of $\kappa_{3,4}$ read

$$\begin{aligned} \kappa_3 &= \frac{\pi}{4\,(\Omega^2 - \delta^2)} \left[(\Omega^2 - \Delta_2^2)\, S_2(\delta) + 2\,(\Delta_2^2 - \delta^2)\, S_2(\Omega) + (\Omega^2 - \Delta_1^2)\, S_1(\delta) \right] \,, \\ \kappa_4 &= \frac{\pi}{4\,(\Omega^2 - \delta^2)} \left[2\,(\Omega^2 - \Delta_2^2)\, S_2(\delta) + (\Delta_2^2 - \delta^2)\, S_2(\Omega) + (\Delta_1^2 - \delta^2)\, S_1(\Omega) \right] \,. \end{aligned} \tag{3.4.35}$$

Making the transition to the Markov-regime, we directly recover the Markov rates (3.4.22) because for high temperatures $S_{1,2}(\omega)$ reduce to the Markov expressions $2/\pi\, \vartheta_{1,2}$. Since $S_{1,2}(\omega)$ describe one-boson exchange processes from or to the bath with energy ω, every term in (3.4.34) and (3.4.35) describes such a process with energy Ω or δ, respectively.

We will focus on the leading order contribution to $\langle \sigma_z \rangle$ in the remainder of this subsection (cf. Eq. (3.4.23)). In the limit $\Delta_2 \to 0$, the spin-spin coupling takes the role of a bias and we should expect the rates $\kappa_{1,2}$ to match the rates of the biased spin-boson model. The limit $\Delta_2 \to 0$ makes $\Omega_\pm$ degenerate and hence $\Omega = \sqrt{\Delta_1^2 + v_z^2}$ and $\delta = 0$. Since δ gets zero, we have to account for the second order contribution to κ_1 that renormalizes δ. That is

$$\begin{aligned} \lambda_{1,2} &= \pm \mathrm{i} \left(\delta - \frac{a^2}{2\,\delta}\right) - \kappa_1 \;\approx\; \pm \mathrm{i} \sqrt{\delta^2 - a^2} - \kappa_1 \\ &\xrightarrow{\delta \to 0} \mp a\, \vartheta_1 - \kappa_1 \,. \end{aligned} \tag{3.4.36}$$

The result of this calculation is

$$a = \frac{1}{2}\left(\frac{v_z^2}{\Omega^2}\,\vartheta_1 + \vartheta_2\right) \tag{3.4.37}$$

and with κ_1 from above, we obtain for $\lambda_{1,2}$

$$\lambda_1 = -\vartheta_1 - \vartheta_2 \quad \text{and} \quad \lambda_2 = -\frac{\Delta_1^2}{\Omega^2}\,\vartheta_1 = -\gamma_\mathrm{r}\,. \tag{3.4.38}$$

The residue of the first term is zero and therefore does not contribute. The second term corresponds to the relaxation rate γ_r in the spin-boson model, whereas v_z adopts the role of the bias ϵ. The rate κ_2 directly simplifies to

$$\gamma = \frac{\gamma_\mathrm{r}}{2} + \frac{v_z^2}{\Omega^2}\,\vartheta_1\,, \tag{3.4.39}$$

which corresponds to the dephasing rate in the spin-boson model from Eq. (2.4.12).

After having checked the spin-boson limit, we can go on and calculate higher orders in $\vartheta_{1,2}$. Using Eq. (3.4.22) we do a series expansion of the denominator up to second order in $\vartheta_{1,2}$ and to first order in $\delta^{(\mathrm{s})}$ and $\Omega^{(\mathrm{s})}$ around $\lambda = \pm\mathrm{i}\left(\delta - \delta^{(\mathrm{s})}\right) - \kappa_1$ and $\lambda = \pm\mathrm{i}\left(\Omega - \Omega^{(\mathrm{s})}\right) - \kappa_2$. That means, in second order of $\vartheta_{1,2}$ we get a frequency shift. The results are

$$\begin{aligned}
\delta^{(\mathrm{s})} = {} & \frac{v_z^2\,\Omega^2\,(\Omega^2 - 5\,\delta^2)}{4\,\delta\,(\Omega^2 - \delta^2)^3}\,\vartheta_1\,\vartheta_2 \\
& + (\Omega^2 - \Delta_1^2)\,\frac{4\,\delta^4 - \Delta_1^2\,\Omega^2 + \Omega^4 - \delta^2\,(3\,\Delta_1^2 + \Omega^2)}{8\,\delta\,(\Omega^2 - \delta^2)^3}\,\vartheta_1^2 \\
& + (\Delta_1^2 - \delta^2)\,\Omega^2\,\frac{\Omega^4\,\Delta_1^2 + \delta^4\,(4\,\Delta_1^2 - 3\,\Omega^2) - \delta^2\,\Omega^2\,(\Delta_1^2 + \Omega^2)}{8\,\Delta_1^4\,\delta\,(\Omega^2 - \delta^2)^3}\,\vartheta_2^2
\end{aligned} \tag{3.4.40}$$

and

$$\begin{aligned}
\Omega^{(\mathrm{s})} = {} & \frac{v_z^2\,\delta^2\,(5\,\Omega^2 - \delta^2)}{4\,\Omega\,(\Omega^2 - \delta^2)^3}\,\vartheta_1\,\vartheta_2 \\
& + (\Delta_1^2 - \delta^2)\,\frac{\delta^4 - 3\,\Delta_1^2\,\Omega^2 + 4\,\Omega^4 - \delta^2\,(\Delta_1^2 + \Omega^2)}{8\,\Omega\,(\Omega^2 - \delta^2)^3}\,\vartheta_1^2 \\
& + (\Omega^2 - \Delta_1^2)\,\delta^2\,\frac{\delta^4\,\Delta_1^2 + \Omega^4\,(4\,\Delta_1^2 - 3\,\delta^2) - \delta^2\,\Omega^2\,(\Delta_1^2 + \delta^2)}{8\,\Delta_1^4\,\Omega\,(\Omega^2 - \delta^2)^3}\,\vartheta_2^2\,.
\end{aligned} \tag{3.4.41}$$

With these results we can calculate the shift of the damping rates in order $\vartheta_{1,2}^3$, i.e we make a series expansion around $\lambda = \pm\mathrm{i}\left(\delta - \delta^{(\mathrm{s})}\right) - \kappa_1 - \kappa_1^{(\mathrm{s})}$ and $\lambda = \pm\mathrm{i}\left(\Omega - \Omega^{(\mathrm{s})}\right) - \kappa_2 - \kappa_2^{(\mathrm{s})}$. We obtain

$$\begin{aligned}
\kappa_1^{(\mathrm{s})} = {} & -\frac{v_z^2\,\Delta_1^2\big[\Omega_+^2\,\Omega_-^2 - \Delta_1^2\,(v_z^2 + \Delta_1^2 - \Delta_2^2)\big]}{2\,\Omega_+^5\,\Omega_-^5}\,\vartheta_1^3 + \frac{v_z^2\,\Delta_2^2\big[\Omega_+^2\,\Omega_-^2 - \Delta_2^2\,(v_z^2 - \Delta_1^2 + \Delta_2^2)\big]}{2\,\Omega_+^5\,\Omega_-^5}\,\vartheta_2^3 \\
& - \frac{3\,v_z^2\,\Delta_1^2\,\Delta_2^2\,(v_z^2 - \Delta_1^2 + \Delta_2^2)}{2\,\Omega_+^5\,\Omega_-^5}\,\vartheta_1^2\,\vartheta_2 + \frac{3\,v_z^2\,\Delta_1^2\,\Delta_2^2\,(v_z^2 + \Delta_1^2 - \Delta_2^2)}{2\,\Omega_+^5\,\Omega_-^5}\,\vartheta_1\,\vartheta_2^2
\end{aligned}$$

(3.4.42)

and

$$\kappa_2^{(\mathrm{s})} = \frac{v_z^2\,\Delta_1^2\left[\Omega_+^2\,\Omega_-^2 - \Delta_1^2\,(v_z^2+\Delta_1^2-\Delta_2^2)\right]}{2\,\Omega_+^5\,\Omega_-^5}\,\vartheta_1^3 - \frac{v_z^2\,\Delta_2^2\left[\Omega_+^2\,\Omega_-^2 - \Delta_2^2\,(v_z^2-\Delta_1^2+\Delta_2^2)\right]}{2\,\Omega_+^5\,\Omega_-^5}\,\vartheta_2^3 + \frac{3\,v_z^2\,\Delta_1^2\,\Delta_2^2\,(v_z^2-\Delta_1^2+\Delta_2^2)}{2\,\Omega_+^5\,\Omega_-^5}\,\vartheta_1^2\,\vartheta_2 - \frac{3\,v_z^2\,\Delta_1^2\,\Delta_2^2\,(v_z^2+\Delta_1^2-\Delta_2^2)}{2\,\Omega_+^5\,\Omega_-^5}\,\vartheta_1\,\vartheta_2^2\,. \tag{3.4.43}$$

The calculation of higher orders is restricted by computer power only.

Within the spin-boson limit, $\Delta_2 \to 0$, and with the generalized temperature dependences, we recover for the Eqs. (3.4.38) and (3.4.39) the one-boson results of the spin-boson model from Eq. (2.4.13)

$$\gamma_{\mathrm{r}} = \frac{\Delta_1^2}{v_z^2+\Delta_1^2}\,\frac{\pi}{2}\,S_1(\Omega) \qquad \text{and} \qquad \gamma = \frac{\gamma_{\mathrm{r}}}{2} + \frac{v_z^2}{v_z^2+\Delta_1^2}\,\frac{\pi}{2}\,S_1(0)\,. \tag{3.4.44}$$

This simple check shows that we indeed derived the correct generalized temperatures in leading order of the bath correlation strength.

A further check of the results is to perform the large coupling limit $v_z \to \infty$. In this regime the two spins are so strongly coupled that they behave as an effective single-spin system with frequency $\widetilde{\delta} = \Delta^2/v_z$ (for equal Δ and equal bathes). The rate κ_1 of Eq. (3.4.33) then changes to

$$\kappa_1 = \pi\,K\,\widetilde{\delta}\coth\left(\frac{\widetilde{\delta}}{2\,T}\right) \tag{3.4.45}$$

and only the residues of $\pm\mathrm{i}\,\delta - \kappa_1$ contribute with 1/2 each. In the high temperature limit this rate obtains the correct form $\kappa_1 = \vartheta$, which is twice the dephasing rate of Eq. (3.4.39). The factor two arises because we have one spin coupled to two identical baths. Setting the coupling to one of the bathes to zero leads to $\kappa_1 = \vartheta/2$. And since we have no bias, there is no relaxation rate.

We can also study the case of vanishing coupling $v_z \to 0$. Only the residues of $\pm\mathrm{i}\,\Omega - \kappa_2$ give a contribution, 1/2 each, and the poles become

$$\pm\mathrm{i}\,\Delta_1 + \frac{1}{2}\,\pi\,K_1\,\Delta_1\,\coth\left(\frac{\Delta_1}{2\,T_1}\right)\,. \tag{3.4.46}$$

The first term describes the oscillation frequency and the second the damping rate. In the high temperature limit the damping term reads $\vartheta_1/2$ which corresponds to the dephasing rate of a single-spin system (cf. (3.4.39)). And again, since we have no bias the relaxation rate is zero.

3.4.2 Large coupling v_z and/or high temperature

For large coupling v_z and/or high temperature only two relaxation poles are relevant in leading order compared to the other frequencies

$$\lambda_{7,8} = -\frac{\Delta_{1,2}^2}{v_z^2 + \vartheta_{1,2}^2} \frac{\Delta_{2,1}^2 + \vartheta_{1,2}\,(\vartheta_1 + \vartheta_2)}{\vartheta_1 + \vartheta_2} \,. \tag{3.4.47}$$

This result can be deduced directly from Eq. (3.4.20). For large coupling the denominator of $\langle \sigma_z \rangle$ can be expanded in a series. The eight dynamical poles are

$$\begin{aligned}
\lambda_{1,2} &= \pm \mathrm{i}\, \widetilde{\Omega} - \vartheta_1 + \frac{\Delta_1^2\, \vartheta_1 - \Delta_2^2\, \vartheta_2}{2 v_z^2} \,, \\
\lambda_{3,4} &= \pm \mathrm{i}\, \widetilde{\Omega} - \vartheta_2 + \frac{\Delta_1^2\, \vartheta_1 - \Delta_2^2\, \vartheta_2}{2 v_z^2} \,, \\
\lambda_{5,6} &= -\vartheta_1 - \vartheta_2 + \frac{\widetilde{\delta}^2}{\vartheta_1 + \vartheta_2} \left(1 + \frac{\vartheta_{2,1}\,(\vartheta_1 + \vartheta_2)}{\Delta_{1,2}^2} \right) \,, \\
\lambda_{7,8} &= -\frac{\widetilde{\delta}^2}{\vartheta_1 + \vartheta_2} \left(1 + \frac{\vartheta_{1,2}\,(\vartheta_1 + \vartheta_2)}{\Delta_{2,1}^2} \right) \,.
\end{aligned} \tag{3.4.48}$$

The relaxation rate λ_4 follows directly from Eq. (3.4.47). The frequencies $\widetilde{\Omega}$ and $\widetilde{\delta}$ are the large v_z expansions of the eigenfrequencies Ω and δ and read

$$\widetilde{\Omega} = v_z + \frac{\Delta_1^2 + \Delta_2^2}{2\, v_z} \,, \qquad \widetilde{\delta} = \frac{\Delta_1\, \Delta_2}{v_z} \,. \tag{3.4.49}$$

Observe that contrary to where weak coupling to the bath prevails, we now have $\widetilde{\Omega}$ as the relevant frequency instead of $\widetilde{\delta}$.
We obtain for the corresponding residues in leading order of large v_z

$$\begin{aligned}
\mathrm{Res}\,[\sigma_z(\lambda_{1,2})] &= 0 \,, \\
\mathrm{Res}\,[\sigma_z(\lambda_{3,4})] &= 0 \,, \\
\mathrm{Res}\,[\sigma_z(\lambda_5)] &= \frac{\pi K_1 \Delta_1^4 \Delta_2^2}{v_z (\Delta_1^2\, \vartheta_1 - \Delta_2^2\, \vartheta_2)\,(\vartheta_1 + \vartheta_2)^{\,2}} \,, \\
\mathrm{Res}\,[\sigma_z(\lambda_6)] &= -\frac{\pi K_1 \Delta_1^4 \Delta_2^2}{v_z (\Delta_1^2\, \vartheta_1 - \Delta_2^2\, \vartheta_2)\,(\vartheta_1 + \vartheta_2)^{\,2}} \,, \\
\mathrm{Res}\,[\sigma_z(\lambda_7)] &= 1 - \frac{\pi K_1 \Delta_1^2 v_z}{\Delta_1^2\, \vartheta_1 - \Delta_2^2\, \vartheta_2} \,, \\
\mathrm{Res}\,[\sigma_z(\lambda_8)] &= \frac{\pi K_1 \Delta_1^2 v_z}{\Delta_1^2\, \vartheta_1 - \Delta_2^2\, \vartheta_2} \,.
\end{aligned} \tag{3.4.50}$$

The leading contribution for $\langle \sigma_z(t) \rangle$ is given in the form

$$\langle \sigma_z(t) \rangle = \left(1 - \frac{\pi K_1 \Delta_1^2 v_z}{\Delta_1^2\, \vartheta_1 - \Delta_2^2\, \vartheta_2} \right) \mathrm{e}^{\lambda_7\, t} + \frac{\pi K_1 \Delta_1^2 v_z}{\Delta_1^2\, \vartheta_1 - \Delta_2^2\, \vartheta_2}\, \mathrm{e}^{\lambda_8\, t} \tag{3.4.51}$$

and therefore describes pure relaxation. The lowest order contribution for the coherent part is of order $\mathcal{O}(1/v_z^2)$.
We can study two interesting limiting expressions

$$\lambda_{7,8} = -\frac{\Delta_{1,2}^2}{v_z^2}\,\vartheta_{1,2} \quad (\Delta_2 \ll \vartheta_{1,2}) \qquad \text{and} \qquad \lambda_{7,8} = -\frac{\delta^2}{\vartheta_1+\vartheta_2} \quad (\Delta_2 \gg \vartheta_{1,2})\ . \tag{3.4.52}$$

The former is the relaxation rate of a biased spin-boson model at low $\vartheta_{1,2}$. The latter describes Kondo-like joint relaxation of locked spins (cf. discussions at the end of Section 2.3 and of the following subsection).

For high temperature we obtain a similar picture. The time evolution is again of the form given in Eq. (3.4.51). The relaxation rate $\lambda_{7,8}$ from Eq. (3.4.47) reduces in the parameter regime $\vartheta_{1,2} \gg v_z$, Δ_2 to

$$\gamma_{\sigma,\tau} \equiv \lambda_{7,8} = -\Delta_{1,2}^2/\vartheta_{1,2} \propto T_{1,2}^{2\,K_{1,2}-1}\ . \tag{3.4.53}$$

The last transformation on the rhs is due to the renormalization of $\Delta_{1,2}$ according to (3.3.2). $\gamma_{\sigma,\tau}$ are defined for subsequent convenience. The coupling v_z is irrelevant for the damping rates in this regime and the rates behave as if they were single-spin damping rates in the Kondo-regime.

3.4.3 Qualitative features of identical spins

In this section the dependence of $\langle\sigma_z\rangle$ on the external parameters is studied for the case of two identical spins, i.e., $\vartheta = \vartheta_1 = \vartheta_2$ and $\Delta = \Delta_1 = \Delta_2$. For simplicity, we will only discuss contributions in leading order of temperature (see Eq. (3.4.23)). Then, the dynamics of $\langle\sigma_z\rangle$ is determined by four dynamical poles of the denominator and the respective amplitudes.

The left part of Fig. 3.4 shows different phases appearing along the coherent-incoherent transition in the T-K-plane. If temperature approaches the order of $\Omega_\pm$, we expect that the results of this section will no longer be valid (cf. (3.3.3)). But, as we will see in Section 4, the regime $T \lesssim \Omega_\pm$ with $K \ll 1$ is properly described with the Bloch-Redfield method. The NIBA is known to give a good description of the coherent-incoherent transition for a single spin [70]. We expect it to do the same for two coupled spins.

If we choose $v_z < v_{\rm cr} = \Delta/\sqrt{2}$ the discriminant of the denominator gives three crossover temperatures (see Figs. 3.4 – 3.6)

$$\vartheta_{0,1}^* = \sqrt{2\,\Delta^2 - v_z^2 \mp 2\Delta\sqrt{\Delta^2 - 2\,v_z^2}} \qquad \text{and} \qquad \vartheta_2^* = \Delta^2/v_z\ . \tag{3.4.54}$$

In the regime $\vartheta < \vartheta_1^*$ the dynamics is coherent and composed of a superposition of two damped oscillations. For $\vartheta < \vartheta_0^*$ the oscillations have different frequencies, the same damping rate, and the amplitudes are comparable in magnitude. On the other hand, in the range $\vartheta_0^* < \vartheta < \vartheta_1^*$, they have the same frequency but differ in the damping rate. Also

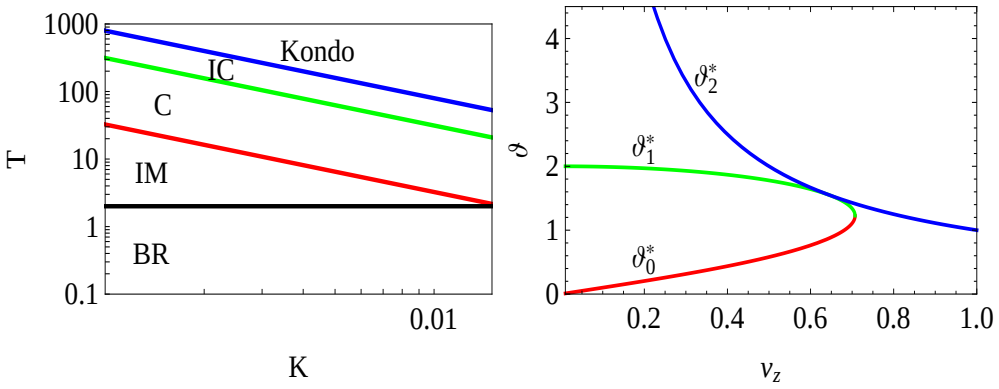

Figure 3.4: $\langle\sigma_z\rangle$: different phases ranging from the Kondo-regime for high temperature/and or coupling strength to the Bloch-Redfield regime valid for low temperature and small coupling $K \ll 1$ are shown in the left figure for $v_z = 0.2$). IC: incoherent-, C: coherent-, IM: intermediate-, BR: Bloch-Redfield-regime. Temperature is given in units of Δ, i.e., $T = \hbar\Delta/k_{\rm B}$. In the right figure are shown crossover temperatures separating the different coherent/incoherent regimes as a function of v_z. $\Delta = 1$. See text for details.

the amplitude belonging to the larger rate can be neglected, compared to the amplitude of the smaller rate.

In the temperature regime $\vartheta > \vartheta_1^*$, the dynamics is incoherent. In the regime $\vartheta_1^* < \vartheta < \vartheta_2^*$ the four poles are real and the two smallest rates have the largest amplitudes and dominate the relaxation process.

In the Kondo regime $\vartheta > \vartheta_2^*$ the dominant pole is real and approaches $-\Delta^2/\vartheta$. As temperature increases, its residuum converges to $1 - \langle\sigma_z\rangle_{\rm eq}$. The other real pole takes the value -2ϑ, while the corresponding amplitude is almost zero. There is also a damped oscillation of which the frequency and rate approach asymptotically v_z and ϑ, but with negligible amplitude. The phenomenon that in the Kondo regime for $K < 1/2$, incoherent relaxation slows down with increasing temperature is already well-known in the single spin-boson problem [2].

Fig. 3.7 shows the transition from coherent to incoherent dynamics as ϑ is raised. One can also see that at high ϑ the effective damping decreases with increasing ϑ.

For $v_z > v_{\rm cr}$, only the crossover temperature ϑ_2^* remains. It separates a regime with two complex conjugate poles from a regime with one pair of complex conjugate poles and two real poles. Above ϑ_2^*, the relaxation is governed by the Kondo pole.

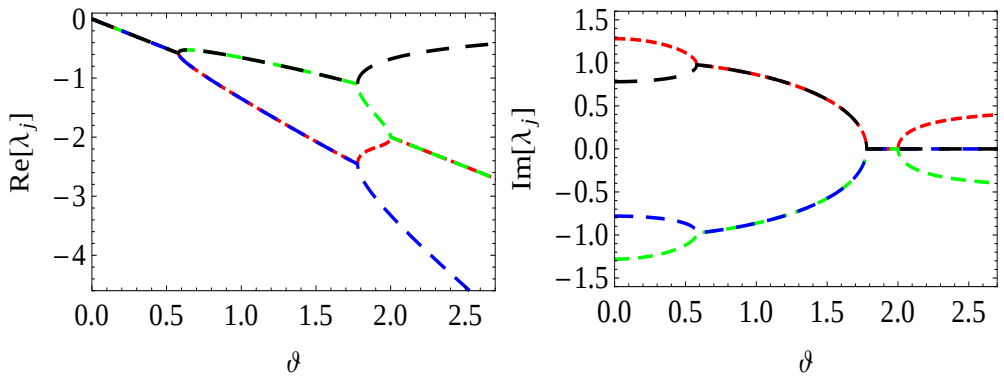

Figure 3.5: $\langle\sigma_z\rangle$: real (left) and imaginary (right) part of λ_j, $v_z = 0.5$, $\Delta = 1$. The colors red, green, blue, and black denote $\mathrm{Re}\,[\lambda_j]$ and $\mathrm{Im}\,[\lambda_j]$, with $j = 1, 2, 3, 4$. See text for details.

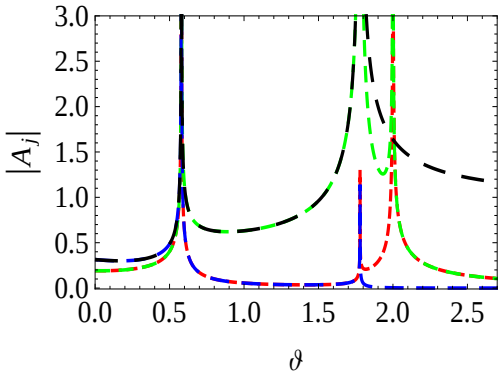

Figure 3.6: $\langle\sigma_z\rangle$: absolute part of $\langle\sigma_z\rangle$ with $v_z = 0.5$, $\Delta = 1$, $K = 0.05$. The singularities are due to degenerate eigenvalues. The colors red, green, blue, and black label $|A_j|$ where $j = 1, 2, 3, 4$. See text for details.

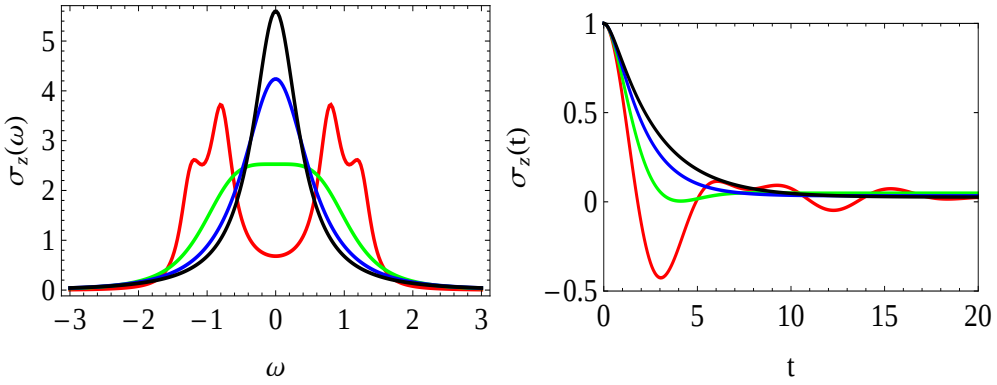

Figure 3.7: $\langle\sigma_z\rangle$: plots of $\langle\sigma_z\rangle$ in the Fourier regime (left) and time regime (right) with $v_z = 0.5$, $\Delta = 1$, $K = 0.05$, red $\vartheta = 0.2$, green $\vartheta = 1.2$, blue $\vartheta = 2.1$, and black $\vartheta = 2.8$. We see the transition from coherent to incoherent behavior for increasing temperature from red $\rightarrow$ green $\rightarrow$ blue. From blue $\rightarrow$ black temperature increases but relaxation decreases. This is due to the Kondo effect.

3.5 $\sigma_z\,\tau_z$

The result for $\langle\sigma_z\tau_z(\lambda)\rangle$ given in Eq. (3.1.28) can also be rewritten, such that we see which transitions contribute. Therefore, we solve the coupled equations of motion in the Heisenberg picture from Appendix A.2 in an iterative way. It is important to keep the ordering of the different contributions from Δ_1 and Δ_2, respectively. At the end, we obtain

$$\begin{aligned}
\langle\sigma_z\tau_z(\lambda)\rangle =&\ \frac{1}{\lambda}\,\frac{1}{D}\ ,\\
D =&\ 1+\Delta_1\,\frac{1}{\lambda^2+v_z^2+\Delta_2^2-\Delta_2\,\Delta_1\,\frac{1}{\lambda^2+v_z^2+\Delta_1^2}\,\Delta_1\,\Delta_2}\,\Delta_1\\
&-\Delta_1\,\frac{1}{\lambda^2+v_z^2+\Delta_2^2-\Delta_2\,\Delta_1\,\frac{1}{\lambda^2+v_z^2+\Delta_1^2}\,\Delta_1\,\Delta_2}\,\Delta_2\,\Delta_1\,\frac{1}{\lambda^2+v_z^2+\Delta_1^2}\,\Delta_2\\
&+\text{terms with } \Delta_1\leftrightarrow\Delta_2\ .
\end{aligned}\tag{3.5.1}$$

Introducing the abbreviations

$$\begin{aligned}
A_1 =&\ \Delta_1\,\frac{1}{\lambda^2+v_z^2+\Delta_2^2-\Delta_2\,\Delta_1\,\frac{1}{\lambda^2+v_z^2+\Delta_1^2}\,\Delta_1\,\Delta_2}\,\Delta_1\\
=&\ \Delta_1\,\frac{1}{\lambda^2+v_z^2+\Delta_2^2}\,\frac{1}{1-\Delta_2\,\Delta_1\,\frac{1}{\lambda^2+v_z^2+\Delta_1^2}\,\Delta_1\,\Delta_2\,\frac{1}{\lambda^2+v_z^2+\Delta_2^2}}\,\Delta_1
\end{aligned}\tag{3.5.2}$$

and

$$\begin{aligned}
A_2 =&\ -\Delta_1\,\frac{1}{\lambda^2+v_z^2+\Delta_2^2}\,\frac{1}{1-\Delta_2\,\Delta_1\,\frac{1}{\lambda^2+v_z^2+\Delta_1^2}\,\Delta_1\,\Delta_2\,\frac{1}{\lambda^2+v_z^2+\Delta_2^2}}\,\Delta_2\\
&\times\ \Delta_1\,\frac{1}{\lambda^2+v_z^2+\Delta_1^2}\,\Delta_2\ ,
\end{aligned}\tag{3.5.3}$$

the denominator from Eq. (3.5.1) can be written in the form

$$D = 1 + A_1 + A_2 + \text{terms with } \Delta_1\leftrightarrow\Delta_2\ .\tag{3.5.4}$$

We further introduce the short hand notations

$$\square_1 = \frac{1}{\lambda^2+v_z^2+\Delta_1^2}\qquad\text{and}\qquad\square_2 = \frac{1}{\lambda^2+v_z^2+\Delta_2^2}\ ,\tag{3.5.5}$$

which describe single spin contributions in the bias v_z of the other spin. Now, A_1 and A_2 can be abbreviated to

$$\begin{aligned}
A_1 =&\ \Delta_1\,\square_2\,\frac{1}{1-\Delta_2\,\Delta_1\,\square_1\,\Delta_1\,\Delta_2\,\square_2}\,\Delta_1\ ,\\
A_2 =&\ -\Delta_1\,\square_2\,\frac{1}{1-\Delta_2\,\Delta_1\,\square_1\,\Delta_1\,\Delta_2\,\square_2}\,\Delta_2\,\Delta_1\,\square_1\,\Delta_2\ .
\end{aligned}\tag{3.5.6}$$

These expressions are in the form of geometrical series (cf. Figs. 3.8 and 3.9).

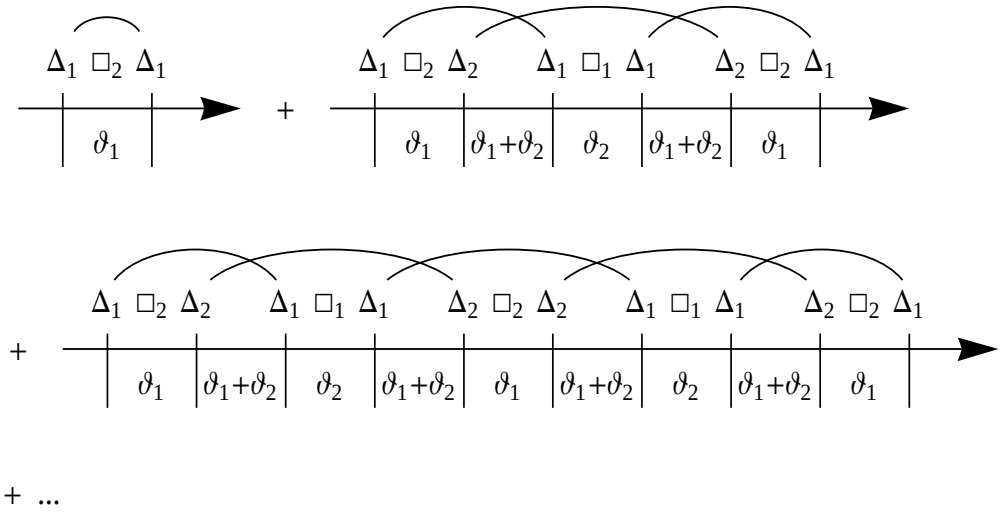

Figure 3.8: Series expansion of contributing transition sequences for A_1. The arrow indicates the time direction.

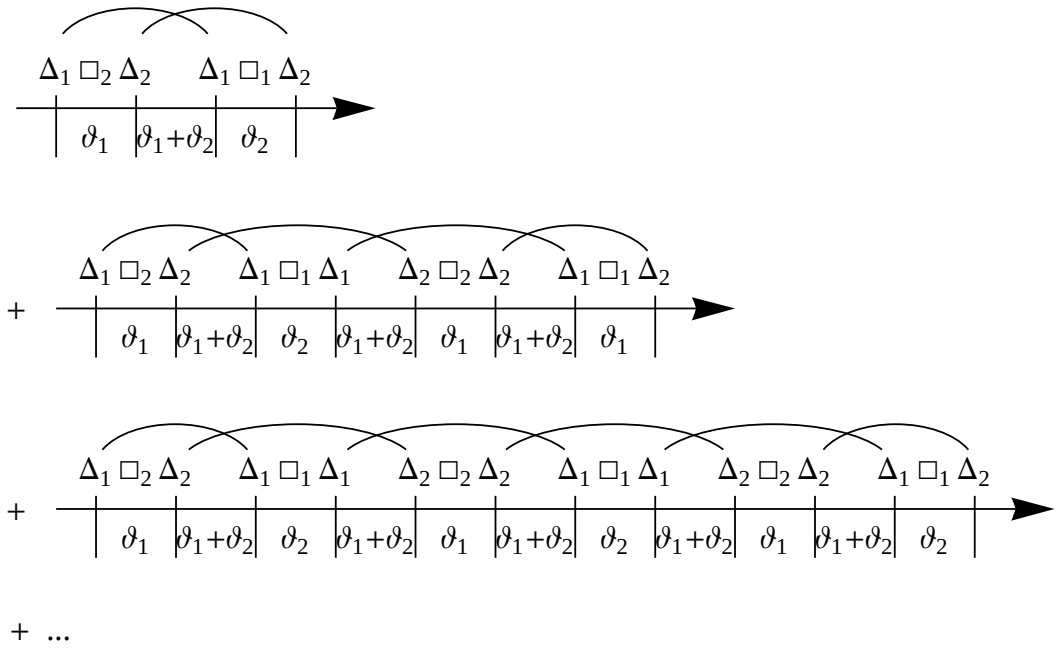

Figure 3.9: Series expansion of contributing transition sequences for A_2. The arrow indicates the time direction.

Further, the bath-induced damping can be inserted. For the first line in Fig. 3.8 and without damping the result is

$$A_{11} = \frac{1}{\lambda}\Delta_1 \frac{1}{\lambda^2 + v_z^2 + \Delta_2^2}\Delta_1 \,. \tag{3.5.7}$$

With damping and up to order $\Delta_1^2\,\Delta_2^2$ we obtain

$$\begin{aligned} &\frac{1}{\lambda}\,\Delta_1 \frac{\lambda+\vartheta_1}{(\lambda+\vartheta_1)^2+v_z^2}\,\Delta_1 \\ &-\frac{1}{\lambda}\,\Delta_1 \frac{\lambda+\vartheta_1}{(\lambda+\vartheta_1)^2+v_z^2}\,\Delta_2 \frac{1}{\lambda+\vartheta_1+\vartheta_2}\,\Delta_2 \frac{\lambda+\vartheta_1}{(\lambda+\vartheta_1)^2+v_z^2}\,\Delta_1 \,. \end{aligned} \tag{3.5.8}$$

Including higher orders results in

$$\begin{aligned} A_{11} &= \frac{\lambda+\vartheta_1}{\lambda}\,\frac{\Delta_1^2}{(\lambda+\vartheta_1)^2+v_z^2}\,\frac{1}{1+\frac{\lambda+\vartheta_1}{\lambda+\vartheta_1+\vartheta_2}\,\frac{\Delta_2^2}{(\lambda+\vartheta_1)^2+v_z^2}} \\ &= \frac{\lambda+\vartheta_1}{\lambda}\,\frac{\Delta_1^2}{(\lambda+\vartheta_1)^2+v_z^2+\frac{\lambda+\vartheta_1}{\lambda+\vartheta_1+\vartheta_2}\,\Delta_2^2} \,. \end{aligned} \tag{3.5.9}$$

The second line in Fig. 3.8 results in a similar expression

$$\begin{aligned} A_{12} = &\frac{\lambda+\vartheta_1}{\lambda}\,\frac{\Delta_1^2}{(\lambda+\vartheta_1)^2+v_z^2+\frac{\lambda+\vartheta_1}{\lambda+\vartheta_1+\vartheta_2}\,\Delta_2^2} \\ &\times \frac{\lambda+\vartheta_2}{\lambda+\vartheta_1+\vartheta_2}\,\frac{\Delta_2^2}{(\lambda+\vartheta_2)^2+v_z^2+\frac{\lambda+\vartheta_2}{\lambda+\vartheta_1+\vartheta_2}\,\Delta_1^2} \\ &\times \frac{\lambda+\vartheta_1}{\lambda+\vartheta_1+\vartheta_2}\,\frac{\Delta_1^2}{(\lambda+\vartheta_1)^2+v_z^2+\frac{\lambda+\vartheta_1}{\lambda+\vartheta_1+\vartheta_2}\,\Delta_2^2} \,. \end{aligned} \tag{3.5.10}$$

For all higher orders (A_{13}, A_{14}, ...) the second and third line of Eq. (3.5.10) contribute in an alternating manner. Introducing

$$\begin{aligned} \alpha_1 &= \frac{\lambda+\vartheta_1}{\lambda+\vartheta_1+\vartheta_2}\,\frac{\Delta_1^2}{(\lambda+\vartheta_1)^2+v_z^2+\frac{\lambda+\vartheta_1}{\lambda+\vartheta_1+\vartheta_2}\,\Delta_2^2} \,, \\ \alpha_2 &= \frac{\lambda+\vartheta_2}{\lambda+\vartheta_1+\vartheta_2}\,\frac{\Delta_2^2}{(\lambda+\vartheta_2)^2+v_z^2+\frac{\lambda+\vartheta_2}{\lambda+\vartheta_1+\vartheta_2}\,\Delta_1^2} \,, \end{aligned} \tag{3.5.11}$$

we can write A_1 as a geometrical series

$$A_1 = \frac{\lambda+\vartheta_1+\vartheta_2}{\lambda}\left\{\alpha_1 + \alpha_1\,\alpha_2\,\alpha_1 + \alpha_1\,\alpha_2\,\alpha_1\,\alpha_2\,\alpha_1 + ...\right\} \,, \tag{3.5.12}$$

which simplifies to

$$A_1 = \frac{\lambda+\vartheta_1+\vartheta_2}{\lambda}\,\frac{\alpha_1}{1-\alpha_2\,\alpha_1} \,. \tag{3.5.13}$$

The derivation of A_2 in Fig. 3.9 is analogous

$$\begin{aligned} A_{21} &= -\frac{\lambda+\vartheta_1+\vartheta_2}{\lambda}\,\alpha_1\,\alpha_2\ , \\ A_{22} &= -\frac{\lambda+\vartheta_1+\vartheta_2}{\lambda}\,\alpha_1\,\alpha_2\,\alpha_1\,\alpha_2\ , \\ &\vdots \end{aligned} \tag{3.5.14}$$

and

$$A_2 = -\,\frac{\lambda+\vartheta_1+\vartheta_2}{\lambda}\,\frac{\alpha_1\,\alpha_2}{1-\alpha_2\,\alpha_1}\ . \tag{3.5.15}$$

Thus, including the bath-induced damping the denominator from (3.5.1) takes the compact form

$$D = 1+\frac{\lambda+\vartheta_1+\vartheta_2}{\lambda}\,\left[\frac{\alpha_1}{1-\alpha_2\,\alpha_1}+\frac{\alpha_2}{1-\alpha_2\,\alpha_1}-\frac{2\,\alpha_1\,\alpha_2}{1-\alpha_2\,\alpha_1}\right]\ . \tag{3.5.16}$$

Again, we have to incorporate the influence phase factors (cf. Eq. (3.3.4), here shown for A_{11}, also cf. Appendix A.2)

$$\begin{aligned} \widetilde{\mathcal{K}}_1(\lambda) &= \frac{1}{\lambda}\,k_1^{(+)}(\lambda)\ , \\ \widetilde{\mathcal{K}}_2(\lambda) &= \frac{1}{\lambda}\,k_1^{(+)}(\lambda)\,\frac{(\lambda+\vartheta_1)\,\Delta_2^2\,\cos(\pi\,K_2)}{(\lambda+\vartheta_1+\vartheta_2)\,[(\lambda+\vartheta_1)^2+v_z^2]}\ , \\ \widetilde{\mathcal{K}}_{n+2}(\lambda) &= (-1)^n\,\widetilde{\mathcal{K}}_2(\lambda)\left(\frac{(\lambda+\vartheta_1)\,\Delta_2^2\,\cos(\pi\,K_2)}{(\lambda+\vartheta_1+\vartheta_2)\,[(\lambda+\vartheta_1)^2+v_z^2]}\right)^n\ , \end{aligned} \tag{3.5.17}$$

with $k_1^{(+)}(\lambda)$ from Eq. (3.4.13),

$$k_1^{(+)}(\lambda) = -\frac{\Delta_1^2}{\lambda}\int_0^\infty \mathrm{d}\tau\,\mathrm{e}^{-(\lambda+\vartheta_1)\,\tau}\,\cos(\pi\,K_1+v_z\,\tau) \tag{3.5.18}$$

and $n = 1, 2, 3, \ldots$. We sum up all contributions and obtain

$$\widetilde{\mathcal{K}}(\lambda) = \frac{1}{\lambda}\,k_1^{(+)}(\lambda)\,\frac{1}{1+\frac{(\lambda+\vartheta_1)\,\Delta_2^2\,\cos(\pi\,K_2)}{(\lambda+\vartheta_1+\vartheta_2)\,[(\lambda+\vartheta_1)^2+v_z^2]}}\ . \tag{3.5.19}$$

This is the basic building block for all other contributions and we obtain in place of Eq. (3.5.11)

$$\begin{aligned} \tilde{\alpha}_1 &= \frac{\lambda+\vartheta_1}{\lambda+\vartheta_1+\vartheta_2}\,\lambda\,k_1^{(+)}(\lambda)\,\frac{1}{1+\frac{(\lambda+\vartheta_1)\,\Delta_2^2\,\cos(\pi\,K_2)}{(\lambda+\vartheta_1+\vartheta_2)\,[(\lambda+\vartheta_1)^2+v_z^2]}}\ , \\ \tilde{\alpha}_2 &= \frac{\lambda+\vartheta_2}{\lambda+\vartheta_1+\vartheta_2}\,\lambda\,k_2^{(+)}(\lambda)\,\frac{1}{1+\frac{(\lambda+\vartheta_2)\,\Delta_1^2\,\cos(\pi\,K_1)}{(\lambda+\vartheta_1+\vartheta_1)\,[(\lambda+\vartheta_2)^2+v_z^2]}}\ . \end{aligned} \tag{3.5.20}$$

The subscript in $k_{1,2}^{(+)}$ denotes the kernels in Eq. (3.4.13) for the σ- and τ-spin respectively. Summing over higher orders, according to Eq. (3.5.16), and with

$$\beta_1^{(+)} = \frac{\lambda+\vartheta_1+\vartheta_2}{\lambda}\,\frac{\tilde\alpha_1-\tilde\alpha_1\,\tilde\alpha_2}{1-\tilde\alpha_2\,\tilde\alpha_1}\,, \qquad \beta_2^{(+)} = \frac{\lambda+\vartheta_1+\vartheta_2}{\lambda}\,\frac{\tilde\alpha_2-\tilde\alpha_1\,\tilde\alpha_2}{1-\tilde\alpha_2\,\tilde\alpha_1}\,, \tag{3.5.21}$$

and

$$\beta_1^{(-)} = \left(1-\frac{v_z}{\lambda+\vartheta_1}\,\tan(\pi\,K_1)\right)\,\beta_1^{(+)}\,, \qquad \beta_2^{(-)} = \left(1-\frac{v_z}{\lambda+\vartheta_2}\,\tan(\pi\,K_2)\right)\,\beta_2^{(+)}\,, \tag{3.5.22}$$

the result for $\langle\sigma_z\tau_z(\lambda)\rangle$ is[1]

$$\langle\sigma_z\tau_z(\lambda)\rangle = \frac{1}{\lambda}\left(1-\frac{\beta_1^{(-)}+\beta_2^{(-)}}{1+\beta_1^{(+)}+\beta_2^{(+)}}\right) = \frac{1}{\lambda}\frac{N(\lambda)}{D(\lambda)}\,. \tag{3.5.23}$$

For equal Δ and ϑ the denominator $D(\lambda)$ reduces to the order λ^4 and the numerator and denominator adopt the form

$$\begin{aligned} N(\lambda) &= 2\,K\,\pi\,v_z\,\Delta^2(2\,\vartheta+\lambda)+\lambda(v_z^2(2\,\vartheta+\lambda)+(\vartheta+\lambda)(2\,\Delta^2+(\vartheta+\lambda)(2\,\vartheta+\lambda)))\,,\\ D(\lambda) &= \lambda^4+\lambda^3\,4\,\vartheta+\lambda^2\,(\Omega_+^2+\Omega_-^2-v_z^2+5\,\vartheta^2)\\ &\quad+\lambda\,(2\,v_z^2\,\vartheta+8\,\Delta^2\,\vartheta+2\,\vartheta^3)+4\,\Delta^2\,\vartheta^2\,. \end{aligned} \tag{3.5.24}$$

In general the denominator $D(\lambda)$ is of order λ^6 and numerator and denominator are

$$\begin{aligned} N(\lambda) &= \left(\left(\pi v_z K_1\Delta_1^2+\lambda\left(v_z^2+(\lambda+\vartheta_1)^{\,2}\right)\right)(\lambda+\vartheta_2)-\pi v_z K_2\Delta_2^2\,(\lambda+\vartheta_1)\right)\Delta_1^2\\ &\quad+\Delta_2^2\left((\lambda+\vartheta_1)\left(\pi v_z K_2\Delta_2^2+\lambda\left(v_z^2+(\lambda+\vartheta_2)^{\,2}\right)\right)-\pi v_z K_1\Delta_1^2\,(\lambda+\vartheta_2)\right)\\ &\quad+(\lambda+\vartheta_1+\vartheta_2)\left\{\pi v_z K_1\left(v_z^2+(\lambda+\vartheta_2)^{\,2}\right)\Delta_1^2\right.\\ &\quad\left.+\left(v_z^2+(\lambda+\vartheta_1)^{\,2}\right)\left(\pi v_z K_2\Delta_2^2+\lambda\left(v_z^2+(\lambda+\vartheta_2)^{\,2}\right)\right)\right\}\,,\\ D(\lambda) &= \lambda\,(\lambda+\vartheta_1+\vartheta_2)\,v_z^4+\left\{\left(\vartheta_1^2+(2\lambda+\vartheta_2)\,\vartheta_1+2\lambda\,(\lambda+\vartheta_2)\right)\Delta_1^2\right.\\ &\quad+\lambda\,(\lambda+\vartheta_1+\vartheta_2)\left(\vartheta_1^2+2\lambda\vartheta_1+\vartheta_2^2+2\lambda\,(\lambda+\vartheta_2)\right)\\ &\quad\left.+\Delta_2^2\left(2\lambda^2+2\,(\vartheta_1+\vartheta_2)\,\lambda+\vartheta_2\,(\vartheta_1+\vartheta_2)\right)\right\}v_z^2\\ &\quad+(\lambda+\vartheta_1)\,(\lambda+\vartheta_2)\left\{\Delta_1^4+\left(2\lambda^2+2\,(\vartheta_1+\vartheta_2)\,\lambda-2\Delta_2^2+\vartheta_2\,(\vartheta_1+\vartheta_2)\right)\Delta_1^2\right.\\ &\quad\left.+\left(\Delta_2^2+\lambda\,(\lambda+\vartheta_2)\right)\left(\Delta_2^2+(\lambda+\vartheta_1)\,(\lambda+\vartheta_1+\vartheta_2)\right)\right\}\,. \end{aligned} \tag{3.5.25}$$

[1] Using the generalized form of the coupled equations of motion given in Appendix A.2 leads to the same result.

Alternatively, written with the eigenfrequencies and ordered by powers of λ

$$
\begin{aligned}
N(\lambda) &= \lambda^6 + 3\left(\vartheta_1+\vartheta_2\right)\lambda^5 + \left(v_z^2 + 3\vartheta_1^2 + 3\vartheta_2^2 + \frac{1}{2}\left(\Omega_-^2+\Omega_+^2\right) + 8\vartheta_1\vartheta_2\right)\lambda^4 \\
&\quad + \Big[\vartheta_1^3 + 7\vartheta_2\vartheta_1^2 + \left(4v_z^2 + 2\Delta_1^2 + \Delta_2^2 + 7\vartheta_2^2\right)\vartheta_1 + \pi v_z K_1\Delta_1^2 + \pi v_z K_2\Delta_2^2 \\
&\qquad + \vartheta_2\left(4v_z^2 + \Delta_1^2 + 2\Delta_2^2 + \vartheta_2^2\right)\Big]\lambda^3 \\
&\quad + \Big[\frac{1}{2}\left(\Omega_-^2+\Omega_+^2+6\vartheta_1^2+6\vartheta_2^2+8\vartheta_1\vartheta_2\right)v_z^2 + \pi K_2\Delta_2^2\left(3\vartheta_1+\vartheta_2\right)v_z \\
&\qquad + \pi K_1\Delta_1^2\left(\vartheta_1+3\vartheta_2\right)v_z + \Delta_1^2\vartheta_1\left(\vartheta_1+2\vartheta_2\right) \\
&\qquad + \vartheta_2\left(2\vartheta_1+\vartheta_2\right)\left(\Delta_2^2 + \vartheta_1\left(\vartheta_1+2\vartheta_2\right)\right)\Big]\lambda^2 \\
&\quad + \Big[\left(v_z^2+\vartheta_2^2\right)\vartheta_1^3 + \vartheta_2\left(v_z^2+\Delta_1^2+\vartheta_2^2\right)\vartheta_1^2 + \left(v_z^2+\Delta_2^2\right)\left(v_z^2+\vartheta_2^2\right)\vartheta_1 \\
&\qquad + \pi v_z K_2\Delta_2^2\left(v_z^2 - \Delta_1^2 + \Delta_2^2 + 3\vartheta_1^2 + 2\vartheta_1\vartheta_2\right) + v_z^2\vartheta_2\left(v_z^2+\Delta_1^2+\vartheta_2^2\right) \\
&\qquad + \pi v_z K_1\Delta_1^2\left(v_z^2 + \Delta_1^2 - \Delta_2^2 + 3\vartheta_2^2 + 2\vartheta_1\vartheta_2\right)\Big]\lambda \\
&\quad + \pi v_z\Big[K_1\left(\vartheta_1\left(v_z^2+\vartheta_2^2\right) + \vartheta_2\left(v_z^2+\Delta_1^2-\Delta_2^2+\vartheta_2^2\right)\right)\Delta_1^2 \\
&\qquad + K_2\Delta_2^2\left(\vartheta_1\left(v_z^2 - \Delta_1^2 + \Delta_2^2 + \vartheta_1^2\right) + \left(v_z^2+\vartheta_1^2\right)\vartheta_2\right)\Big]\,, \\
D(\lambda) &= \lambda^6 + 3\left(\vartheta_1+\vartheta_2\right)\lambda^5 + \left(\Omega_-^2+\Omega_+^2+3\vartheta_1^2+3\vartheta_2^2+8\vartheta_1\vartheta_2\right)\lambda^4 \\
&\quad + \left(\vartheta_1+\vartheta_2\right)\left(4v_z^2 + 4\Delta_1^2 + 4\Delta_2^2 + \vartheta_1^2 + \vartheta_2^2 + 6\vartheta_1\vartheta_2\right)\lambda^3 \\
&\quad + \Big[2\vartheta_2\vartheta_1^3 + \left(2\Delta_1^2 + 5\vartheta_2^2 + 3\left(v_z^2+\Delta_2^2\right)\right)\vartheta_1^2 \\
&\qquad + \vartheta_2\left(4v_z^2 + 7\Delta_1^2 + 7\Delta_2^2 + 2\vartheta_2^2\right)\vartheta_1 + \Omega_-^2\Omega_+^2 + \left(2\Delta_2^2 + 3\left(v_z^2+\Delta_1^2\right)\right)\vartheta_2^2\Big]\lambda^2 \\
&\quad + \left(\vartheta_1+\vartheta_2\right)\Big[\Delta_1^4 + \left(2v_z^2 - 2\Delta_2^2 + \vartheta_2^2 + 3\vartheta_1\vartheta_2\right)\Delta_1^2 + \Delta_2^4 \\
&\qquad + \Delta_2^2\left(2v_z^2 + \vartheta_1^2 + 3\vartheta_1\vartheta_2\right) + \left(v_z^2+\vartheta_1^2\right)\left(v_z^2+\vartheta_2^2\right)\Big]\lambda \\
&\quad + \Delta_1^4\vartheta_1\vartheta_2 + \Delta_2^2\vartheta_2\left(\vartheta_1\left(v_z^2+\Delta_2^2+\vartheta_1^2\right) + \left(v_z^2+\vartheta_1^2\right)\vartheta_2\right) \\
&\quad + \Delta_1^2\vartheta_1\left(\vartheta_1\left(v_z^2+\vartheta_2^2\right) + \vartheta_2\left(v_z^2 - 2\Delta_2^2 + \vartheta_2^2\right)\right)\,.
\end{aligned}
\tag{3.5.26}
$$

The long time behavior is in agreement with the Boltzmann distribution of Eq. (3.1.11) for identical spins in the Markov limit, i.e.,

$$
\langle\sigma_z\tau_z\rangle_{\mathrm{eq}} = \frac{v_z}{2T}\,. \tag{3.5.27}
$$

3.5.1 Low temperature and one-boson self-energy

Again, the next step is to perform a systematic low temperature approximation for the denominator of $\langle\sigma_z\tau_z\rangle$ from Eq. (3.5.23), and further, to derive the one-boson self-energy, which allows us to expand the low temperature approximation to the quantum-noise regime.

First, we make an expansion around $\lambda = \pm\mathrm{i}\,\Omega_+ - \kappa_3$ and $\lambda = \pm\mathrm{i}\,\Omega_- - \kappa_4$ up to first order in the temperatures ϑ_1 and ϑ_2 and to first order in κ_3 and κ_4. The results are

$$\kappa_3 = \frac{\vartheta_1 + \vartheta_2}{2} \qquad \text{and} \qquad \kappa_4 = \frac{\vartheta_1 + \vartheta_2}{2} \,. \tag{3.5.28}$$

A direct expansion around the relaxation poles $\lambda = -\kappa_{5,6}$ does not work because they appear in a quadratic form. We instead make the ansatz

$$(\lambda + \mathrm{i}\,\Omega_+ + \kappa_3)(\lambda - \mathrm{i}\,\Omega_+ + \kappa_3)(\lambda + \mathrm{i}\,\Omega_- + \kappa_4)(\lambda - \mathrm{i}\,\Omega_- + \kappa_4)(\lambda + \kappa_5)(\lambda + \kappa_6) \tag{3.5.29}$$

for the denominator of $\langle \sigma_z \tau_z \rangle$ and identify the coefficients by comparison. This results in six Vieta relations, where we can use those for λ^0 and λ^1 to determine κ_5 and κ_6. By keeping terms of order $\mathcal{O}(\vartheta^2)$, we get

$$\begin{aligned} \kappa_5\,\kappa_6 &= \frac{(\Delta_1^2 - \Delta_2^2)^2\,\vartheta_1\,\vartheta_2 + v_z^2\,(\vartheta_1 + \vartheta_2)(\Delta_1^2\,\vartheta_1 + \Delta_2^2\,\vartheta_2)}{\Omega_+^2\,\Omega_-^2} \,, \\ \kappa_5 + \kappa_6 &= \vartheta_1 + \vartheta_2 \,. \end{aligned} \tag{3.5.30}$$

Solving (3.5.30) for $\kappa_{5,6}$ yields

$$\kappa_5 = \frac{\Omega^2 - \Delta_1^2}{\Omega^2 - \delta^2}\,\vartheta_1 + \frac{\Omega^2 - \Delta_2^2}{\Omega^2 - \delta^2}\,\vartheta_2 \qquad \text{and} \qquad \kappa_6 = \frac{\Delta_1^2 - \delta^2}{\Omega^2 - \delta^2}\,\vartheta_1 + \frac{\Delta_2^2 - \delta^2}{\Omega^2 - \delta^2}\,\vartheta_2 \,. \tag{3.5.31}$$

In next order of $\vartheta_{1,2}$ we get a frequency shift for Ω_+ and Ω_-. It can be calculated by a series expansion of the denominator up to second order in $\vartheta_{1,2}$ and to first order in $\Omega_+^{(\mathrm{s})}$ and $\Omega_-^{(\mathrm{s})}$ around $\lambda = \pm\mathrm{i}\left(\Omega_+ - \Omega_+^{(\mathrm{s})}\right) - \kappa_3$ and $\lambda = \pm\mathrm{i}\left(\Omega_- - \Omega_-^{(\mathrm{s})}\right) - \kappa_4$. The results are

$$\begin{aligned} \Omega_+^{(\mathrm{s})} = &-\frac{v_z^2(v_z^2 + \Delta_1^2 + 3\,\Delta_1\,\Delta_2 + \Delta_2^2)}{4\,\Delta_1\,\Delta_2\,\Omega_+^3}\,\vartheta_1\,\vartheta_2 \\ &+ \frac{v_z^4 + \Delta_2\,(\Delta_1 + \Delta_2)^3 + v_z^2\,\Delta_2\,(3\,\Delta_1 + 2\,\Delta_2)}{8\,\Delta_1\,\Delta_2\,\Omega_+^3}\,\vartheta_1^2 \\ &+ \frac{v_z^4 + \Delta_1\,(\Delta_1 + \Delta_2)^3 + v_z^2\,\Delta_1\,(2\,\Delta_1 + 3\,\Delta_2)}{8\,\Delta_1\,\Delta_2\,\Omega_+^3}\,\vartheta_2^2 \end{aligned} \tag{3.5.32}$$

and

$$\begin{aligned} \Omega_-^{(\mathrm{s})} = &\frac{v_z^2(v_z^2 + \Delta_1^2 - 3\,\Delta_1\,\Delta_2 + \Delta_2^2)}{4\,\Delta_1\,\Delta_2\,\Omega_-^3}\,\vartheta_1\,\vartheta_2 \\ &- \frac{v_z^4 - \Delta_2\,(\Delta_1 - \Delta_2)^3 - v_z^2\,\Delta_2\,(3\,\Delta_1 - 2\,\Delta_2)}{8\,\Delta_1\,\Delta_2\,\Omega_-^3}\,\vartheta_1^2 \\ &- \frac{v_z^4 + \Delta_1\,(\Delta_1 - \Delta_2)^3 + v_z^2\,\Delta_1\,(2\,\Delta_1 - 3\,\Delta_2)}{8\,\Delta_1\,\Delta_2\,\Omega_-^3}\,\vartheta_2^2. \end{aligned} \tag{3.5.33}$$

We do not get a shift of the damping rates in order $\vartheta_{1,2}^3$ for κ_3 and κ_4. This can be seen by using the upper results and performing a series expansion around $\lambda = \pm\mathrm{i}\left(\Omega_+ - \Omega_+^{(\mathrm{s})}\right) - \kappa_3 - \kappa_3^{(\mathrm{s})}$ and $\lambda = \pm\mathrm{i}\left(\Omega_- - \Omega_-^{(\mathrm{s})}\right) - \kappa_4 - \kappa_4^{(\mathrm{s})}$. The results are

$$\kappa_3^{(\mathrm{s})} = 0 \qquad \text{and} \qquad \kappa_4^{(\mathrm{s})} = 0 \,. \tag{3.5.34}$$

For the 5^{th} and 6^{th} pole we do not get a frequency shift, reflecting their pure relaxation pole characteristic.

A similar calculation as in Section (3.4.1) allows us to generalize the temperature dependence to the quantum-noise regime. The rates $\kappa_{3,4}$ generalize to

$$\begin{aligned}
\kappa_{3,4} &= \frac{1}{2}\Big(\theta_1^{(\Omega_\pm)} + \theta_2^{\Omega_\pm)}\Big) \,, \\
\theta_1^{(\Omega_\pm)} &= \frac{\pi}{2}\,\frac{\Omega^2-\Delta_1^2}{\Omega^2-\delta^2}\,S_1(\delta) + \frac{\pi}{2}\,\frac{\Delta_1^2-\delta^2}{\Omega^2-\delta^2}\,S_1(\Omega) \,, \\
\theta_2^{(\Omega_\pm)} &= \frac{\pi}{2}\,\frac{\Omega^2-\Delta_2^2}{\Omega^2-\delta^2}S_2(\delta) + \frac{\pi}{2}\,\frac{\Delta_2^2-\delta^2}{\Omega^2-\delta^2}\,S_2(\Omega) \,.
\end{aligned} \tag{3.5.35}$$

For $\kappa_{5,6}$ we need to be more careful. Since $\kappa_{5,6}$ appear in a quadratic form in λ we need to keep terms of order $\mathcal{O}(K_{1,2}^2)$ in the self-energy. An alternative way is to take the results for the relaxation rates from the Bloch-Redfield calculation in Chapter 4 and determine the temperature generalization reversely starting from the high-temperature rates $\kappa_{5,6}$. In any case, the generalization reads

$$\begin{aligned}
\kappa_5 &= \frac{\pi}{2}\,\frac{\Omega^2-\Delta_1^2}{\Omega^2-\delta^2}\,\theta_1^{(0)} + \frac{\pi}{2}\,\frac{\Omega^2-\Delta_2^2}{\Omega^2-\delta^2}\,\theta_2^{(0)} \,, \\
\kappa_6 &= \frac{\pi}{2}\,\frac{\Delta_1^2-\delta^2}{\Omega^2-\delta^2}\,\theta_1^{(0)} + \frac{\pi}{2}\,\frac{\Delta_2^2-\delta^2}{\Omega^2-\delta^2}\,\theta_2^{(0)} \,,
\end{aligned} \tag{3.5.36}$$

with the generalized temperatures

$$\begin{aligned}
\theta_{1,2}^{(0)} = \frac{\pi}{4}\Big\{ & S_{1,2}(\Omega) + S_{1,2}(\delta) \pm \frac{\Delta_-^4 + v_z^2\Delta_+^2}{(\Omega^2-\delta^2)\Delta_-^2}\,[S_{1,2}(\Omega) - S_{1,2}(\delta)] \\
& \pm \frac{2v_z^2\Delta_{2,1}^2}{(\Omega^2-\delta^2)\Delta_-^2}\,[S_{2,1}(\Omega) - S_{2,1}(\delta)]\Big\} \,.
\end{aligned} \tag{3.5.37}$$

We have used the abbreviation $\Delta_1^2 \pm \Delta_2^2 = \Delta_\pm^2$. These expressions can be significantly simplified to

$$\begin{aligned}
\kappa_5 &= \frac{\pi}{2}\,\frac{\Omega^2-\Delta_1^2}{\Omega^2-\delta^2}\,S_1(\delta) + \frac{\pi}{2}\,\frac{\Omega^2-\Delta_2^2}{\Omega^2-\delta^2}\,S_2(\delta) \,, \\
\kappa_6 &= \frac{\pi}{2}\,\frac{\Delta_1^2-\delta^2}{\Omega^2-\delta^2}\,S_1(\Omega) + \frac{\pi}{2}\,\frac{\Delta_2^2-\delta^2}{\Omega^2-\delta^2}\,S_2(\Omega) \,.
\end{aligned} \tag{3.5.38}$$

This makes clear that the transition to the quantum-noise regime is done by replacing $\vartheta_{1,2}$ with the corresponding $S_{1,2}(\Omega,\delta)$. We see by comparing the above results with (3.5.35), that $\kappa_{3,4}$ may as well be written as $\kappa_{3,4} = (\kappa_5 + \kappa_6)/2$ (also compare Eqs. (3.5.28) and (3.5.30)).

Now, we proceed and calculate the residues of $\langle\sigma_z\tau_z\rangle$. We get for the amplitudes

belonging to the poles $\lambda = \pm\mathrm{i}\,\Omega_+ - \kappa_3$ and $\lambda = \pm\mathrm{i}\,\Omega_- - \kappa_4$

$$\begin{aligned}\mathrm{Res}\,[\sigma_z\tau_z(\lambda = \pm\mathrm{i}\,\Omega_+ - \kappa_3)] &= \frac{1}{4}\left(1 - \frac{v_z^2}{\Omega_+^2}\right)\,,\\ \mathrm{Res}\,[\sigma_z\tau_z(\lambda = \pm\mathrm{i}\,\Omega_- - \kappa_4)] &= \frac{1}{4}\left(1 - \frac{v_z^2}{\Omega_-^2}\right)\,.\end{aligned} \tag{3.5.39}$$

The residues describing the equilibrium contribution and the relaxation rates are

$$\begin{aligned}\mathrm{Res}\,[\sigma_z\tau_z(\lambda = 0)] &= \frac{v_z}{2\,T} = \langle\sigma_z\tau_z\rangle_{\mathrm{eq}}\,,\\ \mathrm{Res}\,[\sigma_z\tau_z(\lambda = \kappa_5)] &= \frac{v_z^2\delta^2}{(\Omega^2-\delta^2)^2} + \frac{\delta^2\,\langle\sigma_z\tau_z\rangle_{\mathrm{eq}}}{\Omega^2-\delta^2}\,,\\ \mathrm{Res}\,[\sigma_z\tau_z(\lambda = \kappa_6)] &= \frac{v_z^2\Omega^2}{(\Omega^2-\delta^2)^2} - \frac{\Omega^2\,\langle\sigma_z\tau_z\rangle_{\mathrm{eq}}}{\Omega^2-\delta^2}\,.\end{aligned} \tag{3.5.40}$$

Observe that the equilibrium contribution is in agreement with the Markov limit of Eq. (3.1.11).

3.5.2 Large coupling v_z and/or high temperature

The dynamics of $\langle\sigma_z\tau_z(t)\rangle$ for large coupling v_z and/or high temperature is described in leading order by pure relaxation

$$\langle\sigma_z\tau_z(t)\rangle = (1 - \langle\sigma_z\tau_z\rangle_{\mathrm{eq}})\;\mathrm{e}^{-\gamma_{\sigma\tau}\,t} + \langle\sigma_z\tau_z\rangle_{\mathrm{eq}}\,. \tag{3.5.41}$$

In the large-coupling limit, $v_z \gg \Delta_{1,2},\,\vartheta_{1,2}$, the relaxation rate $\gamma_{\sigma\tau}$ is calculated to

$$\gamma_{\sigma\tau} \;=\; \frac{\Delta_1^2}{v_z^2}\,\vartheta_1 \;+\; \frac{\Delta_2^2}{v_z^2}\,\vartheta_2\,. \tag{3.5.42}$$

The relaxation rate of the effective single spin receives rate contributions from both the σ- and the τ-spin as if these were independent biased spins in contact with their own heat reservoir. The two terms describe single-spin contributions for large bias.

On the other hand, in the high temperature limit, $\vartheta_{1,2} \gg v_z,\,\Delta_{1,2}$, the relaxation rate adopts a Kondo-like form

$$\gamma_{\sigma\tau} \;=\; \frac{\Delta_1^2}{\vartheta_1} + \frac{\Delta_2^2}{\vartheta_2}\,. \tag{3.5.43}$$

We consider next the regime $\vartheta_1 \gg \Delta_1,\,\Delta_2,\,v_z$. Here, the spin σ behaves Kondo-like as in Eq. (3.4.53). The dynamics of the σ-spin should be almost frozen compared to that of the τ-spin. Therefore, we assume that $\langle\sigma_z\tau_z(t)\rangle$ describes the behavior of a biased single spin-boson model as ϑ_1 is increased. Keeping terms of linear order in γ_σ (see Eq. (3.4.53)) in the pole equation, the expression (3.5.23) with (3.5.25) takes the form

$$\langle\sigma_z\tau_z(\lambda)\rangle = \frac{\lambda^2 \,+\, 2\vartheta_2\lambda \,+\, v_z^2 + \vartheta_2^2 + \pi K_2 v_z\Delta_2^2/\lambda}{\lambda^3 \,+\, 2(\vartheta_2+\gamma_\sigma)\lambda^2 \,+\, (\Delta_2^2 + v_z^2 + \vartheta_2^2 + 3\gamma_\sigma\vartheta_2)\lambda \,+\, \Delta_2^2\vartheta_2 + \gamma_\sigma(v_z^2+\vartheta_2^2)}\,. \tag{3.5.44}$$

In the limit $\gamma_\sigma \to 0$ this form reduces indeed to the expression $\langle\tau_z(\lambda)\rangle$ of a biased spin-boson model in the Markov-regime (see Section 2).

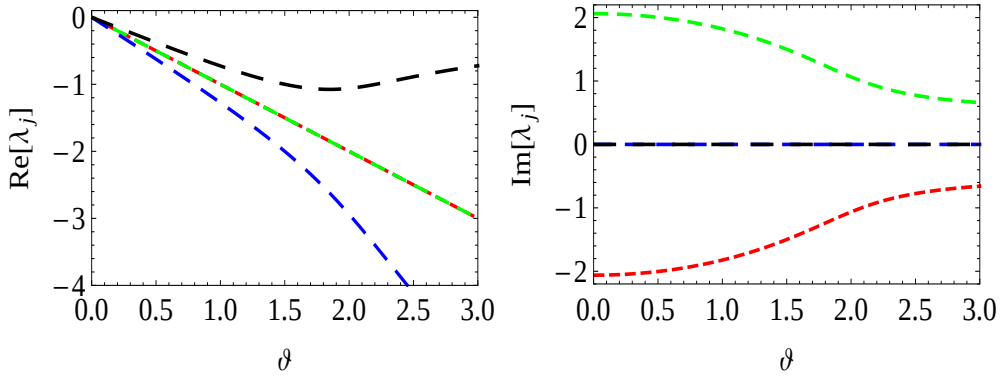

Figure 3.10: $\langle\sigma_z\tau_z\rangle$: real and imaginary part of λ_j with $v_z = 0.5$, $\Delta = 1$. The behavior is the same for all temperature and there are no crossover temperatures. The colors red, green, blue, and black label $\mathrm{Re}\,[\lambda_j]$ and $\mathrm{Im}\,[\lambda_j]$, with $j = 1, 2, 3, 4$.

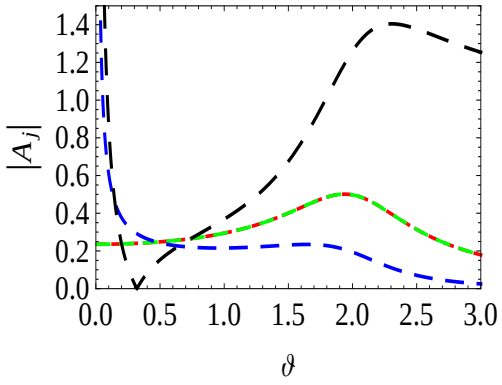

Figure 3.11: $\langle\sigma_z\tau_z\rangle$: absolute part of $\langle\sigma_z\tau_z\rangle$ with $v_z = 0.4$, $\Delta = 1$, and $K = 0.05$. The colors red, green, blue, and black label $|A_j|$ with $j = 1, 2, 3, 4$.

3.5.3 Qualitative features of identical spins

Here we will analyze the dependence of $\langle\sigma_z\tau_z\rangle$ on temperature for the case of two identical spins. This means $\vartheta = \vartheta_1 = \vartheta_2$ and $\Delta = \Delta_1 = \Delta_2$. The resulting equation for $\langle\sigma_z\tau_z\rangle$ is of fourth order in the denominator.
The real and imaginary part of the zeros is shown in Fig. 3.10. In Fig. 3.11 the absolute part is shown. We have two real poles and one complex conjugate pole for all temperature; there is no crossover temperature. The amplitudes of the oscillatory contribution are equal and approach zero for high temperature. The stronger damped relaxation pole has an amplitude below the oscillatory amplitudes and also approaches zero for increasing temperature. The weakly damped relaxation pole is Kondo-like and is dominating for high temperature. Its amplitude approaches zero once for low temperature.

3.6 Other forms of mutual coupling

So far, we have studied two spins interacting via longitudinal v_z coupling, i.e., with $-\frac{v_z}{2}\,\sigma_z\tau_z$. This is an Ising type model. But the two spins might also interact via the transverse x and/or y components. If we include all interaction types and bias terms $\epsilon_{1,2}$ we end up with the Hamiltonian

$$\begin{aligned} H = &-\frac{\Delta_1}{2}(\sigma_x\otimes\mathbb{1}_2) - \frac{\Delta_2}{2}(\mathbb{1}_2\otimes\tau_x) - \frac{v_x}{2}(\sigma_x\otimes\tau_x) - \frac{v_y}{2}(\sigma_y\otimes\tau_y) - \frac{v_z}{2}(\sigma_z\otimes\tau_z) \\ &- \frac{\epsilon_1}{2}(\sigma_z\otimes\mathbb{1}_2) - \frac{\epsilon_2}{2}(\mathbb{1}_2\otimes\tau_z)\,. \end{aligned} \tag{3.6.1}$$

The characteristic polynomial of this Hamiltonian, $\det(H-\omega\,\mathbb{1}_4)$, is of a biquadratic form plus a linear term in ω, which reads $\omega(v_z\,\epsilon_1\,\epsilon_2 + v_x\,\Delta_1\,\Delta_2 - v_x\,v_y\,v_z)$. It vanishes for $v_x = 0$ and if one of the biases is equal to zero. In this case, an analytic solution of the Hamiltonian plus bath can be done. If both biases are zero, it is possible to gain analytic solutions even for $v_x \neq 0$. Otherwise only systematic approximations are feasible.

The equations of motion in the Heisenberg picture for the above Hamiltonian result in a set of 15 coupled equations, which are shown in Appendix A.2.

In the remainder of this section we discuss two spins with simultaneous v_y and v_z coupling. This type of coupling, together with the pure v_z coupling, is most relevant for charge/flux Josephson junction devices[2]. The necessary steps are similar to the analysis of the Sections 3.1 – 3.5. We start with the diagonalization matrix U

$$U = \frac{1}{2}\begin{pmatrix} \frac{\cos(\Theta_1)}{\sqrt{1+\sin(\Theta_1)}} & \sqrt{1+\sin(\Theta_1)} & \sqrt{1+\sin(\Theta_1)} & \frac{\cos(\Theta_1)}{\sqrt{1+\sin(\Theta_1)}} \\ -\frac{\cos(\Theta_2)}{\sqrt{1-\sin(\Theta_2)}} & \sqrt{1-\sin(\Theta_2)} & -\sqrt{1-\sin(\Theta_2)} & \frac{\cos(\Theta_2)}{\sqrt{1-\sin(\Theta_2)}} \\ -\frac{\cos(\Theta_2)}{\sqrt{1+\sin(\Theta_2)}} & -\sqrt{1+\sin(\Theta_2)} & \sqrt{1+\sin(\Theta_2)} & \frac{\cos(\Theta_2)}{\sqrt{1+\sin(\Theta_2)}} \\ \frac{\cos(\Theta_1)}{\sqrt{1-\sin(\Theta_1)}} & -\sqrt{1-\sin(\Theta_1)} & -\sqrt{1-\sin(\Theta_1)} & \frac{\cos(\Theta_1)}{\sqrt{1-\sin(\Theta_1)}} \end{pmatrix}, \tag{3.6.2}$$

where the mixing angles read

$$\Theta_1 = \arctan\left(\frac{v_y - v_z}{\Delta_1 + \Delta_2}\right) \qquad \text{and} \qquad \Theta_2 = \arctan\left(\frac{v_y + v_z}{\Delta_1 - \Delta_2}\right). \tag{3.6.3}$$

This leads to the diagonalized Hamiltonian

$$\widetilde{H} = U\,H\,U^{-1} = -\frac{\Omega}{2}\,(\sigma_z\otimes\mathbb{1}) - \frac{\delta}{2}\,(\mathbb{1}\otimes\tau_z), \tag{3.6.4}$$

with the eigenfrequencies

$$\begin{aligned} \Omega &= \frac{1}{2}(\Omega_+ + \Omega_-)\,, & \delta &= \frac{1}{2}(\Omega_+ - \Omega_-), \\ \Omega_+ &= \sqrt{(\Delta_1+\Delta_2)^2 + (v_y - v_z)^2}\,, & \Omega_- &= \sqrt{(\Delta_1-\Delta_2)^2 + (v_y + v_z)^2}\,. \end{aligned} \tag{3.6.5}$$

[2] In Appendix A.2, we study two spins interacting with v_y coupling alone, afterwards two spins with v_x, v_y, and v_z coupling, and finally two spins with v_y and v_z coupling and a bias ϵ_1.

These eigenfrequencies fulfill the Vieta relations

$$\begin{aligned} \Omega_+^2 + \Omega_-^2 &= 2\,(\Delta_1^2 + \Delta_2^2 + v_y^2 + v_z^2)\;, \quad \Omega^2 + \delta^2 = \Delta_1^2 + \Delta_2^2 + v_y^2 + v_z^2\;, \\ \Omega^2\,\delta^2 &= (v_y\,v_z - \Delta_1\,\Delta_2)^2\;. \end{aligned} \tag{3.6.6}$$

The thermodynamical equilibrium values are calculated to (cf. Sec. 3.1)

$$\langle \sigma_z \rangle_{\rm eq} = \langle \tau_z \rangle_{\rm eq} = 0 \tag{3.6.7}$$

and

$$\langle \sigma_z \tau_z \rangle_{\rm eq} = \frac{(\Omega\,v_y + \delta\,v_z)\tanh\left(\frac{\beta\,\delta}{2}\right) - (\delta\,v_y + \Omega\,v_z)\tanh\left(\frac{\beta\,\Omega}{2}\right)}{\delta^2 - \Omega^2}\;. \tag{3.6.8}$$

Thereby, the leading contributions for high temperature are

$$\langle \sigma_z \tau_z \rangle_{\rm eq} \approx \frac{v_z}{2\,T} - \frac{1}{24\,T^3}\left[v_z\,(\delta^2 + \Omega^2) + v_y\,\delta\,\Omega\right] + \mathcal{O}\left(\frac{1}{T}\right)^5\;. \tag{3.6.9}$$

We see that the v_y coupling is irrelevant for the equilibrium value of $\langle \sigma_z \tau_z \rangle_{\rm eq}$ in leading order of high temperature, regardless of its value.

For the undamped system in Laplace space we obtain the following expressions

$$\begin{aligned} \langle \sigma_z(\lambda) \rangle &= \frac{\lambda\,(\lambda^2 + \Delta_2^2 + v_z^2)}{(\lambda^2 + \Omega^2)(\lambda^2 + \delta^2)}\;, \\ \langle \sigma_z \tau_z(\lambda) \rangle &= N_{\sigma_z\tau_z}/D_{\sigma_z\tau_z}\;, \end{aligned} \tag{3.6.10}$$

where numerator and denominator of $\langle \sigma_z \tau_z(\lambda) \rangle$ are given by

$$\begin{aligned} N_{\sigma_z\tau_z} &= v_y^4 + \left(2\lambda^2 + \Delta_1^2 + \Delta_2^2 - 2v_z^2\right) v_y^2 + 4\Delta_1\Delta_2 v_y\,v_z \\ &\quad + \left(\lambda^2 + v_z^2\right)\left(\lambda^2 + \Delta_1^2 + \Delta_2^2 + v_z^2\right)\;, \\ D_{\sigma_z\tau_z} &= \lambda\left[\lambda^2 + \Omega_+^2\right]\left[\lambda^2 + \Omega_-^2\right]\;. \end{aligned} \tag{3.6.11}$$

The kernel for $\langle \sigma_z(\lambda) \rangle$ in the white-noise limit is calculated straightforward with the equations of motion from Appendix A.2 and reads

$$\mathcal{K}_{\sigma_z}(\lambda) = \frac{\left[(\lambda + \vartheta_1)^2\,v_z^2\right] v_y^2 - 2\Delta_1\Delta_2 v_y v_z + \Delta_1^2\,(\Delta_2^2 + (\lambda + \vartheta_1)\,(\lambda + \vartheta_1 + \theta_2))}{(\lambda + \vartheta_1 + \vartheta_2)\,v_z^2 + (\lambda + \vartheta_1)\,(\Delta_2^2 + (\lambda + \vartheta_1)\,(\lambda + \vartheta_1 + \vartheta_2))}\;. \tag{3.6.12}$$

For $\langle \sigma_z \tau_z(\lambda) \rangle$ the kernel $\mathcal{K}_{\sigma_z\tau_z}(\lambda) = N_{\sigma_z\tau_z}/D_{\sigma_z\tau_z}$ reads

$$\begin{aligned} N_{\sigma_z\tau_z} &= (\lambda + \vartheta_1 + \vartheta_2)\Big[2v_y v_z \Delta_1\Delta_2\,(2\lambda + \vartheta_1 + \vartheta_2) + v_y^2\left((\lambda + \vartheta_2)\,\Delta_1^2 + \Delta_2^2\,(\lambda + \vartheta_1)\right) \\ &\quad + v_z^2\left((\lambda + \vartheta_1)\,\Delta_1^2 + \Delta_2^2\,(\lambda + \vartheta_2)\right)\Big] \\ &\quad + (\lambda + \vartheta_1)\,(\lambda + \vartheta_2)\Big[\Delta_1^4 + \left((\lambda + \vartheta_2)\,(\lambda + \vartheta_1 + \vartheta_2) - 2\Delta_2^2\right)\Delta_1^2 \\ &\quad + \Delta_2^2\left(\Delta_2^2 + (\lambda + \vartheta_1)\,(\lambda + \vartheta_1 + \vartheta_2)\right)\Big]\;, \\ D_{\sigma_z\tau_z} &= (\lambda + \vartheta_1 + \vartheta_2)\,v_y^4 + 2v_z\Delta_1\Delta_2\,(2\lambda + \vartheta_1 + \vartheta_2)\,v_y + v_z^4\,(\lambda + \vartheta_1 + \vartheta_2) \\ &\quad + v_z^2\left((\lambda + \vartheta_2)\,\Delta_1^2 + \Delta_2^2\,(\lambda + \vartheta_1) + (\lambda + \vartheta_1 + \vartheta_2)\left(\vartheta_1^2 + 2\lambda\vartheta_1 + \vartheta_2^2 + 2\lambda\,(\lambda + \vartheta_2)\right)\right) \\ &\quad + (\lambda + \vartheta_1)\,(\lambda + \vartheta_2)\left((\lambda + \vartheta_1)\,\Delta_1^2 + (\lambda + \vartheta_2)\left(\Delta_2^2 + (\lambda + \vartheta_1)\,(\lambda + \vartheta_1 + \vartheta_2)\right)\right) \\ &\quad + v_y^2\left(-2\,(\lambda + \vartheta_1 + \vartheta_2)\,v_z^2 + \Delta_1^2\,(\lambda + \vartheta_1) + (\lambda + \vartheta_2)\left(\Delta_2^2 + 2\,(\lambda + \vartheta_1)\,(\lambda + \vartheta_1 + \vartheta_2)\right)\right). \end{aligned}$$

(3.6.13)

And as usual, with these kernels the form of $\langle\sigma_z(\lambda)\rangle$ and $\langle\sigma_z\tau_z(\lambda)\rangle$ is given by

$$\langle\sigma_z(\lambda)\rangle = \frac{1}{\lambda + \mathcal{K}_{\sigma_z}(\lambda)} \qquad \text{and} \qquad \langle\sigma_z\tau_z(\lambda)\rangle = \frac{1}{\lambda + \mathcal{K}_{\sigma_z\tau_z}(\lambda)}\,. \tag{3.6.14}$$

The influence phase contributions can be calculated with the generalized coupled equations of motion given in Eq. A.2.8. However, we will not note the rather lengthy expressions.

3.6.1 Systematic weak damping approximation for low temperature

Here, we will derive results valid in leading order of low temperature and weak bath coupling. These are obtained by doing a systematic weak damping approximation, i.e., a series expansion of the denominator of $\langle\sigma_z\rangle$ and $\langle\sigma_z\tau_z\rangle$ up to first order in the temperatures ϑ_1 and ϑ_2 and to first order in κ_Ω and κ_δ around $\lambda = \pm\mathrm{i}\,\delta - \kappa_\delta$, $\lambda = \pm\mathrm{i}\,\Omega - \kappa_\Omega$, $\lambda = \pm\mathrm{i}\,\Omega_+ - \kappa_{\Omega_+}$, $\lambda = \pm\mathrm{i}\,\Omega_- - \kappa_{\Omega_-}$, and the two pure relaxation poles of $\langle\sigma_z\tau_z\rangle$, which we call κ_{01}, κ_{02}. The results for the rates of $\langle\sigma_z\rangle$ are

$$\begin{aligned}
\kappa_\Omega &= \frac{3\Omega^2 - 2\Delta_1^2 - \Delta_2^2 - 2v_y^2 - v_z^2}{2\,(\Omega^2 - \delta^2)}\,\vartheta_1 + \frac{\Omega^2 - \Delta_1^2 - v_z^2}{2\,(\Omega^2 - \delta^2)}\,\vartheta_2\,,\\
\kappa_\delta &= \frac{2\Delta_1^2 + \Delta_2^2 + 2v_y^2 + v_z^2 - 3\delta^2}{2\,(\Omega^2 - \delta^2)}\,\vartheta_1 + \frac{\Delta_1^2 + v_z^2 - \delta^2}{2\,(\Omega^2 - \delta^2)}\,\vartheta_2\,.
\end{aligned} \tag{3.6.15}$$

For $\langle\sigma_z\tau_z\rangle$ we obtain the rates

$$\begin{aligned}
\kappa_{\Omega_+} &= \kappa_{\Omega_-} = \frac{\vartheta_1 + \vartheta_2}{2}\,,\\
\kappa_{01} &= \frac{\Delta_1^2 + v_y^2 - \delta^2}{\Omega^2 - \delta^2}\,\vartheta_1 + \frac{\Delta_2^2 + v_y^2 - \delta^2}{\Omega^2 - \delta^2}\,\vartheta_2\,,\\
\kappa_{02} &= \frac{\Omega^2 - \Delta_1^2 - v_y^2}{\Omega^2 - \delta^2}\,\vartheta_1 + \frac{\Omega^2 - \Delta_2^2 - v_y^2}{\Omega^2 - \delta^2}\,\vartheta_2\,.
\end{aligned} \tag{3.6.16}$$

We will postpone the generalization to the quantum-noise regime until Section 4.4, where we use the Bloch-Redfield method to calculate the respective expressions (see Eqs. (4.4.8), (4.4.16), and (4.4.17)).

The calculation of the amplitudes can be readily done in leading order of the damping

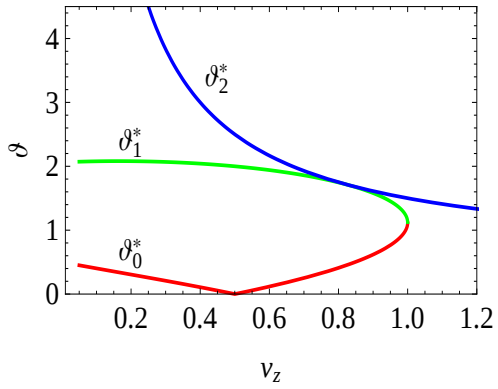

Figure 3.12: $\langle\sigma_z\rangle$: crossover temperatures that are separating coherent and incoherent regimes as functions of v_z, $\Delta = 1$, and $v_y = -0.5$.

strength and we obtain

$$\begin{aligned}
\mathrm{Res}[\langle\sigma_z(\lambda = \pm\mathrm{i}\Omega - \kappa_\Omega)\rangle] &= \frac{\Omega^2 - \Delta_2^2 - v_z^2}{2(\Omega^2 - \delta^2)}\,, \\
\mathrm{Res}[\langle\sigma_z(\lambda = \pm\mathrm{i}\delta - \kappa_\delta)\rangle] &= \frac{\Delta_2^2 + v_z^2 - \delta^2}{2(\Omega^2 - \delta^2)}\,, \\
\mathrm{Res}[\langle\sigma_z\tau_z(\lambda = \pm\mathrm{i}\Omega_+ - \kappa_{\Omega_+})\rangle] &= \frac{(\Delta_1 + \Delta_2)^2}{4\Omega_+^2}\,, \\
\mathrm{Res}[\langle\sigma_z\tau_z(\lambda = \pm\mathrm{i}\Omega_- - \kappa_{\Omega_-})\rangle] &= \frac{(\Delta_1 - \Delta_2)^2}{4\Omega_-^2}\,, \\
\mathrm{Res}[\langle\sigma_z\tau_z(\lambda = -\kappa_{01})\rangle] &= \frac{(\Omega v_z + \delta v_y)^2}{\Omega_+^2\Omega_-^2}\,, \\
\mathrm{Res}[\langle\sigma_z\tau_z(\lambda = -\kappa_{02})\rangle] &= \frac{(\Omega v_y + \delta v_z)^2}{\Omega_+^2\Omega_-^2}\,.
\end{aligned} \tag{3.6.17}$$

3.6.2 Qualitative features

Since simultaneous v_y and v_z coupling is special, as we will see in Section 3.7, we will shortly discuss some qualitative features. These are actually quite similar to sole v_z coupling, which was discussed in the Sections 3.4.3 and 3.5.3. The critical coupling strength for equal tunneling matrix elements and given v_y reads

$$v_z^{\mathrm{cr}} = \frac{1}{2}\left(\sqrt{2\,\Delta^2 + v_y^2} - v_y\right)\,. \tag{3.6.18}$$

If we choose $v_z < v_z^{\mathrm{cr}}$ the denominator contains three crossover temperatures ϑ_0^*, ϑ_1^*, and ϑ_2^* (see Fig. 3.12). For $v_z = -v_y$ one of the crossover temperatures, ϑ_0^*, vanishes. In this regime, we have two dephasing rates for temperatures $0 < \vartheta < \vartheta_1^*$. Otherwise, the discussion of the Sections 3.4.3 and 3.5.3 applies.

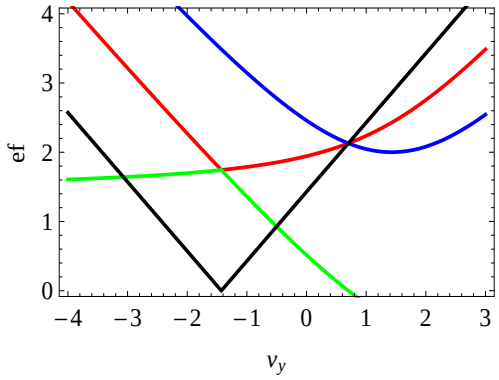

Figure 3.13: The eigenfrequency spectrum is shown for Ω (red), δ (green), Ω_+ (blue), and Ω_- (black) versus the coupling parameter v_y. For the left degeneracy point, we get $\Omega = \delta$ and $\Omega_- = 0$. The right degeneracy point is characterized by $\delta = 0$ and $\Omega = \Omega_\pm$. We used $\Delta_1 = \Delta_2 = 1$ and $v_z = 1.43$.

3.7 Path sums and quantum frustration of decoherence

In 2005 Novais et al. [29, 71] discovered reduced dissipation, when two uncorrelated baths are coupled to different non-commuting components of a single spin with a certain coupling strength. They observed a minimum in the decoherence rate due to the competition of the baths to localize the spin in one or another eigenstate, which are degenerate in energy. The non-commuting characteristic of the bath couplings prevents the spin to localize in one eigenstate. They dubbed this phenomenon *frustration of decoherence*.

We observe a similar behavior, if we take the results of the last subsection for v_y and v_z coupling (Sec. 3.6) and choose $v_{y,z} = v$ and $\Delta_{1,2} = \pm\Delta$, or $v_{y,z} = \pm v$ and $\Delta_{1,2} = \Delta$. For these specific values Ω and δ become degenerate (left degeneracy in Fig. 3.13) and we obtain a minimal damping rate, as can be seen in the time evolution of Fig. 3.14. This can be understood as a competition of two equally preferred ground states. The system could relax to parallel or anti-parallel alignment in y or z direction due to the couplings. And thus, the second spin-spin coupling partially suppresses decoherence. Here, the phenomenon is due to the non-commutative spin-spin couplings [29]. The undamped dynamics of $\langle\sigma_z\rangle$ simplifies for these values to an unbiased single spin problem

$$\langle\sigma_z(\lambda)\rangle\Big|_{\vartheta_1=\vartheta_2=0} = \frac{\lambda}{\lambda^2 + \Delta^2 + v^2} \,, \tag{3.7.1}$$

with the effective frequency $\Omega = \delta = \sqrt{\Delta^2 + v^2}$. Thus, the mutual coupling is only visible in the effective frequency.

It is instructive to study the quality factor of $\langle\sigma_z\rangle$ and compare it with the quality factor of a single spin system with and without bias. The quality factor is defined as

$$Q = \omega_i/\gamma_i \,, \tag{3.7.2}$$

where $\lambda_i = \pm\mathrm{i}\,\omega_i - \gamma_i$ are zeros of the denominator of $\langle\sigma_z(\lambda)\rangle$ given in Eq. (3.6.14) and $i = 1\ldots4$. The quality factor Q describes the ratio of total energy in the system to

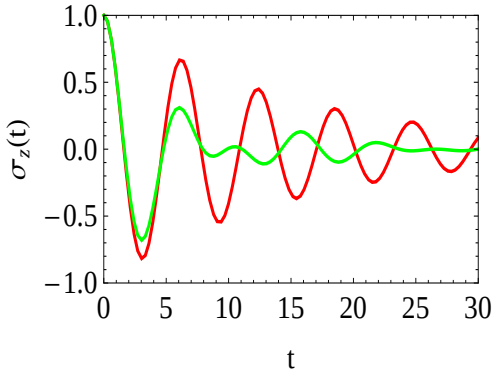

Figure 3.14: Quantum frustration of decoherence for $\langle\sigma_z\rangle$. The damping is much smaller for $v_y = -v_z$ (red), than for $v_y = v_z$ (green). The parameters are $v_z = 0.2$, $\Delta_1 = \Delta_2 = 1$, $K = 0.01$, and $T = 2$.

the energy dissipation rate. The behavior of the quality factor around the degeneracy is shown in Fig. 3.15, with bias for the corresponding single spin, and in Fig. 3.16, without bias for the corresponding single spin. The quality factor shows an increase for two of the rates around the degeneracy, while the other two rates show a decrease in the quality factor. This explains the long coherence time at the degeneracy point observed in Fig. 3.14.

We can study the frustration effect in detail within the low-temperature regime. The systematic weak damping expansion of Sec. 3.6.1 breaks down for equal tunneling matrix $\Delta_{1,2} = \Delta$ and equal coupling strength (but different sign) $v_{y,z} = \pm v$ because the eigenfrequencies become degenerate, i.e., $\Omega = \delta = \sqrt{\Delta^2 + v^2}$. This can be seen by the weak damping rates in Eqs. (3.6.15) – (3.6.17), where most of the denominators diverge. But, we can study the behavior in the vicinity of the degeneracy by choosing small parameters ϵ and η such that $\Delta_{1,2} = \Delta \pm \epsilon/2$ and $v_{y,z} = \pm v + \eta/2$. At the end, we take the limit $\epsilon \to 0$ and $\eta \to 0$. With the damping rates from Eq. (3.6.15), we obtain

$$\kappa_{\Omega,\delta} = \frac{3}{4}\vartheta_1 + \frac{1}{4}\vartheta_2 \mp \frac{\Delta}{4\Omega}(\vartheta_1 + \vartheta_2) \mp \frac{v}{4\Omega}(\vartheta_1 - \vartheta_2) \; . \tag{3.7.3}$$

For a discussion of the results it is easier to use equal baths, i.e., $\vartheta_1 = \vartheta_2 = \vartheta$. Then we obtain

$$\kappa_{\Omega,\delta} = \vartheta \mp \frac{\Delta}{2\Omega}\,\vartheta \; . \tag{3.7.4}$$

Thus, one of the dephasing rates is smaller and the other is larger compared to ϑ. This can be seen in Figs. 3.15 and 3.16 as cups around $v_y = -v_z$, where the quality factor increases or decreases, respectively. κ_Ω approaches $\vartheta/2$ for vanishing coupling v, while $\kappa_\delta \to 3\vartheta/2$. The former is the dephasing rate of the unbiased spin-boson problem in the high temperature limit, the amplitude of the latter vanishes for $v \to 0$. Explicitly, the

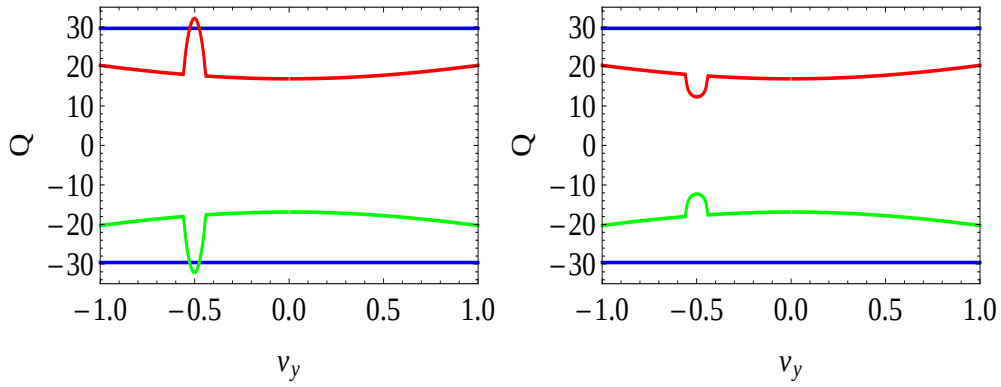

Figure 3.15: $\langle\sigma_z\rangle$: the quality factor Q is plotted versus the coupling v_y. The single spin has a finite bias. Red and green are the two coupled spins, while blue is the single spin. In the left figure is shown λ_3 and λ_4, in the right figure λ_1 and λ_2. In the vicinity of $v_y = -v_z$ an increase of the two-spin quality factor is observed in the left figure that even exceeds the single spin quality factor. In the right figure a decrease of the quality factor occurs. The parameters are $v_z = \epsilon = 0.5$, $\Delta_1 = \Delta_2 = 1$, $K = 0.01$, and $T = 1$.

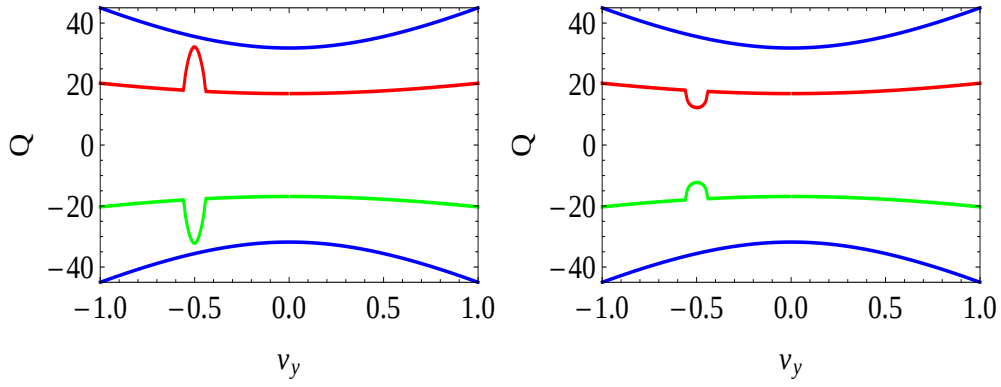

Figure 3.16: $\langle\sigma_z\rangle$: the quality factor versus the coupling v_y is plotted. The bias of the single spin is zero but it has effective frequency $\sqrt{\Delta^2 + v_y^2}$. Red and green are the two coupled spins, while blue is the single spin. In the left figure is shown λ_3 and λ_4, in the right figure λ_1 and λ_2. In the vicinity of $v_y = -v_z$ an increase of the two spin quality factor is observed in the left figure that gets close to the single spin quality factor. In the right figure a decrease of the quality factor occurs. The parameters are $v_z = 0.5$, $\epsilon = 0$, $\Delta_1 = \Delta_2 = 1$, $K = 0.01$, $T = 1$.

amplitudes of $\langle\sigma_z\rangle$ adopt for $v_{y,z} = \pm v$ and $\Delta_{1,2} = \Delta$ the form

$$\begin{aligned} \mathrm{Res}[\langle\sigma_z(\lambda = \pm\mathrm{i}\Omega - \kappa_\Omega)\rangle] &= \frac{1}{4}\left(1 + \frac{\Delta + v}{\Omega}\right), \\ \mathrm{Res}[\langle\sigma_z(\lambda = \pm\mathrm{i}\delta - \kappa_\delta)\rangle] &= \frac{1}{4}\left(1 - \frac{\Delta + v}{\Omega}\right). \end{aligned} \tag{3.7.5}$$

If the coupling v becomes small only $\mathrm{Res}[\langle\sigma_z(\lambda = \pm\mathrm{i}\Omega - \kappa_\Omega)\rangle] \to 1/2$ effectively contributes.

For $\langle\sigma_z\tau_z\rangle$ the picture is similar. The respective eigenfrequencies become $\Omega_+ = 2\Omega$ and $\Omega_- = 0$. The rates change to

$$\begin{aligned} \kappa_{01,02} &= \frac{\vartheta_1 + \vartheta_2}{2} \pm \frac{\Delta}{2\Omega}(\vartheta_1 - \vartheta_2) \pm \frac{v}{2\Omega}(\vartheta_1 + \vartheta_2), \\ \kappa_{\Omega_+} &= \kappa_{\Omega_-} = \frac{\vartheta_1 + \vartheta_2}{2}. \end{aligned} \tag{3.7.6}$$

The amplitudes are

$$\begin{aligned} \mathrm{Res}[\langle\sigma_z\tau_z(\lambda = \pm\mathrm{i}\Omega_+ - \kappa_{\Omega_+})\rangle] &= \frac{\Delta^2}{4\,\Omega^2}, \\ \mathrm{Res}[\langle\sigma_z\tau_z(\lambda = \pm\mathrm{i}\Omega_- - \kappa_{\Omega_-})\rangle] &= \frac{1}{4}, \end{aligned} \tag{3.7.7}$$

and

$$\mathrm{Res}[\langle\sigma_z\tau_z(\lambda = -\kappa_{01,02})\rangle] = \frac{v^2}{4\,\Omega^2}. \tag{3.7.8}$$

Thus for equal baths we obtain

$$\kappa_{01,02} = \vartheta \pm \frac{v}{\Omega}\,\vartheta \tag{3.7.9}$$

and again a decreased and an increased rate compared to ϑ.

There is a second set of parameters leading to a degenerate spectrum of eigenenergies [51, 72]. The studies in [72] were done numerically and restricted to the Bloch-Redfield regime. For the values $v_y\,v_z = \Delta_1\Delta_2$ we get $\Omega_+ = \Omega_-$ and $\delta \to 0$. Additionally, we choose $\Delta_{1,2} = \Delta$ and

$$v_y = \sqrt{\frac{v^2}{2} - \sqrt{\frac{v^4}{4} - \Delta^4\kappa^2}} \qquad \text{and} \qquad v_z = \sqrt{\frac{v^2}{2} + \sqrt{\frac{v^4}{4} - \Delta^4\kappa^2}}, \tag{3.7.10}$$

where $v = \sqrt{v_y^2 + v_z^2}$ is the total length of the coupling vector. Meaningful results are only obtained for $v > \sqrt{2}\,\Delta$. Now, the eigenfrequencies of $\langle\sigma_z\rangle$ become $\Omega = \sqrt{2\,\Delta^2 + v^2}$ and $\delta \to 0$. The energy spectrum becomes degenerate because $\Omega = \Omega_+ = \Omega_-$. We have

introduced in (3.7.10) a parameter κ, which allows to study the behavior of $\langle\sigma_z\rangle$ around the degeneracy point. The undamped dynamics of $\langle\sigma_z\rangle$ reads

$$\langle\sigma_z(\lambda)\rangle = \frac{v^2 + 2\Delta^2 + 2\lambda^2 + \sqrt{v^4 - 4\Delta^4}}{2\lambda\,(\lambda^2 + \Omega^2)}\,. \tag{3.7.11}$$

Performing a weak damping approximation at the degeneracy point $\kappa = 1$ leads to

$$\begin{aligned}\kappa_\Omega &= \frac{1}{4}\left(3 + \frac{\sqrt{v^4 - 4\Delta^4}}{\Omega^2}\right)\vartheta_1 + \frac{1}{4}\left(1 - \frac{\sqrt{v^4 - 4\Delta^4}}{\Omega^2}\right)\vartheta_2\,,\\ \kappa_\delta &= \frac{1}{4}\left(3 - \frac{\sqrt{v^4 - 4\Delta^4}}{\Omega^2}\right)\vartheta_1 + \frac{1}{4}\left(1 + \frac{\sqrt{v^4 - 4\Delta^4}}{\Omega^2}\right)\vartheta_2\,,\end{aligned} \tag{3.7.12}$$

or with equal baths

$$\kappa_\Omega = \kappa_\delta = \vartheta\,. \tag{3.7.13}$$

But, as $\delta \to 0$, the result for κ_δ is altered by a second order contribution (cf. (3.4.36)), which renormalizes κ_δ to

$$\kappa_\delta^\pm = \kappa_\delta \pm \frac{\sqrt{v^2 + \sqrt{v^4 - 4\Delta^4}}}{2\sqrt{2}\,\Omega}\,(\vartheta_1 + \vartheta_2)\,. \tag{3.7.14}$$

And thus leading again to a decreased and an increased relaxation rate. Since $\delta \to 0$, this parameter set gives only rise to a decrease of a relaxation rate within the white-noise regime. We will see within the Bloch-Redfield calculations that also dephasing rates show a minimum with non-vanishing oscillation frequency (see Sec. 4.5 and [72]). The amplitudes stay finite for all contributions and read

$$\begin{aligned}\mathrm{Res}[\langle\sigma_z(\lambda = -\kappa_\delta^\pm)\rangle] &= \frac{1}{2}\left(1 + \frac{\sqrt{v^2 - 2\Delta^2}}{\Omega}\right) \mp \frac{1}{2}\frac{\sqrt{v^2 + \sqrt{v^4 - 4\Delta^4}}}{\sqrt{2}\,\Omega}\,,\\ \mathrm{Res}[\langle\sigma_z(\lambda = \pm\mathrm{i}\Omega - \kappa_\Omega)\rangle] &= \frac{1}{2}\left(1 - \frac{\sqrt{v^2 - 2\Delta^2}}{\Omega}\right)\,.\end{aligned} \tag{3.7.15}$$

The behavior in $\langle\sigma_z\tau_z\rangle$ is similar again. We have a decrease (increase) of the relaxation rate κ_{01} (κ_{02}) around the degeneracy, while $\kappa_{\Omega_\pm}$ do not change,

$$\kappa_{01,\,02} = \left(1 \mp \frac{\sqrt{v^4 - 4\Delta^4}}{\Omega^2}\right)\frac{\vartheta_1 + \vartheta_2}{2} \qquad \text{and} \qquad \kappa_{\Omega_\pm} = \frac{\vartheta_1 + \vartheta_2}{2}\,. \tag{3.7.16}$$

The amplitudes are

$$\begin{aligned}\mathrm{Res}[\langle\sigma_z\tau_z(\lambda = \pm\mathrm{i}\Omega_+ - \kappa_{\Omega_+})\rangle] &= \frac{\Delta^2}{\Omega^2}\,,\\ \mathrm{Res}[\langle\sigma_z\tau_z(\lambda = \pm\mathrm{i}\Omega_- - \kappa_{\Omega_-})\rangle] &= 0\,,\end{aligned} \tag{3.7.17}$$

and

$$\mathrm{Res}[\langle\sigma_z\tau_z(\lambda = -\kappa_{01,\,02})\rangle] = \frac{v^2 \pm \sqrt{v^4 - 4\Delta^4}}{2\,\Omega^2}\,. \tag{3.7.18}$$

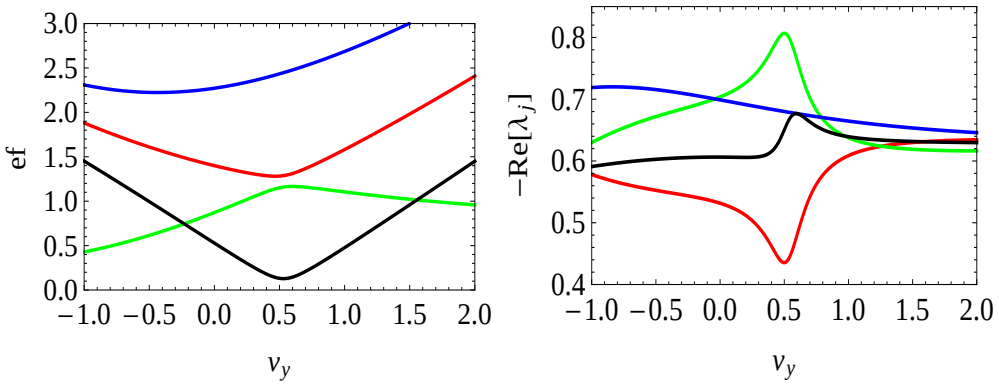

Figure 3.17: Shown are the eigenfrequencies (left) Ω, δ, Ω_+, and Ω_- and the corresponding rates (right) γ_Ω, γ_δ, γ_{Ω_+}, and γ_{Ω_-} in the sequence red, green, blue, and black, respectively. Around $v_y \approx 0.5$ occurs an avoided level crossing of Ω and δ. We have a decrease (increase) of the dephasing rates γ_Ω (γ_δ) around the level crossing. The parameters are $\Delta_1 = \Delta_2 = 1$, $v_z = -0.6$, $K = 0.01$, $T = 10$, and $\epsilon_1 = 0.6$.

Although we do not discuss in detail two coupled spins with bias, it is reasonable to note here that we observe a frustration of decoherence with bias, too. Using the results from Appendix A.2.3, we obtain for v_y and v_z coupling and bias ϵ_1 a decreased and increased decoherence rate around an avoided level crossing of the eigenfrequencies. Here we do not have a complete degeneracy of the eigenfrequencies but a gap remains. The gap is proportional to the bias and the larger the gap, the smaller the frustration of decoherence. The results are shown in Figs. 3.17 and 3.18.

3.8 Density matrix and purity

The purity of a quantum mechanical system is defined as $P = \mathrm{tr}\rho^2$ with the two extremes $P = 1$ for a pure state and $P = 1/N$ for a fully mixed state, where N is given by the dimension of the respective Hilbert space[3]. It follows for the two coupled spins that $P(t = 0) = 1$ because we prepare our system in a pure state and $P(t \to \infty) = 1/4$ because the system equilibrates to a fully mixed state.

The normalized time derivative of the purity

$$\gamma_{\mathrm{eff}} = -\frac{1}{P(t)}\frac{\mathrm{d}P(t)}{\mathrm{d}t}\,, \tag{3.8.1}$$

which characterizes an effective damping rate of the system, is a crucial quantity with prospect to quantum information processing. Since the smaller the effective damping

[3] An alternative measure for the degree of mixture of a state is the von-Neumann entropy given by $S_{\mathrm{N}} = -\mathrm{tr}\rho\ln\rho$, instead of the linear entropy $S_{\mathrm{l}} = 1 - P$

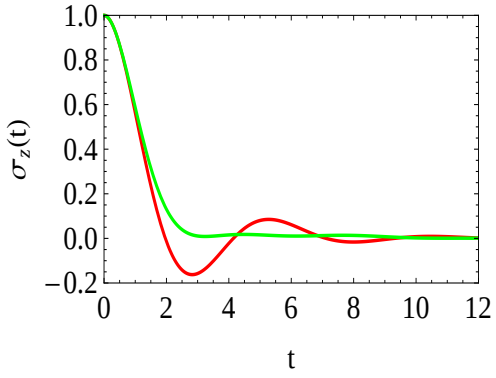

Figure 3.18: Quantum frustration of decoherence for $\langle\sigma_z(t)\rangle$ and bias ϵ_1. The damping is much smaller for $v_y = 0.5$ (red) than for $v_y = -0.5$ (green), i.e., the coherence time is larger around the level crossing. The parameters are $\Delta_1 = \Delta_2 = 1$, $v_z = -0.6$, $K = 0.01$, $T = 10$, and $\epsilon_1 = 0.6$.

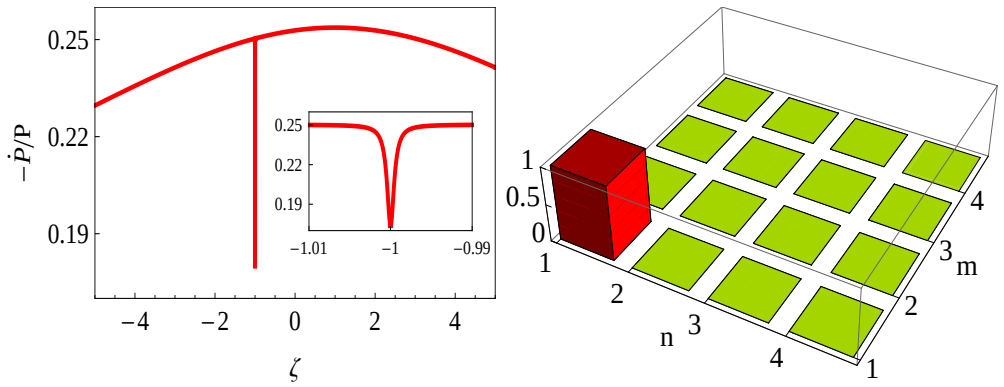

Figure 3.19: Left: a minimum in $\gamma_{\rm eff} = -\frac{1}{P(t)}\frac{{\rm d}P(t)}{{\rm d}t}$ with $\Delta_1 = \Delta_2 = \Delta$, $v_y = \zeta\, v_z$, and $t = 10^{-3}$. For $\zeta = -1$ we obtain $\Omega = \delta$. Right: initial preparation of the density matrix $\rho_{n,m}$ in the RR eigenstate with $n = 1, \ldots, 4$ and $m = 1, \ldots, 4$.

rate, the smaller the dephasing and/or relaxation of the system, and the longer any entanglement may be maintained. We have shown in the last section that we obtain decreased dephasing and/or relaxation rates for degenerate eigenvalues of $H_{\rm S}$, implying a minimum in $\gamma_{\rm eff}$. This is shown in Fig. 3.19.

To obtain the purity, it is necessary to calculate all 16 entries of the density matrix ρ in the time regime. This can be done in leading order of the damping strength within the white-noise regime. For example, the result for $\langle\sigma_z\rangle$ in the time regime is

$$\langle\sigma_z(t)\rangle = \frac{{\rm e}^{-\kappa_\Omega\, t}\cos(\Omega\, t)\,(\Omega^2 - \Delta_2^2 - v_z^2) + {\rm e}^{-\kappa_\delta\, t}\cos(\delta\, t)\,(\Delta_2^2 + v_z^2 - \delta^2)}{\Omega^2 - \delta^2}\,, \tag{3.8.2}$$

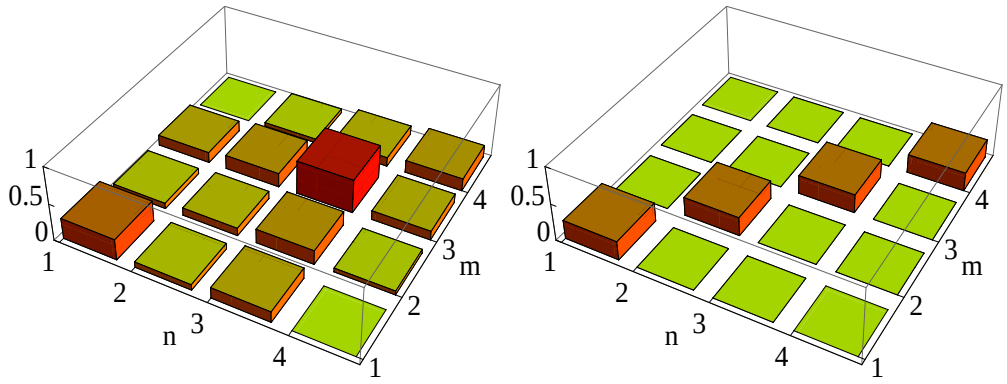

Figure 3.20: Left: density matrix $\rho_{n,m}$ for some intermediate time $0 < t < \infty$. Right: density matrix $\rho_{n,m}$ for $t \to \infty$, where the diagonal states are populated with probability 1/4 each and we are in a fully mixed state.

with $\kappa_{\Omega,\delta}$ from Eq. (3.6.15). Assembling all parts, the purity reads

$$\begin{aligned} P(t) = \frac{1}{4} &+ \frac{1}{8}(1 - C_\sigma)\,\mathrm{e}^{-2\gamma_{\delta,\sigma}t} + \frac{1}{8}(1 + C_\sigma)\,\mathrm{e}^{-2\gamma_{\Omega,\sigma}t} + \frac{1}{8}(1 - C_\tau)\,\mathrm{e}^{-2\gamma_{\delta,\tau}t} + \\ &+ \frac{1}{8}(1 + C_\tau)\,\mathrm{e}^{-2\gamma_{\Omega,\tau}t} + \frac{1}{8}(1 - C_{\Omega_-})\,\mathrm{e}^{-2\gamma_{\Omega_-}t} + \frac{1}{8}(1 - C_{\Omega_+})\,\mathrm{e}^{-2\gamma_{\Omega_+}t} \\ &+ \frac{1}{4}\frac{(v_y\delta + v_z\Omega)^2}{(\Omega^2 - \delta^2)^2}\,\mathrm{e}^{-2\gamma_5 t} + \frac{1}{4}\frac{(v_y\Omega + v_z\delta)^2}{(\Omega^2 - \delta^2)^2}\,\mathrm{e}^{-2\gamma_6 t} \end{aligned} \tag{3.8.3}$$

with the amplitudes

$$C_{\sigma,\tau} = \frac{\Delta_{1,2}^2 - \Delta_{2,1}^2 + v_y^2 - v_z^2}{\Omega^2 - \delta^2}\,, \quad C_{\Omega_\pm} = \frac{(v_y \mp v_z)^2}{\Omega_\pm^2}\,. \tag{3.8.4}$$

The subscript σ, τ identifies the corresponding spin. This function smoothly drops from the initial value $P(t = 0) = 1$ to $P(t \to \infty) = 1/4$.

The time evolution of the RDM $\rho(t)$ is shown for three different times in the Figs. 3.19 and 3.20. This is remarkable as we can really track the decay of the coherences.

3.9 Spin-boson environment

The study of linear environments has attracted a lot of interest in the last decades [1, 2, 12]. The linear environment model is based on a set of infinite many harmonic oscillators, which are weakly coupled to the system. Everything we need to describe the reduced dynamics of the system is the spectral density or power spectrum of the environment. A detailed knowledge of its microscopic structure is not required. The situation changes if the environment has a *memory* on the time scale of the system. For example, such a behavior occurs with solid state qubits surrounded by bistable impurities which gives rise to $1/f$ noise [73]. This might be charges with two states, that are switched by phonon interaction. They appear to play the dominating role in decohering a qubit in solid state

devices [21, 74, 75, 76]. An alternative use of this model is to consider one spin as a measuring device for a spin-boson setup.

To study the effects of a non-linear environment induced by a single bistable impurity, we choose the environment to be a spin-boson setup, i.e., we use the Hamiltonian

$$\begin{aligned} H &= -\frac{\epsilon_1}{2}\,\sigma_z - \frac{\Delta_1}{2}\,\sigma_x - \frac{v_z}{2}\,\sigma_z\tau_z + H_{\mathrm{SB}}\;, \\ H_{\mathrm{SB}} &= -\frac{\epsilon_2}{2}\,\tau_z - \frac{\Delta_2}{2}\,\tau_x - \frac{X}{2}\,\tau_z + \sum_\alpha \omega_\alpha\, a_\alpha^\dagger\, a_\alpha\;, \\ X &= \sum_\alpha c_\alpha\,(b_\alpha^\dagger + b_\alpha)\;. \end{aligned} \tag{3.9.1}$$

It consists of two two-state systems (σ and τ) and the spin-spin coupling term $\propto v_z$. The part H_{SB} corresponds to a spin-boson model. X summarizes the fluctuating bias forces acting on τ_z due to the environment, where the coupling strength to the bath mode α is described by c_α and the bath is characterized in the same way as in Chapter 2. The spin σ is coupled to the environment only via the spin τ.

3.9.1 Gaussian and non-Gaussian behavior

If we consider the ohmic bath and the spin τ as the environment for spin σ we end up with an environment that is in general non-Gaussian and non-Markovian [27, 56]. But nevertheless we can look at the validity range of a standard master equation approach. Therefore, we regard the spin τ plus environment as an effective harmonic model with power spectrum $S_\tau(\omega)$ of the effective coupling operator $v_z\,\tau_z$,

$$S_\tau(\omega) = \int_{-\infty}^{\infty} \mathrm{d}t\; \frac{v_z^2}{2}\left[\langle\tau_z(t)\tau_z(0) + \tau_z(0)\tau_z(t)\rangle_\beta - \langle\tau_z\rangle_{\mathrm{eq}}^2\right] \exp^{\mathrm{i}\,\omega\,t}\,. \tag{3.9.2}$$

We have subtracted the equilibrium population $\langle\tau_z\rangle_{\mathrm{eq}}^2$. The form (3.9.2) is valid as long as the coupling is weak and the dynamics of the SBE is fast enough. Given a range τ_c of the correlation function (3.9.2), the master equation approach is limited to $v_z \ll 1/\tau_{\mathrm{c}}$. This means that for Gaussian behavior the frequencies of the system have to be much smaller than the typical frequencies of the environment, which is also known as motional narrowing. In the limit $\tau_{\mathrm{c}} \to 0$ we have a pure Gaussian bath with ohmic spectral density. This limit is realized in the case of high temperature. Otherwise the system can resolve details of the environmental dynamics and shows non-Gaussian behavior [77, Ch. 4]. This is comparable to Brownian motion, where it is convenient to assume that the mass of the particle is much greater than the masses of the solvent particles, i.e., only the collective action of the solvent particles is relevant, not a single one.

Thus, in the Gaussian case, we get for the relaxation and dephasing rate (see Eq. (2.4.13))

$$\begin{aligned} \frac{1}{T_1} &= \gamma_{\mathrm{r}} = \frac{\pi}{2}\frac{\Delta^2}{\Omega^2}\,S_\tau(\Omega)\;, \\ \frac{1}{T_2} &= \frac{1}{2\,T_1} + \frac{1}{T_2^*} = \frac{\gamma_{\mathrm{r}}}{2} + \frac{\pi}{2}\frac{\epsilon^2}{\Omega^2}\,S_\tau(0)\;, \end{aligned} \tag{3.9.3}$$

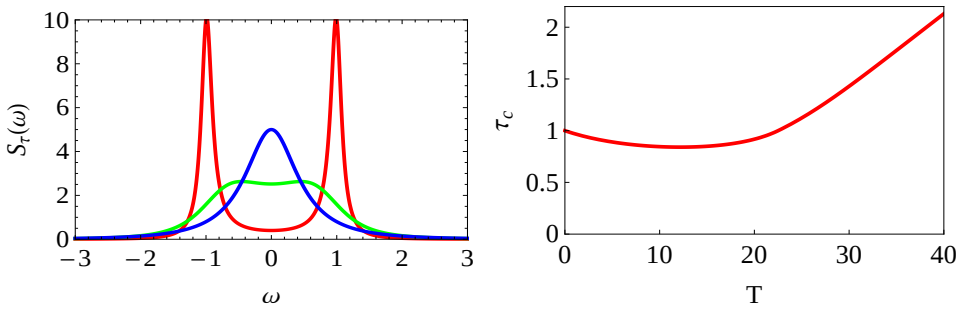

Figure 3.21: Left: power spectrum $S_\tau(\omega)$ for different temperatures (red: $\vartheta = 1/5$, green: $\vartheta = 1.26$, blue: $\vartheta = 2.5$). The transition from under-damped dynamics (red) to the pure incoherent regime (blue) is clearly visible. Right: the correlation time τ_c for $K = 0.01$ and $\Delta = 1$. The condition $v_z\,\tau_c = 1$ separates the Gaussian and non-Gaussian regime.

where $\Omega^2 = \Delta^2 + \epsilon^2$ is the squared eigenfrequency of the system [2, 26, 60].

The spectral density in Eq. (3.9.2) allows us to make a prediction of the typical timescale of the equilibrium fluctuations of a spin-boson impurity, i.e., of the correlation time τ_c. For the uncoupled case $v_z = 0$, the impurity dynamics only depends on the bath coupling K and on the bath temperature. The power spectrum for low and intermediate temperature is approximately described by a superposition of two Lorentzians describing damped oscillations. By increasing temperature, we obtain a single Lorentzian, which is centered around the origin and thus describes pure damped behavior (see Fig. 3.21). The correlation time may be approximately identified by the half-width at half-maximum of the power spectrum

$$S_\tau(1/\tau_c) = S_\tau^{(\max)}/2\,. \tag{3.9.4}$$

The resulting correlation time is shown in Fig. 3.21 [2, 26]. For low effective temperature ϑ, i.e., the under-damped regime, two damped oscillations dominate the dynamics. For growing ϑ, the incoherent contribution gains weight until it dominates for large ϑ. The minimum of the correlation time is an effect of the transition from under-damped to incoherent dynamics. The condition $v_z\,\tau_c = 1$ separates the weak-coupling from the strong-coupling regime where non-Gaussian behavior can be observed.

3.9.2 Inclusion of inter- and intrablip correlations

We begin with the full expressions for $\langle\sigma_z\rangle$ and $\langle\sigma_z\tau_z\rangle$ given in Eqs. (3.4.20) and (3.5.23), where we set $K_1 = 0$. The special case $\Delta_1 = 0$ was studied in [24]. There, we find $[H, \sigma_z] = 0$, which implies that $\langle\sigma_z(t)\rangle = \text{const}$ for all times. Then, there is no relaxation and only dephasing occurs. It follows, that diagonal elements (population) of the RDM are constant, while off-diagonal elements (coherences) decay. Here, we will study the general case with $\Delta_1 \neq 0$. However, we will only consider v_z coupling and zero bias.

With $K_1 = 0$ in Eqs. (3.4.20) and (3.5.23), we obtain the equations describing a

spin-boson environment

$$\begin{aligned}\langle\sigma_z(\lambda)\rangle &= \frac{\lambda\,\Delta_2^2 + (\lambda^2+v_z^2)\,(\lambda+\vartheta_2)}{(\lambda^2+\Delta_1^2)\,\Delta_2^2 + \lambda\,(\lambda^2+\Delta_1^2+v_z^2)\,(\lambda+\vartheta_2)}\,,\\ \langle\tau_z(\lambda)\rangle &= \frac{(\lambda+\vartheta_2)\,(\pi\,v_z\,K_2\,\Delta_2^2 + \lambda\,(v_z^2+\Delta_1^2+(\lambda+\vartheta_2)^{\,2}))}{\lambda\,[((\lambda+\vartheta_2)^{\,2}+\Delta_1^2)\,\Delta_2^2 + \lambda\,(\lambda+\vartheta_2)\,((\lambda+\vartheta_2)^{\,2}+\Delta_1^2+v_z^2)]}\,,\end{aligned} \tag{3.9.5}$$

and correspondingly

$$\langle\sigma_z\tau_z(\lambda)\rangle = \frac{1}{\lambda}\frac{N(\lambda)}{D(\lambda)}\,, \tag{3.9.6}$$

with

$$\begin{aligned}N(\lambda) = \Big\{ &\left(v_z^2+(\lambda+\vartheta_2)^{\,2}\right)\lambda^2 + \pi\,v_z\,K_2\\ &\left[(\lambda+\vartheta_2)\,v_z^2 + \lambda\left(\Delta_2^2-\Delta_1^2+\lambda\,(\lambda+\vartheta_2)\right)\right]\Big\}\Delta_2^2\\ &+\lambda\left(v_z^2+\lambda^2\right)(\lambda+\vartheta_2)\left(v_z^2+\Delta_1^2+(\lambda+\vartheta_2)^{\,2}\right)\,,\\ D(\lambda) = &\left[\left(2\,\lambda^2+2\,\vartheta_2\,\lambda+\vartheta_2^2\right)v_z^2 + \lambda\,(\lambda+\vartheta_2)\left(\Delta_2^2-2\,\Delta_1^2+2\,\lambda\,(\lambda+\vartheta_2)\right)\right]\Delta_2^2\\ &+\lambda\left(v_z^2+\lambda^2+\Delta_1^2\right)(\lambda+\vartheta_2)\left(v_z^2+\Delta_1^2+(\lambda+\vartheta_2)^{\,2}\right)\,.\end{aligned} \tag{3.9.7}$$

By studying the dependence of the oscillation frequencies on K_2 (see Fig. 3.22), we see a crossover from the eigenfrequencies Ω, δ, Ω_+, and Ω_- of the undamped system to the bare eigenfrequencies of $\langle\sigma_z\rangle$, which are $\pm\sqrt{\Delta_1^2+v_z^2}$, for increasing K_2. We find that the visibility of the dynamics of the spin impurity decreases for increasing coupling of the spin impurity to the bath, i.e., the spin-boson-environment becomes a boson-environment. Or equivalently, the non-linear environment becomes a linear environment, as was discussed in Section 3.9.1. This is due to the effect that the dynamics of τ gets more and more frozen as K_2 increases. Thus, the dynamics of τ cannot be resolved by σ.

The Figs. 3.22 – 3.24 show the qualitative behavior of $\langle\sigma_z\rangle$. For low ϑ_2 there is a superposition of two damped oscillations. The amplitude of the smaller frequency is dominating for low temperature, while for intermediate temperature both amplitudes are comparable in magnitude. For increasing ϑ_2 one relaxation and one damped oscillation with non-vanishing oscillation amplitude remain. The high temperature regime is discussed in detail in the following subsection.

3.9.2.1 High temperature

In the limit, where ϑ_2 is the largest energy in the system, $\langle\sigma_z(\lambda)\rangle$ of Eq. (3.9.5) reduces to the form

$$\langle\sigma_z(\lambda)\rangle \;=\; \frac{1}{\lambda\;+\;\mathcal{K}_{\rm ht}^{(\rm s)}(\lambda)} \;=\; \frac{\lambda^2+\gamma_\tau\lambda+v_z^2}{\lambda^3+\gamma_\tau\lambda^2+(\Delta_1^2+v_z^2)\lambda+\Delta_1^2\gamma_\tau}\,, \tag{3.9.8}$$

with

$$\mathcal{K}_{\rm ht}^{(\rm s)}(\lambda) \;=\; -\lambda\,\frac{\Delta_1^2}{\lambda^2+v_z^2}\left(1\;+\;\frac{v_z^2}{\lambda}\,\frac{\gamma_\tau}{\lambda^2+v_z^2+\gamma_\tau\lambda}\right)\,. \tag{3.9.9}$$

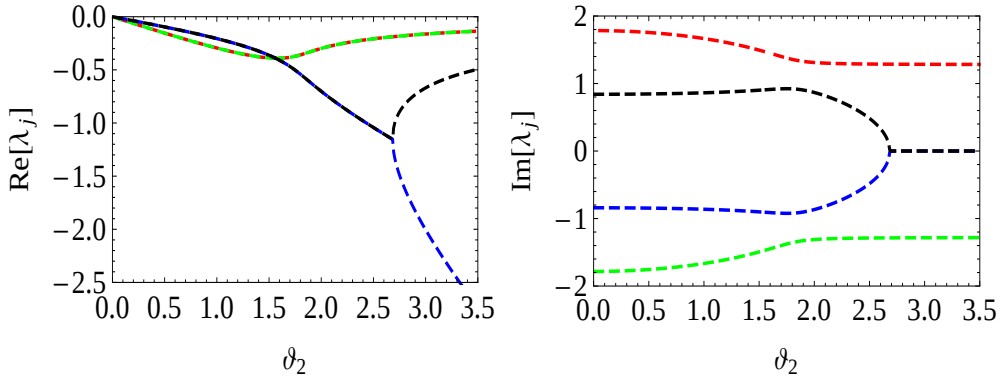

Figure 3.22: $\langle\sigma_z\rangle$ with spin-boson environment: we see the real (left) and imaginary (right) part of λ_j. At low ϑ_2, $\langle\sigma_z(t)\rangle$ is a superposition of two damped oscillations. At high ϑ_2, there is one damped oscillation and one relevant relaxation contribution. The parameters are $v_z = 0.8$, $\Delta_1 = 1$, $\Delta_2 = 1.5$. The colors red, green, blue, and black label $\mathrm{Re}\,[\lambda_j]$ and $\mathrm{Im}\,[\lambda_j]$, with $j = 1, 2, 3, 4$.

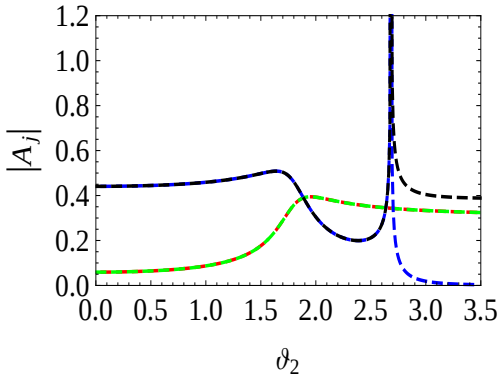

Figure 3.23: $\langle\sigma_z\rangle$ with SBE: here we plotted the absolute part of $\langle\sigma_z\rangle$. Parameters are $v_z = 0.8$, $\Delta_1 = 1$, $\Delta_2 = 1.5$. The colors red, green, blue, and black label $|A_j|$ with $j = 1, 2, 3, 4$.

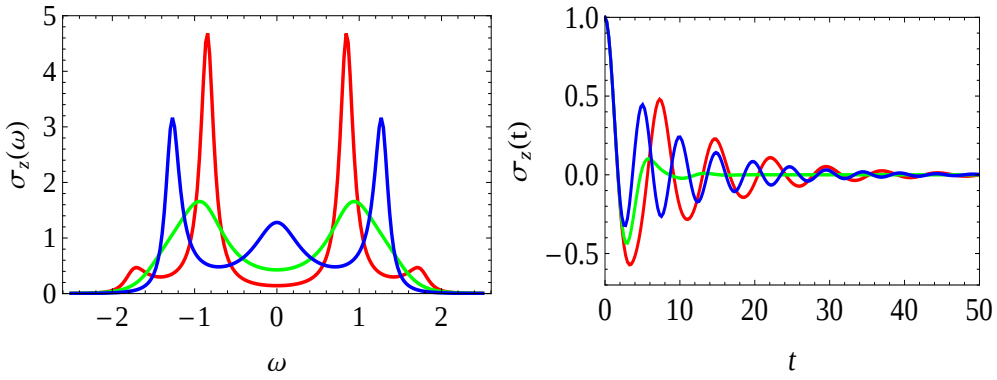

Figure 3.24: $\langle\sigma_z\rangle$ with SBE: shown is a plot in the Fourier regime (left) and time regime (right) of $\langle\sigma_z\rangle$ for different ϑ_2. Red $\vartheta_2 = 0.5$, green $\vartheta_2 = 1.5$, blue $\vartheta_2 = 4.5$. Observe that the amplitude of the oscillation part first decreases with temperature (red $\to$ green) but then increases with ϑ_2 (green $\to$ blue). $v_z = 0.8$, $\Delta_1 = 1$, $\Delta_2 = 1.5$.

The rate $\gamma_\tau = \Delta_2^2/\vartheta_2$ is the relaxation rate of spin τ for high temperature. This expression describes the dynamics of spin σ, which is coupled to a spin-boson environment in the Kondo regime. To leading order in γ_τ (for large ϑ_2), the poles of expression (3.9.8) are

$$\lambda_{1,2} \;=\; \pm\mathrm{i}\sqrt{\Delta_1^2+v_z^2} \;-\; \frac{v_z^2}{2(\Delta_1^2+v_z^2)}\,\frac{\Delta_2^2}{\vartheta_2}\,, \qquad \lambda_3 \;=\; -\,\frac{\Delta_1^2}{\Delta_1^2+v_z^2}\,\frac{\Delta_2^2}{\vartheta_2}\,, \tag{3.9.10}$$

and the amplitudes read

$$A_{1,2} \;=\; \frac{\Delta_1^2}{2(\Delta_1^2+v_z^2)} + \mathcal{O}\Big(\frac{1}{\vartheta_2}\Big)\,, \qquad A_3 \;=\; \frac{v_z^2}{\Delta_1^2+v_z^2} + \mathcal{O}\Big(\frac{1}{\vartheta_2^2}\Big)\,. \tag{3.9.11}$$

It is useful to compare the expressions (3.9.8) – (3.9.11) with the corresponding ones of a fictive single biased spin-boson system with parameters Δ_1 and v_z in the white-noise limit at scaled temperature $\tilde{\vartheta}$. The part that is symmetric in the bias reads

$$\langle\sigma_z^{(\mathrm{sb})}(\lambda)\rangle_{\mathrm{s}} \;=\; \frac{\lambda^2 \,+\, 2\tilde{\vartheta}\lambda \,+\, v_z^2 \,+\, \tilde{\vartheta}^2}{\lambda^3 \,+\, 2\tilde{\vartheta}\lambda^2 \,+\, (\Delta_1^2+v_z^2+\tilde{\vartheta}^2)\lambda + \Delta_1^2\tilde{\vartheta}}\,. \tag{3.9.12}$$

We see that the identification $\tilde{\vartheta} \mathrel{\hat{=}} \gamma_\tau = \Delta_2^2/\vartheta_2$ renders the expressions (3.9.8) and (3.9.12) quite similar. However, the identity is not exact. The damping rate of the oscillation is somewhat different because of the term $2\tilde{\vartheta}\lambda^2$ in Eq. (3.9.12) instead of $\tilde{\vartheta}\lambda^2$ in Eq. (3.9.8) [2]. Surprisingly in the identification, temperature maps on the inverse of itself. This implies that the damping of the fictive spin decreases for increasing temperature, although σ is not in the Kondo-regime, and second, that we have a coherent contribution for large ϑ_2. This can also be seen in Figs. 3.22 – 3.24.

3.9.2.2 Weak spin-spin coupling

We have seen in Section 3.9.1 that the Gaussian and non-Gaussian regime is separated by the condition $v_z\tau_c = 1$. Thus, we expect that in the weak-coupling limit, the spin-boson

environment is Gaussian and can be represented by a resonant power spectrum of a bath of bosons.

On the one hand, the Gaussian approximation of the spin-boson environment is found by matching the power spectrum of the coupling of spin σ to the SBE (see Eq. (3.9.2))

$$S_\tau(\omega) \;=\; \frac{v_z^2}{2}\,\mathrm{Re}\int_{-\infty}^{\infty}\mathrm{d}t\,\big\langle\,[\,\tau_z(t)\tau_z(0)\;+\;\tau_z(0)\tau_z(t)\,]\,\big\rangle\,\mathrm{e}^{\mathrm{i}\,\omega t}, \tag{3.9.13}$$

with that of a harmonic oscillator bath. In the white-noise limit of an unbiased spin, the symmetrized equilibrium correlation function $\mathrm{Re}\,\langle\tau_z(t)\tau_z(0)\rangle$ coincides with the expectation $\langle\tau_z(t)\rangle$. Thus we obtain

$$S_\tau(\omega) \;=\; 2\,v_z^2\,\mathrm{Re}\,\langle\tau_z(\lambda=-\,\mathrm{i}\,\omega)\rangle \quad \text{with} \quad \langle\tau_z(\lambda)\rangle \;=\; \frac{\lambda+\vartheta_2}{\lambda(\lambda+\vartheta_2)+\Delta_2^2}\,. \tag{3.9.14}$$

The resulting power spectrum is that of a structured bath of bosons with a resonance of width ϑ_2 at frequency $\omega=\Delta_2$,

$$S_\tau(\omega) \;=\; 2\vartheta_2\,\frac{v_z^2\Delta_2^2}{(\Delta_2^2-\omega^2)^2+\vartheta_2^2\omega^2}\,. \tag{3.9.15}$$

Due to the coupling to the spin-boson environment, the spin σ performs damped oscillations

$$\langle\sigma_z(t)\rangle = \cos(\Delta_1 t)\,\mathrm{e}^{-\gamma_{\mathrm{dec}}t}\,. \tag{3.9.16}$$

Upon calculating the decoherence rate in order v_z^2, i.e., the one-boson-exchange contribution of the effective boson bath, we obtain

$$\gamma_{\mathrm{dec}} \;=\; \frac{1}{4}\,S_\tau(\Delta_1) \;=\; \frac{v_z^2\Delta_2^2\,\vartheta_2}{2\,[\,(\Delta_2^2-\Delta_1^2)^2+\vartheta_2^2\Delta_1^2\,]}\,. \tag{3.9.17}$$

On the other hand, this form emerges directly by calculating γ_{dec} from the pole equation of the denominator of the full expression for $\langle\sigma_z(\lambda)\rangle$ from (3.4.20). Thus, we have shown that in the weak-coupling limit the spin-boson environment becomes Gaussian.

3.9.2.3 Large spin-spin coupling

For the strong coupling limit we expect a similar behavior as in Section 3.4.2. Starting with the full expression for $\langle\sigma_z(\lambda)\rangle$ from Eq. (3.4.20) or using the results from Eq. (3.4.48), we obtain for the poles

$$\begin{aligned}
&\lambda_1 = -\mathrm{i}\,\widetilde{\Omega} - \frac{\Delta_2^2\,\vartheta_2}{2v_z^2}\,, \quad \lambda_2 = \mathrm{i}\,\widetilde{\Omega} - \frac{\Delta_2^2\,\vartheta_2}{2v_z^2}\,,\\
&\lambda_3 = -\vartheta_2 + \frac{\widetilde{\delta}^2}{\vartheta_2}\left(1+\frac{\vartheta_2^2}{\Delta_1^2}\right)\,, \quad \lambda_4 = -\frac{\widetilde{\delta}^2}{\vartheta_2}\,.
\end{aligned} \tag{3.9.18}$$

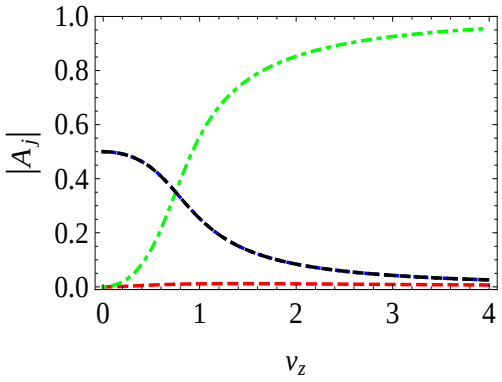

Figure 3.25: $\langle\sigma_z\rangle$ with SBE for large spin-spin coupling: plotted are the absolute values of the amplitudes. See text for details. $\Delta_1 = 1$, $\Delta_2 = 1.5$, $\vartheta_2 = \pi$. The colors red, green, blue, and black label $|A_j|$ with $j = 1, 2, 3, 4$.

$\widetilde{\Omega}$ and $\widetilde{\delta}$ are again the large v_z expansions of the eigenfrequencies Ω and δ (up to $\mathcal{O}(1/v_z^2)$) and read

$$\widetilde{\Omega} = v_z + \frac{\Delta_1^2 + \Delta_2^2}{2\,v_z} \qquad \text{and} \qquad \widetilde{\delta} = \frac{\Delta_1\,\Delta_2}{v_z}\,. \tag{3.9.19}$$

We see that λ_4 is always in a Kondo-like form. The residues can also be obtained directly from Eq. (3.4.50),

$$\begin{aligned} \mathrm{Res}\,[\sigma_z(\lambda_1)] &= \frac{1}{v_z^2}\frac{\Delta_1^2}{2}\,, & \mathrm{Res}\,[\sigma_z(\lambda_2)] &= \frac{1}{v_z^2}\frac{\Delta_1^2}{2}\,, \\ \mathrm{Res}\,[\sigma_z(\lambda_3)] &= -\frac{1}{v_z^2}\frac{\Delta_1^2\Delta_2^2}{\vartheta_2^2}\,, & \mathrm{Res}\,[\sigma_z(\lambda_4)] &= 1 + \frac{\Delta_1^2}{v_z^2}\left(\frac{\Delta_2^2}{\vartheta_2^2} - 1\right)\,. \end{aligned} \tag{3.9.20}$$

The equilibrium amplitude reads $\langle\sigma_z\rangle_{\mathrm{eq}} = 0$. And again, we have pure relaxation, where the leading contribution for $\langle\sigma_z(t)\rangle$ is pure exponential damping

$$\langle\sigma_z(t)\rangle = \mathrm{e}^{\lambda_4\,t} + \mathcal{O}(1/v_z^2)\,. \tag{3.9.21}$$

The results are shown in the Figs. 3.25 and 3.26. For increasing coupling v_z the coherent contribution decreases like $1/v_z^2$, while the system makes a transition from a purely coherent system to an overdamped system.

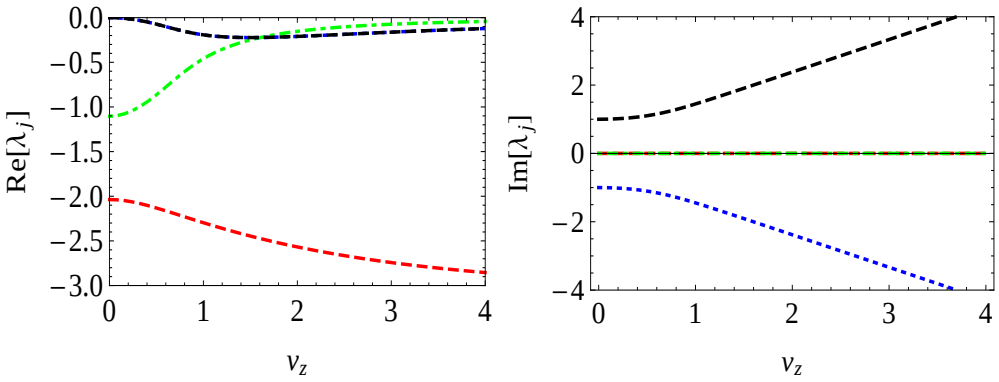

Figure 3.26: $\langle \sigma_z \rangle$ with SBE for large spin-spin coupling: we see the real (left) and imaginary (right) part of λ_j. For large coupling v_z only the incoherent part gives a relevant contribution to the dynamics. See text for details. $\Delta_1 = 1$, $\Delta_2 = 1.5$, $\vartheta_2 = \pi$. The colors red, green, blue, and black label $\mathrm{Re}\,[\lambda_j]$ and $\mathrm{Im}\,[\lambda_j]$, with $j = 1, 2, 3, 4$.

3.10 Comparison with results by Dubé and Stamp

We already mentioned in the introduction that a first study of two coupled spins with path integral techniques was made by Dubé and Stamp [59]. A short derivation of their results is given in Appendix A.4. They used a model, which describes the system well for large spin-spin coupling and high temperature. Also, for low temperature but above the quantum-noise regime, we expect a good agreement with our results because the influence of the environment is small. But, for intermediate temperature and/or small mutual coupling, we expect our results to give a more precise description of the system because Dubé and Stamp neglected inter- and intrablip correlations where both spins are involved. This is indeed the case as we will see now.

There is a qualitative difference concerning the oscillation frequencies of the system. The analysis of Dubé and Stamp gives for the undamped system the eigenfrequencies

$$\begin{aligned} \Omega_{\sigma_z,\tau_z} &= \pm \mathrm{i}\sqrt{\Delta_{1,2}^2 + v_z^2}\,, \\ \Omega^{(1)}_{\sigma_z\tau_z} &= \pm \mathrm{i}\, v_z\,, \qquad \Omega^{(2)}_{\sigma_z\tau_z} = \pm \mathrm{i}\sqrt{\Delta_1^2 + \Delta_2^2 + v_z^2}\,, \end{aligned} \tag{3.10.1}$$

for σ_z, τ_z, and $\sigma_z\tau_z$, respectively. These are not the true eigenfrequencies of two undamped coupled spins, which are given in Eq. (3.1.7). Nevertheless, they are the same in leading order for large mutual coupling.

In Figs. 3.27 – 3.29 damping rates and oscillation frequencies are plotted for $\Delta_{1,2} = 1$ and $v_z = 1$. The calculation by Dubé and Stamp is no more valid for these values because we are not in the strong mutual coupling regime. However, there is a large difference to the exact calculation in this regime. This reveals the importance of inter- and intrablip correlations between the spins. For larger mutual coupling the results of Dubé and Stamp agree well with the results of the Sections 3.4 and 3.5. The damping rates are shown in Figs. 3.27 and 3.28. As expected, the rates by Dubé and Stamp deviate from the new obtained rates for intermediate temperature (Fig. 3.27). The strongest damped pole in Figs. 3.5 and 3.10 is missing in Fig. 3.28. However, its contribution for high temperature is also negligible, when including inter- and intrablip correlations. We see in Fig. 3.29 the different oscillation frequencies. The frequencies are different for low temperature, while for high temperature the frequencies are the same.

Thus, we have a smooth crossover of the new results to the results of Dubé and Stamp for high temperature.

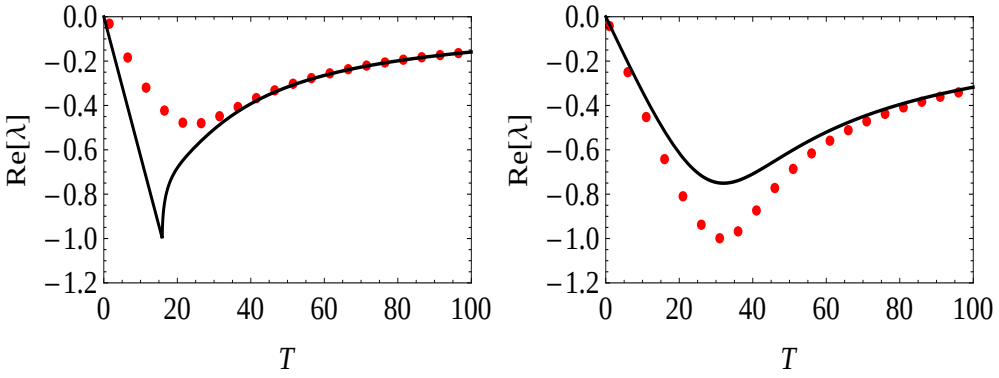

Figure 3.27: Comparison of damping rates with Dubé and Stamp. Left $\langle\sigma_z\rangle$, right $\langle\sigma_z\tau_z\rangle$. Dotted lines (red) are results by Dubé and Stamp, while full lines (black) are with inter- and intrablip correlations as in Figs. 3.5 and 3.10. Shown is the real part of the poles versus temperature T for one of the damping rates. As expected, for large and low temperature the damping rates agree well, while for intermediate temperature a deviation occurs due to the neglected inter- and intrablip correlations. $v_z = 1$, $K = 0.01$, and $\Delta_{1,2} = 1$.

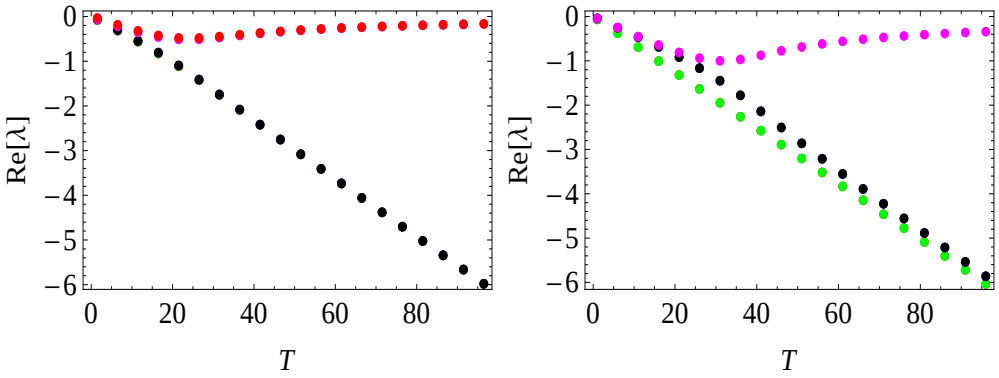

Figure 3.28: Shown are the damping rates calculated by Dubé and Stamp. Left $\langle\sigma_z\rangle$, right $\langle\sigma_z\tau_z\rangle$. The strongest damped rate in Figs. 3.5 and 3.10 is missing, but its contribution for high temperature is also negligible, when including inter- and intrablip correlations. $v_z = 1$, $K = 0.01$, and $\Delta_{1,2} = 1$.

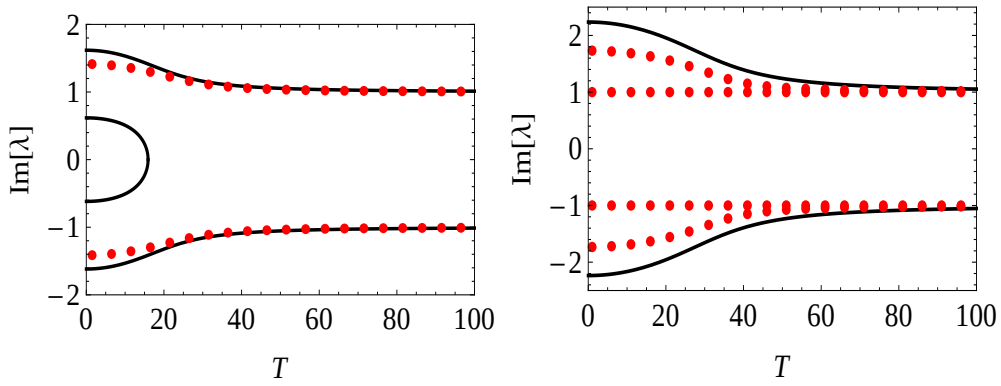

Figure 3.29: Comparison of oscillation frequencies with Dubé and Stamp. Left $\langle\sigma_z\rangle$, right $\langle\sigma_z\tau_z\rangle$. Dotted lines (red) are results by Dubé and Stamp, while full lines (black) are with inter- and intrablip correlations as in Figs. 3.5 and 3.10. Shown is the imaginary part of the poles versus temperature T. Again, we observe that the two approaches match for high temperature. There is a qualitative difference for low temperature regarding the number of relevant frequencies for $\langle\sigma_z\rangle$ and $\langle\sigma_z\tau_z\rangle$, respectively. However, the results by Dubé and Stamp are no more valid there. $v_z = 1$, $K = 0.01$, and $\Delta_{1,2} = 1$.

3.11 Conclusions

We have derived the exact dynamics for two interacting spins with various forms of mutual coupling in the white-noise limit. Thereto we have solved the equations of motion in an iterative way to gain knowledge of the contributing transition sequences. An extension to the one-boson regime was accomplished. One-boson exchange processes between system and bath are dominant for weak coupling and/or low temperature. Additionally, we have discussed the regime of strong coupling and/or high temperature.

An application as spin-boson environment was examined, which is in general a non-Gaussian environment. Here, in the transition to weak bath coupling a crossover from non-Gaussian to Gaussian behavior was observed. The study of non-Gaussian behavior is an important task because $1/f$-noise, which leads to such a behavior, seems to be the limiting factor in achieving long coherence times in solid state devices like SQUIDS. Therefore, a result like (3.9.12), where we find decreasing decoherence with increasing temperature, is remarkable.

In the same sense, the discovered frustration of decoherence phenomenon is not of lesser importance. Here, ground states that are equal in energy but mutually exclusive, lead to extended coherence times.

4 Bloch-Redfield approach

The Bloch-Redfield approach is a perturbative method to obtain the time evolution of the density matrix. It is only valid for low influences of the bath, i.e., for low temperature and/or small coupling to the bath. It is based on three main assumptions.

First, the density matrix of the system plus bath can be factorized into system and bath in thermal equilibrium. This assumption implies that we may neglect any influence of the system on the bath, i.e., the bath is always in thermal equilibrium. The density matrix can thus be written in the factorized form $\rho(t) \to \rho_{\mathrm{S}}(t)\,\rho_{\mathrm{R}}(t)$, where the subscript denotes the system and the reservoir, respectively. Second, it uses the Markov assumption, i.e., there is a small bath correlation time $\tau_c \ll 1/\omega$ after which no memory of the interaction is retained and ω is the smallest frequency of the system (cf. Sec. 3.9.1). The third assumption is the secular approximation. It drops (rapidly) oscillating terms causing a coarse-grained description of the system. The neglected terms are zero on average for $\Delta t \gg 1/\omega_{m,n}$, where $\omega_{m,n}$ describes free motion between eigenstates of the system and Δt is a time step of the master equation. Therefore, we loose any information on a smaller time scale than Δt.

A comparison of Bloch-Redfield and path sum approach is, e.g., given in [56, 57] and the validity of it is, for example, discussed in [78].

After an introduction into the relaxation equation in the following section, we use the Bloch-Redfield method to solve the dissipative TSS. A discussion of two dissipative spins with v_z coupling and simultaneous v_y and v_z coupling follows afterwards. Further, we study decreased and increased dephasing and relaxation rates due to degenerate eigenfrequencies with the Bloch-Redfield method.

4.1 Relaxation equation

It is convenient to separate the Hamiltonian of the two coupled spins into different parts, $H = H_{\mathrm{S}} + H_{\mathrm{R}} + H_{\mathrm{SR}}$, which describe system, reservoir, and the system-reservoir interaction, respectively. Then the von-Neumann equation in the interaction picture reads [55]

$$\mathrm{i}\frac{\partial \rho(t)_{\mathrm{I}}}{\partial t} = [V(t)_{\mathrm{I}}, \rho(t)_{\mathrm{I}}] \ , \tag{4.1.1}$$

whereas an operator O in the interaction picture is defined as

$$O(t)_{\mathrm{I}} = \mathrm{e}^{\mathrm{i}(H_{\mathrm{S}}+H_{\mathrm{R}})\,t}\, O\, \mathrm{e}^{-\,\mathrm{i}(H_{\mathrm{S}}+H_{\mathrm{R}})\,t}. \tag{4.1.2}$$

A formal integration of (4.1.1) yields

$$\rho(t)_{\mathrm{I}} = \rho(0)_{\mathrm{I}} - \mathrm{i}\int_0^t [V(\tau)_{\mathrm{I}}, \rho(\tau)_{\mathrm{I}}]\ \mathrm{d}\tau\ . \tag{4.1.3}$$

We assume that the interaction is switched on at time $t = 0$ and prior to this no interaction of the system with the bath took place. Using the formal solution back in (4.1.1) results in

$$\frac{\partial\rho(t)_{\mathrm{I}}}{\partial t} = -\,\mathrm{i}\,[V(\tau)_{\mathrm{I}}, \rho(0)_{\mathrm{I}}] \ - \int_0^t \mathrm{d}t'\ [V(t)_{\mathrm{I}}, [V(t')_{\mathrm{I}}, \rho(t')_{\mathrm{I}}]]\ . \tag{4.1.4}$$

Now, we use the first and second assumption discussed above. The first allows us to factorize the density matrix. The second, which is the Markov approximation, assumes that correlations drop quickly to zero for $t - t' \gg \tau_c$. Thus it is possible to expand the upper integration limit to infinity. We additionally trace over the bath degrees of freedom to obtain the reduced density matrix $\rho(t)_{\mathrm{SI}} = \mathrm{tr}_{\mathrm{R}}\,\rho(t)_{\mathrm{I}}$ which describes the system alone. The result is

$$\begin{aligned}\dot\rho_{\mathrm{SI}}(t) = &-\mathrm{i}\,\mathrm{tr}_{\mathrm{R}}\ [V(\tau)_{\mathrm{I}}, \rho(0)_{\mathrm{SI}}\,\rho(0)_{\mathrm{R}}] \\ &- \int_0^\infty \mathrm{d}t'\,\mathrm{tr}_{\mathrm{R}}\ [V(t)_{\mathrm{I}}, [V(t')_{\mathrm{I}}, \rho(t')_{\mathrm{SI}}\,\rho(0)_{\mathrm{R}}]]\ .\end{aligned} \tag{4.1.5}$$

To proceed, we have to use a specific interaction type between bath and system. We use one of bilinear form $V = \sum_i Q_i\,F_i$, where Q_i operates only on system variables and F_i only on bath variables. $V(t)_{\mathrm{I}}$ in the interaction picture is obtained with the unitary transformation of Eq. (4.1.2). Inserting $V(t)_{\mathrm{I}}$ into the last equation, using the commutative nature of Q_i and F_i, and also the cyclic property of the trace, leads us to

$$\begin{aligned}\dot\rho_{\mathrm{SI}}(t) = \sum_{ij}\int_0^\infty \mathrm{d}t''\,\Big\{ &[Q_i(t), Q_j(t-t'')\,\rho_{\mathrm{SI}}(t)]\,\langle F_i(t'')\,F_j\rangle \\ &- [Q_i(t), \rho_{\mathrm{SI}}(t)\,Q_j(t-t'')]\,\langle F_j\,F_i(t'')\rangle\Big\}\ .\end{aligned} \tag{4.1.6}$$

The $\langle F_i(t)\,F_j(t')\rangle = \mathrm{tr}_{\mathrm{R}}(F_i(t)\,F_j(t')\,\rho_{\mathrm{R}}(0))$ are time correlation functions describing the correlations of interactions between bath and system at different times. Further, we take the matrix elements between eigenstates $|m\rangle$ of the system and obtain

$$\begin{aligned}\langle m'\,|\,\dot\rho_{\mathrm{SI}}(t)\,|\,m\rangle &= \sum_{n',n}\langle n'\,|\,\rho_{\mathrm{SI}}(t)\,|\,n\rangle\left\{-\sum_k \delta_{mn}\Gamma^+_{m'kkn'} + \Gamma^+_{nmm'n'} + \Gamma^-_{nmm'n'}\right. \\ &\qquad\left. - \sum_k \delta_{n'm'}\Gamma^-_{nkkm}\right\}\exp\left[\mathrm{i}(E_{m'} - E_m - E_{n'} + E_n)t\right] \\ &= \sum_{n',n}\rho_{\mathrm{SI};n'n}(t)R_{m'mn'n}\exp\left[\mathrm{i}(E_{m'} - E_m - E_{n'} + E_n)t\right]\ .\end{aligned} \tag{4.1.7}$$

In the last line, we introduced the so-called Redfield-tensor $R_{m'mn'n}$. We continue the discussion of the Γ's with Eq. (4.1.13). The next step uses the third assumption, the

secular approximation, and (rapidly) oscillating terms are neglected. Therefore, we only hold terms that fulfill the secular condition $E_{m'} - E_m - E_{n'} + E_n = 0$. It is useful to transform the master equation for the reduced density matrix $\rho(t)$ to a more convenient form in the Schrödinger picture. It reads after some transformations [55]

$$\begin{aligned}\langle m' \,|\, \dot{\rho}(t) \,|\, m\rangle = &- \mathrm{i}\, \langle m' \,|\, [H_\mathrm{S}, \rho(t)] \,|\, m\rangle + \delta_{m'm} \sum_{m\neq n} \langle n \,|\, \rho(t) \,|\, n\rangle\, W_{mn} \\ &- \gamma_{m'm}\, \langle m' \,|\, \rho(t) \,|\, m\rangle \ ,\end{aligned} \tag{4.1.8}$$

where $(m \neq n)$

$$W_{mn} = \Gamma^+_{nmmn} + \Gamma^-_{nmmn} \ , \tag{4.1.9}$$

and

$$\gamma_{m'm} = \sum_k \left(\Gamma^+_{m'kkm'} + \Gamma^-_{mkkm}\right) - \Gamma^+_{mmm'm'} - \Gamma^-_{mmm'm'} \ . \tag{4.1.10}$$

The first term on the rhs of (4.1.8) describes time evolution between two states, the second term relaxation of diagonal states, and the third term is mainly responsible for dephasing of off-diagonal terms.

For the following discussion a splitting of the master equation into diagonal and off-diagonal parts is useful. The diagonal elements of the reduced density matrix are determined by the equation of motion

$$\dot{\rho}_{mm}(t) = \sum_{m\neq n} \rho_{nn}(t) W_{mn} - \rho_{mm}(t) \sum_{n\neq m} W_{nm} \ , \tag{4.1.11}$$

which describes the competition of all incoming transitions from a state n to m with all outgoing transitions from state m to n. This is again the relaxation part. On the other side, the off-diagonal elements are governed by

$$\dot{\rho}_{m'm}(t) = -\,\mathrm{i}[H_\mathrm{S}, \rho_{m'm}(t)] - \gamma_{m'm}\, \rho_{m'm}(t) \ , \tag{4.1.12}$$

which consists of an oscillatory part and a damping term.

We still have to define the Γ's that were introduced in (4.1.7). These rates are given by the Golden Rule expressions

$$\begin{aligned}\Gamma^+_{mkln} &= \sum_{ij} \langle m \,|\, Q_i \,|\, k\rangle \langle l \,|\, Q_j \,|\, n\rangle \int_0^\infty \mathrm{d}t''\, \mathrm{e}^{-\mathrm{i}\,\omega_{ln}\, t''}\, \langle F_i(t'')\, F_j\rangle \ , \\ \Gamma^-_{mkln} &= \sum_{ij} \langle m \,|\, Q_j \,|\, k\rangle \langle l \,|\, Q_i \,|\, n\rangle \int_0^\infty \mathrm{d}t''\, \mathrm{e}^{-\mathrm{i}\,\omega_{mk}\, t''}\, \langle F_j\, F_i(t'')\rangle \ .\end{aligned} \tag{4.1.13}$$

$F_i = \sum_\alpha c_\alpha x_\alpha$ describes the coupling to the bath, where c_α is the coupling strength to the bath oscillator α. We are especially interested in the generalized spin-boson Hamiltonian

for two spins like in Eq. (3.2.1) , where the interaction between system and bath is given by

$$V = \frac{\sigma_z}{2} X_1 + \frac{\tau_z}{2} X_2 \,, \tag{4.1.14}$$

with $X_\zeta(t) = \sum_\alpha c_{\zeta,\alpha}\, x_{\zeta,\alpha}(t)$ and $\zeta = 1, 2$. We assume the baths to be uncorrelated, i.e.,

$$\langle X_i(t'')\, X_j \rangle = \langle X_j\, X_i(t'') \rangle = 0 \;, \quad \text{if} \quad i \neq j \,. \tag{4.1.15}$$

Therefore, the $\Gamma' s$ take the form

$$\begin{aligned} \Gamma^+_{mkln} &= \sum_{\zeta=1,2} \langle m \,|\, s_\zeta \,|\, k \rangle \langle l \,|\, s_\zeta \,|\, n \rangle \int_0^\infty \mathrm{d}t''\, \mathrm{e}^{-\mathrm{i}\,\omega_{ln}\, t''} \, \langle X_\zeta(t'')\, X_\zeta \rangle \;, \\ \Gamma^-_{mkln} &= \sum_{\zeta=1,2} \langle m \,|\, s_\zeta \,|\, k \rangle \langle l \,|\, s_\zeta \,|\, n \rangle \int_0^\infty \mathrm{d}t''\, \mathrm{e}^{-\mathrm{i}\,\omega_{mk}\, t''} \, \langle X_\zeta\, X_\zeta(t'') \rangle \;, \end{aligned} \tag{4.1.16}$$

where $s_1 = \sigma_z/2$ and $s_2 = \tau_z/2$. The correlation $\langle X_\zeta(t)\, X_\zeta \rangle$ is the usual bath autocorrelation function (cf. [2])

$$\langle X_\zeta(t)\, X_\zeta \rangle = \int_0^\infty \mathrm{d}\omega\, J_\zeta(\omega)\, [\coth(\omega\beta_\zeta/2)\, \cos(\omega t) - \mathrm{i}\, \sin(\omega t)] \;, \tag{4.1.17}$$

where $J_\zeta(\omega) = 2K_\zeta\, \omega$ is the spectral density of an ohmic bath. In the integral in Eq. (4.1.16),

$$I^\pm_\zeta(\omega) = \int_0^\infty \mathrm{d}t\, \mathrm{e}^{-\mathrm{i}\,\omega\, t} \int_0^\infty \mathrm{d}\omega'\, J_\zeta(\omega')\, [\coth(\omega'\beta_\zeta/2)\, \cos(\omega' t) \mp \mathrm{i}\, \sin(\omega' t)] \;, \tag{4.1.18}$$

we may interchange the time and the frequency integration and split the time integral into a delta function part and a Cauchy principal value. Hence, the integral is divided into a real and an imaginary part. We get

$$\begin{aligned} I^\pm_\zeta(\omega) = \frac{\pi}{2}\, J_\zeta(\omega) \left[\coth\left(\frac{\beta_\zeta \omega}{2}\right) \mp 1 \right] \\ + \mathrm{i}\, \mathcal{P} \int_0^\infty d\omega'\, J_\zeta(\omega') \left[\frac{\omega}{\omega'^2 - \omega^2} \coth\left(\frac{\beta_\zeta \omega'}{2}\right) \mp \frac{\omega'}{\omega'^2 - \omega^2} \right] \,. \end{aligned} \tag{4.1.19}$$

The imaginary part leads to a Lamb-type shift of the relevant frequencies. Since it is usually small, it will be neglected in the following. By using the power spectrum of the collective bath modes $S_\zeta(\omega) = J_\zeta(\omega) \coth(\beta_\zeta \omega/2)$ we can rewrite Eq. (4.1.16) as

$$\begin{aligned} \Gamma^+_{mkln} &= \frac{\pi}{2} \sum_{\zeta=1,2} \langle m \,|\, s_\zeta \,|\, k \rangle \langle l \,|\, s_\zeta \,|\, n \rangle\, S_\zeta(\omega) \left[1 - \tanh\left(\frac{\beta_\zeta \omega}{2}\right) \right] \;, \\ \Gamma^-_{mkln} &= \frac{\pi}{2} \sum_{\zeta=1,2} \langle m \,|\, s_\zeta \,|\, k \rangle \langle l \,|\, s_\zeta \,|\, n \rangle\, S_\zeta(\omega) \left[1 + \tanh\left(\frac{\beta_\zeta \omega}{2}\right) \right] \,. \end{aligned} \tag{4.1.20}$$

We gain more insight, if we introduce a forward rate k_ζ^+ from the system to the bath and the respective backward rate k_ζ^- [2]. Since we assume the bath to be in thermal equilibrium, the forward and backward rate obey detailed balance

$$k_\zeta^- = k_\zeta^+ \exp(-\beta_\zeta \omega) \tag{4.1.21}$$

and thus

$$\frac{k_\zeta^+ - k_\zeta^-}{k_\zeta^+ + k_\zeta^-} = \tanh\left(\frac{\beta_\zeta \omega}{2}\right) . \tag{4.1.22}$$

Using (4.1.22) in (4.1.20) leads to

$$\begin{aligned} \Gamma^+_{mkln} &= \frac{\pi}{2} \sum_{\zeta=1,2} \langle m \,|\, s_\zeta \,|\, k\rangle\langle l \,|\, s_\zeta \,|\, n\rangle \, S_\zeta(\omega) \left(\frac{2\, k_\zeta^-}{k_\zeta^+ + k_\zeta^-}\right) , \\ \Gamma^-_{mkln} &= \frac{\pi}{2} \sum_{\zeta=1,2} \langle m \,|\, s_\zeta \,|\, k\rangle\langle l \,|\, s_\zeta \,|\, n\rangle \, S_\zeta(\omega) \left(\frac{2\, k_\zeta^+}{k_\zeta^+ + k_\zeta^-}\right) . \end{aligned} \tag{4.1.23}$$

This is a product of probabilities, describing the total probability of a one-boson-transfer from or to the bath, which triggers a transition of the system.

There is no boson-exchange from the bath to the system at $T = 0$, as follows from detailed balance. But, the reverse process is still possible. Therefore, the damping rates adopt a non-zero value in the quantum-noise regime even at zero temperature.

4.2 Dissipative two-state system

To become familiar with the procedure, we will first apply the Bloch-Redfield method to the dissipative TSS (cf. Sec. 2) before we proceed with two coupled spins in the next section. Starting with the TSS Hamiltonian

$$H = -\frac{\Delta}{2}\,\sigma_x - \frac{\epsilon}{2}\,\sigma_z \,, \tag{4.2.1}$$

which has the eigenfrequency $\Omega = \sqrt{\Delta^2 + \epsilon^2}$ and further using (4.1.11) and the normalization condition of the density matrix, we obtain the dynamics of the populations in Laplace space

$$\rho_{11}(\lambda) = \frac{W_{12}/\lambda \, + \rho_{11}^{(0)}}{\lambda + W_{12} + W_{21}} = \frac{W_{12}/\lambda \, + \rho_{11}^{(0)}}{\lambda + \gamma_\mathrm{r}} \qquad \text{and} \qquad \rho_{22} = \frac{1}{\lambda} - \rho_{11} \,. \tag{4.2.2}$$

The off-diagonal elements are calculated with Eq. (4.1.12) and read

$$\begin{aligned} \rho_{21}(\lambda) &= \frac{\rho_{21}^{(0)}}{\lambda + \gamma_{21} + \mathrm{i}\,\omega_{21}} = \frac{\rho_{21}^{(0)}}{\lambda + \gamma + \mathrm{i}\,\Omega} \,, \\ \rho_{12}(\lambda) &= \frac{\rho_{12}^{(0)}}{\lambda + \gamma_{12} - \mathrm{i}\,\omega_{21}} = \frac{\rho_{12}^{(0)}}{\lambda + \gamma - \mathrm{i}\,\Omega} \,. \end{aligned} \tag{4.2.3}$$

We identified $W_{12} + W_{21} = W_{12}(1 + \mathrm{e}^{-\beta\omega_{21}})$ as the relaxation rate γ_r of the populations and $\gamma_{21} = \gamma_{12}$ as the dephasing rate γ of the off-diagonal states. The superscript in $\rho_{ij}^{(0)}$ denotes the initial value for $\rho_{ij}(t)$ at $t = 0$.

The explicit expression for γ is

$$\gamma = \frac{1}{2}\left(W_{12} + W_{21}\right) + W_{11} + W_{22} \left(= \frac{1}{2}\left(W_{12} + W_{21}\right)\right) , \tag{4.2.4}$$

where the large bracket on the rhs holds for zero bias only. We also need the damping terms

$$\begin{aligned} W_{11} &= W_{22} = \frac{\pi}{2}\frac{\epsilon^2}{2\,\Omega^2}\,S(0) \\ W_{12} &= \frac{\pi}{2}\left[\frac{K\Delta^2\Omega}{\Omega^2} + \frac{\Delta^2 S(\Omega)}{2\,\Omega^2}\right] = \frac{\pi}{2}\frac{\Delta^2 K\ \left[\coth(\beta\Omega/2) + 1\right]}{\Omega} \\ W_{21} &= \frac{\pi}{2}\left[-\frac{K\Delta^2\Omega}{\Omega^2} + \frac{\Delta^2 S(\Omega)}{2\,\Omega^2}\right] = \frac{\pi}{2}\frac{\Delta^2 K\ \left[\coth(\beta\Omega/2) - 1\right]}{\Omega} = W_{12}\,\exp(-\beta\,\Omega)\,. \end{aligned} \tag{4.2.5}$$

Using the eigenstates from (2.1.3) we can calculate with Eqs. (4.1.8) – (4.1.19) the relaxation rate γ_r for $m' = m$

$$\gamma_\mathrm{r} = \frac{\pi}{2}\,\frac{\Delta^2}{\Omega^2}\,S(\Omega) \tag{4.2.6}$$

and the dephasing rate for $m' \neq m$

$$\gamma = \frac{\pi}{2}\,\frac{\epsilon^2}{\Omega^2}\,S(0) + \frac{\gamma_\mathrm{r}}{2}\ . \tag{4.2.7}$$

These expressions are identical with the corresponding results of the path sum approach in the one-boson exchange limit, Eq. (2.4.13). The proportionality of the dephasing rate with the relaxation rate shows that relaxation also randomizes phase information. We see that $\gamma \geq \gamma_\mathrm{r}/2$. The factor $1/2$ is attributed to the two dephasing channels corresponding to clockwise and counterclockwise Larmor precession. The additional term $\sim S(0)$ is due to flipless dephasing processes, i.e., transitions that start and end in the same state [56]. $S(\omega)$ is the spectral density of the bath, which reads

$$S(\omega) = J(\omega)\,\coth(\omega\beta/2) = 2K\omega\coth(\omega\beta/2)\ . \tag{4.2.8}$$

Observe that in the sum $W_{12} + W_{21}$, the ± 1 terms in the brackets cancel each other. Therefore, the rates are proportional to the spectral density and describe one-boson exchange processes.

For the calculation of $\rho(t)$ we need the initial values given in the eigensystem. If we start in the spin-up state at $t = 0$, we have $\rho^{(0)} = U\,\mathrm{Diag}(1, 0)\,U^{-1}$, where U diagonalizes the Hamiltonian and is given in (2.1.3). In order to calculate the result for $\sigma_z(t) = \mathrm{tr}\,\sigma_z\,\tilde{\rho}(t)$ we have to transform $\rho(t)$, which is given in the basis of the eigensystem of H, to the

up-down-basis which yields $\tilde{\rho}(t)$. At the end, we derive an expression for $\langle\sigma_z(\lambda)\rangle$ that reads

$$\langle\sigma_z(\lambda)\rangle = \frac{1}{\Omega^2}\left[\frac{(\pi K\epsilon\Delta^2+\lambda\epsilon^2)}{\lambda\,(\lambda+\gamma_\mathrm{r})}+\frac{\Delta^2(\lambda+\gamma)}{(\lambda+\gamma)^2+\Omega^2}\right]\,, \tag{4.2.9}$$

with a complex conjugate pole at $\lambda=-\gamma\pm\mathrm{i}\Omega$, a pure relaxation pole at $\lambda=-\gamma_\mathrm{r}$, and an equilibrium contribution at $\lambda=0$. This expression can be Laplace transformed into the time-regime

$$\langle\sigma_z(t)\rangle = \langle\sigma_z\rangle_\mathrm{eq}+\left(\frac{\epsilon^2}{\Omega^2}-\langle\sigma_z\rangle_\mathrm{eq}\right)\mathrm{e}^{-\gamma_\mathrm{r}t}+\frac{\Delta^2}{\Omega^2}\cos\Omega t\,\mathrm{e}^{-\gamma t}\,, \tag{4.2.10}$$

where $\langle\sigma_z\rangle_\mathrm{eq}=\epsilon/\Omega\tanh(\beta\Omega/2)$. So, we have derived in leading order the same result as we did previously with the path sum method in Eq. (2.3.22). Due to the preparation of the spin, the time derivative of $\langle\sigma_z\rangle$ at $t=0$ should be zero. This can be confirmed in leading order of the bath coupling

$$\begin{aligned}\frac{\mathrm{d}}{\mathrm{d}t}\langle\sigma_z(t)\rangle\big|_{t=0} &= \gamma\,\Delta^2+\gamma_\mathrm{r}\left(\langle\sigma_z\rangle_\mathrm{eq}-\frac{\epsilon^2}{\Omega^2}\right)\\ &= 0+\mathcal{O}(K)\,.\end{aligned} \tag{4.2.11}$$

4.3 Two dissipative coupled spins with v_z coupling

The Bloch-Redfield approach for two coupled spins is similar to the single-spin case but has some originalities. So there are terms beyond the secular approximation because of additional degeneracies in the energy spectrum E_m. They are $\omega_{42}=\omega_{31}$ and $\omega_{43}=\omega_{21}$, where $\omega_{mn}=E_m-E_n$ are the transition frequencies of the system (see Fig. 4.1). These regularities alter the master equations for the coherences by introducing additional terms. It is necessary to note that $\Delta_1>\Delta_2$ in the whole section without loss of generality.
Including the additional terms, the coupled equations for the coherences of Eq. (4.1.12) read in Laplace space (the density matrix is written as ρ_{ij} with $i,j=1..4$)

$$\begin{aligned}
\lambda\,\rho_{21}(\lambda)-\rho_{21}^{(0)} &= (-\mathrm{i}\,\omega_{21}-\gamma_{21})\,\rho_{21}(\lambda)+\left(\Gamma^+_{3124}+\Gamma^-_{3124}\right)\rho_{43}(\lambda)\,,\\
\lambda\,\rho_{31}(\lambda)-\rho_{31}^{(0)} &= (-\mathrm{i}\,\omega_{31}-\gamma_{31})\,\rho_{31}(\lambda)+\left(\Gamma^+_{2134}+\Gamma^-_{2134}\right)\rho_{42}(\lambda)\,,\\
\lambda\,\rho_{43}(\lambda)-\rho_{43}^{(0)} &= (-\mathrm{i}\,\omega_{43}-\gamma_{43})\,\rho_{43}(\lambda)+\left(\Gamma^+_{1342}+\Gamma^-_{1342}\right)\rho_{21}(\lambda)\,,\\
\lambda\,\rho_{42}(\lambda)-\rho_{42}^{(0)} &= (-\mathrm{i}\,\omega_{42}-\gamma_{42})\,\rho_{42}(\lambda)+\left(\Gamma^+_{1243}+\Gamma^-_{1243}\right)\rho_{31}(\lambda)\,,\\
\lambda\,\rho_{32}(\lambda)-\rho_{32}^{(0)} &= (-\mathrm{i}\,\omega_{32}-\gamma_{32})\,\rho_{32}(\lambda)\,,\\
\lambda\,\rho_{41}(\lambda)-\rho_{41}^{(0)} &= (-\mathrm{i}\,\omega_{41}-\gamma_{41})\,\rho_{41}(\lambda)\,.
\end{aligned} \tag{4.3.1}$$

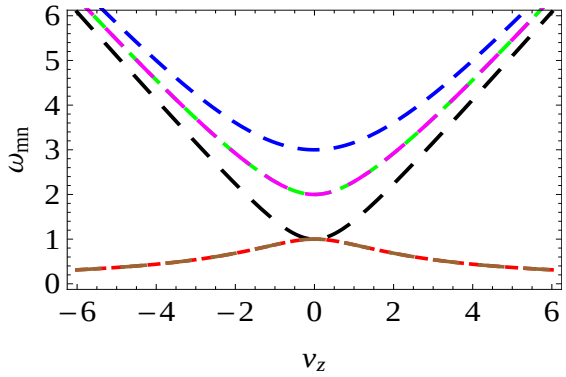

Figure 4.1: Transition frequencies $\omega_{mn} = E_m - E_n$ for two spins coupled with v_z coupling. $\Delta_1 = 2$ and $\Delta_2 = 1$. Color coding is: red, green, blue, black, magenta, brown corresponding to ω_{21}, ω_{31}, ω_{41}, ω_{32}, ω_{42}, ω_{43}. Observe the degeneracies for $\omega_{42} = \omega_{31}$ and $\omega_{43} = \omega_{21}$ for $v_z \neq 0$. The identification with the corresponding eigenfrequencies of two coupled spins in Eq. (3.1.7) is: $\omega_{21} = \delta$, $\omega_{31} = \Omega$, $\omega_{41} = \Omega_+$, and $\omega_{32} = \Omega_-$.

On the other hand, the populations defined in Eq. (4.1.11) are determined by the set of equations

$$\begin{aligned}
\rho_{11}(\lambda) &= -\frac{-W_{12}\,\rho_{22}(\lambda) - W_{13}\,\rho_{33}(\lambda) - \rho_{11}^{(0)}}{\lambda + W_{21} + W_{31}}\ , \\
\rho_{22}(\lambda) &= -\frac{-W_{13}/\lambda + W_{13}\,\rho_{11}(\lambda) - W_{21}\,\rho_{11}(\lambda) + W_{13}\,\rho_{33}(\lambda) - \rho_{22}^{(0)}}{\lambda + W_{12} + W_{13} + W_{31}}\ , \\
\rho_{33}(\lambda) &= -\frac{-W_{12}/\lambda + W_{12}\,\rho_{11}(\lambda) - W_{31}\,\rho_{11}(\lambda) + W_{12}\,\rho_{22}(\lambda) - \rho_{33}^{(0)}}{\lambda + W_{12} + W_{13} + W_{21}}\ .
\end{aligned} \tag{4.3.2}$$

We have used the normalization condition $\mathrm{tr}[\rho_{ij}(\lambda)] = 1/\lambda$. Again, the superscript in $\rho_{ij}^{(0)}$ denotes the initial value for $\rho_{ij}(t)$ at $t = 0$. Since the density matrix is Hermitian, these are all matrix elements that we actually need. We also find the following relations

$$\begin{aligned}
&W_{43} = W_{21}, \qquad W_{42} = W_{31}\ , \\
&W_{41} = W_{14} = W_{32} = W_{23} = 0\ ,
\end{aligned} \tag{4.3.3}$$

and

$$\begin{aligned}
\gamma_{21} &= \frac{1}{2}\,(W_{12} + W_{42} + W_{21} + W_{31})\ , \quad \gamma_{31} = \frac{1}{2}\,(W_{13} + W_{43} + W_{21} + W_{31})\ , \\
\gamma_{32} &= \frac{1}{2}\,(W_{13} + W_{43} + W_{12} + W_{42})\ , \quad \gamma_{41} = \frac{1}{2}\,(W_{24} + W_{34} + W_{21} + W_{31})\ , \\
\gamma_{42} &= \frac{1}{2}\,(W_{24} + W_{34} + W_{12} + W_{42})\ , \quad \gamma_{43} = \frac{1}{2}\,(W_{24} + W_{34} + W_{13} + W_{43})\ .
\end{aligned} \tag{4.3.4}$$

It is useful to remark that the expressions in (4.3.4) are valid for zero bias only. Some of the transition frequencies can be identified with the eigenfrequencies in Eq. (3.1.7)

$$\begin{aligned}
&\omega_{31} = \Omega = (\Omega_+ + \Omega_-)/2 \quad , \quad \omega_{21} = \delta = (\Omega_+ - \Omega_-)/2\,, \\
&\omega_{41} = \Omega_+ \quad , \qquad\qquad\qquad \omega_{32} = \Omega_-\,,
\end{aligned} \tag{4.3.5}$$

where $\Omega_\pm = \sqrt{(\Delta_1 \pm \Delta_2)^2 + v_z^2}$. Ω and δ are the eigenfrequencies of $\langle\sigma_z\rangle$ and $\Omega_\pm$ those of $\langle\sigma_z\tau_z\rangle$ (cf. Eq. (3.1.28)). The rather lengthy expressions for the $W_{i,j}$'s and $\Gamma^\pm$'s are given in Appendix A.5.1.

4.3.1 σ_z

Transforming the density matrix to the up-down-basis, $\tilde{\rho}(\lambda)$, we can calculate $\langle\sigma_z(\lambda)\rangle = \operatorname{tr}\sigma_z\,\tilde{\rho}(\lambda)$. Again, we prepare our system in $\langle\sigma_z(t=0)\rangle = 1$. Expressing the result in terms of the corresponding quantities in the energy basis yields

$$\begin{aligned}\langle\sigma_z(\lambda)\rangle = &-\frac{1}{2}\left[\sqrt{(1+\sin\Theta_1)(1-\sin\Theta_2)}+\sqrt{(1-\sin\Theta_1)(1+\sin\Theta_2)}\right]\\ &\times\Big[\rho_{13}(\lambda)+\rho_{24}(\lambda)+\rho_{31}(\lambda)+\rho_{42}(\lambda)\Big]\\ &+\frac{1}{2}\left[\sqrt{(1-\sin\Theta_1)(1-\sin\Theta_2)}-\sqrt{(1+\sin\Theta_1)(1+\sin\Theta_2)}\right]\\ &\times\Big[\rho_{12}(\lambda)+\rho_{21}(\lambda)-\rho_{34}(\lambda)-\rho_{43}(\lambda)\Big]\,.\end{aligned} \tag{4.3.6}$$

Here, we used again the mixing angles (3.1.4), i.e.,

$$\Theta_1 = \arctan\left[v_z/(\Delta_1+\Delta_2)\right] \qquad \text{and} \qquad \Theta_2 = \arctan\left[v_z/(\Delta_1-\Delta_2)\right]\,. \tag{4.3.7}$$

Alternatively, we can use the eigenfrequencies and obtain

$$\begin{aligned}&\langle\sigma_z(\lambda)\rangle =\\ &-\frac{1}{2}\left[\sqrt{\frac{\Omega^2-(v_z-\delta)^2}{\Omega^2-\delta^2}}+\sqrt{\frac{\Omega^2-(v_z+\delta)^2}{\Omega^2-\delta^2}}\right]\Big[\rho_{13}(\lambda)+\rho_{24}(\lambda)+\rho_{31}(\lambda)+\rho_{42}(\lambda)\Big]\\ &+\frac{1}{2}\left[\sqrt{\frac{(\Omega-v_z)^2-\delta^2}{\Omega^2-\delta^2}}-\sqrt{\frac{(\Omega+v_z)^2-\delta^2}{\Omega^2-\delta^2}}\right]\Big[\rho_{12}(\lambda)+\rho_{21}(\lambda)-\rho_{34}(\lambda)-\rho_{43}(\lambda)\Big].\end{aligned} \tag{4.3.8}$$

The dynamics of $\langle\sigma_z(\lambda)\rangle$ is determined by the poles of $\rho_{13}(\lambda)$, $\rho_{24}(\lambda)$, $\rho_{31}(\lambda)$, and $\rho_{42}(\lambda)$, which are located at

$$\lambda_\Omega^{\pm,\pm} \;=\; \pm\mathrm{i}\,\omega_{31} - \gamma_\Omega^\pm \;=\; \pm\mathrm{i}\,\Omega - \gamma_\Omega^\pm\,, \tag{4.3.9}$$

and for ρ_{12}, ρ_{21}, ρ_{34}, and ρ_{43} at

$$\lambda_\delta^{\pm,\pm} \;=\; \pm\mathrm{i}\,\omega_{21} - \gamma_\delta^\pm \;=\; \pm\mathrm{i}\,\delta - \gamma_\delta^\pm\,. \tag{4.3.10}$$

Here, the rates are given by

$$\begin{aligned}\gamma_{\Omega}^{\pm} &= \frac{1}{2}\Bigg[W_{12}+W_{21}+W_{13}+W_{31} \\ &\qquad \pm \sqrt{4\left(\Gamma_{2134}^{+}+\Gamma_{2134}^{-}\right)\left(\Gamma_{1243}^{+}+\Gamma_{1243}^{-}\right)+\left(W_{12}-W_{21}\right)^{2}}\Bigg], \\ \gamma_{\delta}^{\pm} &= \frac{1}{2}\Bigg[W_{12}+W_{21}+W_{13}+W_{31} \\ &\qquad \pm \sqrt{4\left(\Gamma_{3124}^{+}+\Gamma_{3124}^{-}\right)\left(\Gamma_{1342}^{+}+\Gamma_{1342}^{-}\right)+\left(W_{13}-W_{31}\right)^{2}}\Bigg].\end{aligned} \tag{4.3.11}$$

The rates in Eqs. (4.3.9) – (4.3.11) correspond to the respective rates that we obtained with the path sum method in the Eqs. (3.4.34) and (3.4.35). The approximate equivalence of the expressions can be shown if we neglect terms of order $\mathcal{O}\left(K_{\zeta}\right)$ but retain terms of $\mathcal{O}\left(K_{\zeta}\coth(1/T_{\zeta})\right)$. This is the weak damping limit for high (low) temperature in the Bloch-Redfield (path sum) method. Explicitly, within this regime we get for the rates

$$\begin{aligned}\gamma_{\delta}^{\mp} &= \frac{\pi}{4\left(\Omega^{2}-\delta^{2}\right)}\left[\left(\Omega^{2}-\Delta_{1,2}^{2}\right)S_{1,2}(\delta)+2\left(\Delta_{1,2}^{2}-\delta^{2}\right)S_{1,2}(\Omega)+\left(\Omega^{2}-\Delta_{2,1}^{2}\right)S_{2,1}(\delta)\right], \\ \gamma_{\Omega}^{\pm} &= \frac{\pi}{4\left(\Omega^{2}-\delta^{2}\right)}\left[2\left(\Omega^{2}-\Delta_{1,2}^{2}\right)S_{1,2}(\delta)+\left(\Delta_{1,2}^{2}-\delta^{2}\right)S_{1,2}(\Omega)+\left(\Delta_{2,1}^{2}-\delta^{2}\right)S_{2,1}(\Omega)\right].\end{aligned} \tag{4.3.12}$$

By comparing these results with the corresponding rates that we obtained within the one-boson self-energy calculation given in Eqs. (3.4.34) and (3.4.35), we see that $\kappa_{1,3}=\gamma_{\delta}^{\mp}$ and $\kappa_{2,4}=\gamma_{\Omega}^{\pm}$. This implies a smooth crossover from the quantum-noise regime to the Markov-regime, which is shown in Fig. 4.2. As can be seen, the rates smoothly match in the intermediate regime. Thus, we have an exact description of two coupled spins from low to high temperature in leading order of the bath coupling. The size of the intermediate regime and the validity of Bloch-Redfield and path sum results were already discussed in Section 3.4.3 and Fig. 3.4.

After having analyzed the poles, we may proceed and calculate the residues of $\langle\sigma_z\rangle$. For notational simplicity, the prefactors in Eq. (4.3.8) are already included in $\rho_{ij}(\lambda)$. We introduce auxiliary variables a,b,c,d to collect amplitudes which sum up to a cosine contribution in the time regime. These are

$$\begin{aligned}\mathrm{Res}\left[a\right] &= \mathrm{Res}\left[\rho_{13}(\lambda_{\Omega}^{+,+})\right]+\mathrm{Res}\left[\rho_{31}(\lambda_{\Omega}^{-,+})\right]+\mathrm{Res}\left[\rho_{24}(\lambda_{\Omega}^{+,+})\right]+\mathrm{Res}\left[\rho_{42}(\lambda_{\Omega}^{-,+})\right], \\ \mathrm{Res}\left[b\right] &= \mathrm{Res}\left[\rho_{31}(\lambda_{\Omega}^{-,-})\right]+\mathrm{Res}\left[\rho_{13}(\lambda_{\Omega}^{+,-})\right]+\mathrm{Res}\left[\rho_{42}(\lambda_{\Omega}^{-,-})\right]+\mathrm{Res}\left[\rho_{24}(\lambda_{\Omega}^{+,-})\right],\end{aligned} \tag{4.3.13}$$

and

$$\begin{aligned}\mathrm{Res}\left[c\right] &= \mathrm{Res}\left[\rho_{12}(\lambda_{\delta}^{+,+})\right]+\mathrm{Res}\left[\rho_{21}(\lambda_{\delta}^{-,+})\right]-\mathrm{Res}\left[\rho_{34}(\lambda_{\delta}^{+,+})\right]-\mathrm{Res}\left[\rho_{43}(\lambda_{\delta}^{-,+})\right], \\ \mathrm{Res}\left[d\right] &= \mathrm{Res}\left[\rho_{21}(\lambda_{\delta}^{-,-})\right]+\mathrm{Res}\left[\rho_{12}(\lambda_{\delta}^{+,-})\right]-\mathrm{Res}\left[\rho_{43}(\lambda_{\delta}^{-,-})\right]-\mathrm{Res}\left[\rho_{34}(\lambda_{\delta}^{+,-})\right].\end{aligned}$$

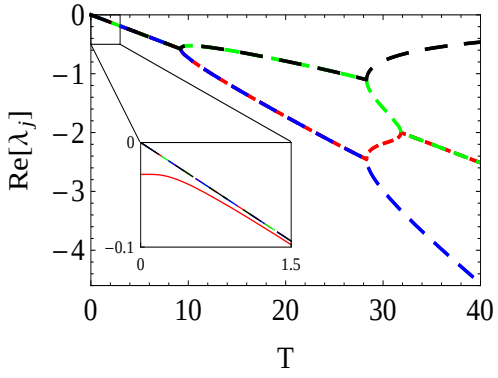

Figure 4.2: Crossover from the quantum-noise regime to the Markov-regime for $\langle\sigma_z\rangle$. For intermediate temperature the Bloch-Redfield and path sum rates smoothly merge, as can be seen in the inset. The solid red line is a Bloch-Redfield rate. We also see in the inset, how the shown Bloch-Redfield rate approaches a constant value for $T = 0$, while the path sum rates go to zero. The parameters are the same as in Fig. 3.5, i.e., we use an equal tunneling frequency $\Delta = 1$ and $v_z = 0.5$. Additionally, we use $K = 0.01$.

(4.3.14)

There is no sine contribution in the time regime as follows from the corresponding sums, which add up to zero,

$$\begin{aligned} \mathrm{Res}\left[\rho_{13}(\lambda_\Omega^{+,+})\right] - \mathrm{Res}\left[\rho_{31}(\lambda_\Omega^{-,+})\right] + \mathrm{Res}\left[\rho_{24}(\lambda_\Omega^{+,+})\right] - \mathrm{Res}\left[\rho_{42}(\lambda_\Omega^{-,+})\right] = 0\,, \\ -\mathrm{Res}\left[\rho_{31}(\lambda_\Omega^{-,-})\right] + \mathrm{Res}\left[\rho_{13}(\lambda_\Omega^{+,-})\right] - \mathrm{Res}\left[\rho_{42}(\lambda_\Omega^{-,-})\right] + \mathrm{Res}\left[\rho_{24}(\lambda_\Omega^{+,-})\right] = 0\,, \end{aligned} \tag{4.3.15}$$

and

$$\begin{aligned} \mathrm{Res}\left[\rho_{12}(\lambda_\delta^{+,+})\right] - \mathrm{Res}\left[\rho_{21}(\lambda_\delta^{-,+})\right] - \mathrm{Res}\left[\rho_{34}(\lambda_\delta^{+,+})\right] + \mathrm{Res}\left[\rho_{43}(\lambda_\delta^{-,+})\right] = 0\,, \\ -\mathrm{Res}\left[\rho_{21}(\lambda_\delta^{-,-})\right] + \mathrm{Res}\left[\rho_{12}(\lambda_\delta^{+,-})\right] + \mathrm{Res}\left[\rho_{43}(\lambda_\delta^{-,-})\right] - \mathrm{Res}\left[\rho_{34}(\lambda_\delta^{+,-})\right] = 0\,. \end{aligned} \tag{4.3.16}$$

The dynamics of $\langle\sigma_z\rangle$ in the time regime follows as

$$\begin{aligned} \langle\sigma_z(t)\rangle = \mathrm{Res}\left[a\right] \mathrm{e}^{-\gamma_\Omega^+ t}\cos\Omega t + \mathrm{Res}\left[b\right] \mathrm{e}^{-\gamma_\Omega^- t}\cos\Omega t \\ + \mathrm{Res}\left[c\right] \mathrm{e}^{-\gamma_\delta^+ t}\cos\delta t + \mathrm{Res}\left[d\right] \mathrm{e}^{-\gamma_\delta^- t}\cos\delta t\,. \end{aligned} \tag{4.3.17}$$

To be explicit, we calculate the amplitudes in the high-temperature regime in $\mathcal{O}(1/T_\zeta)$. With the condition $\Delta_1 > \Delta_2$ and equal bathes, i.e., $T_1 = T_2 = T$ and $K_1 = K_2 = K$, we

finally obtain

$$\begin{aligned}
\mathrm{Res}\,[a] &= \frac{\Omega^2-\Delta_2^2-v_z^2}{\Omega^2-\delta^2} - \frac{v_z}{2T}\frac{\Delta_1^2\,(\Delta_2^2-\delta^2)}{(\Omega^2-\delta^2)\,(\Delta_1^2-\Delta_2^2)}\;,\\
\mathrm{Res}\,[b] &= \frac{v_z}{2T}\frac{\Delta_1^2\,(\Delta_2^2-\delta^2)}{(\Omega^2-\delta^2)\,(\Delta_1^2-\Delta_2^2)}\;,\\
\mathrm{Res}\,[c] &= \frac{v_z}{2T}\frac{\Delta_1^2\,(\Omega^2-\Delta_2^2)}{(\Omega^2-\delta^2)\,(\Delta_1^2-\Delta_2^2)}\;,\\
\mathrm{Res}\,[d] &= \frac{\Delta_2^2+v_z^2-\delta^2}{\Omega^2-\delta^2} - \frac{v_z}{2T}\frac{\Delta_1^2\,(\Omega^2-\Delta_2^2)}{(\Omega^2-\delta^2)\,(\Delta_1^2-\Delta_2^2)}\;.
\end{aligned} \tag{4.3.18}$$

These are the same amplitudes that we obtained with the path sum method in Eq. (3.4.23). Also the rates $\gamma_\Omega^\pm$ and $\gamma_\delta^\mp$ smoothly match with the path sum results from Eqs. (3.4.33) – (3.4.35) if we neglect terms of order $\mathcal{O}\,(K_\zeta)$ but retain terms of $\mathcal{O}\,(K_\zeta\,T_\zeta)$ (see analysis above). Thus, in leading order of high temperature the dynamics of $\langle\sigma_z\rangle$ is in perfect agreement with the path sum result within the systematic weak damping approximation.

4.3.2 $\sigma_z\,\tau_z$

The study of $\langle\sigma_z\tau_z\rangle$ is similar. We get for $\langle\sigma_z\tau_z(\lambda)\rangle = \mathrm{tr}\,\sigma_z\tau_z\,\tilde{\rho}(\lambda)$ the result

$$\begin{aligned}
\langle\sigma_z\tau_z(\lambda)\rangle = {}& \sin\Theta_1\,[\rho_{11}(\lambda)-\rho_{44}(\lambda)] + \sin\Theta_2\,[\rho_{22}(\lambda)-\rho_{33}(\lambda)]\\
&+ \cos\Theta_1\,[\rho_{14}(\lambda)+\rho_{41}(\lambda)] + \cos\Theta_2\,[\rho_{23}(\lambda)+\rho_{32}(\lambda)]\;,
\end{aligned} \tag{4.3.19}$$

or written with the eigenfrequencies

$$\begin{aligned}
\langle\sigma_z\tau_z(\lambda)\rangle = {}& \frac{v_z}{\Omega_+}\,[\rho_{11}(\lambda)-\rho_{44}(\lambda)] + \frac{v_z}{\Omega_-}\,[\rho_{22}(\lambda)-\rho_{33}(\lambda)]\\
&+ \frac{\Delta_1+\Delta_2}{\Omega_+}\,[\rho_{14}(\lambda)+\rho_{41}(\lambda)] + \frac{\Delta_1-\Delta_2}{\Omega_-}\,[\rho_{23}(\lambda)+\rho_{32}(\lambda)]\;.
\end{aligned} \tag{4.3.20}$$

We obtain for the poles of $\rho_{23}(\lambda)$, $\rho_{32}(\lambda)$, $\rho_{14}(\lambda)$, and $\rho_{41}(\lambda)$,

$$\begin{aligned}
\lambda_{\Omega_+}^\pm &= \pm i\omega_{41} - \gamma_{\Omega_\pm} = \pm i\omega_{41} - \frac{1}{2}\,(W_{12}+W_{21}+W_{13}+W_{31})\;,\\
\lambda_{\Omega_-}^\pm &= \pm i\omega_{32} - \gamma_{\Omega_\pm} = \pm i\omega_{32} - \frac{1}{2}\,(W_{12}+W_{21}+W_{13}+W_{31})\;.
\end{aligned} \tag{4.3.21}$$

The frequencies ω_{41} and ω_{32} correspond to $\Omega_\pm$, i.e., the eigenfrequencies of $\langle\sigma_z\tau_z\rangle$. The poles of $\rho_{11}(\lambda)$, $\rho_{22}(\lambda)$, $\rho_{33}(\lambda)$, and $\rho_{44}(\lambda)$ are relaxation poles and read

$$\gamma_0 = 0\;,\quad \gamma_5 = W_{12}+W_{21}\;,\quad \text{and}\quad \gamma_6 = W_{13}+W_{31}\;. \tag{4.3.22}$$

The relaxation rates are given by

$$\begin{aligned}
\gamma_5 &= \frac{\Omega^2-\Delta_1^2}{\Omega^2-\delta^2}\frac{\pi}{2}\,S_1(\delta) + \frac{\Omega^2-\Delta_2^2}{\Omega^2-\delta^2}\frac{\pi}{2}\,S_2(\delta)\;,\\
\gamma_6 &= \frac{\Delta_1^2-\delta^2}{\Omega^2-\delta^2}\frac{\pi}{2}\,S_1(\Omega) + \frac{\Delta_2^2-\delta^2}{\Omega^2-\delta^2}\frac{\pi}{2}\,S_1(\Omega)\;.
\end{aligned} \tag{4.3.23}$$

We immediately find the identities $\kappa_{5,6} = \gamma_{5,6}$, with the generalized form of $\kappa_{5,6}$ in Eq. (3.5.38) that was calculated via the one-boson self-energy. Also, the dephasing rates in (4.3.21) match the one-boson rates from Eq. (3.5.35) and are given by the sum of the relaxation rates, $\gamma_{\Omega_\pm} = (\gamma_{01} + \gamma_{02})/2$.

As the next step, we calculate the residues. In the following the prefactors of Eq. (4.3.20) are already included in $\rho(\lambda)$. The result for $\rho_{23}(\lambda)$ and $\rho_{32}(\lambda)$ is

$$\mathrm{Res}[\rho_{23,32}(\lambda^{\pm}_{\Omega_-})] = \frac{1}{4}\left(1 - \frac{v_z^2}{\Omega_-^2}\right) . \tag{4.3.24}$$

For $\rho_{14}(\lambda)$ and $\rho_{41}(\lambda)$ we get

$$\mathrm{Res}[\rho_{14,41}(\lambda^{\pm}_{\Omega_+})] = \frac{1}{4}\left(1 - \frac{v_z^2}{\Omega_+^2}\right) . \tag{4.3.25}$$

The equilibrium and relaxation poles $\rho_{11}(\lambda)$, $\rho_{22}(\lambda)$, $\rho_{33}(\lambda)$, and $\rho_{44}(\lambda)$ have the following residues

$$\begin{aligned}
\sum_{i=1,..,4} \mathrm{Res}\left[\rho_{ii}(\gamma_0)\right] &= \frac{v_z}{\delta^2 - \Omega^2}\left[\delta\,\tanh\left(\frac{\beta\,\delta}{2}\right) - \Omega\,\tanh\left(\frac{\beta\,\Omega}{2}\right)\right] , \\
\sum_{i=1,..,4} \mathrm{Res}\left[\rho_{ii}(\gamma_5)\right] &= \frac{v_z\,\Delta_1\,\Delta_2\,\left[v_z(\Omega_+ - \Omega_-) + 2\,\Omega_+\,\Omega_-\,\tanh\left(\frac{\beta\,(\Omega_+ - \Omega_-)}{4}\right)\right]}{\Omega_+^2\,\Omega_-^2\,(\Omega_+ + \Omega_-)} , \\
\sum_{i=1,..,4} \mathrm{Res}\left[\rho_{ii}(\gamma_6)\right] &= \frac{v_z\,\Delta_1\,\Delta_2\,\left(v_z\,(\Omega_+ + \Omega_-) - 2\,\Omega_+\,\Omega_-\,\tanh\left[\frac{\beta\,(\Omega_+ + \Omega_-)}{4}\right]\right)}{\Omega_+^2\,\Omega_-^2\,(\Omega_+ - \Omega_-)} ,
\end{aligned} \tag{4.3.26}$$

or rewritten with the frequencies Ω and δ

$$\begin{aligned}
\sum_{i=1,..,4} \mathrm{Res}\left[\rho_{ii}(\gamma_5)\right] &= \frac{v_z^2\delta^2}{(\Omega^2 - \delta^2)^2} + \frac{v_z\,\delta}{\Omega^2 - \delta^2}\,\tanh\left(\frac{\beta\delta}{2}\right) , \\
\sum_{i=1,..,4} \mathrm{Res}\left[\rho_{ii}(\gamma_6)\right] &= \frac{v_z^2\Omega^2}{(\Omega^2 - \delta^2)^2} - \frac{v_z\,\Omega}{\Omega^2 - \delta^2}\,\tanh\left(\frac{\beta\Omega}{2}\right) .
\end{aligned} \tag{4.3.27}$$

These results for the amplitudes and the rates are in agreement with the path sum results discussed in Sec. (3.5.1).

4.4 Two dissipative coupled spins with v_y and v_z coupling

The additional v_y spin-spin coupling does not alter the relevant equations that are valid for exclusive v_z coupling. Hence, Eqs. (4.3.1) – (4.3.4) are still the starting point, and we have to perform basically the same steps as for sole v_z coupling. So we will skip the details and concentrate on the results. The resulting expressions for the $W_{i,j}$'s and $\Gamma^{\pm}$'s are given in Appendix A.5.2.

4.4.1 σ_z

First, we calculate $\langle\sigma_z(\lambda)\rangle$,

$$\begin{aligned}\langle\sigma_z(\lambda)\rangle = &-\frac{1}{2}\left(\sqrt{(1-\sin\Theta_1)\,(1-\sin\Theta_2)}+\sqrt{(1+\sin\Theta_1)\,(1+\sin\Theta_2)}\right)\\ &\times\Big[\rho_{13}(\lambda)+\rho_{24}(\lambda)+\rho_{31}(\lambda)+\rho_{42}(\lambda)\Big]\\ &+\frac{1}{2}\left(\sqrt{(1-\sin\Theta_1)\,(1+\sin\Theta_2)}-\sqrt{(1+\sin\Theta_1)\,(1-\sin\Theta_2)}\right)\\ &\times\Big[\rho_{12}(\lambda)+\rho_{21}(\lambda)-\rho_{34}(\lambda)-\rho_{43}(\lambda)\Big]\,,\end{aligned} \tag{4.4.1}$$

with the mixing angles from Eq. (3.6.3)

$$\Theta_1=\arctan\left(\frac{v_y-v_z}{\Delta_1+\Delta_2}\right),\qquad \Theta_2=\arctan\left(\frac{v_y+v_z}{\Delta_1-\Delta_2}\right)\,. \tag{4.4.2}$$

Equivalently, with the eigenfrequencies Ω and δ we obtain

$$\begin{aligned}\langle\sigma_z(\lambda)\rangle = &\frac{\big[\Delta_1(v_z-\Omega)+\Delta_2(v_y+\delta)\big]\,\sqrt{\Omega+\delta+v_z-v_y}}{(\Delta_1+\Delta_2)\sqrt{(\Omega^2-\delta^2)(\Omega-\delta-v_z-v_y)}}\\ &\times\Big[\rho_{13}(\lambda)+\rho_{24}(\lambda)+\rho_{31}(\lambda)+\rho_{42}(\lambda)\Big]\\ &-\frac{\big[\Delta_1(v_z-\delta)+\Delta_2(v_y+\Omega)\big]\,\sqrt{\Omega+\delta+v_z-v_y}}{(\Delta_1+\Delta_2)\sqrt{(\Omega^2-\delta^2)(\Omega-\delta+v_z+v_y)}}\\ &\times\Big[\rho_{12}(\lambda)+\rho_{21}(\lambda)-\rho_{34}(\lambda)-\rho_{43}(\lambda)\Big]\,.\end{aligned} \tag{4.4.3}$$

The poles of $\rho_{13}(\lambda)$, $\rho_{24}(\lambda)$, $\rho_{31}(\lambda)$, and $\rho_{42}(\lambda)$ are located at

$$\lambda_\Omega^{\pm,\pm}=\pm\mathrm{i}\,\omega_{31}-\gamma_\Omega^{\pm}\,, \tag{4.4.4}$$

and for $\rho_{12}(\lambda)$, $\rho_{21}(\lambda)$, $\rho_{34}(\lambda)$, and $\rho_{43}(\lambda)$ at

$$\lambda_\delta^{\pm,\pm}=\pm\mathrm{i}\,\omega_{21}-\gamma_\delta^{\pm}\,. \tag{4.4.5}$$

Again, the rates take the form

$$\begin{aligned}\gamma_\Omega^{\pm}=\frac{1}{2}\Bigg[&W_{12}+W_{21}+W_{13}+W_{31}\\ &\pm\sqrt{4\,(\Gamma^+_{2134}+\Gamma^-_{2134})\,(\Gamma^+_{1243}+\Gamma^-_{1243})+(W_{12}-W_{21})^{\,2}}\Bigg]\,,\\ \gamma_\delta^{\pm}=\frac{1}{2}\Bigg[&W_{12}+W_{21}+W_{13}+W_{31}\\ &\pm\sqrt{4\,(\Gamma^+_{3124}+\Gamma^-_{3124})\,(\Gamma^+_{1342}+\Gamma^-_{1342})+(W_{13}-W_{31})^{\,2}}\Bigg]\,.\end{aligned} \tag{4.4.6}$$

We have the identities $\Omega = \omega_{31} = (\Omega_+ + \Omega_-)/2$ and $\delta = \omega_{21} = (\Omega_+ - \Omega_-)/2$, where

$$\Omega_+ = \sqrt{(\Delta_1 + \Delta_2)^2 + (v_y - v_z)^2} \quad \text{and} \quad \Omega_- = \sqrt{(\Delta_1 - \Delta_2)^2 + (v_y + v_z)^2} \,. \tag{4.4.7}$$

The frequencies Ω and δ are the eigenfrequencies of $\langle \sigma_z \rangle$ and $\Omega_\pm$ those of $\langle \sigma_z \tau_z \rangle$. And once more, we can show in order $\mathcal{O}\left(K_\zeta\, T_\zeta\right)$ that the identities $\kappa_\delta = \gamma_\delta^-$ and $\kappa_\Omega = \gamma_\Omega^+$ hold, with κ_δ and κ_Ω from Section 3.6.1. Thus, we have a smooth crossover to the path sum results that were previously derived. Explicitly, within $\mathcal{O}\left(K_\zeta \coth(1/T_\zeta)\right)$ the rates take the forms

$$\begin{aligned}
\gamma_\delta^\mp = \frac{\pi}{4(\Omega^2 - \delta^2)} \Big[& 2\left(\Omega^2 - \Delta_{2,1}^2 - v_z^2\right) S_{1,2}(\Omega) + \left(\Delta_{2,1}^2 + v_z^2 - \delta^2\right) S_{1,2}(\delta) \\
& + \left(\Delta_{1,2}^2 + v_z^2 - \delta^2\right) S_{2,1}(\delta) \Big] \,, \\
\gamma_\Omega^\pm = \frac{\pi}{4(\Omega^2 - \delta^2)} \Big[& \left(\Omega^2 - \Delta_{2,1}^2 - v_z^2\right) S_{1,2}(\Omega) + 2\left(\Delta_{2,1}^2 + v_z^2 - \delta^2\right) S_{1,2}(\delta) \\
& + \left(\Omega^2 - \Delta_{1,2}^2 - v_z^2\right) S_{2,1}(\Omega) \Big] \,.
\end{aligned} \tag{4.4.8}$$

It is convenient to rewrite the Markov expressions of the rates from Eq. (3.6.15) as

$$\begin{aligned}
\kappa_\delta &= \frac{1}{2\left(\Omega^2 - \delta^2\right)} \left[2\left(\Omega^2 - \Delta_2^2 - v_z^2\right) \vartheta_1 + \left(\Delta_2^2 + v_z^2 - \delta^2\right) \vartheta_1 + \left(\Delta_1^2 + v_z^2 - \delta^2\right) \vartheta_2 \right] \,, \\
\kappa_\Omega &= \frac{1}{2\left(\Omega^2 - \delta^2\right)} \left[\left(\Omega^2 - \Delta_2^2 - v_z^2\right) \vartheta_1 + 2\left(\Delta_2^2 + v_z^2 - \delta^2\right) \vartheta_1 + \left(\Omega^2 - \Delta_1^2 - v_z^2\right) \vartheta_2 \right] \,.
\end{aligned} \tag{4.4.9}$$

Comparing (4.4.8) with (4.4.9) reveals that the transition from the Markov-regime to the quantum-noise regime is again done by the replacement of ϑ_ζ with the corresponding $S_\zeta(\Omega, \delta)$. The two remaining poles in (4.4.8), γ_δ^+ and γ_Ω^-, are absent in the path sum derivation, when the influence phase contributions to $\langle \sigma_z(\lambda) \rangle$ are disregarded (see (A.2.8)).

As the same arguments apply that led to (4.3.17), the dynamics of $\langle \sigma_z \rangle$ in the time regime and for high temperature is described by

$$\begin{aligned}
\langle \sigma_z(t) \rangle = {} & \mathrm{Res}\,[a]\ \mathrm{e}^{-\gamma_\Omega^+ t} \cos \Omega t + \mathrm{Res}\,[b]\ \mathrm{e}^{-\gamma_\Omega^- t} \cos \Omega t \\
& + \mathrm{Res}\,[c]\ \mathrm{e}^{-\gamma_\delta^+ t} \cos \delta t + \mathrm{Res}\,[d]\ \mathrm{e}^{-\gamma_\delta^- t} \cos \delta t \,.
\end{aligned} \tag{4.4.10}$$

The amplitudes are of the same form as in (4.3.13) and (4.3.14). The four amplitudes simplify in the high temperature limit to the following expressions:

$$\begin{aligned}
\mathrm{Res}\,[a] &= \frac{\Omega^2 - \Delta_2^2 - v_z^2}{\Omega^2 - \delta^2} + \mathcal{O}(1/T) \,, \\
\mathrm{Res}\,[b] &= \mathrm{Res}\,[c] = \mathcal{O}(1/T) \,, \\
\mathrm{Res}\,[d] &= \frac{\Delta_2^2 + v_z^2 - \delta^2}{\Omega^2 - \delta^2} + \mathcal{O}(1/T) \,.
\end{aligned} \tag{4.4.11}$$

These are the same as we calculated in Eq. (3.6.17) with the path sum method.

4.4.2 $\sigma_z\,\tau_z$

For $\langle\sigma_z\tau_z(\lambda)\rangle$ we get

$$\begin{aligned}\langle\sigma_z\tau_z(\lambda)\rangle = &-\sin\Theta_1\left[\rho_{11}(\lambda)-\rho_{44}(\lambda)\right]+\sin\Theta_2\left[\rho_{22}(\lambda)-\rho_{33}(\lambda)\right]\\ &+\cos\Theta_1\left[\rho_{14}(\lambda)+\rho_{41}(\lambda)\right]+\cos\Theta_2\left[\rho_{23}(\lambda)+\rho_{32}(\lambda)\right]\ ,\end{aligned} \tag{4.4.12}$$

or written in terms of the eigenfrequencies

$$\begin{aligned}\langle\sigma_z\tau_z(\lambda)\rangle = &\frac{v_z-v_y}{\Omega_+}\Big[\rho_{11}(\lambda)-\rho_{44}(\lambda)\Big]+\frac{v_z+v_y}{\Omega_-}\Big[\rho_{22}(\lambda)-\rho_{33}(\lambda)\Big]\\ &+\frac{\Delta_1+\Delta_2}{\Omega_+}\Big[\rho_{14}(\lambda)+\rho_{41}(\lambda)\Big]+\frac{\Delta_1-\Delta_2}{\Omega_-}\Big[\rho_{23}(\lambda)+\rho_{32}(\lambda)\Big]\ .\end{aligned} \tag{4.4.13}$$

The pole conditions for $\rho_{23}(\lambda)$, $\rho_{32}(\lambda)$ and $\rho_{14}(\lambda)$, $\rho_{41}(\lambda)$ are

$$\begin{aligned}\lambda^{\pm}_{\Omega_+} &= \pm\mathrm{i}\,\Omega_+ - \gamma_{\Omega_\pm} = \pm\mathrm{i}\,\omega_{41} - \frac{1}{2}\left(W_{12}+W_{21}+W_{13}+W_{31}\right)\ ,\\ \lambda^{\pm}_{\Omega_-} &= \pm\mathrm{i}\,\Omega_- - \gamma_{\Omega_\pm} = \pm\mathrm{i}\,\omega_{32} - \frac{1}{2}\left(W_{12}+W_{21}+W_{13}+W_{31}\right)\ .\end{aligned} \tag{4.4.14}$$

The frequencies ω_{41} and ω_{32} correspond to Ω_+ and Ω_-, i.e., they are the eigenfrequencies of $\langle\sigma_z\tau_z\rangle$. The different $W_{i,j}$'s are defined in the Eqs. (A.5.13)–(A.5.16). The poles from $\rho_{11}(\lambda)$, $\rho_{22}(\lambda)$, $\rho_{33}(\lambda)$, and $\rho_{44}(\lambda)$ form three relaxation poles and read

$$\gamma_0 = 0\ , \qquad \gamma_{01} = W_{12}+W_{21}\ , \qquad \gamma_{02} = W_{13}+W_{31}\ . \tag{4.4.15}$$

Within the high-temperature limit, we immediately find the identities $\kappa_{01} = \gamma_{01}$ and $\kappa_{02} = \gamma_{02}$, with $\kappa_{01,02}$ from Eq. (3.6.16). Explicitly, we have

$$\begin{aligned}\gamma_{01} &= \frac{\Delta_1^2+v_y^2-\delta^2}{\Omega^2-\delta^2}\frac{\pi}{2}S_1(\Omega)+\frac{\Delta_2^2+v_y^2-\delta^2}{\Omega^2-\delta^2}\frac{\pi}{2}S_2(\Omega)\ ,\\ \gamma_{02} &= \frac{\Omega^2-v_y^2-\Delta_1^2}{\Omega^2-\delta^2}\frac{\pi}{2}S_1(\delta)+\frac{\Omega^2-v_y^2-\Delta_2^2}{\Omega^2-\delta^2}\frac{\pi}{2}S_2(\delta)\ .\end{aligned} \tag{4.4.16}$$

The dephasing rates in (4.4.14) smoothly match the path sum rates of Eq. (3.6.16) in the high-temperature limit, i.e., $\kappa_{\Omega_\pm} = (\vartheta_1+\vartheta_2)/2$. The generalized rate $\kappa_{\Omega_\pm}$ in the one-boson exchange is immediately obtained by the sum of the last two equations and reads

$$\gamma_{\Omega_\pm} = (\gamma_{01}+\gamma_{02})/2\ . \tag{4.4.17}$$

Thus, the generalization of the two pure relaxation poles $\kappa_{01,02}$ and the dephasing poles $\kappa_{\Omega_\pm}$ to the one-boson exchange regime is again based on replacing $\vartheta_{1,2}$ with the corresponding power spectra $S_{1,2}(\Omega,\delta)$.

The oscillatory amplitude of $\langle\sigma_z\tau_z\rangle$ for ρ_{23} and ρ_{32} is

$$\mathrm{Res}[\langle\sigma_z\tau_z(\lambda=\lambda^{\pm}_{\Omega_-})\rangle] = \frac{(\Delta_1-\Delta_2)^2}{4\Omega_-^2}\ , \tag{4.4.18}$$

and for ρ_{14} and ρ_{41} we get

$$\mathrm{Res}[\langle\sigma_z\tau_z(\lambda=\lambda^{\pm}_{\Omega_+})\rangle] = \frac{(\Delta_1+\Delta_2)^2}{4\Omega_+^2}\,. \tag{4.4.19}$$

The equilibrium pole and the pure relaxation poles have the amplitudes

$$\begin{aligned}
\mathrm{Res}[\langle\sigma_z\tau_z(\lambda=0)\rangle] &= \frac{(\Omega v_z+\delta v_y)\tanh\left(\frac{\beta\Omega}{2}\right)-(\Omega v_y+\delta v_z)\tanh\left(\frac{\beta\delta}{2}\right)}{\Omega^2-\delta^2}\,,\\
\mathrm{Res}[\langle\sigma_z\tau_z(\lambda=-\kappa_{01})\rangle] &= \frac{(\Omega v_z+\delta v_y)\left(\Omega v_z+\delta v_y-(\Omega^2-\delta^2)\tanh\left(\frac{\beta\Omega}{2}\right)\right)}{(\Omega^2-\delta^2)^2}\,,\\
\mathrm{Res}[\langle\sigma_z\tau_z(\lambda=-\kappa_{02})\rangle] &= \frac{(\Omega v_y+\delta v_z)\left(\Omega v_y+\delta v_z+(\Omega^2-\delta^2)\tanh\left(\frac{\beta\delta}{2}\right)\right)}{(\Omega^2-\delta^2)^2}\,.
\end{aligned} \tag{4.4.20}$$

As we see, these results for $\langle\sigma_z\tau_z\rangle$ are the same as the path sum results.

4.5 Bloch-Redfield and quantum frustration of decoherence

We have shown in Section 3.7 that we obtain minimal damping rates if two or more of the eigenvalues become degenerate. Now, we will study this feature in the Bloch-Redfield regime (see Fig. 4.3). In Figure 3.13 are shown the eigenfrequencies of $\langle\sigma_z\rangle$ and $\langle\sigma_z\tau_z\rangle$ with the two degeneracy points.

For the first degeneracy point, which is the left in Figure 3.13, we simplify the calculation by only keeping terms of $\mathcal{O}\left(K_\zeta\,\coth(1/T_\zeta)\right)$ and neglecting terms of $\mathcal{O}\left(K_\zeta\right)$. The degeneracy occurs where

$$\Delta_{1,2} = \Delta \pm \epsilon/2 \quad \text{and} \quad v_{y,z} = \pm v + \eta/2\,, \tag{4.5.1}$$

and therefore $\Omega = \delta = \sqrt{\Delta^2+v^2}$ for $\epsilon \to 0$ and $\eta \to 0$. Using the expressions (4.4.6) and (A.5.11) – (A.5.20), we can calculate the rates at this degeneracy point

$$\begin{aligned}
\gamma_\delta^- &= \frac{3\,\pi}{8}\,S_1(\Omega)+\frac{\pi}{8}\,S_2(\Omega)+\frac{\pi\,\Delta}{8\,\Omega}\,[S_1(\Omega)+\,S_2(\Omega)]+\frac{\pi\,v}{8\,\Omega}\,[S_1(\Omega)-\,S_2(\Omega)]\,,\\
\gamma_\Omega^+ &= \frac{3\,\pi}{8}\,S_1(\Omega)+\frac{\pi}{8}\,S_2(\Omega)-\frac{\pi\,\Delta}{8\,\Omega}\,[S_1(\Omega)+\,S_2(\Omega)]-\frac{\pi\,v}{8\,\Omega}\,[S_1(\Omega)-\,S_2(\Omega)]\,,\\
\gamma_\delta^+ &= \frac{\pi}{8}\,S_1(\Omega)+\frac{3\,\pi}{8}\,S_2(\Omega)-\frac{\pi\,\Delta}{8\,\Omega}\,[S_1(\Omega)+\,S_2(\Omega)]-\frac{\pi\,v}{8\,\Omega}\,[S_1(\Omega)-\,S_2(\Omega)]\,,\\
\gamma_\Omega^- &= \frac{\pi}{8}\,S_1(\Omega)+\frac{3\,\pi}{8}\,S_2(\Omega)+\frac{\pi\,\Delta}{8\,\Omega}\,[S_1(\Omega)+\,S_2(\Omega)]+\frac{\pi\,v}{8\,\Omega}\,[S_1(\Omega)-\,S_2(\Omega)]\,,
\end{aligned} \tag{4.5.2}$$

and

$$\begin{aligned}
\gamma_{\Omega_\pm} &= \frac{\pi}{4}\,[S_1(\Omega)+S_2(\Omega)]\,,\\
\gamma_{01,02} &= \frac{\pi}{4}\,[S_1(\Omega)+S_2(\Omega)]\pm\frac{\pi\,\Delta}{4\,\Omega}\,[S_1(\Omega)-S_2(\Omega)]\pm\frac{\pi\,v}{4\,\Omega}\,[S_1(\Omega)+S_2(\Omega)]\,.
\end{aligned} \tag{4.5.3}$$

By comparing these rates with the corresponding results in the Markov-regime, i.e., Eqs. (3.7.3) and (3.7.6), we see that the Markov rates are easily expanded to the quantum-noise regime by replacing ϑ_ζ with $S_\zeta(\Omega)$. Since the rates and the amplitudes have the same structure as in Section 3.7, we observe the frustration of decoherence phenomenon in the quantum-noise regime, too.

For the second degeneracy point, we set $\Delta_1 = \Delta_2 = \Delta$, $v_y\, v_z = \Delta^2$,

$$v_y = \sqrt{\frac{v^2}{2} - \sqrt{\frac{v^4}{4} - \Delta^4\kappa^2}}\,, \qquad v_z = \sqrt{\frac{v^2}{2} + \sqrt{\frac{v^4}{4} - \Delta^4\kappa^2}}\,, \tag{4.5.4}$$

where $v = \sqrt{v_y^2 + v_z^2}$ is the total length of the coupling vector (see Eq. (3.7.10)). Then, we obtain $\Omega = \Omega_+ = \Omega_-$ and therefore $\delta \to 0$. This time, the transition to the quantum-noise regime is not only performed by replacing ϑ_ζ with $S_\zeta(\Omega)$. Since $\delta \to 0$, we get for the power spectrum $S_\zeta(\delta)$ at the degeneracy point $\kappa = 1$ the same form as in the Markov-regime, i.e.,

$$\lim_{\delta\to 0} \frac{\pi}{2}\, S_\zeta(\delta) = \vartheta_\zeta\,. \tag{4.5.5}$$

Then we obtain for the dephasing rates of $\langle\sigma_z\rangle$ in $\mathcal{O}\left(K_\zeta\, \coth(1/T_\zeta)\right)$

$$\begin{aligned}
\gamma_\delta^- &= \frac{1}{4}\left(1 + \frac{\sqrt{v^2 - 2\,\Delta^2}}{\sqrt{v^2 + 2\,\Delta^2}}\right)\,[\vartheta_1 + \vartheta_2] + \frac{\pi}{4}\left(1 - \frac{\sqrt{v^2 - 2\,\Delta^2}}{\sqrt{v^2 + 2\,\Delta^2}}\right)\,S_1(\Omega)\,,\\
\gamma_\Omega^+ &= \frac{1}{2}\left(1 + \frac{\sqrt{v^2 - 2\,\Delta^2}}{\sqrt{v^2 + 2\,\Delta^2}}\right)\,\vartheta_1 + \frac{\pi}{8}\left(1 - \frac{\sqrt{v^2 - 2\,\Delta^2}}{\sqrt{v^2 + 2\,\Delta^2}}\right)\,[S_1(\Omega) + S_2(\Omega)]\,,
\end{aligned} \tag{4.5.6}$$

and

$$\begin{aligned}
\gamma_\delta^+ &= \frac{1}{4}\left(1 + \frac{\sqrt{v^2 - 2\,\Delta^2}}{\sqrt{v^2 + 2\,\Delta^2}}\right)\,[\vartheta_1 + \vartheta_2] + \frac{\pi}{4}\left(1 - \frac{\sqrt{v^2 - 2\,\Delta^2}}{\sqrt{v^2 + 2\,\Delta^2}}\right)\,S_2(\Omega)\,,\\
\gamma_\Omega^- &= \frac{1}{2}\left(1 + \frac{\sqrt{v^2 - 2\,\Delta^2}}{\sqrt{v^2 + 2\,\Delta^2}}\right)\,\vartheta_2 + \frac{\pi}{8}\left(1 - \frac{\sqrt{v^2 - 2\,\Delta^2}}{\sqrt{v^2 + 2\,\Delta^2}}\right)\,[S_1(\Omega) + S_2(\Omega)]\,.
\end{aligned} \tag{4.5.7}$$

For high temperature, the rates γ_δ^- and γ_Ω^+ adopt the forms of the path sum derivation given in Eq. (3.7.12). Unfortunately, a shift of $\gamma_\delta^\pm$ due to a renormalization by a second order contribution (like in Eq. (3.7.14) because $\delta \to 0$) is not accessible because Bloch-Redfield is valid in first order of the bath correlations only. For $\langle\sigma_z\tau_z\rangle$, the relaxation rates and the dephasing rate of Eq. (3.7.16) change to

$$\begin{aligned}
\gamma_{01} &= \frac{\pi}{4}\left(1 - \frac{\sqrt{v^4 - 4\Delta^4}}{\Omega^2}\right)\,[S_1(\Omega) + S_2(\Omega)]\,,\\
\gamma_{02} &= \frac{1}{2}\left(1 + \frac{\sqrt{v^4 - 4\Delta^4}}{\Omega^2}\right)\,[\vartheta_1 + \vartheta_2]\,,\\
\gamma_{\Omega_\pm} &= \frac{\gamma_{01} + \gamma_{02}}{2}\,.
\end{aligned} \tag{4.5.8}$$

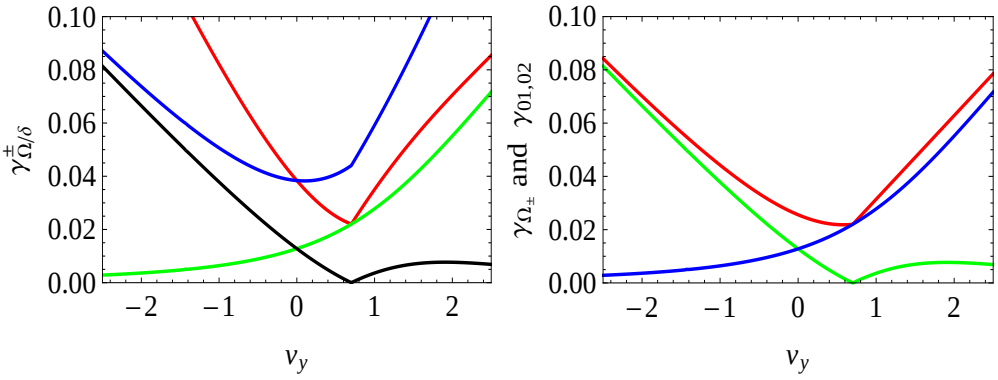

Figure 4.3: Minima in damping rates with $v_z = 1.43$, $\Delta = 1$, $T = 10^{-4}$, $K = 0.01$. We see a minimum for a coupling strength as in Eq. (4.5.4). Plots were done with the full expressions for the rates and not approximated by neglecting terms of $\mathcal{O}(K_\zeta)$. See text for details. Left: red is γ^+_Ω, green is γ^-_Ω, blue is γ^+_δ, and black is γ^-_δ. Right: red is $\gamma_{\Omega_\pm}$, green is γ_{01}, and blue is γ_{02}.

The minima in the rates due to a frustration of decoherence do not show up until reaching very low temperature. Therefore, we cannot neglect any term in the rate expressions, i.e., we have to use the rates given in the Eqs. (4.4.6), (4.4.15), and (4.4.17). By performing a numerical analysis, we see a minimum for the dephasing rates γ^-_δ, γ^+_Ω, $\gamma_{\Omega_\pm}$ and for the relaxation rate γ_{01} at the degeneracy point. The other rates do not show a minimum. This is different to the Markov-regime, where only two of the relaxation rates have a minimum (cf. Sec. 3.7). The rates are shown in Fig. 4.3 (cf. [72]). A numerical analysis of the amplitudes (not shown) reveals that only γ^+_Ω, γ^+_δ, γ_{Ω_+} give rise to a coherent contribution around the degeneracy point.

4.6 Conclusions

We applied the Bloch-Redfield equations both to a single spin and to two coupled spins with v_z coupling and simultaneous v_y and v_z coupling. In the case of two coupled spins we had to extend the usual secular approximation to include additional terms due to degeneracies of the relevant frequencies.

We obtained a smooth crossover from Bloch-Redfield to the path sum results of the previous chapter in the one-boson exchange regime and for intermediate temperature. This is not obvious because both theories are based on different procedures. We closed the gap between Bloch-Redfield results, valid for low temperature, and path sum results by Dubé and Stamp, valid for high temperature and strong mutual spin-spin coupling. Now, it is possible to describe two coupled spins for all temperatures in leading order of the bath coupling. The connection between the low temperature regime, where the Bloch-Redfield method is valid, and the high temperature regime, where the path sum method is valid, is analytically exact.

5 Summary

Two dissipative coupled spins were analyzed with the path sum and the Bloch-Redfield method. We focused on the case, where each of the spins is coupled to its own boson bath. Our studies begun in the white-noise Markov-regime, where multi-boson exchange processes between system and bath prevail. Then, an extension to the low temperature and weak bath coupling quantum-noise regime, where one-boson exchange processes dominate was made.

Various regimes were examined in detail with the path sum method. We studied the one-boson exchange regime, which is valid for low temperature, and the high-temperature and/or large spin-spin coupling regime. An extension to linear combinations of longitudinal and transverse spin-spin coupling was discussed. For simultaneous v_y and v_z spin-spin coupling we found degenerate eigenenergies for certain coupling strengths. There we obtained equally preferred but mutually exclusive ground states. Since both ground states are exclusive, we observed a frustration of decoherence, which lead to extended coherence times. This is crucial with regard to quantum information processing, where long coherence times are essential. With bias, we obtained an avoided level crossing and no more a complete degeneracy of the eigenenergies. Nevertheless, we found a frustration of decoherence, too. Non-Gaussian behavior of an environment was studied with a spin-boson environment and the path sum method. We found for high temperature of the resonant boson-bath that damping decreases with increasing temperature, and more important, a coherent contribution with relevant amplitude remains, with the result that we obtained an unexpected long coherence time. So we found another possibility to minimize the influence of the environment.

We further applied the Bloch-Redfield method to two coupled spins which are weakly coupled to boson baths. Thereto, we had to include additional terms in the Bloch-Redfield equations beyond the usual secular approximation. We found for the first time an analytically exact crossover from the Bloch-Redfield results to the path sum results for weak bath coupling, i.e., in the one-boson exchange regime. This is not obvious a priori because the Bloch-Redfield method uses a perturbative expansion of the system-bath coupling, while the path sum method is based on an expansion of the tunnel matrix element.

By filling the gap between Bloch-Redfield results, valid for low temperature, and former path sum results by Dubé and Stamp, valid for high temperature and strong mutual spin-spin coupling, it is now possible to describe two coupled spins with weak bath coupling for all temperatures between $T = 0$ and $T = \infty$. It was also shown that the transition from the quantum-noise regime to the white-noise regime is analytically exact.

The description of two dissipative coupled spins with bias was only begun in this thesis. Unfortunately, the analytic handling is complicated by the size of the occurring

expressions. We hope that further research can circumvent this drawback. Also driven coupled qubits were not discussed in this thesis, which remains an open topic for future research [79].

A Appendix

A.1 Preparation effects

A.1.1 One spin

Assume that we prepare our spin at $t = 0$ only to a fraction α in $|L\rangle$ and $1 - \alpha$ in $|R\rangle$. Then, we have $\langle\sigma_z(t = 0)\rangle = \alpha\,|L\rangle + (1 - \alpha)\,|R\rangle$, with $0 \leq \alpha \leq 1$ at $t = 0$, and therefore

$$\begin{aligned}\rho_{R,\alpha} &= \alpha\,\rho_{R,L} + (1 - \alpha)\,\rho_{R,R}\,,\\ \rho_{L,\alpha} &= \alpha\,\rho_{L,L} + (1 - \alpha)\,\rho_{L,R}\,.\end{aligned} \tag{A.1.1}$$

Summing these equations results in 1, or $1/\lambda$, because $\rho_{R,L}+\rho_{L,L} = 1$ and $\rho_{R,R}+\rho_{L,R} = 1$. Subtracting these equations gives

$$\begin{aligned}\rho_{R,\alpha} - \rho_{L,\alpha} &= \alpha(\rho_{R,L} - \rho_{L,L}) + (1 - \alpha)(\rho_{R,R} - \rho_{L,R})\\ &= \alpha\,\langle\sigma_z\rangle^{L} + (1 - \alpha)\,\langle\sigma_z\rangle^{R}\\ &(= (1 - 2\,\alpha)\,\langle\sigma_z\rangle^{R})\,.\end{aligned} \tag{A.1.2}$$

The upper index in $\langle\cdot\rangle^{R,L}$ means that $\langle\sigma_z(t = 0)\rangle$ starts either in R or L.

A.1.2 Two spins

Now, assume that we prepare spin σ at $t = 0$ to a fraction α in $|L\rangle$ and $1 - \alpha$ in $|R\rangle$. Similarly, the second spin, τ, is prepared to a fraction δ in $|L\rangle$ and $1 - \delta$ in $|R\rangle$. Then we have $\langle\sigma_z(t = 0)\rangle = \alpha\,|L\rangle + (1 - \alpha)\,|R\rangle$ and $\langle\tau_z(t = 0)\rangle = \delta\,|L\rangle + (1 - \delta)\,|R\rangle$, with $0 \leq \alpha, \delta \leq 1$ at $t = 0$. It follows

$$\begin{aligned}\rho_{R,R;\alpha\,\delta} &= \alpha\,\delta\,\rho_{RR,LL} + \alpha(1 - \delta)\,\rho_{RR,LR}\\ &\quad + (1 - \alpha)\,\delta\,\rho_{RR,RL} + (1 - \alpha)(1 - \delta)\,\rho_{RR,RR}\,,\\ \rho_{R,L;\alpha\,\delta} &= \alpha\,\delta\,\rho_{RL,LL} + \alpha(1 - \delta)\,\rho_{RL,LR}\\ &\quad + (1 - \alpha)\,\delta\,\rho_{RL,RL} + (1 - \alpha)(1 - \delta)\,\rho_{RL,RR}\,,\\ \rho_{L,R;\alpha\,\delta} &= \alpha\,\delta\,\rho_{LR,LL} + \alpha(1 - \delta)\,\rho_{LR,LR}\\ &\quad + (1 - \alpha)\,\delta\,\rho_{LR,RL} + (1 - \alpha)(1 - \delta)\,\rho_{LR,RR}\,,\\ \rho_{L,L;\alpha\,\delta} &= \alpha\,\delta\,\rho_{LL,LL} + \alpha(1 - \delta)\,\rho_{LL,LR}\\ &\quad + (1 - \alpha)\,\delta\,\rho_{LL,RL} + (1 - \alpha)(1 - \delta)\,\rho_{LL,RR}\,.\end{aligned} \tag{A.1.3}$$

Summing these equations gives 1 or $1/\lambda$, respectively. Labeling the four equations in (A.1.3) with (1) – (4), we can show the relations

$$\begin{aligned}
&(1)+(2)-(3)-(4) = \alpha\,\langle\sigma_z\rangle^L + (1-\alpha)\,\langle\sigma_z\rangle^R\,,\\
&(1)-(2)+(3)-(4) = \delta\,\langle\tau_z\rangle^L + (1-\delta)\,\langle\tau_z\rangle^R\,,\\
&(1)-(2)-(3)+(4) = (1-\alpha-\delta+2\,\alpha\,\delta)\,\langle\sigma_z\tau_z\rangle_R^R + (\alpha+\delta-2\,\alpha\,\delta)\,\langle\sigma_z\tau_z\rangle_R^L\,.
\end{aligned} \tag{A.1.4}$$

The lower index in $\langle\cdot\rangle_{R,L}$ means that $\langle\tau_z(t=0)\rangle$ starts either in $|R\rangle$ or $|L\rangle$.
Eq. (A.1.4) can be understood if we look at the corresponding expressions for $\langle\sigma_z\rangle$, $\langle\tau_z\rangle$, and $\langle\sigma_z\tau_z\rangle$. $\langle\sigma_z\rangle^R$ reads

$$\langle\sigma_z\rangle^R = \sum_{X,Y=R,L} \rho_{RX,RY} \;-\; \sum_{X,Y=R,L} \rho_{LX,RY}\,, \tag{A.1.5}$$

where we have to sum over all possibilities of the spin τ,

$$\begin{aligned}
\langle\sigma_z\rangle^R = {}& \rho_{RR,RR} + \rho_{RL,RR} + \rho_{RR,RL} + \rho_{RL,RL}\\
&- \rho_{LR,RR} - \rho_{LL,RR} - \rho_{LR,RL} - \rho_{LL,RL}\,.
\end{aligned} \tag{A.1.6}$$

This can be written as

$$\langle\sigma_z\rangle^R = \langle\sigma_z\rangle_R^R + \langle\sigma_z\rangle_L^R = 2\,\langle\sigma_z\rangle_R^R = 2\,\langle\sigma_z\rangle_L^R\,. \tag{A.1.7}$$

Further, we obtain

$$\begin{aligned}
\langle\sigma_z\rangle^L &= \sum_{X,Y=R,L} \rho_{RX,LY} \;-\; \sum_{X,Y=R,L} \rho_{LX,LY}\,,\\
\langle\tau_z\rangle^R &= \sum_{X,Y=R,L} \rho_{XR,YR} \;-\; \sum_{X,Y=R,L} \rho_{XL,YR}\,,\\
\langle\tau_z\rangle^L &= \sum_{X,Y=R,L} \rho_{XR,YL} \;-\; \sum_{X,Y=R,L} \rho_{XL,YL}\,.
\end{aligned} \tag{A.1.8}$$

$\langle\sigma_z\tau_z\rangle$ is given by

$$(\rho^\sigma_{R,X} - \rho^\sigma_{L,X})(\rho^\tau_{R,Y} - \rho^\tau_{L,Y})\,, \tag{A.1.9}$$

where X and Y stand for R and L and we have to take all possibilities. To give an example, $\langle\sigma_z\tau_z\rangle_R^R$ reads

$$\begin{aligned}
\langle\sigma_z\tau_z\rangle_R^R &= (\rho^\sigma_{R,R} - \rho^\sigma_{L,R})(\rho^\tau_{R,R} - \rho^\tau_{L,R})\\
&= \rho_{RR,RR} + \rho_{LL,RR} - \rho_{LR,RR} - \rho_{RL,RR}\,.
\end{aligned} \tag{A.1.10}$$

Now, we can express $\rho_{R,R;\alpha\,\delta}$, $\rho_{R,L;\alpha\,\delta}$, $\rho_{L,R;\alpha\,\delta}$ and $\rho_{L,L;\alpha\,\delta}$ in terms of $\langle\sigma_z\rangle$, $\langle\tau_z\rangle$ and $\langle\sigma_z\tau_z\rangle$. Using $\langle\sigma_z\rangle^R = -\langle\sigma_z\rangle^L$, $\langle\tau_z\rangle_R = -\langle\tau_z\rangle_L$, and $\langle\sigma_z\tau_z\rangle_R^R = -\langle\sigma_z\tau_z\rangle_L^R$, we get

$$\begin{aligned}
\rho_{R,R;\alpha\,\delta} &= \frac{1}{4}\Big[1 + (1-2\,\alpha)\langle\sigma_z\rangle^R + (1-2\,\delta)\langle\tau_z\rangle_R + (1-2\,\alpha)(1-2\,\delta)\langle\sigma_z\tau_z\rangle_R^R\Big]\,,\\
\rho_{R,L;\alpha\,\delta} &= \frac{1}{4}\Big[1 + (1-2\,\alpha)\langle\sigma_z\rangle^R - (1-2\,\delta)\langle\tau_z\rangle_R - (1-2\,\alpha)(1-2\,\delta)\langle\sigma_z\tau_z\rangle_R^R\Big]\,,\\
\rho_{L,R;\alpha\,\delta} &= \frac{1}{4}\Big[1 - (1-2\,\alpha)\langle\sigma_z\rangle^R + (1-2\,\delta)\langle\tau_z\rangle_R - (1-2\,\alpha)(1-2\,\delta)\langle\sigma_z\tau_z\rangle_R^R\Big]\,,\\
\rho_{L,L;\alpha\,\delta} &= \frac{1}{4}\Big[1 - (1-2\,\alpha)\langle\sigma_z\rangle^R - (1-2\,\delta)\langle\tau_z\rangle_R + (1-2\,\alpha)(1-2\,\delta)\langle\sigma_z\tau_z\rangle_R^R\Big]\,.
\end{aligned} \tag{A.1.11}$$

A.2 General form of equations of motion

The equations of motion are obtained by calculating the time evolution of all relevant operators. The time evolution in the Heisenberg picture reads

$$\frac{\mathrm{d}}{\mathrm{d}\,t}A(t) = \mathrm{i}\,\mathrm{e}^{\mathrm{i}\,H\,t}\,[H,A]\,\mathrm{e}^{-\mathrm{i}\,H\,t}\;, \tag{A.2.1}$$

where $[H,A]$ is the usual commutator. Therefore, the full set of coupled equations reads in Laplace space

$$\begin{array}{rlcrlrlrlrlrl}
\lambda & \langle\sigma_z\rangle & = & -\Delta_1 & \langle\sigma_y\rangle & -v_x & \langle\sigma_y\tau_x\rangle & +v_y & \langle\sigma_x\tau_y\rangle & + & \langle\sigma_z^0\rangle & & \\
\lambda_1 & \langle\sigma_y\rangle & = & \Delta_1 & \langle\sigma_z\rangle & -\epsilon_1 & \langle\sigma_x\rangle & +v_x & \langle\sigma_z\tau_x\rangle & -v_z & \langle\sigma_x\tau_z\rangle & & \\
\lambda_1 & \langle\sigma_x\rangle & = & \epsilon_1 & \langle\sigma_y\rangle & -v_y & \langle\sigma_z\tau_y\rangle & +v_z & \langle\sigma_y\tau_z\rangle & & & & \\
\lambda & \langle\tau_z\rangle & = & -\Delta_2 & \langle\tau_y\rangle & -v_x & \langle\sigma_x\tau_y\rangle & +v_y & \langle\sigma_y\tau_x\rangle & + & \langle\tau_z^0\rangle & & \\
\lambda_2 & \langle\tau_y\rangle & = & \Delta_2 & \langle\tau_z\rangle & -\epsilon_2 & \langle\tau_x\rangle & +v_x & \langle\sigma_x\tau_z\rangle & -v_z & \langle\sigma_z\tau_x\rangle & & \\
\lambda_2 & \langle\tau_x\rangle & = & \epsilon_2 & \langle\tau_y\rangle & -v_y & \langle\sigma_y\tau_z\rangle & +v_z & \langle\sigma_z\tau_y\rangle & & & & \\
\lambda_{12} & \langle\sigma_x\tau_y\rangle & = & \Delta_2 & \langle\sigma_x\tau_z\rangle & +\epsilon_1 & \langle\sigma_y\tau_y\rangle & -\epsilon_2 & \langle\sigma_x\tau_x\rangle & +v_x & \langle\tau_z\rangle & -v_y & \langle\sigma_z\rangle \\
\lambda_{12} & \langle\sigma_y\tau_x\rangle & = & \Delta_1 & \langle\sigma_z\tau_x\rangle & -\epsilon_1 & \langle\sigma_x\tau_x\rangle & +\epsilon_2 & \langle\sigma_y\tau_y\rangle & +v_x & \langle\sigma_z\rangle & -v_y & \langle\tau_z\rangle \\
\lambda_2 & \langle\sigma_z\tau_y\rangle & = & -\Delta_1 & \langle\sigma_y\tau_y\rangle & +\Delta_2 & \langle\sigma_z\tau_z\rangle & -\epsilon_2 & \langle\sigma_z\tau_x\rangle & +v_y & \langle\sigma_x\rangle & -v_z & \langle\tau_x\rangle \\
\lambda_1 & \langle\sigma_y\tau_z\rangle & = & \Delta_1 & \langle\sigma_z\tau_z\rangle & -\Delta_2 & \langle\sigma_y\tau_y\rangle & -\epsilon_1 & \langle\sigma_x\tau_z\rangle & +v_y & \langle\tau_x\rangle & -v_z & \langle\sigma_x\rangle \\
\lambda_1 & \langle\sigma_x\tau_z\rangle & = & -\Delta_2 & \langle\sigma_x\tau_y\rangle & +\epsilon_1 & \langle\sigma_y\tau_z\rangle & -v_x & \langle\tau_y\rangle & +v_z & \langle\sigma_y\rangle & & \\
\lambda_2 & \langle\sigma_z\tau_x\rangle & = & -\Delta_1 & \langle\sigma_y\tau_x\rangle & +\epsilon_2 & \langle\sigma_z\tau_y\rangle & -v_x & \langle\sigma_y\rangle & +v_z & \langle\tau_y\rangle & & \\
\lambda_{12} & \langle\sigma_y\tau_y\rangle & = & \Delta_1 & \langle\sigma_z\tau_y\rangle & +\Delta_2 & \langle\sigma_y\tau_z\rangle & -\epsilon_1 & \langle\sigma_x\tau_y\rangle & -\epsilon_2 & \langle\sigma_y\tau_x\rangle & & \\
\lambda_{12} & \langle\sigma_x\tau_x\rangle & = & \epsilon_1 & \langle\sigma_y\tau_x\rangle & +\epsilon_2 & \langle\sigma_x\tau_y\rangle & & & & & & \\
\lambda & \langle\sigma_z\tau_z\rangle & = & -\Delta_1 & \langle\sigma_y\tau_z\rangle & -\Delta_2 & \langle\sigma_z\tau_y\rangle & + & \langle\sigma_z\tau_z^0\rangle\;. & & & &
\end{array} \tag{A.2.2}$$

We have used ($\zeta = 1, 2$)

$$\lambda_\zeta = \lambda + \vartheta_\zeta\;, \quad \text{and} \quad \lambda_{12} = \lambda + \vartheta_1 + \vartheta_2\;. \tag{A.2.3}$$

The superscript in, e.g., $\langle\sigma_z\tau_z^0\rangle \equiv \langle\sigma_z\tau_z(t=0)\rangle$ denotes the corresponding initial state at $t = 0$.

To include influence phase factors it is convenient to rewrite the coupled equations of motion in terms of the density matrix states. Labeling these states as

$$\rho = \begin{pmatrix} s_1 & s_3 & s_5 & s_7 \\ s_2 & s_4 & s_6 & s_8 \\ s_9 & s_{11} & s_{13} & s_{15} \\ s_{10} & s_{12} & s_{14} & s_{16} \end{pmatrix} \tag{A.2.4}$$

and using the normalization $s_{16} = 1/\lambda - s_1 - s_4 - s_{13}$, we obtain for the coupled equations

of motion (cf. (3.1.14) – (3.1.17), we set $v_x = 0$)

$$\begin{aligned}
&\lambda s_1 - \frac{\mathrm{i}}{2}\left[(s_7 - s_{10})\, v_y + (s_9 - s_5)\,\Delta_1 + (s_2 - s_3)\,\Delta_2 - \mathrm{i}\right] = 0\,, \\
&\lambda s_4 + \frac{\mathrm{i}}{2}\left[(s_6 - s_{11})\, v_y + (s_8 - s_{12})\,\Delta_1 + (s_2 - s_3)\,\Delta_2 + \mathrm{i}\right] = 0\,, \\
&\lambda s_{13} - \frac{\mathrm{i}}{2}\left[(s_6 - s_{11})\, v_y + (s_5 - s_9)\,\Delta_1 + (s_{14} - s_{15})\,\Delta_2 - \mathrm{i}\right] = 0\,,
\end{aligned} \tag{A.2.5}$$

and

$$\begin{aligned}
&s_2\left[\mathrm{i}\,(v_z + \epsilon_2) + \lambda_2\right] - \frac{\mathrm{i}}{2}\left[(s_{10} - s_6)\,\Delta_1 + (s_8 v_y - s_4\Delta_2)\, I_2^- + (s_9 v_y + s_1\Delta_2)\, I_2^+\right] = 0\,, \\
&s_3\left[\mathrm{i}(v_z + \epsilon_2) - \lambda_2\right] - \frac{\mathrm{i}}{2}\left[(s_7 - s_{11})\,\Delta_1 + (s_5 v_y + s_1\Delta_2)\, I_2^- + (s_{12} v_y - s_4\Delta_2)\, I_2^+\right] = 0\,, \\
&s_5\left[\mathrm{i}(v_z + \epsilon_1) - \lambda_1\right] - \frac{\mathrm{i}}{2}\left[(s_7 - s_6)\,\Delta_2 + (s_3 v_y + s_1\Delta_1)\, I_1^- + (s_{14} v_y - s_{13}\Delta_1)\, I_1^+\right] = 0\,, \\
&s_6\left[\mathrm{i}(\epsilon_2 - \epsilon_1) + \lambda_{12}\right] + \frac{\mathrm{i}}{2}\big[\left(s_2 I_1^- - s_{14} I_1^+\right)\Delta_1 + \left(s_8 I_2^- - s_5 I_2^+\right)\Delta_2 \\
&\qquad\qquad + \left(s_4 I_{12}^- - s_{13} I_{12}^+\right) v_y\big] = 0\,, \\
&s_7\left[\mathrm{i}\,(\epsilon_1 + \epsilon_2) - \lambda_{12}\right] + \frac{\mathrm{i}}{2}\big[\left(s_{15} I_1^+ - s_3 I_1^-\right)\Delta_1 + \left(s_8 I_2^+ - s_5 I_2^-\right)\Delta_2 \\
&\qquad\qquad + \left(s_1 I_{12}^- - s_{16} I_{12}^+\right) v_y\big] = 0\,, \\
&s_8\left[\mathrm{i}\,(\epsilon_1 - v_z) - \lambda_1\right] + \frac{\mathrm{i}}{2}\left[(s_7 - s_6)\,\Delta_2 + (s_2 v_y - s_4\Delta_1)\, I_1^- + (s_{15} v_y + s_{16}\Delta_1)\, I_1^+\right] = 0\,, \\
&s_9\left[\mathrm{i}\,(v_z + \epsilon_1) + \lambda_1\right] - \frac{\mathrm{i}}{2}\left[(s_{10} - s_{11})\,\Delta_2 + (s_{15} v_y - s_{13}\Delta_1)\, I_1^- + (s_2 v_y + s_1\Delta_1)\, I_1^+\right] = 0\,, \\
&s_{10}\left[\mathrm{i}\,(\epsilon_1 + \epsilon_2) + \lambda_{12}\right] + \frac{\mathrm{i}}{2}\big[\left(s_{14} I_1^- - s_2 I_1^+\right)\Delta_1 + \left(s_{12} I_2^- - s_9 I_2^+\right)\Delta_2 \\
&\qquad\qquad + \left(s_1 I_{12}^+ - s_{16} I_{12}^-\right) v_y\big] = 0\,, \\
&s_{11}\left[\mathrm{i}(\epsilon_2 - \epsilon_1) - \lambda_{12}\right] + \frac{\mathrm{i}}{2}\big[\left(s_3 I_1^+ - s_{15} I_1^-\right)\Delta_1 + \left(s_{12} I_2^+ - s_9 I_2^-\right)\Delta_2 \\
&\qquad\qquad + \left(s_4 I_{12}^+ - s_{13} I_{12}^-\right) v_y\big] = 0\,, \\
&s_{12}\left[\mathrm{i}(\epsilon_1 - v_z) + \lambda_1\right] + \frac{\mathrm{i}}{2}\left[(s_{10} - s_{11})\,\Delta_2 + (s_{14} v_y + s_{16}\Delta_1)\, I_1^- + (s_3 v_y - s_4\Delta_1)\, I_1^+\right] = 0\,, \\
&s_{14}\left[\mathrm{i}(\epsilon_2 - v_z) + \lambda_2\right] + \frac{\mathrm{i}}{2}\left[(s_{10} - s_6)\,\Delta_1 + (s_{12} v_y + s_{16}\Delta_2)\, I_2^- + (s_5 v_y - s_{13}\Delta_2)\, I_2^+\right] = 0\,, \\
&s_{15}\left[\mathrm{i}\,(\epsilon_2 - v_z) - \lambda_2\right] + \frac{\mathrm{i}}{2}\left[(s_7 - s_{11})\,\Delta_1 + (s_9 v_y - s_{13}\Delta_2)\, I_2^- + (s_8 v_y + s_{16}\Delta_2)\, I_2^+\right] = 0\,.
\end{aligned} \tag{A.2.6}$$

Here, the system was prepared in $\langle\sigma_z^0\rangle = \langle\tau_z^0\rangle = \langle\sigma_z\tau_z^0\rangle = 1$ and we have introduced the influence phase factors $I_{1,2,12}^{\pm}$, which read

$$I_{1,2}^{\pm} = \exp[\pm\,\mathrm{i}\,\pi K_{1,2}] \quad \text{and} \quad I_{12}^{\pm} = \exp[\pm\,\mathrm{i}\,\pi\,(K_1 + K_2)]\,. \tag{A.2.7}$$

Again in the representation with $\langle\sigma_z\rangle$, $\langle\tau_z\rangle$, and so on, we get

$$
\begin{aligned}
&\lambda\langle\sigma_z\rangle + \Delta_1\langle\sigma_y\rangle - v_y\langle\sigma_x\tau_y\rangle = 1\\
&\lambda\langle\tau_z\rangle + \Delta_2\langle\tau_y\rangle - v_y\langle\sigma_y\tau_x\rangle = 1\\
&\lambda\langle\sigma_z\tau_z\rangle + \Delta_1\langle\sigma_y\tau_z\rangle + \Delta_2\langle\sigma_z\tau_y\rangle = 1\\
&\lambda_1\langle\sigma_x\rangle - \Delta_1\sin(\pi K_1)/\lambda - \epsilon_1\langle\sigma_y\rangle + v_y\langle\sigma_z\tau_y\rangle\cos(\pi K_1) - v_z\langle\sigma_y\tau_z\rangle = 0\,,\\
&\lambda_2\langle\tau_x\rangle - \Delta_2\sin(\pi K_2)/\lambda - \epsilon_2\langle\tau_y\rangle + v_y\langle\sigma_y\tau_z\rangle\cos(\pi K_2) - v_z\langle\sigma_z\tau_y\rangle = 0\,,\\
&\lambda_1\langle\sigma_y\rangle - \Delta_1\langle\sigma_z\rangle\cos(\pi K_1) + \epsilon_1\langle\sigma_x\rangle - v_y\langle\tau_y\rangle\sin(\pi K_1) + v_z\langle\sigma_x\tau_z\rangle = 0\,,\\
&\lambda_2\langle\tau_y\rangle - \Delta_2\langle\tau_z\rangle\cos(\pi K_2) + \epsilon_2\langle\tau_x\rangle - v_y\langle\sigma_y\rangle\sin(\pi K_2) + v_z\langle\sigma_z\tau_x\rangle = 0\,,\\
&\lambda_1\langle\sigma_x\tau_z\rangle - [\Delta_1\langle\tau_z\rangle + v_y\langle\sigma_z\tau_x\rangle]\sin(\pi K_1) + \Delta_2\langle\sigma_x\tau_y\rangle - \epsilon_1\langle\sigma_y\tau_z\rangle - v_z\langle\sigma_y\rangle = 0\,,\\
&\lambda_2\langle\sigma_z\tau_x\rangle - [\Delta_2\langle\sigma_z\rangle + v_y\langle\sigma_x\tau_z\rangle]\sin(\pi K_2) + \Delta_1\langle\sigma_y\tau_x\rangle - \epsilon_2\langle\sigma_z\tau_y\rangle - v_z\langle\tau_y\rangle = 0\,,\\
&\lambda_1\langle\sigma_y\tau_z\rangle - [\Delta_1\langle\sigma_z\tau_z\rangle + v_y\langle\tau_x\rangle]\cos(\pi K_1) + \Delta_2\langle\sigma_y\tau_y\rangle + \epsilon_1\langle\sigma_x\tau_z\rangle + v_z\langle\sigma_x\rangle = 0\,,\\
&\lambda_2\langle\sigma_z\tau_y\rangle - [\Delta_2\langle\sigma_z\tau_z\rangle + v_y\langle\sigma_x\rangle]\cos(\pi K_2) + \Delta_1\langle\sigma_y\tau_y\rangle + \epsilon_2\langle\sigma_z\tau_x\rangle + v_z\langle\tau_x\rangle = 0\,,\\
&\lambda_{12}\langle\sigma_y\tau_x\rangle - \big[\Delta_1\langle\sigma_z\tau_x\rangle\cos(\pi K_1) + \Delta_2\langle\sigma_y\rangle\sin(\pi K_2) - \epsilon_1\langle\sigma_x\tau_x\rangle + \epsilon_2\langle\sigma_y\tau_y\rangle\\
&\qquad\qquad - v_y\langle\tau_z\rangle\cos(\pi K_{12})\big] = 0,\\
&\lambda_{12}\langle\sigma_x\tau_y\rangle - \big[\Delta_1\langle\tau_y\rangle\sin(\pi K_1) + \Delta_2\langle\sigma_x\tau_z\rangle\cos(\pi K_2) + \epsilon_1\langle\sigma_y\tau_y\rangle - \epsilon_2\langle\sigma_x\tau_x\rangle\\
&\qquad\qquad - v_y\langle\sigma_z\rangle\cos(\pi K_{12})\big] = 0,\\
&\lambda_{12}\langle\sigma_x\tau_x\rangle - \big[\Delta_1\langle\tau_x\rangle\sin(\pi K_1) + \Delta_2\langle\sigma_x\rangle\sin(\pi K_2) + \epsilon_1\langle\sigma_y\tau_x\rangle + \epsilon_2\langle\sigma_x\tau_y\rangle\\
&\qquad\qquad - v_y\langle\sigma_z\tau_z\rangle\sin(\pi K_{12})\big] = 0,\\
&\lambda_{12}\langle\sigma_y\tau_y\rangle - \big[\Delta_1\langle\sigma_z\tau_y\rangle\cos(\pi K_1) + \Delta_2\langle\sigma_y\tau_z\rangle\cos(\pi K_2) - \epsilon_1\langle\sigma_x\tau_y\rangle - \epsilon_2\langle\sigma_y\tau_x\rangle\\
&\qquad\qquad + v_y\sin(\pi K_{12})/\lambda\big] = 0.
\end{aligned}
\tag{A.2.8}
$$

These are the generalized coupled equations of motion for two coupled dissipative spins in the white-noise regime including influence phase factors in all orders.

A.2.1 v_y coupling

We begin the analysis with the diagonalization of the corresponding Hamiltonian. Therefore, we need the diagonalization matrix U,

$$U = \frac{1}{2}\begin{pmatrix} \frac{\cos(\Theta_1)}{\sqrt{1+\sin(\Theta_1)}} & \sqrt{1+\sin(\Theta_1)} & \sqrt{1+\sin(\Theta_1)} & \frac{\cos(\Theta_1)}{\sqrt{1+\sin(\Theta_1)}} \\ -\frac{\cos(\Theta_2)}{\sqrt{1-\sin(\Theta_2)}} & \sqrt{1-\sin(\Theta_2)} & -\sqrt{1-\sin(\Theta_2)} & \frac{\cos(\Theta_2)}{\sqrt{1-\sin(\Theta_2)}} \\ -\frac{\cos(\Theta_2)}{\sqrt{1+\sin(\Theta_2)}} & -\sqrt{1+\sin(\Theta_2)} & \sqrt{1+\sin(\Theta_2)} & \frac{\cos(\Theta_2)}{\sqrt{1+\sin(\Theta_2)}} \\ \frac{\cos(\Theta_1)}{\sqrt{1-\sin(\Theta_1)}} & -\sqrt{1-\sin(\Theta_1)} & -\sqrt{1-\sin(\Theta_1)} & \frac{\cos(\Theta_1)}{\sqrt{1-\sin(\Theta_1)}} \end{pmatrix}, \tag{A.2.9}$$

together with the mixing angles

$$\Theta_1 = \arctan\left(\frac{v_y}{\Delta_1+\Delta_2}\right) \qquad \text{and} \qquad \Theta_2 = \arctan\left(\frac{v_y}{\Delta_1-\Delta_2}\right). \tag{A.2.10}$$

We can transform the Hamiltonian into a diagonalized form

$$\widetilde{H} = U\,H\,U^{-1} = -\frac{\Omega}{2}\,(\sigma_z \otimes \mathbb{1}) - \frac{\delta}{2}\,(\mathbb{1} \otimes \tau_z), \tag{A.2.11}$$

with

$$\begin{aligned} \Omega &= \frac{1}{2}(\Omega_+ + \Omega_-)\,, & \delta &= \frac{1}{2}(\Omega_+ - \Omega_-), \\ \Omega_+ &= \sqrt{(\Delta_1+\Delta_2)^2 + v_y^2}\,, & \Omega_- &= \sqrt{(\Delta_1-\Delta_2)^2 + v_y^2}\,. \end{aligned} \tag{A.2.12}$$

The equilibrium values are calculated to (cf. Sec. 3.1)

$$\langle\sigma_z\rangle_{\text{eq}} = \langle\tau_z\rangle_{\text{eq}} = 0 \tag{A.2.13}$$

and

$$\langle\sigma_z\tau_z\rangle_{\text{eq}} = \frac{v_y}{\delta^2-\Omega^2}\,\left[\Omega\,\tanh\left(\frac{\beta\,\delta}{2}\right) - \delta\,\tanh\left(\frac{\beta\,\Omega}{2}\right)\right]\,. \tag{A.2.14}$$

Observe that the term $\tanh\left(\frac{\beta\,\delta}{2}\right)$ is multiplied with Ω and $\tanh\left(\frac{\beta\,\Omega}{2}\right)$ with δ (cf. (3.1.12)). Thus the leading contribution for high temperature is

$$\langle\sigma_z\tau_z\rangle_{\text{eq}} \approx -\frac{1}{24}\,v_y\,\delta\,\Omega\,\beta^3 + \mathcal{O}(\beta^5)\,. \tag{A.2.15}$$

The eigenfrequencies are again in the form of (3.1.7) but with v_y instead of v_z

$$\Omega_\pm = \sqrt{(\Delta_1 \pm \Delta_2)^2 + v_y^2}\,, \quad \Omega = \frac{1}{2}(\Omega_+ + \Omega_-)\,, \quad \delta = \frac{1}{2}(\Omega_+ - \Omega_-)\,. \tag{A.2.16}$$

With the useful Vieta relations

$$\begin{aligned} \Omega_+^2 + \Omega_-^2 &= 2\,(\Delta_1^2 + \Delta_2^2 + v_y^2)\,, & \Omega_+^2\,\Omega_-^2 &= (\Delta_1^2 + \Delta_2^2 + v_y^2)^2 - 4\,\Delta_1^2\,\Delta_2^2\,, \\ \Omega^2 + \delta^2 &= \Delta_1^2 + \Delta_2^2 + v_y^2\,, & \Omega^2\,\delta^2 &= \Delta_1^2\,\Delta_2^2\,, \end{aligned} \tag{A.2.17}$$

we obtain for the undamped dynamics (cf. Sec. 3.1)

$$\langle\sigma_z(\lambda)\rangle = \frac{\lambda\,(\lambda^2+\Delta_2^2)}{(\lambda^2+\Omega^2)\,(\lambda^2+\delta^2)}\,, \qquad \langle\sigma_z\tau_z(\lambda)\rangle = \frac{\left(\lambda^2+v_y^2\right)\left(\lambda^2+v_y^2+\Delta_1^2+\Delta_2^2\right)}{\lambda\,(\lambda^2+\Omega_+^2)\,(\lambda^2+\Omega_-^2)}\,. \tag{A.2.18}$$

The kernels in the Markov limit read

$$\mathcal{K}_{\sigma_z}(\lambda) = \frac{\Delta_1^2}{\lambda+\vartheta_1} + v_y\,\frac{1}{1+\frac{1}{\lambda+\vartheta_1+\vartheta_2}\Delta_2\frac{1}{\lambda+\vartheta_1}\Delta_2}\,\frac{1}{\lambda+\vartheta_1+\vartheta_2}\,v_y \tag{A.2.19}$$

and

$$\begin{aligned}
\mathcal{K}_{\sigma_z\tau_z}(\lambda) &= \frac{N}{D}\,,\\
N &= (\lambda+\vartheta_1)\,(\lambda+\vartheta_2)\,\Delta_1^4 + (\lambda+\vartheta_2)\Big[\,(\lambda+\vartheta_1+\vartheta_2)\,v_y^2\\
&\quad + (\lambda+\vartheta_1)\left((\lambda+\vartheta_2)\,(\lambda+\vartheta_1+\vartheta_2) - 2\Delta_2^2\right)\Big]\Delta_1^2\\
&\quad + \Delta_2^2\,(\lambda+\vartheta_1)\Big[\,(\lambda+\vartheta_1+\vartheta_2)\,v_y^2\\
&\quad + (\lambda+\vartheta_2)\left(\Delta_2^2 + (\lambda+\vartheta_1)\,(\lambda+\vartheta_1+\vartheta_2)\right)\Big]\,,\\
D &= \left(v_y^2 + (\lambda+\vartheta_1)\,(\lambda+\vartheta_2)\right)\\
&\quad \times\Big[\,(\lambda+\vartheta_1+\vartheta_2)\,v_y^2 + \Delta_1^2\,(\lambda+\vartheta_1)\\
&\quad + (\lambda+\vartheta_2)\left(\Delta_2^2 + (\lambda+\vartheta_1)\,(\lambda+\vartheta_1+\vartheta_2)\right)\Big]\,.
\end{aligned} \tag{A.2.20}$$

With these kernels the form of $\langle\sigma_z(\lambda)\rangle$ and $\langle\sigma_z\tau_z(\lambda)\rangle$ is given by

$$\langle\sigma_z(\lambda)\rangle = \frac{1}{\lambda+\mathcal{K}_{\sigma_z}(\lambda)} \qquad \text{and} \qquad \langle\sigma_z\tau_z(\lambda)\rangle = \frac{1}{\lambda+\mathcal{K}_{\sigma_z\tau_z}(\lambda)}\,. \tag{A.2.21}$$

Now, we make the systematic weak damping approximation, i.e., the series expansion of the denominator of $\langle\sigma_z\rangle$ and $\langle\sigma_z\tau_z\rangle$ up to first order in the temperatures ϑ_1 and ϑ_2 and to first order in κ_Ω, κ_δ, κ_{Ω_+}, and κ_{Ω_-} around $\lambda = \pm\mathrm{i}\,\delta - \kappa_\delta$, $\lambda = \pm\mathrm{i}\,\Omega - \kappa_\Omega$, $\lambda = \pm\mathrm{i}\,\Omega_+ - \kappa_{\Omega_+}$, $\lambda = \pm\mathrm{i}\,\Omega_- - \kappa_{\Omega_-}$, and the two pure relaxation poles of $\langle\sigma_z\tau_z\rangle$, which we call κ_{01}, κ_{02}. The resulting rates for $\langle\sigma_z\rangle$ are

$$\begin{aligned}
\kappa_\Omega &= \frac{2\Omega^2-\Delta_1^2-v_y^2-\delta^2}{2\,(\Omega^2-\delta^2)}\,\vartheta_1 + \frac{\Omega^2-\Delta_1^2}{2\,(\Omega^2-\delta^2)}\,\vartheta_2\,,\\
\kappa_\delta &= \frac{\Omega^2+\Delta_1^2+v_y^2-2\delta^2}{2\,(\Omega^2-\delta^2)}\,\vartheta_1 + \frac{\Delta_1^2-\delta^2}{2\,(\Omega^2-\delta^2)}\,\vartheta_2\,.
\end{aligned} \tag{A.2.22}$$

And the rates for $\langle\sigma_z\tau_z\rangle$ are

$$\begin{aligned}
\kappa_{\Omega_+} &= \kappa_{\Omega_-} = \frac{\vartheta_1+\vartheta_2}{2}\,,\\
\kappa_{01} &= \frac{\Delta_1^2+v_y^2-\delta^2}{\Omega^2-\delta^2}\,\vartheta_1 + \frac{\Delta_2^2+v_y^2-\delta^2}{\Omega^2-\delta^2}\,\vartheta_2\,,\\
\kappa_{02} &= \frac{\Omega^2-v_y^2-\Delta_1^2}{\Omega^2-\delta^2}\,\vartheta_1 + \frac{\Omega^2-v_y^2-\Delta_2^2}{\Omega^2-\delta^2}\,\vartheta_2\,.
\end{aligned} \tag{A.2.23}$$

A.2.2 v_x coupling

There are two characteristic features for v_x coupling: first, it leads to a shift of the eigenfrequencies such that $\Omega \to \Omega \pm v_x$ and $\delta \to \delta \pm v_x$. Second, the low temperature rates are of the form $(\vartheta_1+\vartheta_2)/2$ for the rates around Ω, δ, and $\Omega_\pm$. In the following some results are given for different combinations of v_x, v_y, and v_z coupling without influence phase contributions.

A.2.2.1 Sole v_x coupling

For sole v_x coupling the eigenfrequencies of $\langle\sigma_z(\lambda)\rangle$ depend on Δ_1, while the eigenfrequencies of $\langle\tau_z(\lambda)\rangle$ depend on Δ_2. The eigenfrequencies of $\langle\sigma_z\tau_z(\lambda)\rangle$ depend on both, Δ_1 and Δ_2. We obtain without bath coupling

$$\begin{aligned}
\langle\sigma_z(\lambda)\rangle &= \frac{\lambda\,(\lambda^2+\Delta_1^2+v_x^2)}{[\lambda^2+(\Omega+v_x)^2]\,[\lambda^2+(\Omega-v_x)^2]}\,,\\
\langle\tau_z(\lambda)\rangle &= \frac{\lambda\,(\lambda^2+\Delta_2^2+v_x^2)}{[\lambda^2+(\delta+v_x)^2]\,[\lambda^2+(\delta-v_x)^2]}\,,\\
\langle\sigma_z\tau_z(\lambda)\rangle &= \frac{\lambda\,(\lambda^2+\Delta_1^2+\Delta_2^2)}{(\lambda^2+\Omega_+^2)\,(\lambda^2+\Omega_-^2)}\,,
\end{aligned} \tag{A.2.24}$$

with the expressions

$$\Omega_\pm = \Delta_1 \pm \Delta_2\,,\quad \Omega = \frac{1}{2}(\Omega_+ + \Omega_-) = \Delta_1\,,\quad \text{and}\quad \delta = \frac{1}{2}(\Omega_+ - \Omega_-) = \Delta_2\,. \tag{A.2.25}$$

The long time expectation values are

$$\langle\sigma_z\rangle_{\rm eq} = \langle\tau_z\rangle_{\rm eq} = \langle\sigma_z\tau_z\rangle_{\rm eq} = 0\,. \tag{A.2.26}$$

We can calculate the kernels in the Markov limit and get

$$\begin{aligned}
\mathcal{K}_{\sigma_z}(\lambda) &= \frac{v_x^4+((\lambda+\vartheta_1)\,(\lambda+\vartheta_2)-2\Delta_1^2)\,v_x^2+\Delta_1^2\,(\Delta_1^2+(\lambda+\vartheta_2)\,(\lambda+\vartheta_1+\vartheta_2))}{(\lambda+\vartheta_1+\vartheta_2)\,v_x^2+(\lambda+\vartheta_1)\,(\Delta_1^2+(\lambda+\vartheta_2)\,(\lambda+\vartheta_1+\vartheta_2))}\,,\\
\mathcal{K}_{\sigma_z\tau_z}(\lambda) &= \frac{\Delta_1^4+((\lambda+\vartheta_2)\,(\lambda+\vartheta_1+\vartheta_2)-2\Delta_2^2)\,\Delta_1^2+\Delta_2^2\,(\Delta_2^2+(\lambda+\vartheta_1)\,(\lambda+\vartheta_1+\vartheta_2))}{(\lambda+\vartheta_1)\,\Delta_1^2+(\lambda+\vartheta_2)\,(\Delta_2^2+(\lambda+\vartheta_1)\,(\lambda+\vartheta_1+\vartheta_2))}\,.
\end{aligned} \tag{A.2.27}$$

The kernel $\mathcal{K}_{\tau_z}(\lambda)$ for $\langle\tau_z(\lambda)\rangle$ is obtained by interchanging $1 \leftrightarrow 2$ in $\mathcal{K}_{\sigma_z}(\lambda)$. With these kernels the form of $\langle\sigma_z(\lambda)\rangle$, $\langle\tau_z(\lambda)\rangle$, and $\langle\sigma_z\tau_z(\lambda)\rangle$ is given in the usual way

$$\langle\sigma_z(\lambda)\rangle = \frac{1}{\lambda + \mathcal{K}_{\sigma_z}(\lambda)}\,, \quad \langle\tau_z(\lambda)\rangle = \frac{1}{\lambda + \mathcal{K}_{\tau_z}(\lambda)}\,, \quad \langle\sigma_z\tau_z(\lambda)\rangle = \frac{1}{\lambda + \mathcal{K}_{\sigma_z\tau_z}(\lambda)}\,. \tag{A.2.28}$$

The systematic low temperature approximation, i.e., the series expansion of the denominator of $\langle\sigma_z\rangle$ and $\langle\sigma_z\tau_z\rangle$ up to first order in the temperatures ϑ_1 and ϑ_2 and to first order in the rates$\kappa_{\Omega\pm v_x}$, $\kappa_{\delta\pm v_x}$, κ_{Ω_+}, and κ_{Ω_-} around $\lambda = \pm\mathrm{i}\,(\delta\pm v_x) - \kappa_{\delta\pm v_x}$, $\lambda = \pm\mathrm{i}\,(\Omega\pm v_x) - \kappa_{\Omega\pm v_x}$, $\lambda = \pm\mathrm{i}\,\Omega_+ - \kappa_{\Omega_+}$, and $\lambda = \pm\mathrm{i}\,\Omega_- - \kappa_{\Omega_-}$ results in

$$\kappa_{\delta\pm v_x} = \kappa_{\Omega\pm v_x} = \kappa_{\Omega_+} = \kappa_{\Omega_-} = \frac{\vartheta_1 + \vartheta_2}{2}\,. \tag{A.2.29}$$

There are no pure relaxation poles for $\langle\sigma_z\tau_z\rangle$.

A.2.2.2 v_x and v_y coupling

For simultaneous v_x and v_y coupling we obtain for the denominators of $\langle\sigma_z(\lambda)\rangle = N_{\sigma_z}/D_{\sigma_z}$ and $\langle\sigma_z\tau_z(\lambda)\rangle = N_{\sigma_z\tau_z}/D_{\sigma_z\tau_z}$ in the undamped case the expressions

$$\begin{aligned} D_{\sigma_z} &= \left(\lambda^2 + (\Omega + v_x)^{\,2}\right)\left(\lambda^2 + (\Omega - v_x)^{\,2}\right)\left(\lambda^2 + (\delta + v_x)^{\,2}\right)\left(\lambda^2 + (\delta - v_x)^{\,2}\right)\,, \\ D_{\sigma_z\tau_z} &= \lambda\left(\lambda^2 + \Omega_+^2\right)\left(\lambda^2 + \Omega_-^2\right)\,, \end{aligned} \tag{A.2.30}$$

with the frequencies

$$\begin{aligned} \Omega &= \frac{1}{2}(\Omega_+ + \Omega_-)\,, & \delta &= \frac{1}{2}(\Omega_+ - \Omega_-), \\ \Omega_+ &= \sqrt{(\Delta_1 + \Delta_2)^2 + v_y^2}\,, & \Omega_- &= \sqrt{(\Delta_1 - \Delta_2)^2 + v_y^2}\,. \end{aligned} \tag{A.2.31}$$

The numerators are

$$\begin{aligned} N_{\sigma_z} = \lambda\Big\{ & v_x^6 + 2v_y v_x^5 + \left(3\lambda^2 + v_y^2 + \Delta_1^2 - 2\Delta_2^2\right) v_x^4 + 4\lambda^2 v_y v_x^3 + 2v_x\, v_y \left(\lambda^4 - \Delta_1^2\Delta_2^2\right) \\ & + \left[3\lambda^4 + 2\left(v_y^2 + \Delta_1^2\right)\lambda^2 + \Delta_2^2\left(v_y^2 - 2\Delta_1^2 + \Delta_2^2\right)\right] v_x^2 \\ & + \left(\lambda^2 + \Delta_2^2\right)\left[\lambda^2 v_y^2 + \left(\lambda^2 + \Delta_1^2\right)\left(\lambda^2 + \Delta_2^2\right)\right] \Big\}\,, \\ N_{\sigma_z\tau_z} = {} & \left(\lambda^2 + v_y^2\right)\left(\lambda^2 + v_y^2 + \Delta_1^2 + \Delta_2^2\right)\,. \end{aligned} \tag{A.2.32}$$

We obtain for the equilibrium values

$$\langle\sigma_z\rangle_{\mathrm{eq}} = \langle\tau_z\rangle_{\mathrm{eq}} = 0 \tag{A.2.33}$$

and

$$\langle\sigma_z\tau_z\rangle_{\mathrm{eq}} = \frac{\left[\sinh\left(\frac{\beta\Omega_-}{2}\right)\Omega_+ - \mathrm{e}^{\beta v_x}\sinh\left(\frac{\beta\Omega_+}{2}\right)\Omega_-\right] v_y}{\left[\cosh\left(\frac{\beta\Omega_-}{2}\right) + \mathrm{e}^{\beta v_x}\cosh\left(\frac{\beta\Omega_+}{2}\right)\right]\Omega_+\Omega_-}\,. \tag{A.2.34}$$

The leading contribution for high temperature is

$$\langle \sigma_z \tau_z \rangle_{\mathrm{eq}} \approx -\frac{v_x v_y}{4} \left(\frac{1}{T}\right)^2 + \mathcal{O}\left(\frac{1}{T}\right)^3 . \tag{A.2.35}$$

Since the results for $\langle \sigma_z(\lambda) \rangle$ and $\langle \sigma_z \tau_z(\lambda) \rangle$ with bath coupling are too long, we will not note them here. However, they can be calculated with appropriate software and the coupled equations of motion given in (A.2.2).

The low temperature approximation yields for the rates (cf. Eq. (A.2.29))

$$\begin{aligned} \kappa_{\Omega \pm v_x} = \kappa_{\delta \pm v_x} = \kappa_{\Omega_+} = \kappa_{\Omega_-} &= \frac{\vartheta_1 + \vartheta_2}{2} , \\ \kappa_{01} &= \frac{\Delta_1^2 + v_y^2 - \delta^2}{\Omega^2 - \delta^2} \vartheta_1 + \frac{\Delta_2^2 + v_y^2 - \delta^2}{\Omega^2 - \delta^2} \vartheta_2 , \\ \kappa_{02} &= \frac{\Omega^2 - v_y^2 - \Delta_1^2}{\Omega^2 - \delta^2} \vartheta_1 + \frac{\Omega^2 - v_y^2 - \Delta_2^2}{\Omega^2 - \delta^2} \vartheta_2 , \end{aligned} \tag{A.2.36}$$

where κ_{01} and κ_{02} are the two pure relaxation poles of $\langle \sigma_z \tau_z \rangle$.

A.2.2.3 v_x and v_z coupling

In the case of v_x and v_z coupling we obtain in the undamped case for the denominators of $\langle \sigma_z(\lambda) \rangle = N_{\sigma_z}/D_{\sigma_z}$ and $\langle \sigma_z \tau_z(\lambda) \rangle = N_{\sigma_z \tau_z}/D_{\sigma_z \tau_z}$ the expressions

$$\begin{aligned} D_{\sigma_z} &= \left(\lambda^2 + (\Omega + v_x)^2\right) \left(\lambda^2 + (\Omega - v_x)^2\right) \left(\lambda^2 + (\delta + v_x)^2\right) \left(\lambda^2 + (\delta - v_x)^2\right) , \\ D_{\sigma_z \tau_z} &= \lambda \left(\lambda^2 + \Omega_+^2\right) \left(\lambda^2 + \Omega_-^2\right) , \end{aligned} \tag{A.2.37}$$

with the expressions

$$\begin{aligned} \Omega &= \frac{1}{2}(\Omega_+ + \Omega_-) , & \delta &= \frac{1}{2}(\Omega_+ - \Omega_-), \\ \Omega_+ &= \sqrt{(\Delta_1 + \Delta_2)^2 + v_z^2} , & \Omega_- &= \sqrt{(\Delta_1 - \Delta_2)^2 + v_z^2} . \end{aligned} \tag{A.2.38}$$

We obtain for the numerators

$$\begin{aligned} N_{\sigma_z} = \lambda \Big\{ & v_x^6 + \left(3\lambda^2 - 2v_z^2 + \Delta_1^2 - 2\Delta_2^2\right) v_x^4 - 2v_z \Delta_1 \Delta_2 \left(2\lambda^2 + v_z^2 + \Delta_1^2 + \Delta_2^2\right) v_x \\ & + \left[3\lambda^4 + v_z^4 + \Delta_2^4 + 2\Delta_1^2 \left(\lambda^2 - \Delta_2^2\right) + v_z^2 \left(\Delta_1^2 + 2\Delta_2^2\right)\right] v_x^2 \\ & + \left(\lambda^2 + v_z^2 + \Delta_2^2\right) \left[\lambda^2 v_z^2 + \left(\lambda^2 + \Delta_1^2\right) \left(\lambda^2 + \Delta_2^2\right)\right] + 4 v_z \Delta_1 \Delta_2 v_x^3 \Big\} , \\ N_{\sigma_z \tau_z} = & \left(\lambda^2 + v_z^2\right) \left(\lambda^2 + v_z^2 + \Delta_1^2 + \Delta_2^2\right) . \end{aligned} \tag{A.2.39}$$

The equilibrium values are given by

$$\langle \sigma_z \rangle_{\mathrm{eq}} = \langle \tau_z \rangle_{\mathrm{eq}} = 0 \tag{A.2.40}$$

and

$$\langle\sigma_z\tau_z\rangle_{\rm eq} = \frac{\left[{\rm e}^{\beta v_x}\sinh\left(\frac{\beta\Omega_+}{2}\right)\Omega_- + \sinh\left(\frac{\beta\Omega_-}{2}\right)\Omega_+\right]v_z}{\left[\cosh\left(\frac{\beta\Omega_-}{2}\right) + {\rm e}^{\beta v_x}\cosh\left(\frac{\beta\Omega_+}{2}\right)\right]\Omega_-\Omega_+}\,. \tag{A.2.41}$$

For high temperature the leading contribution is given by

$$\langle\sigma_z\tau_z\rangle_{\rm eq} \approx \frac{v_z}{2\,T} + \mathcal{O}\left(\frac{1}{T}\right)^3\,. \tag{A.2.42}$$

The full expressions for $\langle\sigma_z(\lambda)\rangle$ and $\langle\sigma_z\tau_z(\lambda)\rangle$ with bath coupling are too long to be noted here. However, they are computable with appropriate software and by using the coupled equations of motion from (A.2.2).

The systematic weak damping approximation yields for the rates

$$\begin{aligned}
\kappa_{\Omega\pm v_x} = \kappa_{\delta\pm v_x} = \kappa_{\Omega_+} = \kappa_{\Omega_-} &= \frac{\vartheta_1+\vartheta_2}{2}\,,\\
\kappa_{01} &= \frac{\Delta_1^2-\delta^2}{\Omega^2-\delta^2}\,\vartheta_1 + \frac{\Delta_2^2-\delta^2}{\Omega^2-\delta^2}\,\vartheta_2\,,\\
\kappa_{02} &= \frac{\Omega^2-\Delta_1^2}{\Omega^2-\delta^2}\,\vartheta_1 + \frac{\Omega^2-\Delta_2^2}{\Omega^2-\delta^2}\,\vartheta_2\,.
\end{aligned} \tag{A.2.43}$$

A.2.2.4 v_x, v_y, and v_z coupling

Finally, if all coupling types are present, i.e., v_x, v_y, and v_z, we get for vanishing bath coupling for the denominators of $\langle\sigma_z(\lambda)\rangle = N_{\sigma_z}/D_{\sigma_z}$ and $\langle\sigma_z\tau_z(\lambda)\rangle = N_{\sigma_z\tau_z}/D_{\sigma_z\tau_z}$ the results

$$\begin{aligned}
D_{\sigma_z} &= \left(\lambda^2+(\Omega+v_x)^{\,2}\right)\left(\lambda^2+(\Omega-v_x)^{\,2}\right)\left(\lambda^2+(\delta+v_x)^{\,2}\right)\left(\lambda^2+(\delta-v_x)^{\,2}\right)\,,\\
D_{\sigma_z\tau_z} &= \lambda^2\left(\lambda^2+\Omega_+^2\right)\left(\lambda^2+\Omega_-^2\right)\,,
\end{aligned} \tag{A.2.44}$$

with the frequencies

$$\begin{aligned}
\Omega &= \frac{1}{2}(\Omega_+ + \Omega_-)\,, & \delta &= \frac{1}{2}(\Omega_+ - \Omega_-),\\
\Omega_+ &= \sqrt{(\Delta_1+\Delta_2)^2+(v_y-v_z)^2}\,, & \Omega_- &= \sqrt{(\Delta_1-\Delta_2)^2+(v_y+v_z)^2}\,.
\end{aligned} \tag{A.2.45}$$

The numerators are given by

$$\begin{aligned}
N_{\sigma_z} = \lambda\Big\{ & v_x^6 + \left(3\lambda^2+v_y^2-2v_z^2+\Delta_1^2-2\Delta_2^2\right)v_x^4 + \left[3\lambda^4+2\Delta_1^2\lambda^2+v_z^4+\Delta_2^4-2\Delta_1^2\Delta_2^2\right.\\
&+ 6v_yv_z\Delta_1\Delta_2 + v_y^2\left(2\lambda^2-2v_z^2+\Delta_2^2\right)+v_z^2\left(\Delta_1^2+2\Delta_2^2\right)\Big]v_x^2 + \left(\lambda^2+v_z^2+\Delta_2^2\right)\\
&\times\left[\left(\lambda^2+v_z^2+\Delta_2^2\right)\lambda^2 + v_y^2\left(\lambda^2+v_z^2\right) - 2v_yv_z\Delta_1\Delta_2 + \Delta_1^2\left(\lambda^2+\Delta_2^2\right)\right]\Big\}\,,\\
N_{\sigma_z\tau_z} = {} & \lambda v_y^4 + \left[\lambda\Delta_1^2 - 2\lambda v_z^2 + \lambda\left(2\lambda^2+\Delta_2^2\right)\right]v_y^2 + 4\lambda v_z\Delta_1\Delta_2 v_y + \lambda v_z^4\\
&+ v_z^2\left[\lambda\Delta_2^2+\lambda\left(2\lambda^2+\Delta_1^2\right)\right] + \lambda^2\left[\lambda\Delta_1^2+\lambda\left(\lambda^2+\Delta_2^2\right)\right]\,.
\end{aligned}$$

(A.2.46)

We get for the long time expectation values $\langle\sigma_z\rangle_{\rm eq} = \langle\tau_z\rangle_{\rm eq} = 0$ and

$$\begin{aligned}\langle\sigma_z\tau_z\rangle_{\rm eq} = {\rm e}^{\frac{\beta\Omega_+}{2}} \Big[{\rm e}^{\frac{1}{2}\beta(\Omega_- - \Omega_+ + 2v_x)}\,\Omega_-\,(v_y - v_z) - {\rm e}^{\frac{1}{2}\beta(\Omega_- + \Omega_+ + 2v_x)}\,\Omega_-\,(v_y - v_z) \\ + {\rm e}^{\beta\Omega_-}\,\Omega_+\,(v_y + v_z) - \Omega_+\,(v_y + v_z)\Big] \\ \Big/ \left({\rm e}^{\frac{\beta\Omega_+}{2}}\left(1 + {\rm e}^{\beta\Omega_-}\right) + {\rm e}^{\frac{\beta\Omega_-}{2} + \beta v_x} + {\rm e}^{\frac{\beta\Omega_-}{2} + \beta\Omega_+ + \beta v_x}\right)\Omega_-\Omega_+ \,.\end{aligned} \tag{A.2.47}$$

Then, the leading contribution for high temperature is

$$\langle\sigma_z\tau_z\rangle_{\rm eq} \approx \frac{v_z}{2\,T} - \frac{v_x v_y}{4}\left(\frac{1}{T}\right)^2 + \mathcal{O}\left(\frac{1}{T}\right)^3 \,. \tag{A.2.48}$$

The corresponding expressions for $\langle\sigma_z(\lambda)\rangle$ and $\langle\sigma_z\tau_z(\lambda)\rangle$ with coupling to the baths are too long and will not note them here. Anyhow, they can be calculated with the coupled equations of motion in (A.2.2).
We obtain for the rates within the low temperature approximation the results

$$\begin{aligned}\kappa_{\Omega\pm v_x} = \kappa_{\delta\pm v_x} = \kappa_{\Omega_+} = \kappa_{\Omega_-} &= \frac{\vartheta_1 + \vartheta_2}{2}\,, \\ \kappa_{01} &= \frac{\Delta_1^2 + v_y^2 - \delta^2}{\Omega^2 - \delta^2}\,\vartheta_1 + \frac{\Delta_2^2 + v_y^2 - \delta^2}{\Omega^2 - \delta^2}\,\vartheta_2\,, \\ \kappa_{02} &= \frac{\Omega^2 - v_y^2 - \Delta_1^2}{\Omega^2 - \delta^2}\,\vartheta_1 + \frac{\Omega^2 - v_y^2 - \Delta_2^2}{\Omega^2 - \delta^2}\,\vartheta_2\,.\end{aligned} \tag{A.2.49}$$

A.2.3 v_y and v_z coupling and bias ϵ_1

The denominator of $\langle\sigma_z(\lambda)\rangle = N_{\sigma_z}/D_{\sigma_z}$ and $\langle\sigma_z\tau_z(\lambda)\rangle = N_{\sigma_z\tau_z}/D_{\sigma_z\tau_z}$ is a polynomial of degree nine in λ and is composed of

$$D_{\sigma_z} = D_{\sigma_z\tau_z} = \lambda(\lambda^2 + \Omega^2)(\lambda^2 + \delta^2)(\lambda^2 + \Omega_+^2)(\lambda^2 + \Omega_-^2)\,, \tag{A.2.50}$$

i.e., the bias ϵ_1 mixes the eigenfrequencies of both spins. The denominator of $\langle\tau_z(\lambda)\rangle = N_{\tau_z}/D_{\tau_z}$ keeps the same form as without bias

$$D_{\tau_z} = \lambda(\lambda^2 + \Omega^2)(\lambda^2 + \delta^2)\,. \tag{A.2.51}$$

The eigenfrequencies are

$$\begin{aligned}\Omega_+ &= \sqrt{\Delta_1^2 + \Delta_2^2 + v_y^2 + v_z^2 + \epsilon_1^2 + 2\Omega^{(0)}}\quad, \qquad \Omega = \frac{1}{2}(\Omega_+ + \Omega_-)\,, \\ \Omega_- &= \sqrt{\Delta_1^2 + \Delta_2^2 + v_y^2 + v_z^2 + \epsilon_1^2 - 2\Omega^{(0)}}\quad, \qquad \delta = \frac{1}{2}(\Omega_+ - \Omega_-)\,,\end{aligned} \tag{A.2.52}$$

where $\Omega^{(0)} = \sqrt{\left(v_y v_z - \Delta_1\Delta_2\right)^2 + \epsilon_1^2\left(v_z^2 + \Delta_2^2\right)}$. The numerator of $\langle\sigma_z(\lambda)\rangle$ reads

$$\begin{aligned}
&\left(\lambda^2+\epsilon_1^2\right)v_z^6 + \left[\left(2\lambda^2+\epsilon_1^2\right)\Delta_1^2 + \left(3\lambda^2+3\Delta_2^2-2\epsilon_1^2\right)\left(\lambda^2+\epsilon_1^2\right)\right]v_z^4 - 2v_y^3\Delta_1\Delta_2\epsilon_1^2 v_z + \Big[\lambda^2\Delta_1^4 \\
&+ \left(4\lambda^4+\epsilon_1^2\lambda^2+\epsilon_1^4-\Delta_2^2\epsilon_1^2\right)\Delta_1^2 + \left(\lambda^2+\epsilon_1^2\right)\left[3\lambda^4+3\Delta_2^4+\epsilon_1^4+\Delta_2^2\left(6\lambda^2-4\epsilon_1^2\right)\right]\Big]v_z^2 \\
&+ 2v_y\Delta_1\Delta_2\left[4\lambda^4+4\Delta_2^2\lambda^2-\epsilon_1^2\lambda^2-\epsilon_1^4-\Delta_1^2\epsilon_1^2+3\Delta_2^2\epsilon_1^2+v_z^2\left(4\lambda^2+3\epsilon_1^2\right)\right]v_z \\
&+ \left(\lambda^2+\Delta_2^2\right)\left(\lambda^2+\epsilon_1^2\right)\left[\Delta_1^4+2\left(\lambda^2-\Delta_2^2+\epsilon_1^2\right)\Delta_1^2+\Delta_2^4+\left(\lambda^2+\epsilon_1^2\right)^2-2\Delta_2^2\left(\epsilon_1^2-\lambda^2\right)\right] \\
&+ v_y^4\left(\left(\lambda^2+\Delta_2^2+\epsilon_1^2\right)\lambda^2+v_z^2\left(\lambda^2+\epsilon_1^2\right)\right) + v_y^2\Big[2\lambda^6+4\Delta_2^2\lambda^4+4\epsilon_1^2\lambda^4+2\Delta_2^4\lambda^2+2\epsilon_1^4\lambda^2 \\
&+ \Delta_2^2\epsilon_1^2\lambda^2+\Delta_2^2\epsilon_1^4+\Delta_2^4\epsilon_1^2-2v_z^4\left(\lambda^2+\epsilon_1^2\right)+\Delta_1^2\left(2\left(\lambda^2+\epsilon_1^2\right)\lambda^2+\Delta_2^2\left(2\lambda^2+\epsilon_1^2\right)\right) \\
&+ v_z^2\left(\left(2\lambda^2+\epsilon_1^2\right)\Delta_1^2+\epsilon_1^2\left(2\left(\lambda^2+\epsilon_1^2\right)-\Delta_2^2\right)\right)\Big],
\end{aligned} \tag{A.2.53}$$

that for $\langle\tau_z(\lambda)\rangle$ is

$$\left(\lambda^2+\Delta_1^2+\epsilon_1^2\right)\lambda^2 + v_z^2\left(\lambda^2+\epsilon_1^2\right), \tag{A.2.54}$$

and we obtain for the numerator of $\langle\sigma_z\tau_z(\lambda)\rangle$

$$\begin{aligned}
&\left(\lambda^2+v_z^2\right)v_y^6 - 2v_z\Delta_1\Delta_2 v_y^5 + \Big[3\lambda^4+\left(3\epsilon_1^2+2\left(\Delta_1^2+\Delta_2^2\right)\right)\lambda^2 - 2v_z^4 + \Delta_1^2\Delta_2^2 \\
&+ v_z^2\left(\lambda^2+\Delta_1^2+\Delta_2^2+3\epsilon_1^2\right)\Big]v_y^4 + 2v_z\Delta_1\Delta_2\left(4v_z^2-\Delta_1^2-\Delta_2^2-2\epsilon_1^2\right)v_y^3 + v_z^6\left(\lambda^2+\epsilon_1^2\right) \\
&+ \Big[3\lambda^6+2\left(3\epsilon_1^2+2\left(\Delta_1^2+\Delta_2^2\right)\right)\lambda^4+\left(\Delta_1^4+4\left(\Delta_2^2+\epsilon_1^2\right)\Delta_1^2+\Delta_2^4+3\epsilon_1^4\right)\lambda^2+v_z^6 \\
&+ v_z^4\left(\lambda^2+\Delta_1^2+\Delta_2^2-4\epsilon_1^2\right)+\Delta_1^2\Delta_2^2\left(\Delta_1^2+\Delta_2^2+\epsilon_1^2\right)+v_z^2\Big[3\lambda^4+2\epsilon_1^2\lambda^2+3\epsilon_1^4 \\
&+ \Delta_2^2\left(\lambda^2-\epsilon_1^2\right)+\Delta_1^2\left(\lambda^2-10\Delta_2^2+2\epsilon_1^2\right)\Big]\Big]v_y^2 - 2v_z\Delta_1\Delta_2\Big[v_z^4+\left(\Delta_1^2+\Delta_2^2-4\epsilon_1^2\right)v_z^2 \\
&- \left(\lambda^2+\Delta_2^2-\epsilon_1^2\right)\left(\lambda^2+\epsilon_1^2\right)+\Delta_1^2\left(-\lambda^2-2\Delta_2^2+\epsilon_1^2\right)\Big]v_y + \lambda^2\left(\lambda^2+\Delta_1^2+\epsilon_1^2\right) \\
&\times\left[\Delta_2^4+2\left(\lambda^2-\epsilon_1^2\right)\Delta_2^2+\left(\lambda^2+\epsilon_1^2\right)^2+\Delta_1^2\left(\lambda^2+\Delta_2^2+\epsilon_1^2\right)\right]+v_z^4\Big[\left(2\lambda^2+\Delta_2^2+\epsilon_1^2\right)\Delta_1^2 \\
&+ \left(3\lambda^2+2\Delta_2^2-2\epsilon_1^2\right)\left(\lambda^2+\epsilon_1^2\right)\Big]+v_z^2\Big[\left(\lambda^2+\Delta_2^2\right)\Delta_1^4 \\
&+ \left[4\lambda^4+\left(4\Delta_2^2+\epsilon_1^2\right)\lambda^2+\left(\Delta_2^2-\epsilon_1^2\right)^2\right]\Delta_1^2+\left(\lambda^2+\epsilon_1^2\right)\left(3\lambda^4+4\Delta_2^2\lambda^2+\left(\Delta_2^2-\epsilon_1^2\right)^2\right)\Big].
\end{aligned} \tag{A.2.55}$$

Then we can calculate the equilibrium values

$$\begin{aligned}
\langle\sigma_z\rangle_{\mathrm{eq}} &= \Big[\mathrm{e}^{\frac{1}{2}\beta(2\Omega_-+\Omega_+)}\,\Omega_+\left(-v_z^2-\Delta_2^2+\Omega^{(0)}\right)+\mathrm{e}^{\frac{\beta\Omega_+}{2}}\,\Omega_+\left(v_z^2+\Delta_2^2-\Omega^{(0)}\right) \\
&\quad -\mathrm{e}^{\frac{\beta\Omega_-}{2}}\,\Omega_-\left(v_z^2+\Delta_2^2+\Omega^{(0)}\right)+\mathrm{e}^{\frac{1}{2}\beta(\Omega_-+2\Omega_+)}\,\Omega_-\left(v_z^2+\Delta_2^2+\Omega^{(0)}\right)\Big]\epsilon_1 \\
&\quad /\ \left[\left(\mathrm{e}^{\frac{\beta\Omega_-}{2}}+\mathrm{e}^{\frac{\beta\Omega_+}{2}}+\mathrm{e}^{\frac{1}{2}\beta(2\Omega_-+\Omega_+)}+\mathrm{e}^{\frac{1}{2}\beta(\Omega_-+2\Omega_+)}\right)\Omega^{(0)}\Omega_-\Omega_+\right]\,, \\
\langle\tau_z\rangle_{\mathrm{eq}} &= \left(1-\frac{2\cosh\left(\beta\Omega_-/2\right)}{\cosh\left(\beta\Omega_-/2\right)+\cosh\left(\beta\Omega_+/2\right)}\right)\frac{v_z\epsilon_1}{\Omega^{(0)}}\,, \\
\langle\sigma_z\tau_z\rangle_{\mathrm{eq}} &= \mathrm{e}^{\frac{1}{2}\beta(2\Omega_-+\Omega_+)}\,\Omega_+\left(-v_zv_y^2+\Delta_1\Delta_2v_y-v_z\epsilon_1^2+\Omega^{(0)}v_z\right) \\
&\quad +\mathrm{e}^{\frac{\beta\Omega_+}{2}}\,\Omega_+\left(v_zv_y^2-\Delta_1\Delta_2v_y+v_z\epsilon_1^2-\Omega^{(0)}v_z\right) \\
&\quad -\mathrm{e}^{\frac{\beta\Omega_-}{2}}\,\Omega_-\left(v_zv_y^2-\Delta_1\Delta_2v_y+v_z\left(\epsilon_1^2+\Omega^{(0)}\right)\right) \\
&\quad +\mathrm{e}^{\frac{1}{2}\beta(\Omega_-+2\Omega_+)}\,\Omega_-\left(v_zv_y^2-\Delta_1\Delta_2v_y+v_z\left(\epsilon_1^2+\Omega^{(0)}\right)\right) \\
&\quad /\ \left[\left(\mathrm{e}^{\frac{\beta\Omega_-}{2}}+\mathrm{e}^{\frac{\beta\Omega_+}{2}}+\mathrm{e}^{\frac{1}{2}\beta(2\Omega_-+\Omega_+)}+\mathrm{e}^{\frac{1}{2}\beta(\Omega_-+2\Omega_+)}\right)\Omega^{(0)}\Omega_-\Omega_+\right]\,.
\end{aligned} \tag{A.2.56}$$

So, the leading contributions for high temperature are

$$\begin{aligned}
\langle\sigma_z\rangle_{\mathrm{eq}} &\approx \frac{\epsilon_1}{2\,T}+\mathcal{O}\left(\frac{1}{T}\right)^3\,, \\
\langle\tau_z\rangle_{\mathrm{eq}} &\approx \frac{1}{16\,T^2}\left(\Omega_+^2v_z\epsilon_1-\Omega_-^2v_z\epsilon_1\right)+\mathcal{O}\left(\frac{1}{T}\right)^4\,, \\
\langle\sigma_z\tau_z\rangle_{\mathrm{eq}} &\approx \frac{v_z}{2\,T}+\mathcal{O}\left(\frac{1}{T}\right)^3\,.
\end{aligned} \tag{A.2.57}$$

The leading contribution for $\langle\sigma_z\rangle_{\mathrm{eq}}$ is what we expect from the corresponding result of the TSS in Eq. (2.3.16).

It is not possible to note here the results with bath coupling for $\langle\sigma_z(\lambda)\rangle$ or $\langle\sigma_z\tau_z(\lambda)\rangle$ simply because they are too long. Also the dephasing and relaxation rates of the systematic weak damping approximation are too long. However, they can be calculated with appropriate software. In Fig. 3.17 are shown the rates of $\langle\sigma_z(\lambda)\rangle$ and the eigenfrequencies. We see a level crossing of the eigenfrequencies Ω and δ around $v_y\approx 0.5$ and a decrease (increase) of the corresponding rates γ_Ω (γ_δ). This is again a manifestation of the quantum frustration of decoherence, as illustrated for $\langle\sigma_z(t)\rangle$ in Fig. 3.18. Here, coherence is maintained longer around the level crossing compared to other parameters.

A.3 Propagator approach

The time dependence of the propagator reads

$$\partial_t\,k(t)=-\mathrm{i}H\,\mathrm{e}^{-\mathrm{i}\,H\,t}\,. \tag{A.3.1}$$

Then, the probability to be in the state $|RR\rangle$ at time t when we start in the state $|RR\rangle$ at time t_0 reads

$$\rho_{RR,RR}(t) = |k_{RR,RR}(t)|^2 \,. \tag{A.3.2}$$

The propagator

$$\partial_t \, k_{RR,RR}(t) = -\mathrm{i}\langle RR|H \, \mathrm{e}^{-\mathrm{i}\,H\,t}|RR\rangle \tag{A.3.3}$$

can be solved by using the completeness relation

$$\mathbb{1} = \; |RR\rangle\langle RR| + |RL\rangle\langle RL| + |LR\rangle\langle LR| + |LL\rangle\langle LL| \; . \tag{A.3.4}$$

We obtain

$$\begin{aligned} \mathrm{i}\partial_t \, k_{RR,RR}(t) = {} & \langle RR|H|RR\rangle\langle RR|\mathrm{e}^{-\mathrm{i}\,H\,t}|RR\rangle + \langle RR|H|RL\rangle\langle RL|\mathrm{e}^{-\mathrm{i}\,H\,t}|RR\rangle \\ & + \langle RR|H|LR\rangle\langle LR|\mathrm{e}^{-\mathrm{i}\,H\,t}|RR\rangle + \langle RR|H|LL\rangle\langle LL|\mathrm{e}^{-\mathrm{i}\,H\,t}|RR\rangle \,. \end{aligned} \tag{A.3.5}$$

Here $\langle RR|\mathrm{e}^{-\mathrm{i}\,H\,t}|RR\rangle$ is again $k_{RR,RR}(t)$, $\langle RL|\mathrm{e}^{-\mathrm{i}\,H\,t}|RR\rangle$ corresponds to $k_{RL,RR}(t)$, and so on. This step has to be repeated for $k_{RR,RR}(t)$, $k_{RL,RR}(t)$, $k_{LR,RR}(t)$ and $k_{LL,RR}(t)$, respectively. Taking the Laplace transform of these equations and abbreviating the propagators as $\alpha = k_{RR,RR}(\lambda)$, $\beta = k_{RL,RR}(\lambda)$, $\gamma = k_{LR,RR}(\lambda)$, $\delta = k_{LL,RR}(\lambda)$, we arrive at a set of coupled equations in Laplace space (written with bias ϵ_1, ϵ_2)

$$\begin{aligned} \mathrm{i}\,\lambda\,\alpha - \mathrm{i} &= -\frac{v}{2}\,\alpha - \frac{\Delta_2}{2}\,\beta - \frac{\Delta_1}{2}\,\gamma + \frac{\epsilon_1+\epsilon_2}{2}\,\alpha \,, \\ \mathrm{i}\,\lambda\,\beta &= -\frac{\Delta_2}{2}\,\alpha + \frac{v}{2}\,\beta - \frac{\Delta_1}{2}\,\delta + \frac{\epsilon_1-\epsilon_2}{2}\,\beta \,, \\ \mathrm{i}\,\lambda\,\gamma &= -\frac{\Delta_1}{2}\,\alpha + \frac{v}{2}\,\gamma - \frac{\Delta_2}{2}\,\delta + \frac{-\epsilon_1+\epsilon_2}{2}\,\gamma \,, \\ \mathrm{i}\,\lambda\,\delta &= -\frac{\Delta_1}{2}\,\beta - \frac{\Delta_2}{2}\,\gamma - \frac{v}{2}\,\delta - \frac{\epsilon_1+\epsilon_2}{2}\,\delta \,. \end{aligned} \tag{A.3.6}$$

A.4 Path sum derivation of Dubé and Stamp

Dubé and Stamp studied the dynamics of coupled spins in four different parameter regimes for sole v_z coupling [59]:

1. The locked phase regime ($v_z \gg T$, Δ/α)
   There is a high energy cost if a blip on one path overlaps with a sojourn on the other. The dynamics corresponds to that of a single spin-boson system with the effective frequency $\Delta_\mathrm{c} = \Delta_1\,\Delta_2\,/\,v_z$ and $\alpha_\mathrm{c} = \alpha_1 + \alpha_2 \pm 2\,\alpha_{12}$. The $\pm$ is for ferromagnetic or antiferromagnetic coupling.

2. The correlated relaxation or high T-phase regime ($T \gg \Delta/\alpha$, v_z)
   Temperature breaks the locking of the spins. For $v_z \gg \Delta_{1,2}$ blips on one path virtually always overlap with a sojourn on the other path. Interactions between blips on the same path and to blips on the other path can be neglected (cf. Fig. A.1 and A.2).

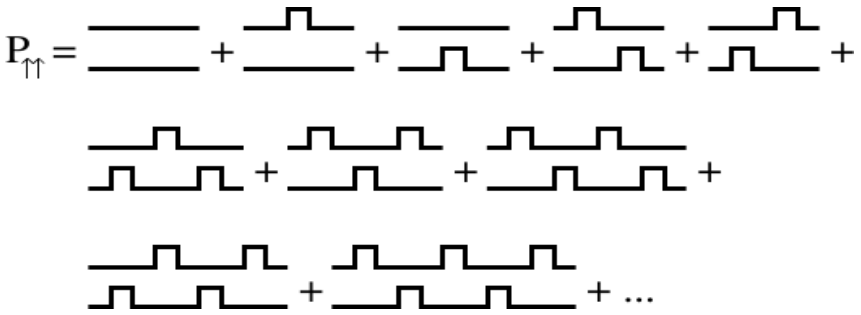

Figure A.1: NIBA analog for coupled spins.

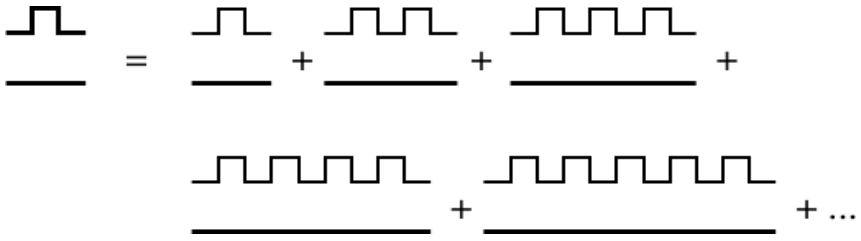

Figure A.2: NIBA analog for coupled spins of a single cluster.

3. The mutual coherence regime ($\Delta/\alpha \gg T \gg v_z$)
   Temperature breaks the locking of the spins but does not destroy coherence. For $v_z \gg \Delta_{1,2}$ the oscillation frequencies are $\propto v_z$ and the same approximations as in the correlated relaxation regime apply.

4. The perturbative regime ($v_z \ll \Delta$)
   The two spins are almost independent. The correlations can be treated perturbatively.

The inter-spin power spectrum of the coupling, which describes correlations between the two baths, reads

$$\begin{aligned} S_{12}(R,\omega) = S_{21}(R,\omega) &= \mathrm{Re}\int \mathrm{d}t\, \mathrm{e}^{-\mathrm{i}\,\omega t}\langle X(R_1,t)\, X(R_2,t)\rangle_\beta \\ &= \frac{\pi}{2}\sum_\alpha \frac{c_\alpha^{(1)}\, c_\alpha^{(2)*}}{m_\alpha\,\omega_\alpha}\, D(R,\omega_\alpha)\,\delta(\omega-\omega_\alpha)\ . \end{aligned} \tag{A.4.1}$$

$R_{1,2}$ are the positions of spin σ and τ, respectively. $D(R,\omega_\alpha) = \sum_\alpha \mathrm{e}^{\mathrm{i}\alpha R}\, D_\alpha(\omega)$ is the propagator for the bath modes. This is in general a retarded function. Retardation effects can be neglected for distances $|R| = |R_1 - R_2| \ll v_\alpha/\omega_\alpha$, where v_α is the propagation velocity of bath mode α. This leads to the limit $R \lesssim 50\mu m$ for an electronic bath and $R \lesssim 250\mu m$ for a phonon bath [59]. Below this limit, the inter-spin power spectrum is separable and adopts for an ohmic bath the form

$$S_{12}(R,\omega) = S_{21}(R,\omega) = 2\,(K_1K_2)^{1/2}\,\mathrm{e}^{-|\omega|/\omega_\mathrm{c}}\ . \tag{A.4.2}$$

Bath mediated effects induce an extra interaction term $\tilde{\epsilon}\,\sigma_z\tau_z$ to the direct interaction term $-v_z/2\,\sigma_z\tau_z$, where $\tilde{\epsilon} \sim \int_0^\infty \mathrm{d}\omega S_{12}(R,\omega)/\omega$. This extra interaction reads for ohmic dissipation and without retardation effects $\tilde{\epsilon} = (K_1K_2)^{1/2}\,\omega_c$. Interestingly, this extra interaction depends only on the cutoff frequency ω_c and the bath coupling $K_{1/2}$. This means that the bath mediated extra interaction is solely determined by the highest frequency (adiabatic) mode of the bath and the coupling strengths. In the following this extra interaction is already included in the coupling v_z.

For the correlated relaxation and the mutual coherence regime we have to consider contributions of the kind shown in Figs. A.1 and A.2. For a cluster from Fig. A.2 we can write

$$\begin{aligned}(\tilde{g}^{(\alpha)})_\tau^\sigma &= (g^{(\alpha)})_\tau^\sigma \sum_{n=0}^{\infty} \left[(g^{(\alpha)})_\tau^+ + (g^{(\alpha)})_\tau^-\right]^n \\ &= (g^{(\alpha)})_\tau^\sigma \frac{1}{1-(g^{(\alpha)})_\tau^+ - (g^{(\alpha)})_\tau^-}\ ,\end{aligned} \tag{A.4.3}$$

with $(g^{(\alpha)})_\tau^\sigma$ a contribution of a blip of type α. The index σ refers to the sojourn on the path $\alpha = 1,2$ preceding the blip and τ refers to the sojourn overlapping the blip. $(g^{(\alpha)})_\tau^\sigma$ is a contribution of a blip of type α

$$\begin{aligned}(g^{(\alpha)})_\tau^\sigma &= -\frac{\Delta_\alpha^2}{2\,\lambda}\int_0^\infty \mathrm{d}t\,\mathrm{e}^{-\lambda\,t}\,\mathrm{e}^{-Q_2^{(\alpha)}(t)}\,\cos\left[\tau\,v_z\,t - \sigma\,Q_1^{(\alpha)}(t)\right] \\ &= -\frac{1}{2\,\lambda}(g_\alpha + \sigma\,\tau\,h_\alpha)\ .\end{aligned} \tag{A.4.4}$$

The symmetric and antisymmetric kernels, g_α and h_α, can be calculated analytically within the NIBA and the scaling limit [2]

$$\begin{aligned}g_\alpha &= f(\lambda + \mathrm{i}\,\epsilon) + f(\lambda - \mathrm{i}\,\epsilon)\ , \\ h_\alpha &= \mathrm{i}\,\tan(\pi\,K)\,\left[f(\lambda + \mathrm{i}\,\epsilon) - f(\lambda - \mathrm{i}\,\epsilon)\right]\ ,\end{aligned} \tag{A.4.5}$$

with

$$f(\lambda) = \frac{\Delta_{\mathrm{eff}}}{2}\,\left(\frac{\beta\,\Delta_{\mathrm{eff}}}{2\,\pi}\right)^{1-2\,K}\,\frac{\Gamma(K + \lambda\,\beta/2\,\pi)}{\Gamma(1-K+\lambda\,\beta/2\,\pi)}\ . \tag{A.4.6}$$

The effective tunnel matrix element Δ_{eff}, given by

$$\Delta_{\mathrm{eff}} = \left[\Gamma(1-2\,K)\,\cos(\pi K)\right]^{1/2(1-K)}\,(\Delta/\omega_{\mathrm{c}})^{K/(1-K)}\,\Delta\ , \tag{A.4.7}$$

is valid as long as $K < 1$. The expression

$$\frac{1}{\lambda}\left(\frac{1}{1-(g^{(\alpha)})_\tau^+ - (g^{(\alpha)})_\tau^-} + (\tilde{g}^{(\alpha)})_\tau^+ - (\tilde{g}^{(\alpha)})_\tau^-\right) = \frac{1}{\lambda}\,\frac{\lambda - h_\alpha}{\lambda + g_\alpha} = P(\lambda) \tag{A.4.8}$$

corresponds to $P(\lambda) = P_{\mathrm{R}} - P_{\mathrm{L}}$, which describes a spin-boson system in the static bias $\tau\,v_z$ within the NIBA [2]. Now, we can sum over a chain of clusters beginning with a

cluster of type α and ending with a cluster of type β, with n clusters of type α, $C_n^{\alpha,\beta}$ (cf. Fig. A.1). We always start in the state RR. Then, we obtain

$$P_{\mathrm{RR}} = \frac{1}{\lambda} + \frac{1}{\lambda}\sum_{n=1}^{\infty} C_n^{(1,1)} + \frac{1}{\lambda}\sum_{n=1}^{\infty} C_n^{(1,2)} + \frac{1}{\lambda}\sum_{n=1}^{\infty} C_n^{(2,1)} + \frac{1}{\lambda}\sum_{n=1}^{\infty} C_n^{(2,2)} \,. \tag{A.4.9}$$

Since the clusters are one after the other, we have the restriction $\sigma_{j+1} = \tau_j$. A chain, where two limiting clusters are of the same type, reads

$$\sum_{n=1}^{\infty} C_n^{(\alpha,\alpha)} = (\tilde{g}^{(\alpha)})_+^+ \sum_{n=0}^{\infty} \left(\sum_{\{\sigma_j\}} (\tilde{g}^{(\beta)})_{2\,j-1}^{2\,j-2} \, (\tilde{g}^{(\alpha)})_{2\,j}^{2\,j-1} \right)^n \,. \tag{A.4.10}$$

The summation index $\{\sigma_j\}$ marks that we have to sum over all possible orderings of σ. This can be written more elegant in matrix notation as (with the restriction $\sigma_{2\,n+1} = 1$)

$$\sum_{n=1}^{\infty} C_n^{(\alpha,\alpha)} = (\tilde{g}^{(\alpha)})_+^+ \left[\left(\mathbb{1}_2 - (\underline{\tilde{g}}^{(\beta)}) \, (\underline{\tilde{g}}^{(\alpha)}) \right)^{-1} \right]_+^+ \,, \tag{A.4.11}$$

with

$$(\underline{\tilde{g}}^{(\alpha)}) = \begin{pmatrix} (\tilde{g}^{(\alpha)})_+^+ & (\tilde{g}^{(\alpha)})_-^+ \\ (\tilde{g}^{(\alpha)})_+^- & (\tilde{g}^{(\alpha)})_-^- \end{pmatrix} \,. \tag{A.4.12}$$

The upper and lower index on the square bracket label the accordant matrix element. We get for two limiting clusters of a different type the expression (again with the restriction $\sigma_{2\,n+1} = 1$)

$$\sum_{n=1}^{\infty} C_n^{(\alpha,\beta)} = \sum_{n=0}^{\infty} (\tilde{g}^{(\alpha)})_+^+ \, (\tilde{g}^{(\beta)})_{\sigma_1}^+ \left(\sum_{\{\sigma_j\}} (\tilde{g}^{(\alpha)})_{2\,j}^{2\,j-1} \, (\tilde{g}^{(\beta)})_{2\,j+1}^{2\,j} \right)^n \tag{A.4.13}$$

or in matrix notation

$$\sum_{n=1}^{\infty} C_n^{(\alpha,\beta)} = (\tilde{g}^{(\alpha)})_+^+ \left[(\underline{\tilde{g}}^{(\beta)}) \left(\mathbb{1}_2 - (\underline{\tilde{g}}^{(\alpha)}) \, (\underline{\tilde{g}}^{(\beta)}) \right)^{-1} \right]_+^+ \,. \tag{A.4.14}$$

Now we can write for P_{RR} from Eq. (A.4.9)

$$\begin{aligned} P_{\mathrm{RR}} = \frac{1}{\lambda} &+ \frac{1}{\lambda} \, (\tilde{g}^{(1)})_+^+ \left[\left(\mathbb{1}_2 - (\underline{\tilde{g}}^{(2)}) \, (\underline{\tilde{g}}^{(1)}) \right)^{-1} \right]_+^+ \\ &+ \frac{1}{\lambda} \, (\tilde{g}^{(2)})_+^+ \left[\left(\mathbb{1}_2 - (\underline{\tilde{g}}^{(1)}) \, (\underline{\tilde{g}}^{(2)}) \right)^{-1} \right]_+^+ \\ &+ \frac{1}{\lambda} \, (\tilde{g}^{(1)})_+^+ \left[(\underline{\tilde{g}}^{(2)}) \, \left(\mathbb{1}_2 - (\underline{\tilde{g}}^{(1)}) \, (\underline{\tilde{g}}^{(2)}) \right)^{-1} \right]_+^+ \\ &+ \frac{1}{\lambda} \, (\tilde{g}^{(2)})_+^+ \left[(\underline{\tilde{g}}^{(1)}) \, \left(\mathbb{1}_2 - (\underline{\tilde{g}}^{(2)}) \, (\underline{\tilde{g}}^{(1)}) \right)^{-1} \right]_+^+ \,. \end{aligned} \tag{A.4.15}$$

Observe the factor $1/\lambda$ in the last two lines, which is missing in the derivation of [59]. In a similar way we obtain P_{LL} (now with the restriction $\sigma_{2\,n+1} = -1$)

$$\begin{aligned} P_{\mathrm{LL}} = & \frac{1}{\lambda}\,(\tilde{g}^{(1)})_{+}^{+}\,\left[(\underline{\tilde{g}}^{(2)})\,\left(\mathbb{1}_2 - (\underline{\tilde{g}}^{(1)})\,(\underline{\tilde{g}}^{(2)})\right)^{-1}\right]_{-}^{+} \\ & + \frac{1}{\lambda}\,(\tilde{g}^{(2)})_{+}^{+}\,\left[(\underline{\tilde{g}}^{(1)})\,\left(\mathbb{1}_2 - (\underline{\tilde{g}}^{(2)})\,(\underline{\tilde{g}}^{(1)})\right)^{-1}\right]_{-}^{+} \\ & + \frac{1}{\lambda}\,(\tilde{g}^{(1)})_{+}^{+}\,\left[(\underline{\tilde{g}}^{(2)})\,(\underline{\tilde{g}}^{(1)})\,\left(\mathbb{1}_2 - (\underline{\tilde{g}}^{(2)})\,(\underline{\tilde{g}}^{(1)})\right)^{-1}\right]_{-}^{+} \\ & + \frac{1}{\lambda}\,(\tilde{g}^{(2)})_{+}^{+}\,\left[(\underline{\tilde{g}}^{(1)})\,(\underline{\tilde{g}}^{(2)})\,\left(\mathbb{1}_2 - (\underline{\tilde{g}}^{(1)})\,(\underline{\tilde{g}}^{(2)})\right)^{-1}\right]_{-}^{+}\,. \end{aligned} \tag{A.4.16}$$

Finally, for P_{RL} we get

$$\begin{aligned} P_{\mathrm{RL}} = & -\frac{1}{\lambda}\,(\tilde{g}^{(1)})_{+}^{+}\,\left[(\underline{\tilde{g}}^{(2)})\,\left(\mathbb{1}_2 - (\underline{\tilde{g}}^{(1)})\,(\underline{\tilde{g}}^{(2)})\right)^{-1}\right]_{+}^{+} \\ & - \frac{1}{\lambda}\,(\tilde{g}^{(2)})_{+}^{+}\,\left[\left(\mathbb{1}_2 - (\underline{\tilde{g}}^{(1)})\,(\underline{\tilde{g}}^{(2)})\right)^{-1}\right]_{+}^{+} \\ & - \frac{1}{\lambda}\,(\tilde{g}^{(1)})_{+}^{+}\,\left[(\underline{\tilde{g}}^{(2)})\,(\underline{\tilde{g}}^{(1)})\,\left(\mathbb{1}_2 - (\underline{\tilde{g}}^{(2)})\,(\underline{\tilde{g}}^{(1)})\right)^{-1}\right]_{-}^{+} \\ & - \frac{1}{\lambda}\,(\tilde{g}^{(2)})_{+}^{+}\,\left[(\underline{\tilde{g}}^{(1)})\,\left(\mathbb{1}_2 - (\underline{\tilde{g}}^{(2)})\,(\underline{\tilde{g}}^{(1)})\right)^{-1}\right]_{-}^{+}\,. \end{aligned} \tag{A.4.17}$$

P_{LR} is the same as P_{RL} but $(1) \leftrightarrow (2)$. Here we have the restriction $\sigma_{2\,n+1} = 1$ if the last cluster is on path 2 and $\sigma_{2\,n+1} = -1$ if the last cluster is on path 1.

With g_1 and h_1 from Eq. (A.4.4) we can write

$$\begin{aligned} P_{\mathrm{RR}} = & \frac{1}{\lambda} - \frac{1}{4\,\lambda}\frac{g_1 + g_2 + h_1 + h_2}{\lambda + g_1 + g_2} - \frac{1}{4}\frac{g_1 + g_2 + h_1 + h_2}{(\lambda + g_1)(\lambda + g_2) - h_1\,h_2} \\ & - \frac{1}{2\,\lambda}\frac{g_1\,g_2 - h_1\,h_2}{(\lambda + g_1)(\lambda + g_2) - h_1\,h_2} \end{aligned} \tag{A.4.18}$$

and similar expressions follow correspondingly for P_{LL}, P_{RL}, and P_{LR} [59].

The steady state for long times can be derived directly from the limit $\lambda\,P_{\mathrm{RR}}(\lambda)$ as $\lambda \to 0$ (within the scaling limit) or from the general thermodynamic relation given in Eq. (2.1.9). In either case we get within the limits $T \gg v_z$ and $v_z \gg \Delta$ the long time probabilities

$$\begin{aligned} P_{\mathrm{RR}}(t \to \infty) &= P_{\mathrm{LL}}(t \to \infty) = \frac{1}{4}\left[1 + \tanh\left(\frac{v_z}{2\,T}\right)\right] \\ P_{\mathrm{RL}}(t \to \infty) &= P_{\mathrm{LR}}(t \to \infty) = \frac{1}{4}\left[1 - \tanh\left(\frac{v_z}{2\,T}\right)\right]\,. \end{aligned} \tag{A.4.19}$$

A.5 Explicit results of Bloch-Redfield method

A.5.1 v_z coupling

The matrix elements that we need to calculate the $W_{i,j}$'s and $\Gamma^{\pm}$'s are

$$\begin{aligned}
\left\langle 1 \left| \frac{\sigma_z}{2} \right| 2 \right\rangle \left\langle 1 \left| \frac{\sigma_z}{2} \right| 2 \right\rangle &= \frac{v_z^2 - \delta^2 - \Delta 1^2 + \Delta 2^2 + \Omega^2}{8(\Omega^2 - \delta^2)}\,, \\
\left\langle 1 \left| \frac{\sigma_z}{2} \right| 3 \right\rangle \left\langle 1 \left| \frac{\sigma_z}{2} \right| 3 \right\rangle &= -\frac{v_z^2 + \delta^2 - \Delta 1^2 + \Delta 2^2 - \Omega^2}{8(\Omega^2 - \delta^2)}\,, \\
\left\langle 1 \left| \frac{\tau_z}{2} \right| 2 \right\rangle \left\langle 1 \left| \frac{\tau_z}{2} \right| 2 \right\rangle &= \frac{v_z^2 - \delta^2 + \Delta 1^2 - \Delta 2^2 + \Omega^2}{8(\Omega^2 - 2\delta^2)}\,, \\
\left\langle 1 \left| \frac{\tau_z}{2} \right| 3 \right\rangle \left\langle 1 \left| \frac{\tau_z}{2} \right| 3 \right\rangle &= -\frac{v_z^2 + \delta^2 + \Delta 1^2 - \Delta 2^2 - \Omega^2}{8(\Omega^2 - 2\delta^2)}\,,
\end{aligned} \tag{A.5.1}$$

and

$$\begin{aligned}
\langle 1 \,|\, \sigma_z \,|\, 2 \rangle \langle 3 \,|\, \sigma_z \,|\, 4 \rangle &= -\langle 1 \,|\, \sigma_z \,|\, 2 \rangle \langle 1 \,|\, \sigma_z \,|\, 2 \rangle\,, \\
\langle 1 \,|\, \tau_z \,|\, 2 \rangle \langle 3 \,|\, \tau_z \,|\, 4 \rangle &= \langle 1 \,|\, \tau_z \,|\, 2 \rangle \langle 1 \,|\, \tau_z \,|\, 2 \rangle\,, \\
\langle 1 \,|\, \sigma_z \,|\, 3 \rangle \langle 2 \,|\, \sigma_z \,|\, 4 \rangle &= \langle 1 \,|\, \sigma_z \,|\, 3 \rangle \langle 1 \,|\, \sigma_z \,|\, 3 \rangle\,, \\
\langle 1 \,|\, \tau_z \,|\, 3 \rangle \langle 2 \,|\, \tau_z \,|\, 4 \rangle &= -\langle 1 \,|\, \tau_z \,|\, 3 \rangle \langle 1 \,|\, \tau_z \,|\, 3 \rangle\,.
\end{aligned} \tag{A.5.2}$$

With these expressions and with (4.1.9) and (4.1.20) we obtain

$$\begin{aligned}
W_{1,2} = -\frac{\pi}{8\left(\delta^2 - \Omega^2\right)} \Bigg[& S_1(\delta) \left(1 + \tanh\left(\frac{\delta}{2T_1}\right)\right) \left(v_z^2 - \delta^2 + \Omega^2 - \Delta_1^2 + \Delta_2^2\right) \\
& + S_2(\delta) \left(1 + \tanh\left(\frac{\delta}{2T_2}\right)\right) \left(v_z^2 - \delta^2 + \Omega^2 + \Delta_1^2 - \Delta_2^2\right) \Bigg]\,,
\end{aligned} \tag{A.5.3}$$

$$\begin{aligned}
W_{1,2} = -\frac{\pi}{8\left(\delta^2 - \Omega^2\right)} \Bigg[& S_1(\delta) \left(1 - \tanh\left(\frac{\delta}{2T_1}\right)\right) \left(v_z^2 - \delta^2 + \Omega^2 - \Delta_1^2 + \Delta_2^2\right) \\
& + S_2(\delta) \left(1 - \tanh\left(\frac{\delta}{2T_2}\right)\right) \left(v_z^2 - \delta^2 + \Omega^2 + \Delta_1^2 - \Delta_2^2\right) \Bigg]\,,
\end{aligned} \tag{A.5.4}$$

and

$$\begin{aligned}
W_{1,3} = \frac{\pi}{8\left(\delta^2 - \Omega^2\right)} \Bigg[& S_1(\Omega) \left(1 + \tanh\left(\frac{\Omega}{2T_1}\right)\right) \left(v_z^2 + \delta^2 - \Omega^2 - \Delta_1^2 + \Delta_2^2\right) \\
& + S_2(\Omega) \left(1 + \tanh\left(\frac{\Omega}{2T_2}\right)\right) \left(v_z^2 + \delta^2 - \Omega^2 + \Delta_1^2 - \Delta_2^2\right) \Bigg]\,,
\end{aligned} \tag{A.5.5}$$

$$W_{3,1} = \frac{\pi}{8\left(\delta^2-\Omega^2\right)}\Bigg[S_1(\Omega)\left(1-\tanh\left(\frac{\Omega}{2T_1}\right)\right)\left(v_z^2+\delta^2-\Omega^2-\Delta_1^2+\Delta_2^2\right) + S_2(\Omega)\left(1-\tanh\left(\frac{\Omega}{2T_2}\right)\right)\left(v_z^2+\delta^2-\Omega^2+\Delta_1^2-\Delta_2^2\right)\Bigg]. \tag{A.5.6}$$

We see that $W_{2,1}$ and $W_{3,1}$ vanish for zero temperature, i.e., there is no bath mediated transition from a lower to an upper state at zero temperature. We also obtain

$$\Gamma^+_{2134}+\Gamma^-_{2134} = \frac{\pi}{8\left(\delta^2-\Omega^2\right)}\Bigg[S_1(\delta)\left(1+\tanh\left(\frac{\delta}{2T_1}\right)\right)\left(\Omega^2-\delta^2+v_z^2-\Delta_1^2+\Delta_2^2\right) + S_2(\delta)\left(1+\tanh\left(\frac{\delta}{2T_2}\right)\right)\left(\delta^2-\Omega^2-v_z^2-\Delta_1^2+\Delta_2^2\right)\Bigg], \tag{A.5.7}$$

$$\Gamma^+_{1243}+\Gamma^-_{1243} = \frac{\pi}{8\left(\delta^2-\Omega^2\right)}\Bigg[S_1(\delta)\left(1-\tanh\left(\frac{\delta}{2T_1}\right)\right)\left(\Omega^2-\delta^2+v_z^2-\Delta_1^2+\Delta_2^2\right) + S_2(\delta)\left(1-\tanh\left(\frac{\delta}{2T_2}\right)\right)\left(\delta^2-\Omega^2-v_z^2-\Delta_1^2+\Delta_2^2\right)\Bigg], \tag{A.5.8}$$

and

$$\Gamma^+_{2134}+\Gamma^-_{2134} = -\frac{\pi}{8\left(\delta^2-\Omega^2\right)}\Bigg[S_1(\Omega)\left(1+\tanh\left(\frac{\Omega}{2T_1}\right)\right)\left(\Omega^2-\delta^2-v_z^2+\Delta_1^2-\Delta_2^2\right) + S_2(\Omega)\left(1+\tanh\left(\frac{\Omega}{2T_2}\right)\right)\left(\delta^2-\Omega^2+v_z^2+\Delta_1^2-\Delta_2^2\right)\Bigg], \tag{A.5.9}$$

$$\Gamma^+_{1243}+\Gamma^-_{1243} = -\frac{\pi}{8\left(\delta^2-\Omega^2\right)}\Bigg[S_1(\Omega)\left(1-\tanh\left(\frac{\Omega}{2T_1}\right)\right)\left(\Omega^2-\delta^2-v_z^2+\Delta_1^2-\Delta_2^2\right) + S_2(\Omega)\left(1-\tanh\left(\frac{\Omega}{2T_2}\right)\right)\left(\delta^2-\Omega^2+v_z^2+\Delta_1^2-\Delta_2^2\right)\Bigg]. \tag{A.5.10}$$

A.5.2 v_y and v_z coupling

The matrix elements that we need to calculate the $W_{i,j}$'s and $\Gamma^{\pm}$'s are

$$\begin{aligned}
\left\langle 1 \left| \frac{\sigma_z}{2} \right| 2 \right\rangle \left\langle 1 \left| \frac{\sigma_z}{2} \right| 2 \right\rangle &= \frac{((\delta+v_y)^2-(v_z-\Omega)^2+\Delta_1^2-\Delta_2^2)^2}{16\,(\delta^2-\Omega^2)\,((\delta+v_y)^2-(v_z-\Omega)^2)}\,,\\
\left\langle 1 \left| \frac{\sigma_z}{2} \right| 3 \right\rangle \left\langle 1 \left| \frac{\sigma_z}{2} \right| 3 \right\rangle &= -\frac{((v_z-\delta)^2-(\Omega+v_y)^2-\Delta_1^2+\Delta_2^2)^2}{16\,(\delta^2-\Omega^2)\,((\Omega+v_y)^2-(\delta-v_z)^2)}\,,\\
\left\langle 1 \left| \frac{\tau_z}{2} \right| 2 \right\rangle \left\langle 1 \left| \frac{\tau_z}{2} \right| 2 \right\rangle &= \frac{((\delta+v_y)^2-(v_z-\Omega)^2-\Delta_1^2+\Delta_2^2)^2}{16\,(\delta^2-\Omega^2)\,((\delta+v_y)^2-(v_z-\Omega)^2)}\,,\\
\left\langle 1 \left| \frac{\tau_z}{2} \right| 3 \right\rangle \left\langle 1 \left| \frac{\tau_z}{2} \right| 3 \right\rangle &= -\frac{((v_z-\delta)^2-(\Omega+v_y)^2+\Delta_1^2-\Delta_2^2)^2}{16\,(\delta^2-\Omega^2)\,((\Omega+v_y)^2-(\delta-v_z)^2)}\,,
\end{aligned} \tag{A.5.11}$$

and

$$\begin{aligned}
\left\langle 1 \left| \frac{\sigma_z}{2} \right| 2 \right\rangle \left\langle 3 \left| \frac{\sigma_z}{2} \right| 4 \right\rangle &= \frac{\delta^2-\Omega^2+v_y^2-v_z^2+\Delta_1^2-\Delta_2^2}{8\,(\Omega^2-\delta^2)}\,,\\
\left\langle 1 \left| \frac{\tau_z}{2} \right| 2 \right\rangle \left\langle 3 \left| \frac{\tau_z}{2} \right| 4 \right\rangle &= \frac{\Omega^2-\delta^2-v_y^2+v_z^2+\Delta_1^2-\Delta_2^2}{8\,(\Omega^2-\delta^2)}\,,\\
\left\langle 1 \left| \frac{\sigma_z}{2} \right| 3 \right\rangle \left\langle 2 \left| \frac{\sigma_z}{2} \right| 4 \right\rangle &= \frac{\Omega^2-\delta^2+v_y^2-v_z^2+\Delta_1^2-\Delta_2^2}{8\,(\Omega^2-\delta^2)}\,,\\
\left\langle 1 \left| \frac{\tau_z}{2} \right| 3 \right\rangle \left\langle 2 \left| \frac{\tau_z}{2} \right| 4 \right\rangle &= \frac{\delta^2-\Omega^2-v_y^2+v_z^2+\Delta_1^2-\Delta_2^2}{8\,(\Omega^2-\delta^2)}\,.
\end{aligned} \tag{A.5.12}$$

With these expressions and with (4.1.9) and (4.1.20) we obtain

$$\begin{aligned}
W_{1,2} = {} & \frac{\pi}{16\,(\delta^2-\Omega^2)\,[(\delta+v_y)^2-(v_z-\Omega)^2]}\\
& \times \left[S_1(\delta) \left(1+\tanh\left(\frac{\delta}{2T_1}\right)\right) \left[(\delta+v_y)^2-(v_z-\Omega)^2+\Delta_1^2-\Delta_2^2\right]^2 \right.\\
& \left. + S_2(\delta) \left(1+\tanh\left(\frac{\delta}{2T_2}\right)\right) \left[(\delta+v_y)^2-(v_z-\Omega)^2-\Delta_1^2+\Delta_2^2\right]^2 \right],
\end{aligned} \tag{A.5.13}$$

$$\begin{aligned}
W_{2,1} = {} & \frac{\pi}{16\,(\delta^2-\Omega^2)\,[(\delta+v_y)^2-(v_z-\Omega)^2]}\\
& \times \left[S_1(\delta) \left(1-\tanh\left(\frac{\delta}{2T_1}\right)\right) \left[(\delta+v_y)^2-(v_z-\Omega)^2+\Delta_1^2-\Delta_2^2\right]^2 \right.\\
& \left. + S_2(\delta) \left(1-\tanh\left(\frac{\delta}{2T_2}\right)\right) \left[(\delta+v_y)^2-(v_z-\Omega)^2-\Delta_1^2+\Delta_2^2\right]^2 \right],
\end{aligned} \tag{A.5.14}$$

and

$$W_{1,3} = -\frac{\pi}{16\left(\delta^2-\Omega^2\right)\left[\left(\Omega+v_y\right)^2-\left(v_z-\delta\right)^2\right]} \times\left[S_1(\Omega)\left(1+\tanh\left(\frac{\Omega}{2T_1}\right)\right)\left[\left(v_z-\delta\right)^2-\left(\Omega+v_y\right)^2-\Delta_1^2+\Delta_2^2\right]^2 + S_2(\Omega)\left(1+\tanh\left(\frac{\Omega}{2T_2}\right)\right)\left[\left(v_z-\delta\right)^2-\left(\Omega+v_y\right)^2+\Delta_1^2-\Delta_2^2\right]^2\right], \tag{A.5.15}$$

$$W_{3,1} = -\frac{\pi}{16\left(\delta^2-\Omega^2\right)\left[\left(\Omega+v_y\right)^2-\left(v_z-\delta\right)^2\right]} \times\left[S_1(\Omega)\left(1-\tanh\left(\frac{\Omega}{2T_1}\right)\right)\left[\left(v_z-\delta\right)^2-\left(\Omega+v_y\right)^2-\Delta_1^2+\Delta_2^2\right]^2 + S_2(\Omega)\left(1-\tanh\left(\frac{\Omega}{2T_2}\right)\right)\left[\left(v_z-\delta\right)^2-\left(\Omega+v_y\right)^2+\Delta_1^2-\Delta_2^2\right]^2\right]. \tag{A.5.16}$$

We see that $W_{2,1}$ and $W_{3,1}$ vanish for zero temperature, i.e., there is no bath mediated transition from a lower to an upper state at zero temperature. We get

$$\Gamma^+_{2134}+\Gamma^-_{2134} = \frac{\pi}{8\left(\delta^2-\Omega^2\right)}\left[S_1(\delta)\left(1+\tanh\left(\frac{\delta}{2T_1}\right)\right)\left(\Omega^2-\delta^2-v_y^2+v_z^2-\Delta_1^2+\Delta_2^2\right) + S_2(\delta)\left(1+\tanh\left(\frac{\delta}{2T_2}\right)\right)\left(\delta^2-\Omega^2+v_y^2-v_z^2-\Delta_1^2+\Delta_2^2\right)\right], \tag{A.5.17}$$

$$\Gamma^+_{1243}+\Gamma^-_{1243} = \frac{\pi}{8\left(\delta^2-\Omega^2\right)}\left[S_1(\delta)\left(1-\tanh\left(\frac{\delta}{2T_1}\right)\right)\left(\Omega^2-\delta^2-v_y^2+v_z^2-\Delta_1^2+\Delta_2^2\right) + S_2(\delta)\left(1-\tanh\left(\frac{\delta}{2T_2}\right)\right)\left(\delta^2-\Omega^2+v_y^2-v_z^2-\Delta_1^2+\Delta_2^2\right)\right], \tag{A.5.18}$$

and

$$\Gamma^+_{2134}+\Gamma^-_{2134} = -\frac{\pi}{8\left(\delta^2-\Omega^2\right)}\left[S_1(\Omega)\left(1+\tanh\left(\frac{\Omega}{2T_1}\right)\right)\left(\Omega^2-\delta^2+v_y^2-v_z^2+\Delta_1^2-\Delta_2^2\right) + S_2(\Omega)\left(1+\tanh\left(\frac{\Omega}{2T_2}\right)\right)\left(\delta^2-\Omega^2-v_y^2+v_z^2+\Delta_1^2-\Delta_2^2\right)\right],$$

(A.5.19)

$$\Gamma^{+}_{1243} + \Gamma^{-}_{1243} = - \frac{\pi}{8\left(\delta^2 - \Omega^2\right)} \Bigg[S_1(\Omega) \left(1 - \tanh\left(\frac{\Omega}{2T_1}\right)\right) \left(\Omega^2 - \delta^2 + v_y^2 - v_z^2 + \Delta_1^2 - \Delta_2^2\right) + S_2(\Omega) \left(1 - \tanh\left(\frac{\Omega}{2T_2}\right)\right) \left(\delta^2 - \Omega^2 - v_y^2 + v_z^2 + \Delta_1^2 - \Delta_2^2\right) \Bigg] .$$

(A.5.20)

Bibliography

[1] A. J. Leggett, S. Chakravarty, A. T. Dorsey, M. P. A. Fisher, A. Garg, and W. Zwerger, *Rev. Mod. Phys.* **59**, 1 (1987), erratum *Rev. Mod. Phys.* **67**, 725 (1995).

[2] U. Weiss, *Quantum Dissipative Systems*, World Scientific, 3rd edition, 2007.

[3] M. N. Baibich, J. M. Broto, A. Fert, F. N. Van Dau, F. Petroff, P. Eitenne, G. Creuzet, A. Friederich, and J. Chazelas, *Phys. Rev. Lett.* **61**, 2472 (1988).

[4] D. Sellmyer and R. Skomski, *Advanced Magnetic Nanostructures*, Springer, 2006.

[5] P. Shor, *Foundations of Computer Science, 1994 Proceedings., 35th Annual Symposium on* , 124 (1994).

[6] P. W. Shor, *Phys. Rev. A* **52**, R2493 (1995).

[7] P. W. Shor, *SIAM Rev.* **41**, 303 (1999).

[8] D. Aharonov, *Quantum Computation* (1998), in: *Annual Review of Computational Physics VI*, p.259, ed. by D. Stauffer, World Scientific, 1999.

[9] D. Loss and D. P. DiVincenzo, *Phys. Rev. A* **57**, 120 (1998).

[10] R. Feynman, *Int. J. Theo. Phys.* **21**, 467 (1982).

[11] I. Kassal, S. P. Jordan, P. J. Love, M. Mohseni, and A. Aspuru-Guzik, *PNAS* **105**, 18681 (2008).

[12] Y. Makhlin, G. Schön, and A. Shnirman, *Rev. Mod. Phys.* **73**, 357 (2001).

[13] W. H. Zurek, *Rev. Mod. Phys.* **75**, 715 (2003).

[14] M. Schlosshauer, *Rev. Mod. Phys.* **76**, 1267 (2005).

[15] W. H. Zurek, *Nat. Phys.* **5**, 181 (2009).

[16] J. Fischer and D. Loss, *Science* **324**, 1277 (2009).

[17] M. Dubé and P. Stamp, *Chem. Phys.* **268**, 257 (2001).

[18] N. Prokof'ev and P. Stamp, *Rep. Prog. Phys.* **63**, 669 (2000).

[19] D. J. V. Harlingen, T. L. Robertson, B. L. T. Plourde, P. A. Reichardt, T. A. Crane, and J. Clarke, *Phys. Rev. B* **70**, 064517 (2004).

[20] A. Lupascu, P. Bertet, E. F. C. Driessen, C. J. P. M. Harmans, and J. E. Mooij, *http://arxiv.org/abs/0810.0590* (2008).

[21] J. Bergli, Y. M. Galperin, and B. L. Altshuler, *New. J. Phys.* **11**, 025002 (2009).

[22] C. Müller, A. Shnirman, and Y. Makhlin, *http://arxiv.org/abs/0905.2332* (2009).

[23] H. Gassmann, F. Marquardt, and C. Bruder, *Phys. Rev. E* **66**, 041111 (2002).

[24] E. Paladino, M. Sassetti, and G. Falci, *Chem. Phys.* **296**, 325 (2004).

[25] H. Gassmann and C. Bruder, *Phys. Rev. B* **72**, 035102 (2005).

[26] E. Paladino, A. Maugeri, M. Sassetti, G. Falci, and U. Weiss, *Physica E* **40**, 198 (2007).

[27] E. Paladino, M. Sassetti, G. Falci, and U. Weiss, *Chem. Phys.* **322**, 98 (2006).

[28] E. Paladino, M. Sassetti, G. Falci, and U. Weiss, *Phys. Rev. B* **77**, 041303 (2008).

[29] E. Novais, A. H. C. Neto, L. Borda, I. Affleck, and G. Zarand, *Phys. Rev. B* **72**, 014417 (2005).

[30] P. Nägele and U. Weiss, *Physica E* (2009), in press, http://dx.doi.org/10.1016/j.physe.2009.06.060.

[31] E. Paladino, A. Mastellone, A. D'Arrigo, and G. Falci, *Phys. Rev. Lett.* (2009), submitted.

[32] H. Häffner, W. Hänsel, C. F. Roos, J. Benhelm, D. C. al kar, M. Chwalla, T. Körber, U. D. Rapol, M. Riebe, P. O. Schmidt, C. Becher, O. Gühne, W. Dür, and R. Blatt, *Nature* **438**, 643 (2005).

[33] S. C. Benjamin, A. Ardavan, G. A. D. Briggs, D. A. Britz, D. Gunlycke, J. Jefferson, M. A. G. Jones, D. F. Leigh, B. W. Lovett, A. N. Khlobystov, S. A. Lyon, J. J. L. Morton, K. Porfyrakis, M. R. Sambrook, and A. M. Tyryshkin, *J. Phys.: Cond. Matter* **18**, S867 (2006).

[34] L. Childress, M. V. G. Dutt, J. M. Taylor, A. S. Zibrov, F. Jelezko, J. Wrachtrup, P. R. Hemmer, and M. D. Lukin, *Science* **314**, 281 (2006).

[35] R. Hanson and D. D. Awschalom, *Nature* **453**, 1043 (2008).

[36] J. Baugh, J. Chamilliard, C. M. Chandrashekar, M. Ditty, A. Hubbard, R. Laflamme, M. Laforest, D. Maslov, O. Moussa, C. Negrevergne, M. Silva, S. Simmons, C. A. Ryan, D. G. Cory, J. S. Hodges, and C. Ramanathan, *http://arxiv.org/abs/0710.1447* (2007).

[37] C.-Y. Lu, X.-Q. Zhou, O. Guhne, W.-B. Gao, J. Zhang, Z.-S. Yuan, A. Goebel, T. Yang, and J.-W. Pan, *Nat. Phys.* **3**, 91 (2007).

[38] R. Hanson, L. P. Kouwenhoven, J. R. Petta, S. Tarucha, and L. M. K. Vandersypen, *Rev. Mod. Phys.* **79**, 1217 (2007).

[39] J. M. Martinis, S. Nam, J. Aumentado, and C. Urbina, *Phys. Rev. Lett.* **89**, 117901 (2002).

[40] I. Chiorescu, Y. Nakamura, C. J. P. M. Harmans, and J. E. Mooij, *Science* **299**, 1869 (2003).

[41] Y. A. Pashkin, T. Yamamoto, O. Astafiev, Y. Nakamura, D. V. Averin, and J. S. Tsai, *Nature* **421**, 823 (2003).

[42] T. Yamamoto, Y. A. Pashkin, O. Astafiev, Y. Nakamura, and J. S. Tsai, *Nature* **425**, 941 (2003).

[43] I. Chiorescu, P. Bertet, K. Semba, Y. Nakamura, C. J. P. M. Harmans, and J. E. Mooij, *Nature* **431**, 159 (2004).

[44] R. McDermott, R. W. Simmonds, M. Steffen, K. B. Cooper, K. Cicak, K. D. Osborn, S. Oh, D. P. Pappas, and J. M. Martinis, *Science* **307**, 1299 (2005).

[45] J. Clarke and F. K. Wilhelm, *Nature* **453**, 1031 (2008).

[46] G. Chen, D. A. Church, B.-G. Englert, C. Henkel, and B. Rohwedder, *Quantum computing devices: principles, designs, and analysis*, Chapman & Hall, 2006.

[47] R. L. Rivest, A. Shamir, and L. Adleman, *Commun. ACM* **21**, 120 (1978).

[48] A. Shnirman, Y. Makhlin, and G. Schön, *Physica Scripta* **T102**, 147 (2002).

[49] O. Astafiev, Y. A. Pashkin, Y. Nakamura, T. Yamamoto, and J. S. Tsai, *Phys. Rev. Lett.* **93**, 267007 (2004).

[50] F. Yoshihara, K. Harrabi, A. O. Niskanen, Y. Nakamura, and J. S. Tsai, *Phys. Rev. Lett.* **97**, 167001 (2006).

[51] D. Vion, A. Aassime, A. Cottet, P. Joyez, H. Pothier, C. Urbina, D. Esteve, and M. H. Devoret, *Science* **296**, 886 (2002).

[52] J. Koch, T. M. Yu, J. Gambetta, A. A. Houck, D. I. Schuster, J. Majer, A. Blais, M. H. Devoret, S. M. Girvin, and R. J. Schoelkopf, *Phys. Rev. A* **76**, 042319 (2007).

[53] F. Nesi, E. Paladino, M. Thorwart, and M. Grifoni, *Europhys. Let.* **80**, 40005 (2007).

[54] F. Nesi, E. Paladino, M. Thorwart, and M. Grifoni, *Phys. Rev. B* **76**, 155323 (2007).

[55] K. Blum, *Density matrix theory and applications*, Plenum Pr., 2nd edition, 1996.

[56] F. K. Wilhelm, S. Kleff, and J. von Delft, *Chem. Phys.* **296**, 345 (2004).

[57] L. Hartmann, I. Goychuk, M. Grifoni, and P. Hänggi, *Phys. Rev. E* **61**, R4687 (2000).

[58] R. Feynman and F. Vernon, *Ann. Phys. (N.Y.)* **24**, 118 (1963).

[59] M. Dubé and P. Stamp, *Int. J. of Mod. Phys. B* **12**, 1191 (1998).

[60] M. Governale, M. Grifoni, and G. Schön, *Chem. Phys.* **268**, 273 (2001).

[61] G. Campagnano, A. Hamma, and U. Weiss, *http://de.arxiv.org/abs/0807.1987* (2008).

[62] M. B. Plenio, *Science* **324**, 342 (2009).

[63] D. DiVincenzo, *Fortschr. Phys.* **48**, 771 (2000).

[64] M. Grajcar, S. H. W. van der Ploeg, A. Izmalkov, E. Il'ichev, H.-G. Meyer, A. Fedorov, A. Shnirman, and G. Schön, *Nat. Phys.* **4**, 612 (2008).

[65] F. Nori, *Nat. Phys.* **4**, 589 (2008).

[66] P. Nägele, G. Campagnano, and U. Weiss, *New. J. Phys.* **10**, 115010 (2008).

[67] M. Storcz and F. Wilhelm, *Phys. Rev. A* **67**, 042319 (2003).

[68] M. J. Storcz, F. Hellmann, C. Hrelescu, and F. K. Wilhelm, *Phys. Rev. A* **72**, 052314 (2005).

[69] T. Zell, F. Queisser, and R. Klesse, *Phys. Rev. Lett.* **102**, 160501 (2009).

[70] C. H. Mak and D. Chandler, *Phys. Rev. A* **44**, 2352 (1991).

[71] D. D. B. Rao, H. Kohler, and F. Sols, *New. J. Phys.* **10**, 115017 (2008).

[72] I. A. Grigorenko and D. V. Khveshchenko, *Phys. Rev. Lett.* **94**, 040506 (2005).

[73] M. B. Weissman, *Rev. Mod. Phys.* **60**, 537 (1988).

[74] A. B. Zorin, F.-J. Ahlers, J. Niemeyer, T. Weimann, H. Wolf, V. A. Krupenin, and S. V. Lotkhov, *Phys. Rev. B* **53**, 13682 (1996).

[75] R. W. Simmonds, K. M. Lang, D. A. Hite, S. Nam, D. P. Pappas, and J. M. Martinis, *Phys. Rev. Lett.* **93**, 077003 (2004).

[76] K. B. Cooper, M. Steffen, R. McDermott, R. W. Simmonds, S. Oh, D. A. Hite, D. P. Pappas, and J. M. Martinis, *Phys. Rev. Lett.* **93**, 180401 (2004).

[77] C. Cohen-Tannoudji, J. Dupont-Roc, and G. Grynberg, *Atom-Photon Interactions*, John Wiley & Sons, Inc., 1992.

[78] Y. Makhlin, G. Schön, and A. Shnirman, (2003), in: New Directions in Mesoscopic Physics, pp. 197-224, eds. R. Fazio, V. F. Gantmakher, and Y. Imry, Kluwer, Dordrecht, 2003.

[79] S. Ashhab, J. R. Johansson, and F. Nori, *New. J. Phys.* **8**, 103 (2006).

Lebenslauf

Name:	Peter Nägele	
Geburtsdatum:	12.05.1980	
Geburtsort:	Schwäbisch Gmünd	
Schule:	1986 – 1990	Grundschule in Ottenbach
	1990 – 1996	Erich-Kästner Gymnasium in Eislingen
	1996 – 1999	Abitur am Technischen Gymnasium Öde in Göppingen
Studium:	1999 – 2000	Studium der Informatik an der Universiät Stuttgart
	2000 – 2006	Studium der Physik an der Universiät Stuttgart
	März 2006	Diplom in Physik
	Seit März 2006	Wissenschaftlicher Mitarbeiter am II. Institut für Theoretische Physik der Universiät Stuttgart

Danksagung

An dieser Stelle möchte ich mich bei allen bedanken, die zum Gelingen dieser Arbeit beigetragen haben.

Mein besonderer Dank gilt Herrn Prof. Dr. U. Weiß für das nie nachlassende Interesse während allen Teilen dieser Arbeit, die ständige Unterstützung und anregenden Diskussionen.

Ich danke Prof. Dr. G. Mahler für die freundliche Übernahme des Mitberichtes.

Herrn Prof. Dr. U. Seifert und allen Kollegen des 2. Instituts für Theoretische Physik danke ich für das freundliche und offene Institutsklima. Besonderer Dank gilt R. Bedau und G. Campagnano für die vielen fruchtbaren Diskussionen in- und außerhalb der Physik.

Ich danke R. Nägele für das hilfreiche Korrekturlesen.

Ohne die fortwährende Unterstützung und des Korrekturlesens von M. Löffler wäre diese Arbeit nicht möglich gewesen.

Auch ohne die Unterstützung meiner Eltern, T. und E. Nägele, und meiner Familie wäre nichts von alledem möglich gewesen. So gilt ihnen der größte Dank.